ANALYSIS OF FUNCTIONAL ORGANIC MOLECULES AT NOBLE METAL SURFACES BY MEANS OF VIBRATIONAL SPECTROSCOPIES

Im Fachbereich Physik
der Freien Universität Berlin
eingereichte Dissertation

Felix Leyßner

August 2011

This work was started in September 2007 in the group of Professor Martin Wolf and finished in August 2011 in the group of Professor Petra Tegeder at the Physics Department of the Freie Universität Berlin.

Berlin, August 2011

Erstgutachterin: Prof. Dr. Petra Tegeder
Zweitgutachter: Prof. Dr. José Ignacio Pascual

Datum der Disputation: 24.10.2011

Abstract

The goal of this work is to optimize the efficiency of photoinduced molecular switching processes on surfaces *via* controlled variations of the adsorption and electronic properties of the switch. We investigated the influence of external stimuli, *i.e.* photons and thermal activation, on surface bound molecular switches undergoing *trans/cis*-isomerizations and ring-opening/closing-reactions, respectively. *High resolution electron energy loss spectroscopy* (HREELS) and *sum-frequency generation* (SFG) spectroscopy have been used as the main tools to investigate the adsorption behavior and the molecular switching properties. Two basic concepts of coupling the molecular switch to the surface have been studied: (i) physisorbed or weakly chemisorbed systems deposited on noble metal surfaces under UHV conditions and (ii) molecular switches bound covalently *via* anchor groups.

In the HREELS study following concept (i), we investigated the adsorption geometry and isomerization behavior of various molecular switches on metal substrates which are able to undergo a photoinduced *trans/cis*-isomerization in solution. We investigated three isoelectronic molecules on Au where we systematically changed the photochemically active group from the diazo-group in an azobenzene-derivative (on Cu(111)) to the imine-group, and the vinylene-group, respectively. Finding the photoisomerization quenched for all systems we observed considerable differences in their thermal isomerization behavior. Comparable we find the photoinduced ring-opening/closing-reaction of spiropyran quenched on Au(111) but a thermally induced ring-opening reaction resulting in the open form being strongly stabilized by the metal. SFG spectroscopy is employed to investigate the reversible, photoinduced *trans/cis*-isomerization of an azobenzene-functionalized self-assembled monolayer (SAM) on gold using a tripodal linker system. In consequence of the decoupling provided by the tripodal linker, the switching behavior of the azobenzene incorporated into the SAM is analogous to the free molecule in solution with the determined cross sections being similar. Therefore we propose a direct (intramolecular) electronic excitation mechanism. Additionally we studied graphene nanoribbons (GNRs), which are thin flakes of graphene, characterized by their width and edge-structure. Electronic HREELS has been proven to be a powerful tool which enables us to directly measure the band gap of the GNRs on Au(111). Regarding sub-nanometer wide atomically precise GNRs we report the first measurement of the band gap.

We gained insight into the dependence of the switching process regarding molecule-/substrate-interactions and molecule/molecule-interactions. These interactions govern the adsorption geometry and electronic structure of the surface bound species as well as they are responsible for steric hindrance and intra-layer electronic coupling strength. We conclude that the physical mechanism governing the desired functionality may be influenced drastically by the electronic interaction with the substrate, so that purely geometrical arguments to predict the functionality of adsorbed molecules have to be taken with great caution. Our study demonstrates that both, the geometric and electronic structure of the complete molecule–substrate complex have to be taken into account for a successful reversible photoisomerization of surface bound molecular switches.

Kurzfassung

Das Ziel dieser Arbeit ist es, die Effizienz photoinduzierter Schaltvorgänge auf Festkörperoberflächen über gezielte Variation der Adsorptions- und elektronischen Eigenschaften molekularer Schalter zu optimieren. Wir untersuchten den Einfluss von externen Stimuli (Photonen und thermische Aktivierung) auf adsorbierte molekulare Schalter. Die untersuchten Systeme können in Lösung entweder eine *trans/cis*-Isomerisierung oder eine Ringöffnungs/-schluss Reaktion vollführen. *Hochaufgelöste Elektronenenergie Verlustspektroskopie* (HREELS) und Summenfrequenzerzeugung (SFG) wurden verwendet um das Adsorptionsverhalten und die molekularen Schalteigenschaften zu untersuchen. Zwei Konzepte bezüglich der Ankopplung der Schaltermoleküle an die Oberfläche wurden verfolgt: (i) physisorbierte oder schwach chemisorbierte Systeme auf Edelmetalloberflächen und (ii) molekulare Schalter kovalent an Gold über Anker-/Linkergruppen gebunden.

Die Adsorptionsgeometrie und das Schaltverhalten von drei isoelektronischen molekularen Schaltern nach Adsorption auf Au(111) (bzw. Cu(111)) wurde untersucht. Die photochemisch aktive Guppe ist systematisch von der Diazo-Gruppe in Azobenzol (auf Cu(111)) zu der Imin und Vinylen-Gruppe variiert worden, um den Einfluss auf die Schaltfähigkeit zu untersuchen. Für alle Derivate konnte kein photoinduzierter Schaltvorgang nach Adsorption nachgewiesen werden. Allerdings wurden erhebliche Unterschiede im thermischen Isomerisierungsverhalten gefunden. Vergleichbar ist das Verhalten von Spiropyran auf Au(111), bei der die photoinduzierte Ringöffnungs/-schluss Reaktion unterdrückt wird. Es wurde eine thermische Ring-Öffnungs Reaktion beobachtet bei der das resultierende Isomer stark durch die Oberfläche stabilisiert wird. SFG Spektroskopie wurde verwendet, um die reversible, lichtinduzierte *trans/cis*-Isomerisierung von Azobenzol-funktionalisierten *selbstorganisierten Monolagen* (SAMs) auf Gold zu untersuchen. Die Verankerung wurde durch ein Tripod-Linker-System realisiert, resultierend in einer schwachen Molekül/Molekül und Molekül/Metall-Wechselwirkung. Dadurch ist das Photoisomerisierungsverhalten analog zu dem der freien Moleküle in Lösung. Daher schlagen wir eine direkte, intramolekulare Anregung als verantwortlichen Mechanismus vor. Zusätzlich untersuchten wir kohlenstoff-basierte Nanodrähte, die durch ihre Breite und Chiralität ausgezeichnet sind. Elektronische HREELS Messungen erwiesen sich als leistungsfähiges Werkzeug, das die Messung der Bandlücke der Nanodrähte auf Au(111) ermöglicht.

Der Schaltvorgang ist abhängig von der Stärke der Molekül/Substrat- und der Molekül/Molekül-Wechselwirkungen. Diese Wechselwirkungen sind verantwortlich für die Adsorptionsgeometrie und elektronische Struktur der auf der Oberfläche gebundenen Schalter sowie für sterische Effekte und die Stärke der intermolekularen elektronischen Kopplung. Wir schlußfolgern, dass die gewünschte Funktionalität drastisch durch die elektronische Wechselwirkung mit dem Substrat beeinflusst wird, so dass rein strukturelle Argumente für die Vorhersage der Funktionalität der adsorbierten Moleküle hinterfragt werden müssen. Es zeigt sich, dass sowohl die geometrische als auch die elektronische Struktur des gesamten Molekül-Substrat-Komplexes für eine erfolgreiche reversible Photoisomerisierung zu berücksichtigen ist.

Contents

List of Figures

List of Tables

1 Introduction

Molecular switching is a basic concept found in nature, where a certain functionality is achieved by a reversible change of state. This is often accomplished *via* conformational changes induced by external stimuli. In particular photoabsorption processes are often found responsible for a molecular change of state with a high conversion quantum efficiency. As an example, in the human vision process the signal processing is activated by the reversible *cis*⇄*trans*-isomerization of the retinal molecule. The retinal molecule is a photochromic molecule located in a protein called rhodopsin. Twisted chains of amino acids (opsins) are enclosing the chromophore. When a visible photon enters the receptor cell it is adsorbed by this small, chain-like molecule leading to a *cis*→*trans*-isomerization of the molecule connected to a change of its geometry, from an overall bent structure to one that is nearly linear. The change in shape of the retinal is affecting the opsin proteins leading to signal transduction. Interactions of the chromophore with a cluster of key residues determines the wavelength of the maximum absorption. Changes in these interactions among rhodopsins facilitate color discrimination [Pal00]. This example shows that the functionality of the switch, *i.e.* color discrimination and signal processing, is determined by the interplay with its surrounding.

Anchoring of molecular switches on solid state surfaces opens up new perspectives for the control of the switching ability and their integration in larger ensembles. The reversible switching of surface properties, *e.g.* wetting and non-linear optical properties, could deliver important concepts for applications. The basic understanding of the elementary processes governing the interaction between adsorbate and substrate is significant and essential to tailor well-defined architectures. The use of organic molecules as building blocks opens up a multitude of variations regarding the control of molecule/substrate- and molecule/molecule-interactions by the right choice of substituents and substrates. Adsorption of molecules can lead to changes in the energetic positions of electronic states and the potential energy landscape of the molecule. In addition steric interactions and energy dissipation govern the switching ability of the functionalized surface. Understanding these interactions, capable of altering, facilitating and even quenching the switching process, is a necessity to achieve selective, reversible changes of the physical properties at the nanoscale.

Contact to a (metal) surface is as well a basic requirement for electric transport through a molecular switch in metal/molecule/metal junctions opening up the field of molecular electronic. The vision of the usage of single molecules as building blocks for signal processing is rather old and was already addressed by R. Feynman in 1959 [Fey60]. This idea is attracting attention again since the 30-year-long trend in microelectronics to increase both speed and density by device scaling has come to an end for structures smaller than the ”22-nm technology node” [Zhi03]. In this region of miniaturization quantum-mechanical limitations on the device performance become apparent.

The goal of this work is to optimize the efficiency of photoinduced switching processes *via* controlled variations of the adsorption and electronic properties of the molecular

switches. We investigated the influence of external stimuli, *i.e.* photons and thermal activation, on surface bound molecular switches undergoing *trans/cis*-isomerizations and ring-opening/closing-reactions. Vibrational and electronic *high resolution electron energy loss spectroscopy* (HREELS) and *sum-frequency generation* (SFG) spectroscopy have been used as the main tools to investigate the adsorption behavior and the molecular switching properties. Both techniques are highly surface sensitive and are excellent tools to investigate the orientation of the molecules on the surface. For the here studied molecular switches the switching is accompanied by conformational changes detectable by our spectroscopy tools. Both techniques are averaging over larger sample areas and thus probing ensembles of molecules. In this work two basic concepts of the coupling of the molecular switch to the surface have been investigated: (i) physisorbed or weakly chemisorbed systems deposited on noble metal surfaces under UHV conditions and (ii) molecular switches coupled covalently *via* anchor groups on gold, resulting in upright geometries. We performed coverage dependent measurements investigate lateral molecule/molecule-interactions. Whereas the results of this thesis are closely related to elementary processes in surface bound molecular switches they could be of fundamental interest for future applications, since the functionality achieved at the atomic scale is an enormous progress in miniaturization.

Presented in chapter 4, we investigated the class of molecular switches undergoing *trans/cis*-isomerizations. The molecules are deposited on (111) coinage metal surfaces under UHV conditions and analyzed with HREELS. We studied the prototypical azobenzene and the structural similar and isoelectronic imine and stilbene specifically tailored for the adsorption on surfaces via the substitution with bulky *tert*-butyl-groups. These groups are supposed to act as *molecular spacers* in order to decouple the switch from the surface. Differences for the three investigated systems are found in their optically active groups, *i.e.* –N=N–, –HC=N–, and –HC=CH–, respectively, which result in a comparable switching behavior for the free molecules (in solution) with differences found in their geometry and energetics of the isomerization processes. The systematic variation of the studied molecules results in strong differences found for the respective thermal and photoinduced isomerization behavior when they are in direct contact with the metal surface.

Second, a discussion of a HREELS study on a second class of molecular switches is given for the system spiropyran on Au(111) in chapter 5. In solution spiropyran is capable of undergoing a light induced and thermally activated ring-opening/closing reaction. In this chemical reaction, involving the cleavage of the C-O bond in spiropyran (SP), the isomeric merocyanine (MC) can be formed. We have been able to observe a thermally induced ring-opening reaction on Au(111) from the SP to the MC form but the reversibility of the reaction and photoexcitation channel driving the reaction in solution is quenched by the presence of the substrate. We demonstrate that adsorption on the inert gold surface is capable of inverting the thermal stability.

The approach of covalent anchored molecular switches has been followed in chapter 6. Here the results are presented for SFG spectroscopy investigations of self-assembled

monolayers (SAMs) consisting of azobenzene functionalized molecules formed under wet-chemical conditions on thin gold films. A covalent bond between photoswitchable molecules and substrate is hereby established via an anchoring group (head group) by sulphur-gold bonds. A linker connects the head group with the terminal group, i.e. the azobenzene. Via modification of the anchor group (and the linker) the strength of the electronic coupling between the molecular switch and the metal surface can be adjusted. The self assembly leads to molecular structures with defined geometry and orientation We followed two different approaches: (i) Utilizing a three dimensional tripodal linker should provide the molecule with sufficient free space to exclude steric hindrance and (ii) using one-dimensional biphenyl linkers is supposed to result in tightly packed SAMs where the molecule/molecule interaction is intentionally increased based on an expected π-stacking of neighboring molecules resulting in supramolecular structures.

Our results show that photoinduced switching is suppressed for most investigated system on metal substrates, which is believed to be caused mainly from the strong electronic interaction able to quench the isomerization channels present for the systems in solution. We observed an "inverted" thermal isomerization behavior for ground state potential energy surfaces and the energetic barriers determining the followed reactional pathways are strongly altered by the presence of the metal. The results clarify the delicate balance of the adsorbate/substrate interaction which is needed to establish functionalization for adsorbed molecular switches.

Additionally to the already presented systems we studied graphene nanoribbons (GNRs), which are thin flakes of graphene, characterized by their width and edge-structure. For this strictly two dimensional sp^2 carbon based material a width dependent band gap is predicted making it a promising material which could serve a wide range of applications from molecular wires to transistors. The fabrication follows a surface-based chemical method where the GNR is formed by an on-surface-polymerization on Au(111) by a thermally activated dehalogenation followed by a thermal dehydrogenation step of a 10,10'-dibromo-9,9'-bianthryl precursor. The successful fabrication of resulting subnanometer wide GNRs could be proven by vibrational HREELS. Employing electronic HREELS the first measurement of the band gap of a ≤ 1 nm wide, atomically precise GNR is presented. The measured band gap could be of use as a benchmark for theoretical calculations. Our results emphasize the strength of the bottom-up (on-surface synthesis) fabrication leading to chemically well-defined structures with a high output.

2 Studied Systems

In this chapter the basic properties of the investigated organic molecules, *i.e.* molecular switches and graphene nanoribbons, as well as the important features of the used coinage metal substrates are discussed.

At first the choice of the noble metal substrates and their basic structural and electronic properties are illustrated. As a member group of the Sonderforschungsbereich (SFB) 658 *Elementarprozesse in molekularen Schaltern an Oberflächen/Elementary Processes in Molecular Switches at Surfaces* our motivation is to study different types of molecular photo-switches which may undergo conformational changes on metal surfaces and gain a deeper insight into the underlying elementary processes governing the switching reaction in surface bound functional molecules. If the functionality of the free molecules is conserved on the surface is primarily determined by the role of the molecule-substrate interaction.

Secondly the characteristics of the photochromic molecules are discussed. We studied two classes of molecules which undergo photoexcited conformational changes *via*: (i) a ring-opening/closure reaction or (ii) a *trans/cis*-isomerization. The possible interactions resulting from the deposition of the molecules onto the metal surface are discussed in chapter 2.3.

Finally the basic properties of graphene nanoribbons are presented, this work is motivated by their outstanding variable electronic and transport properties, which makes it an extremely interesting material for a new generations of nano-devices.

2.1 Metal Substrates

Investigation of different functional molecules on the (111)-surface for two different noble metal substrates have been carried out in this thesis. In this chapter the fundamental aspects regarding the important features of these surfaces are given. Noble metals are chosen as the underlying substrates because they are thoroughly investigated, easy to prepare and are expected to show a rather weak interaction with the adsorbing molecules due to their inertness.

2.1.1 Au(111) and Cu(111)

Both metals belong to the first subgroup of the periodic table and have therefore many properties in common. Gold and copper crystalize in the face centered cubic (fcc) crystalline structure, so that cutting the bulk crystal in the respective plane exposes a trigonal surface symmetry in the (111) direction (see figure 2.1). The resulting surface exhibits tightest packing with six bonds per atom, with the Au(111) surface showing the characteristic herringbone reconstruction due to an lattice mismatch resulting in $(22\times\sqrt{3})$ unit cells. This leads to stripes with alternating domains exhibiting fcc and hexagonally closed packed (hcp) properties forming the famous zigzag pattern where the angle at the elbows between the stripes is 120° [Bar90]. At the crossing of the unit-cell domains with the domain walls separating the fcc and hcp domains, the so-called elbows, a pair of atoms is found exhibiting 5 and 7 bonds, respectively. This can create an energetically favorable situation for adsorption.

The electronic configuration for the metals is $[Xe]$ $5d^{10}6s^1$ and $[Ar]$ $3d^{10}4s^1$ for gold and copper, respectively, resulting in a comparable band-structure as can be seen in figure 2.2. Cu(111) and Au(111) in general exhibit a low reactivity attributed to their filled d-shells [Ham95]. The reactivity of the substrates for chemisorption differs, Au is the most inert metal, whereas Cu is generally more reactive. In the theoretical work of Hammer and Nørskov [Ham95] the nobleness of a material is given by two factors: (i) the degree of filling of the antibonding states on adsorption and (ii) the degree of orbital overlap with the adsorbate. These two factors, which determine the strength of the adsorbate-metal interaction and energy barrier for dissociation, operate together to the maximal detriment of adsorbate binding and subsequent reactivity of gold. Note that, almost all successful switching experiments investigating surface-bound molecular

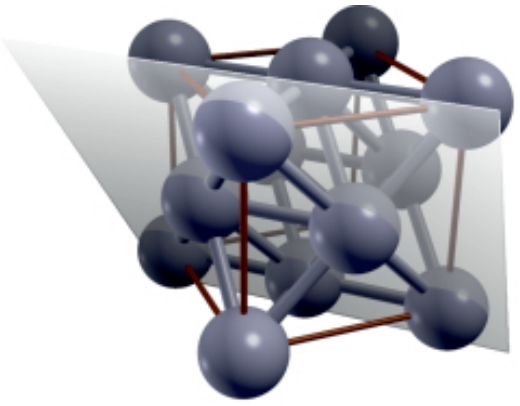

Figure 2.1: Face centered cubic (fcc) crystalline structure and the respective (111) plane [Kok06].

switches have been performed on Au(111) as the supporting substrate. As a further step in the detailed understanding of molecular switching processes on surfaces, it is important to study the influence of the molecule-substrate interaction on the switching process. Therefore the change of the substrate from Au(111) to Cu(111) offers the opportunity to tune the chemical reactivity and the surface corrugation while the electronic structure, that is for instance believed to be of fundamental importance in the successful photo-induced switching of TBA/Au(111) [Hag08a, Ley10], is comparable. Comparing the band structures of both surfaces along the Γ-L (G-L) points shows that the filled d-band edge is located ≈ 2 eV below the Fermi level for both metals. Furthermore the energetic position and dispersion of the conduction band consisting of the respective s- and p-bands shows a high agreement. The filled d-band has a high density of states (see exemplary the calculated density of states for Cu in figure 2.2 (b)) for both coinage metals.

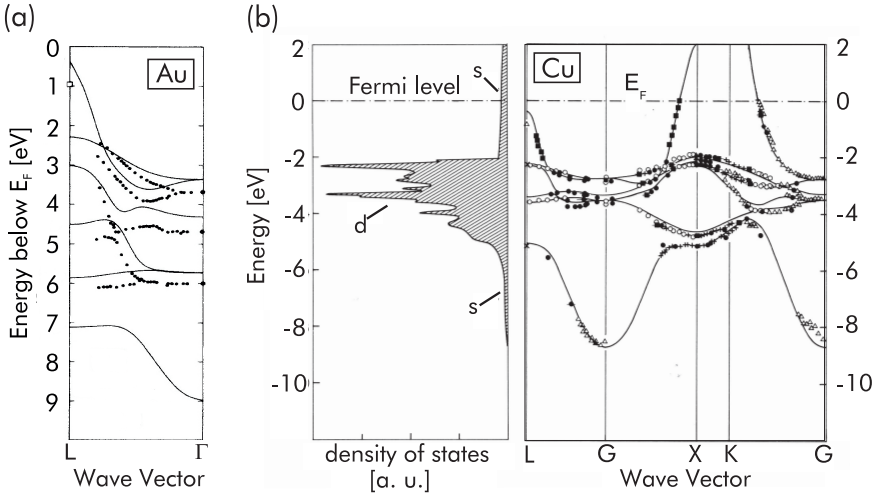

Figure 2.2: (a) Bulk band structure of Au below the Fermi-energy. Solid lines represent calculated bands adopted from [Eck84], points represent experimental data adopted from [Cou86]. (b) Bulk band structure along high symmetry points in the Brioullin zone derived from theoretical and experimental investigations and calculated density of states of Cu [Eck84]. Adopted from [Iba90].

2.1.2 Substrate preparation

For both surfaces, *i.e.* Au(111) and Cu(111), the preparation has been performed in the UHV preparation chamber which is separated from the UHV spectrometer chamber *via* a gate valve. Therefore the complete measurement cycle, starting from the surface preparation to the deposition of the molecules and the final transfer to the spectrometer chamber were performed under UHV conditions.

The aim of the preparation is to produce well defined surfaces for adsorption studies which are clean and offer large defect-free terraces of the respective type. The single crystal samples have been prepared using the standard sputter and anneal approach.

During the sputter process Ar^+-ions are accelerated with a ion gun with 0.9 - 1 keV towards the sample under an incident angle of 45°. The Argon gas is inserted *via* a leak valve to the nozzle of the ion gun and an overall pressure of 2×10^{-6} mbar is established during the sputter process. The ion current between sample and ground is in the order of 2 μA and is used as a probe during sputtering the sample for 10 min. The ion bombardment is intended to remove the topmost atomic layers. Afterwards the now roughened surface is annealed for 20 min at sample temperatures of:

$$\mathrm{T}_{Au(111)} = 800 \text{ K, and } \mathrm{T}_{Cu(111)} = 700 \text{ K.}$$

This procedure has been established as a standard for the preparation of many metal surfaces and an overview is given in reference [Mus82]. For the first preparation of a newly installed sample the above listed steps have been performed with longer times and have been repeated 20 to 30 times. At least one full preparation cycle has been performed prior to each experiment to remove residual gas contaminations.

2.2 Molecular Switches

Molecular switches permit the control of molecular structure and resulting functional properties (*e.g.* electronic and geometric structure, color, dipole-moment, conductance) by the use of external stimuli [Fer01]. Thereby the molecules are interconverted reversibly between at least two (meta)- stable states. In nature molecular switching is a frequently found concept to induce a certain functionality which is often realized by light driven processes. The *cis/trans*-isomerization of the retinal molecule in rhodopsin acting as the photoreceptor in the vision process in the human eye is a prominent example [Wil93]. In this work we performed investigations on two different classes of molecular switches, which address completely different switching mechanisms:

(i) *trans/cis*-isomerization, and (ii) ring opening/closure-reactions.

Unifying for the two classes is that the respective reaction can be caused *via* excitation with light at appropriate wavelengths for the free molecules in solution. This behavior is referred to as photochromism which is defined as the reversible transformation of a chemical species between two forms by the absorption of electromagnetic radiation resulting in two distinct species of the molecule exhibiting different absorption spectra [Iri00, Dür03]. Photochromism can therefore be described as a reversible change of color upon exposure to light with different wavelength. Most photochromic systems, including the investigated ones, undergo a photochromic reaction in a single photon induced process. Usually all photochromic systems react back after optical excitation to their meta-stable to the stable ground state with a temperature dependent rate.

Among the most representative photochromes, azobenzene, imine, and stilbene and their derivatives undergo a reversible photoinduced *trans* $\rightleftarrows$ *cis* isomerization (see figures 2.3, 2.6, 2.8) between a planar (imine is an exception), thermodynamically more stable *trans*-isomer and the three dimensional *cis*-form. Note that for stilbene the thermal barrier is too high excluding thermally induced isomerization. Optical excitation followed by a rotation around the N=N (C=N, C=C) double bond in azobenzene (imine, stilbene) or N inversion in azobenzenes and imine drives the photoisomerization.

The ring-opening/closing reaction between spiropyran and its meta-stable merocyanine form is a prototypical thermally and optically induced reversible reaction. Illumination with UV light leads to the fission of a bond in the three dimensional, colorless spiropyran followed by a ring opening towards the conjugated, planar merocyanine which adsorbs light in the visible regime.

2.2.1 Azobenzene

Molecular switches like azobenzene represent promising systems for applications, *e.g.* molecular electronic devices and sensor applications, due to their ability to undergo a reversible, photoinduced conformational change between two stereoisomers, the *trans*- and the *cis*-isomer [Tam00, Rau03a, Fan90]. Stereoisomers are molecules that have the same molecular formula and sequence of bonded atoms, differing only in the three-dimensional orientations of their atoms in space.

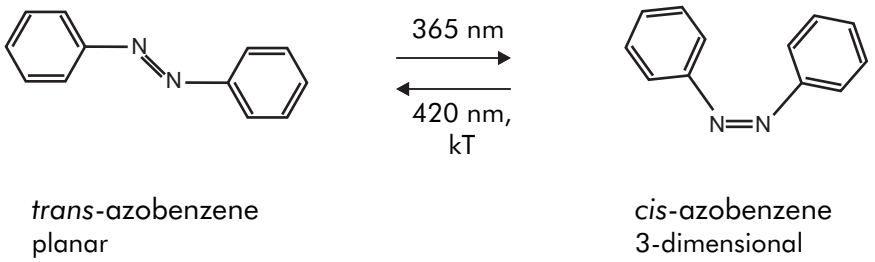

Figure 2.3: Structure of azobenzene in its planar *trans*-state (left) and after the optically induced ($\lambda = 365$ nm) isomerization resulting in the three-dimensional *cis*-conformation (right). In the *trans*-isomer the double bond of the diazo group is 120° aligned to the single bonds between the nitrogen atoms to the phenyl rings as a consequence of the sp^2-hybridized orbitals of the nitrogen. The back reaction can be induced by light ($\lambda = 420$ nm) or by thermal activation.

In solution the photoinduced switching process is a well-studied phenomena. When not stated elsewise the following considerations are in relation of the properties of the molecules in solution. Azobenzene consists of the namesake diazo-group (–N=N–). Figure 2.3 shows the two isomers of azobenzene. The origin of the functionality of this molecule, *i.e.* possessing two geometrically different isomers upon illumination with appropriate wavelength, is given by the electronic structure of the diazo group. The two nitrogen atoms are sp^2-hybridized and bonded by a σ- and a π-bond. Additionally the lone pair electrons of the nitrogen features an antibonding orbital n. The conformational change can be induced by either exciting an electron from the S_0 ground state to the first excited state S_1 or by excitation from the ground state to the second excited state S_2.

For the *trans*-isomer the $S_0 \rightarrow S_1$ excitation is dominated by the transition from the highest occupied molecular orbital (HOMO) in the lowest unoccupied molecular orbital (LUMO). The HOMO is composed of the non-bonding orbital n of the lone pair electrons, whereas the composition of the LUMO is for the most part deduced from the antibonding π^*-orbital. The $S_0 \rightarrow S_2$ excitation is essentially given by the HOMO-1$\rightarrow$LUMO transition. The HOMO-1 is dominated by the π-orbital of the diazo unit. In summary the photoexcited electronic transitions are the n$\rightarrow\pi^*$ excitation ($S_0 \rightarrow S_1$) and the $\pi\rightarrow\pi^*$ excitation ($S_0 \rightarrow S_2$) [Füc06].

The *trans*$\rightarrow$*cis*-isomerization can occur involving two different reaction pathways: inversion and rotation. The first step for both pathways is the excitation from the ground state (n and π, respectively) to the excited state π^* by photons of appropriate

energy.
This weakens the stiff N=N double bond and a rotation of the phenyl ring around the diazo group is feasible. Note that this rotation is occurring out of the molecular plane. In the inversion pathway one phenylring moves in the molecular plane by an angle of 120° around an axis perpendicular to the N=N double bond.

The orientation of the two phenylrings at the same side of the molecule leads to steric repulsion between the moieties. Regarding the resulting *cis*-isomer the steric reorientation causes a rotational angle of about 60° regarding the planes of the phenylrings leading to its three dimensionality. Whereas the trans-isomer does not possess a dipole moment, the cis-isomer exhibits a dipole moment of ≈ 3 Debye [Ber36, Füc06]. In the case of azobenzene and its derivatives also a thermally activated *cis* → *trans* reaction is possible which involves a thermal barrier of around 1 eV. The isomerization processes and the underlying excitations are schematically drawn in figure 2.4, as well as the activation energy for the thermal back reaction and the energy difference between the stable *trans*- and the meta-stable *cis*-isomer [Rau03b, Füc06].

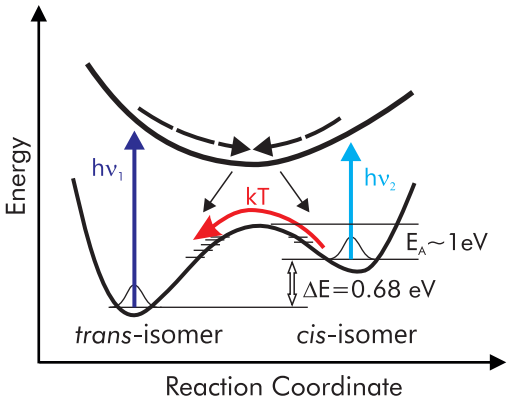

Figure 2.4: Schematic drawing of the potential energy diagram of azobenzene in solution. The ground state potential energy surface exhibiting the characteristic double well, representing the two isomers.

In this work we studied the the switching ability of the azobenzene derivative 3, 3‘, 5, 5‘-tetra-*tert*-butyl-azobenzene (TBA) upon adsorption on noble metal surfaces (see figure 2.5 for the corresponding UV/Vis-absorption spectra and the structural model). The TBA has been synthesized in the group of St. Hecht (HU Berlin, Institut für organische Chemie). TBA is equipped with four bulky *tert*-butyl-groups[1] which are expected to act as a *molecular spacer*[2]. This concept has been already introduced and discussed in literature and it has been shown for lander molecules that the *molecular spacers* can lead to a decoupling of the active part of the molecule, *i.e.* the π-system, from the surface [Mor04, Jun97].

Figure 2.5 shows the UV/Vis absorption spectrum of TBA solved in cyclohexane in the photostationary state before (dotted red line) and after (solid red line) illumination with light at an energy of hν = 3.96 eV (λ = 313 nm). The absorption spectrum of the *trans*-isomer is dominated by a strong absorption band with its maximum at 3.81 eV ($h\nu$ = 325 nm) which is attributed to optical excitation of the $\pi \rightarrow \pi^*$ transition. A second, weaker absorption band with is visible at lower photon energies with its maximum located at 2.82 eV ($h\nu$ = 440 nm) is associated to the symmetry forbidden

[1] *tert*-butyl-groups: $(CH_3)_3C$–

[2] The TBA has been synthesized by St. Hecht *et al.* [Pet08], Chemistry Department, HU Berlin; member of the SFB 658.

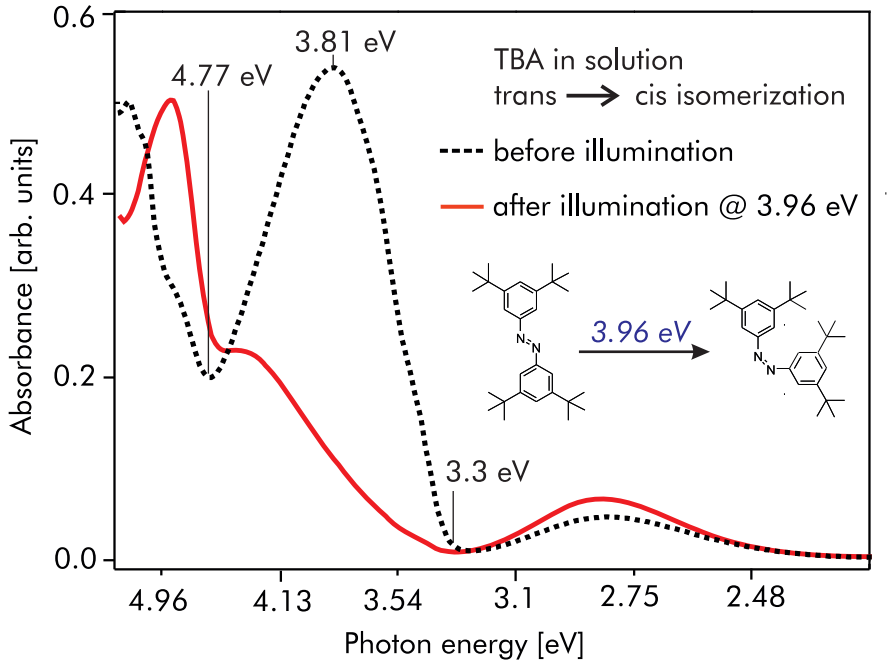

Figure 2.5: UV/Vis-spectrum of TBA in solution before and after illumination at a photon energy of 3.96 eV. Adopted from ref. [Hag08b].

$n \rightarrow \pi^*$ transition. When the photostationary state is established a strong decrease in the absorbance of the $\pi \rightarrow \pi^*$ transition at 3.81 eV ($h\nu$ = 325 nm) and an increase of the absorbance of the $n \rightarrow \pi^*$ transition is observed at 2.82 eV ($h\nu$ = 440 nm). This behavior is the fingerprint for the occurrence of the *cis*-isomer. The different adsorption cross-sections of the two isomers are of fundamental importance for the optical excited switching process, in particular for the addressability of the wanted conformation.

For excitation with wavelength around 320 nm the absorbance of the *trans*-isomer is much more pronounced, whereas the cis-isomer shows a higher cross-section for excitation with light in the visible regime ($h\nu \approx$ 440 nm). This enhances the probability to selectively excite one conformational state until the switching process in the respective direction (UV-light ($h\nu \approx$ 325 nm):*trans*→*cis*; blue-light ($h\nu \approx$ 440 nm): *cis*→*trans*) is carried out. The measured absorption spectra express the fact that the switching process is feasible for the molecule with substituted *tert*-butyl-groups[3] [Hec06].

Density functional theory (DFT) calculations show for azobenzene and its derivative TBA comparable values for the dipole moment $\mid \vec{\mu} \mid$ and the energetic difference between the *trans*- and the *cis*-state $\triangle E$ [Füc06]. The values are combined in table 2.1. The expected advantages of the substituted azobenzene derivative (TBA) for our surface supported investigations are:

(i) Responsible for the switching process, the electronic structure of the diazo group is substantially unchanged upon substitution with *tert*-butyl-groups in comparison

[3]The absorption spectra of the un-substituted azobenzene is almost identical [Näg97].

to the bare, unsubstituted azobenzene.

(ii) The *tert*-butyl-groups do not lead to steric hindrance during the isomerization process.

(iii) The idea behind the bulky *tert*-butyl groups is to reduce the electronic coupling between substrate and adsorbate.

isomer	$\mid \vec{\mu} \mid$ [D]	$\triangle E$ [eV]
cis-TBA	3,600	
trans-TBA	0,001	0,65
cis-azobenzene	3,211	
trans-azobenzene	0	0,68

Table 2.1: Fundamental properties of azobenzene and tetra-*tert*-butyl-azobenzene: dipole moment $\mid \vec{\mu} \mid$ and energy difference between the *cis*- and the *trans*-isomer $\triangle E$ in the respective groundstate according to ref. [Füc06].

2.2.2 Imine

Another class of molecular switches investigated in this thesis, closely related to azobenzene, are N-benzylideneaniline molecules. Such compounds, containing a carbon-nitrogen (–N=CH–) double bond, show as well the characteristic reversible photo-induced *trans/cis*-isomerization in solution, resulting in an alteration of the molecular geometrical conformation comparable to the *trans/cis*-isomerization of azobenzene described in the previous chapter 2.2.1.

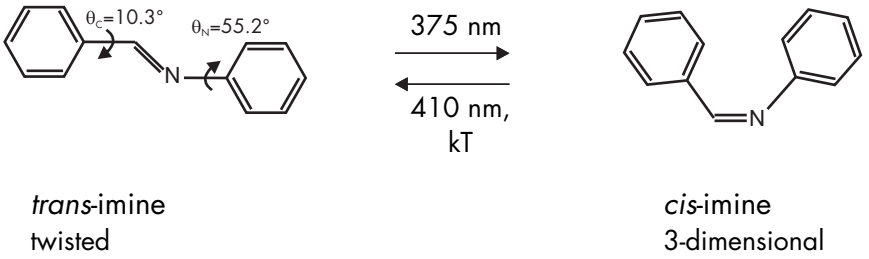

Figure 2.6: Structure of imine in its *trans*-state (left) and after the optically induced (λ = 375 nm) isomerization resulting in the three-dimensional *cis*-conformation (right). The *trans*-isomer shows as well twisted geometry, induced by the electron lone pair of the nitrogen atom. The rotational angles are $\Theta_C = 10.3°$ for the aniline-ring and $\Theta_N = 55.2°$ for the benzylidene-ring around the double bond of the imine group as shown in the figure. The back reaction can be induced by light (λ = 410 nm) or by thermal activation.

Despite the fact that the N-benzylideneaniline, also called imine, is isoelectronic to the already discussed azobenzene it exhibits several variations regarding its geometry and physical properties. In imines the lone pair of the nitrogen forms a conjugated system with the adjacent phenyl ring. This leads to an non-planar, twisted geometry of the *trans*-isomer [Gae07].

The first spectroscopic observation of the *trans/cis*-photoisomerization of imines was reported by Fischer and Frei in 1957 [Fis57]. Figure 2.6 shows the structural model of imine with the known excitation wavelengths for the photoisomerization, i.e. *trans* $\rightarrow$ *cis*: 375 nm and *cis* $\rightarrow$ *trans*: 410 nm. The values of the rotational angles, $\Theta_C = 10.3°$ for the aniline-ring and $\Theta_N = 55.2°$ for the benzylidene-ring with respect to the double bond of the imine group as shown in figure 2.6, are derived from X-ray experiments of the molecule in the condensed phase [Bür70]. A theoretical study resulted in values of $\Theta_C = 4.8°$ and $\Theta_N = 36.6°$ confirming the assignment [Mei93]. The asymmetry of both isomers leads to almost equal dipole moments of 1.8 Debye for the *trans*- and 2.1 Debye for the *cis*-isomer [Wei71].

Substituent and solvent effects for the *trans/cis*-isomerization of imine compounds were also studied experimentally and by theoretical calculations [Ber76, Asa93, Kin97]. Optical excitation in the UV regime is followed by either –HC=N– bond rotation or N inversion leading to the *cis*-isomer. It was demonstrated that in most cases the photochemical *trans* to *cis* isomerization was achieved by out-of-plane rotation around the C=N double bond, while the thermal back relaxation underwent in-plane nitrogen inversion through a "linear" transition state. Differently to azobenzene the inversion

pathway is blocked for the phenyl ring located at the carbon atom due to the sp^4 hybridized nature of this atom. The activation barrier separating the *trans* from the *cis* state[4] is rather low with $E_A \approx 0.69$ eV, whereas it is $E_A \approx 1$ eV for azobenzenes [Wet65]. This leads to a much faster $cis \rightarrow trans$ thermal relaxation in comparison to azobenzene molecules. The half-life time of the cis-isomer is only about one second at 25°C [Wet65]. Accordingly, the cis-isomer can only be found for temperatures below 173 K (IR-spectroscopy found in reference [Lew82]) and was first observed in a cooled solution at 130 K where the speed of the thermal back reaction is lowered [Fis57]. Our motivation to study this class of photoswitchable molecules is in view of their isomerization behavior adsorbed on metal-surfaces and in comparison to the studies of adsorbed azobenzene and its derivatives. Figure 2.7 shows the ball-and-stick model of 3,3',5,5'-tetra-tert-butyl-imine (TBI) used in this work for the studies on Au(111). The imine has been equipped as well with for bulky *tert*-butyl-groups due to our successful previous investigations of TBA on Au(111) (compare with chapter 2.2.1) with the intention to analyze the adsorption and in particular switching ability of the adsorbed molecules when changing the functional unit from the diazo (–N=N–) to the imine group[5].

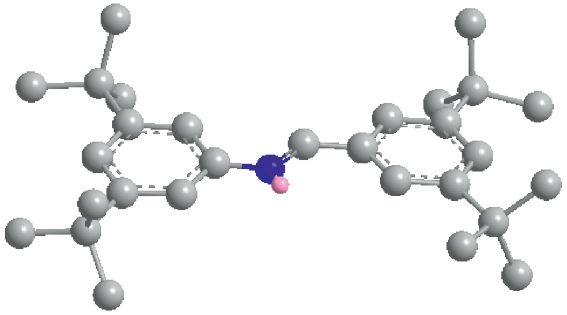

Figure 2.7: Ball-and-stick model of 3,3',5,5'-tetra-tert-butyl-imine (TBI) investigated in this work.

[4]Similar to the potential energy diagram of azobenzene in figure 2.4

[5]The TBI has been synthesized by R. Haag *et al.*, Chemistry Department, FU Berlin; member of the SFB 658.

2.2.3 Stilbene

A third molecular switch, *i.e.* stilbene, completes the group of investigated molecular switches undergoing a photoinduced *trans/cis*-isomerization. Stilbene, isoelectronic to azobenzene and imine, possesses a –HC=CH– double bond as the functional unit between the phenyl rings.

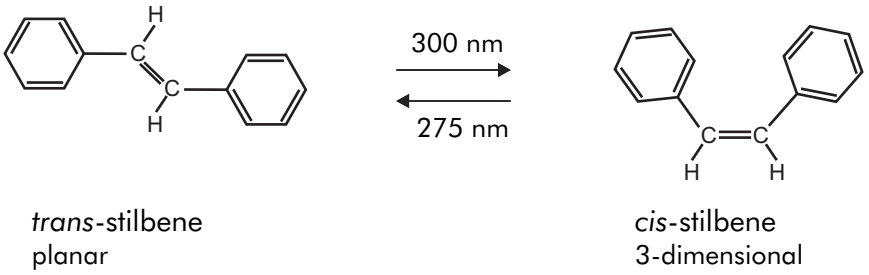

Figure 2.8: Structure of stilbene in its planar *trans*-state (left) and after the optically induced ($\lambda = 300$ nm) isomerization resulting in the three-dimensional *cis*-conformation (right). Optical excitation leads to a rotation around the C=C bond. The back reaction can be induced by light at $\lambda = 275$ nm. Note that for stilbene the thermally activated back reaction is unlikely, due to a high barrier.

Figure 2.6 shows the structural model of stilbene with the known excitation wavelengths for the photoisomerization, i.e. *trans*→*cis*: 300 nm and *cis*→*trans*: 275 nm. Comparable to azobenzene in solution stilbene isomerizes under illumination with UV-light from a planar *trans*- to a three dimensional *cis*-isomer [Han02]. The planar *trans*-stilbene has a vanishing dipole moment and is thermodynamically more stable in analogy to azobenzene. The hydrogen atoms bound to the carbons at the photochemically active group influence the electronic structure and the behavior of the double bond at the isomerization. The underlying electronic excitation, *i.e.* the excitation of an electron from the HOMO to the LUMO level of the molecule, is found at fundamentally lower wavelength. The larger HOMO-LUMO gap leads to a blueshift of ≈ 70 nm compared to azobenzene and imine. Isomerization is only possible for the rotational pathway involving a preceding breaking of the double bond.

In the case of azobenzene and its derivatives also a thermally activated *cis* → *trans* reaction is possible. In contrast, for stilbenoid compounds the thermal back reaction is unlikely since the activation barrier (E_A) is on the order of 1.9 eV [Wal91, Fer01] and thus much higher compared to azobenzenes and imines (see table 2.2).

All the given distinctions to azobenzene make stilbene an interesting molecule for investigations on the switching ability according to adsorption on metal surfaces. 3,3',5,5'-tetra-tert-butyl-stilbine (TBS) has been used in this work for the investigation on Au(111). Again, the stilbene has been equipped with for bulky *tert*-butyl-groups due to our successful previous investigations of TBA on Au(111) (compare with chapter 2.2.1). The intention is to systematically vary the functional unit and to investigate the

effect on adsorption and in particular switching behavior of the adsorbed molecules[6].

2.2.4 Summary

In table 2.2 the activation barrier E_A, the energetic stabilization ΔE, and the respective photon energies for the underlying excitations of the *trans*→*cis* and the *cis*→*trans* photoisomerization of the three introduced photochromes, *i.e.* azobenzene, imine, stilbene (, and their derivatives), are summarized.

	azobenzene	imine	stilbene
E_A [eV]	≈ 1	0.69	1.9
Δ E [eV]	0.68	≈ 0.3	–
$h\nu_{trans\rightarrow cis}$ [$h\nu$]	365	375	300
$h\nu_{cis\rightarrow trans}$ [$h\nu$]	420	410	275

Table 2.2: Fundamental properties of the investigated molecules which can undergo *trans/cis*-isomerizations. The activation barrier E_A, the energetic stabilization ΔE, and the respective photon energies for the underlying excitations of the *trans*→*cis* and the *cis*→*trans* photoisomerization are summarized for the three introduced photochromes, *i.e.* azobenzene, imine, stilbene, and their derivatives.

[6]The TBS has been synthesized by St. Hecht *et al.* [Pet08], Chemistry Department, HU Berlin; member of the SFB 658.

2.2.5 The Ring-Opening/Closing Reaction of Spiropyran

We investigated the molecule 1,3,3-trimethylindolino-6-nitrobenzopyrylospiran (spiropyran, SP) which can undergo a thermally and optically induced reversible configurational change from the three dimensional SP into the planar merocyanine (MC) isomer. The structure of the molecule in its open and closed form is given in figure 2.9.

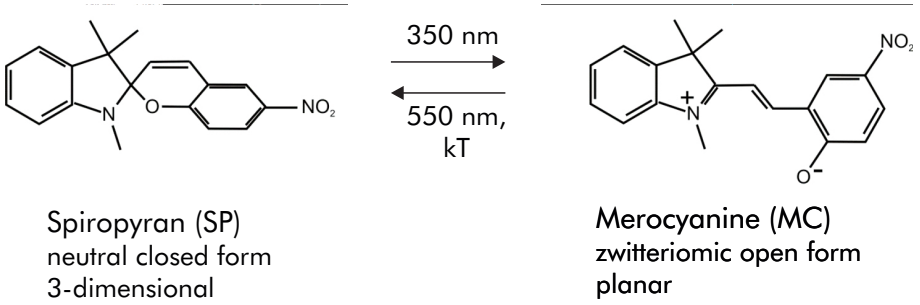

Figure 2.9: Structure of trimethyl-6-nitro-spiropyran in its closed, three-dimensional form (left) and after the ring-opening reaction resulting in the open merocyanine conformation (right). The closed spiropyran isomer possesses two halves with orthogonal planes The merocyanine can be found in a zwitterionic state, the locations of the charges are indicated by + and -, respectively.

Excitation with wavelength around 350 nm (dependent on the solvent) converts the closed, colorless form to an open colored form which was first reported by E. Fischer *et al.* [Fis52, Ber71]. Whereas spiropyran is inert the merocyanine is chemically highly reactive and is a resonance hybrid between a neutral form and a zwitterionic one, possessing a large dipole moment [Gar00]. The dipole moment changes from $\mid \vec{\mu} \mid = 5.4$ Debye for the closed Sp form to $\mid \vec{\mu} \mid = 11.3$ Debye in the open MC form [Cot00]. Merocyanine can be closed in the presence of visible light and by thermal activation.

Due to its large change of the molecular properties the use of these molecules to form part of sensors and detectors [Byr06], perform logic operations in molecule-based devices [Par89, Ber00, Ray02], and to induce reversible changes of chemical or optical properties of organic-inorganic interfaces [Rad07] is discussed in the literature.

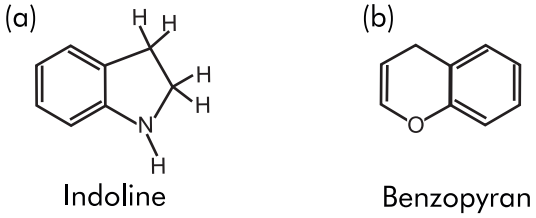

Figure 2.10: Structural formula of (a) indoline and (b) benzopyran.

Spiropyran consists basically of two moieties that are build up from the indoline and benzopyran molecules. The structural formula of the respective molecules is displayed

in figure 2.10. The benzopyran moiety is equipped with an additional NO_2 group. In the open merocyanine configuration the C–O bond of the benzopyran is broken, which is as well the first step in the ring-opening reaction followed by unfolding steps involving rotation around the C=C bond [Cot04]. The fission of the C-O bond is especially of importance for our investigations utilizing vibrational spectroscopy. The bond fission is the rate determining step with solvent dependent activation energies of 0.9 to 1.2 eV [Gor01, Fla68]. For non polar solvents the lowest activation energies are reported, therefore the activation barrier of the free molecule can be expected to be close to these values. For the closed form the geometry is determined by the sp^3 hybridized carbon atom connecting the two major groups indoline and benzopyran resulting in a twisted orientation with a perpendicular alignment between the indoline and the benzopyran group.

Due to the resulting planar configuration after the ring-opening the π-orbitals overlap resulting in an extended conjugated system. Therefore the absorption peak for the merocyanine is found to be considerably red-shifted at 560 to 600 nm [Chi97]

Additionally the molecular interconversion can be activated by thermal activation (E_A = 0.77 - 0.98 eV) with an SP to MC ratio increasing with the polarity of the solvent at room temperature [Gor01].

2.3 Molecular Switches on Metal Substrates

Recently, increasing interest has been directed toward research on molecular switches at surfaces due to their potential use in nanotechnology ranging from information storage and processing to adaptive surfaces [Fer01, Bal03, Bro06, Bal08]. A major goal, relevant to the development of future applications, is to understand and control structural changes of molecular switches on solid substrate surfaces. For this purpose, it is crucial to gain a detailed knowledge about the adsorption geometry (molecular orientation) and in particular the switching properties of the molecules in contact with (metal) substrates [Ley10].

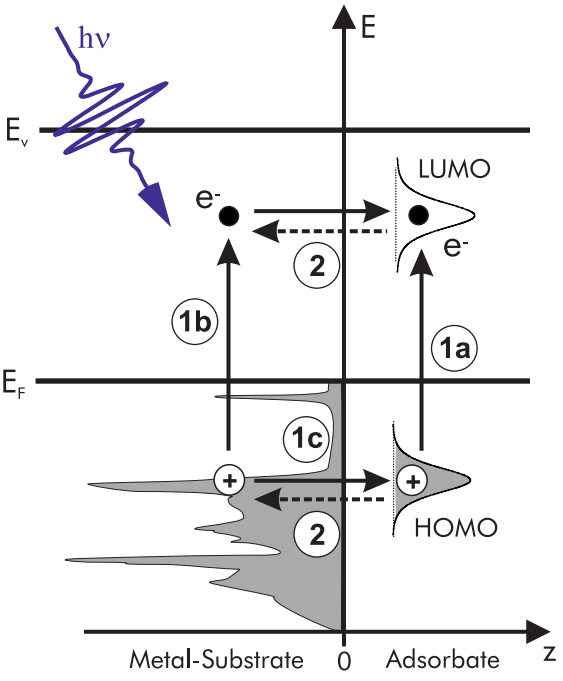

Figure 2.11: Possible excitation/decay channels for molecular switches adsorbed on metal-surfaces after optical excitation. (1a) Intramolecular direct excitation (similar to the known excitation mechanism of photochromic molecules in solution); (1b) Substrate mediated electron transfer resulting in a negative ion resonance; (1c) Substrate mediated hole transfer resulting in a positive ion resonance; (2) Back transfer from the electron (hole) to the substrate as possible de-excitations of the molecule in its excited neutral or ionic state.

In comparison to photo-isomerization processes of molecules in the liquid phase, which are well understood for many systems, the presence of a (metallic) substrate might cause significant modifications of the switching properties as discussed in reference [Óvá10]: (i) Steric hindrance might play a role, since the molecules lose the freedom to freely change their conformation if the atomic motion is constrained by the surface and/or neighboring molecules. (ii) At metal substrates effective quenching processes of electronic excitations occur, leading to short lifetimes (typically in the order of $\approx$ 100 fs) of excited states. (iii) New substrate-mediated excitation mechanisms in the photoisomerization could be accessible instead of the well-known intramolecular electronic excitation, i.e. due to a HOMO-LUMO transition, which is operative for free molecules in the solution.

The presence of the substrate can create possible additional excitation channels such as optically induced electron or hole transfer processes between the substrate and the molecular switch, leading to the creation of negative or positive ion resonances,

respectively.
Figure 2.11 shows possible excitation channels of molecules in contact with a metal substrate: (1a) Intramolecular direct excitation (similar to the known excitation mechanism of photochromic molecules in solution); (1b) Substrate-mediated electron transfer resulting in a negative ion resonance; (1c) Substrate-mediated hole transfer resulting in a positive ion resonance; (2) Back-transfer from the electron (hole) to the substrate as possible de-excitations of the molecule in its excited neutral or ionic state.

In the framework of this thesis two different concepts have been followed regarding the anchoring of the molecular switches on the metal substrate:

(i) Physisorbed or weakly chemisorbed systems, which were prepared by evaporating the molecules under UHV conditions on noble metal single crystals. Here we investigated equally substituted molecular switches undergoing *trans/cis*-isomerizations (TBA, TBI, and TBS see chapter 4) where the systematic variation of the photochemically active group provides a selective modification of the switching behavior. Furthermore we changed the substrate from Au(111) to Cu(111) for TBA to gain insight into the adsorbate/substrate interaction. Furthermore we performed coverage dependent measurements to study phenomena of lateral interaction. Our study of a prototypical ring-opening/closing reaction on Au(111) (see chapter 5) is in line.

(ii) Covalently bond switches, where the functional molecule, *i.e.* azobenzene, is covalently connected to the substrate via an anchoring group (and linker) (see chapter 6). The terminal functional group is separated from the anchoring group by a spacer unit (linker) and thereby determines the chemical and physical properties of the surface. The preparation is achieved under wet-chemical conditions. The goal is to establish well-ordered molecular ensembles with a preferential molecular orientation towards the surface. The choice of the linker enables one to specifically vary the strength of the electronic coupling between the functional molecule and the substrate as well as the adsorbate/adsorbate-interaction. The latter can determine the switching properties by steric hindrance/packing density and the electronic coupling between the adjacent molecules (*e.g.* by π-stacking of the functional units).

Recently, photo- and electron-induced isomerizations of several molecular switches have been investigated mostly on the chemically inert gold surface where the molecules have been physisorbed [Hen06, Ale06, Com07, Ova07, Hen07b, Gri08, Baz11, Mor11] or covalently attached via anchoring groups incorporated in a self-assembled monolayer [Pac07, Sch08, Elb08, Wag09, Cri11]. Most of the surface bound molecular switches studied are azobenzene derivatives, which are well-known photochromic systems in solution undergoing a photoinduced reversible trans/cis isomerization (for details see the chapter 2.2.1). Using scanning tunneling microscopy (STM) reversible conformational changes of various azobenzene derivatives on Au(111) have been achieved by inelastic [Hen06] and resonant tunneling [Cho06] and via the applied electric field [Ale06]. For the latter example the electric field of the tip is believed to deform the potential energy landscape along the isomerization pathway [Gri08]. Photoinduced trans/cis isomerization of physisorbed molecules at metal surfaces has so far been demonstrated only for a specifically designed azobenzene derivative, namely, tetra-*tert*-butyl-azobenzene

adsorbed on Au(111) [Ale06, Hag07, Wol09].

HREELS [Ova07] and 2PPE [Hag07] measurements show a reversible isomerization for TBA/Au(111) induced by light and thermal activation. Light with energies $h\nu \geq 2$ eV induces the *trans*→*cis*, whereas the back reaction is driven by thermal activation.

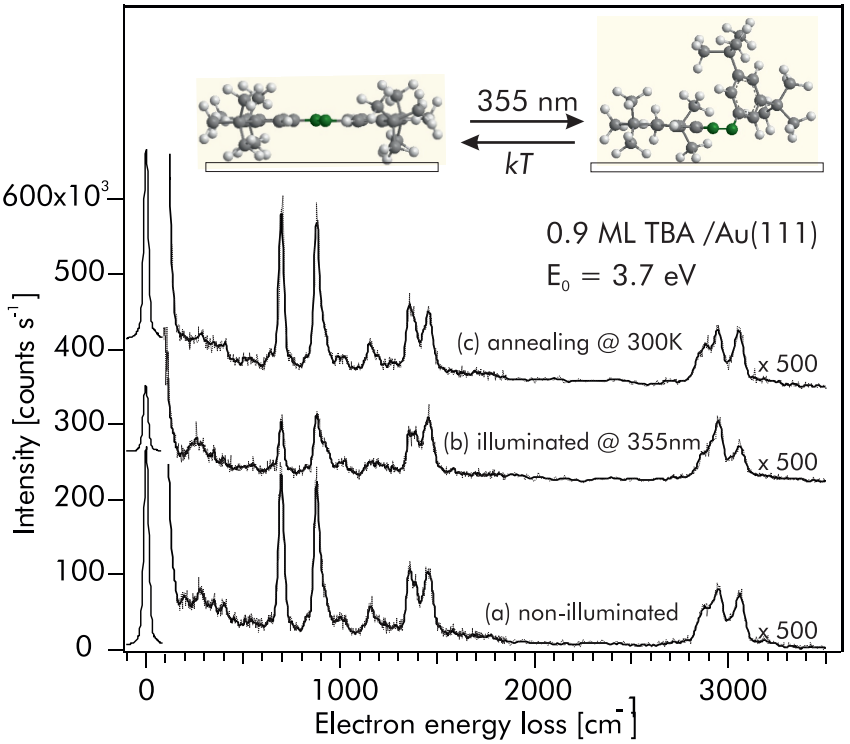

Figure 2.12: Reversible switching of 0.9 ML TBA molecules adsorbed on Au(111) induced by light and thermal activation. HREEL spectra recorded at a primary energy of 3.7 eV (a) before illumination (b) after illumination with UV-light at $h\nu = 355$ nm as well as (c) after annealing the illuminated sample to 300 K. Adopted from reference [Ova07].

Figure 2.12 shows the HREELS spectra of 0.9 ML TBA/Au(111) (a) before and (b) after illumination with UV-light at $h\nu = 355$ nm as well as (c) after annealing the illuminated sample to 300 K [Ova07]. Dominant in the spectra are the modes at around 700 and 880 cm^{-1} assigned to torsion modes of the phenyl rings. The high intensity indicates that the phenyl rings are orientated parallel to the surface (see chapter 4). Therefore the measured intensity decrease due to illumination is associated with a tilting of the phenyl rings out of their previous plane, which is assigned to the *cis*-isomer. Annealing leads to a full recovery of the modes equivalent to a planar *trans*-geometry. In analogy to the molecule in solution the *trans*-state is thermally stable.

Differences are found for the photoinduced isomerization behavior. While in the free molecule the direct (intramolecular) optical electronic excitation provokes the confor-

mational change, the switching properties of the surface-bound species are strongly modified by the interaction with the metal surface. The photoisomerization of the adsorbed TBA is driven by an indirect substrate-mediated charge transfer process.

In the 2PPE study by S. Hagen *et al.* [Hag08a] the cross section of the photoexcitation has been measured as a function of photon energy. Here the change in the electronic structure, *i.e.* the change in the workfunction, due to the *trans*→*cis* isomerization is used as a measure for the isomerization. Figure 2.13 shows the cross section of the isomerization as a function of excitation wavelength. The effective cross section for the light-induced isomerization as a function of photon energy possesses a remarkable shape. It exhibits a threshold-like decrease below 2.2 eV and increase above 4.4 eV as can be seen in figure 2.13. This behavior correlates with the energy of the d-band edge (≈ 2eV below the Fermi level) and the photon energy dependent hole formation process in the Au d-band [Hag08a]. The second increase for photon energies above 4.4 eV, which is twice the energy of the d-band edge, the population of holes is believed to be enhanced by an Auger-like decay mechanism. It is obvious that no resonant behavior is found (as can be seen figure 2.13) excluding an intramolecular mechanism, comparable to the known direct intramolecular excitation of the molecule in solution.

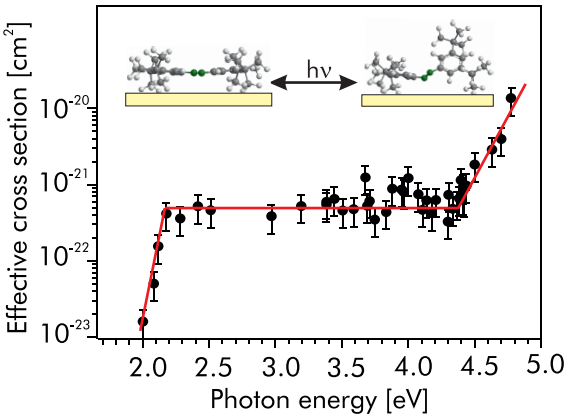

Figure 2.13: Effective cross section for the photoinduced *trans/cis*-isomerization of TBA adsorbed on Au(111) as a function of photon energy. Adopted from reference [Hag08a].

Figure 2.14 summarizes the proposed underlying mechanism. For photon energies above 2.1 eV excitation of electrons from the gold d-bands, leading to a hole creation in the Au d-band (step 1). The holes rapidly relax to the top of the d-band (step 2) followed by a subsequent transfer to the HOMO level of the TBA (step 3). The transient formation of a cationic species is resulting in the isomerization.

Therefore it is a key goal to determine the switching properties of different surface-bound molecular switches to gain insight into the underlying elementary processes. With future applications in molecule-based devices in mind, a detailed knowledge of the adsorption geometry, i.e. the molecular orientation, is essential.

Note, that the photoinduced isomerization of bare azobenzene on Au(111), i.e. the molecule bound to Au(111) without *tert*-butyl spacers, is suppressed presumably because of the stronger interaction with the metal substrate and corresponding differences in the electronic and geometric structures [Com07]. This considerations concerning the influence of the electronic structure on the switching ability are disproved by 2PPE measurements on the electronic structure of azobenzene on Au(111) [Sch11]. It has been determined that the electronic structure underlying the indirect photoisomeriza-

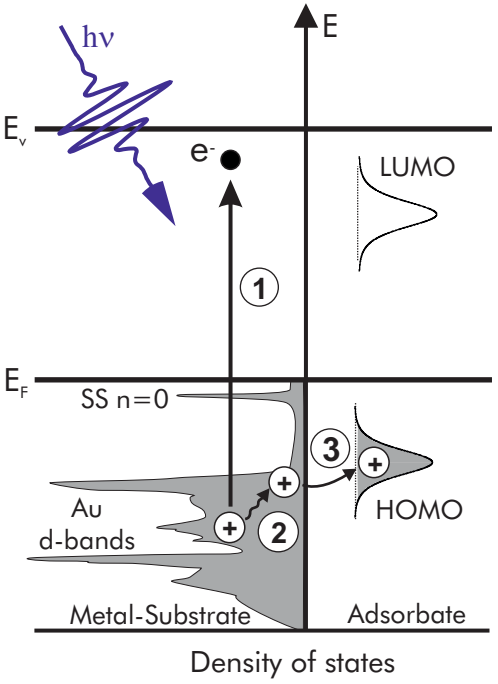

Figure 2.14: Proposed excitation mechanism for the photoinduced trans/cis isomerization of TBA adsorbed on Au(111) via the creation of a positive ion resonance. Thereby photoexcitation at photon energies above $\approx$ 2.1 eV leads in the first step to electron-hole pair formation. The holes in the Au d-band relax to the top of the d-band (step 2) followed by a hole transfer to the HOMO of TBA (step 3). Adopted from reference [Hag08a].

tion mechanism, i.e. the energetic positions of the HOMO and the d-bands, respectively, exhibit similar energies for azobenzene and TBA on Au(111). The idea behind the usage of the *tert*-butyl-groups has been given by structural argument: The bulky spacer legs should lift the photochemical diazo-group above the surface resulting in a weakened electronic interaction with the substrate. However, recent normal incidence X-ray standing wave experiments and DFT calculations indicate a similar distance of the photochemically active diazo bridge to the noble metal (Ag, Au) substrate for both the bare and the *tert*-butyl functionalized azobenzene [McN10b, McN10a, Mer10]. This expresses the delicate balance between the switching ability and the strength of the coupling to the surface in combination with the electronic structure of the molecule/metal-system governing the optically induced isomerization process.

2.4 Graphene Nanoribbons

A more detailed introduction with respect to the properties of graphene nanoribbons (GNRs) is given in the respective chapter of our investigations on GNRs formed on Au(111) following a bottom-up approach (see chapter 7). A central question in the field of graphene-related research is how graphene behaves when it is patterned at the nanometer scale with different edge geometries. So called graphene nanoribbons are a narrow stripe of graphene, that can exhibit different chiralities depending on the angle at which the graphene layer is cut. Figure 2.15 shows the possible types of GNRs: Zigzag and armchair type. The corresponding chiral vector angle is $\Theta = 0°$ for the zigzag type and $\Theta = 30°$ for the armchair type. The angles are in reference to one of the basis vectors of graphene.

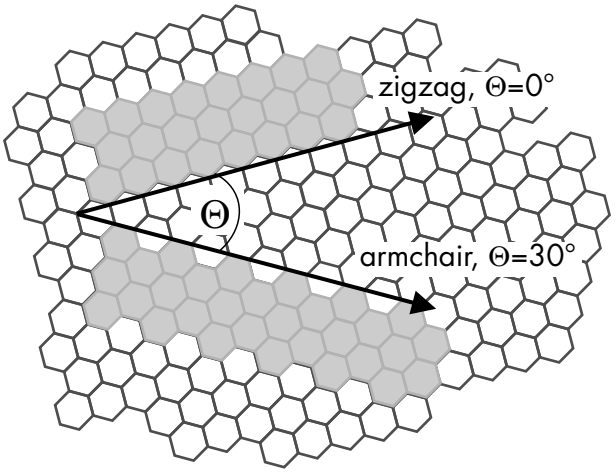

Figure 2.15: Schematic drawing of the possible types of GNRs, *i.e.* zigzag or armchair GNR, depending on the corresponding chiral angles of $\Theta = 0°$ and $\Theta = =30°$ with respect to the basis vector of the graphene lattice.

Studies on graphene nanoribbons are hindered by their limited availability. Although there have been numerous publications, the reliable production of GNRs smaller than 10 nm width with a clean edge structure remains an experimental challenge [Eza06, Son06a, Son06b, Han07, Gil10, Ren10, Tao11]. In our study we follow the bottom-up approach, which is an on-surface synthesis resulting in structures with atomic precision, utilizing a 10,10'-dibromo-9,9'-bianthryl monomer as the precursor molecule as reported in reference [Cai10].

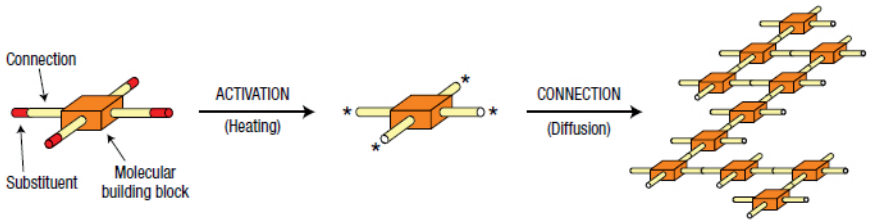

Figure 2.16: Concept of the on surface-synthesis by connecting activated molecular building blocks to covalently bond networks [Gri07].

L. Grill (FHI Berlin) and St. Hecht (HU Berlin) introduced the concept of the on-surface synthesis. In a publication from 2007 they showed that such covalently bound molecular nanostructures can be formed on a gold surface upon thermal activation of molecular building blocks and their subsequent chemical reaction at predefined connec-

tion points [Gri07]. The concept is schematically shown in figure 2.16. At each leg of the used building block (porphyrin) bromine was used as a labile substituent atom, which is supposed to be dissociated in a controlled manner by surface heating. Afterwards the activated precursor molecule is able to connect to the other precursor molecules due to thermal diffusion. The connection is due to a covalent bond formation happening at the activated connections. The results clearly show that a network with high precision and high purity can be formed on the surface. This represent a versatile route for bottom-up construction of various surface bound structures based on individual functionalized molecules. The same concept has been utilized for the fabrication of GNRs [Cai10] where surface adsorption and heating of the 10,10'-dibromo-9,9'-bianthryl precursor molecule on Au(111) leads to the removal of the bromine atoms and to C-C coupling. After a second heating step the graphene nanoribbons are established by cyclodehydrogenation and are investigated in this thesis by vibrational and electronic HREELS in chapter 7.

2.5 Sample Preparation

The sample preparation of the studied adsorbate/substrate systems is generally given in detail at the beginning of the respective chapter. Here a summary of the used evaporation T_D and sample temperatures T_S for the molecules investigated on coinage metal single crystal surfaces under UHV conditions is given in table 2.3. The experimental parameters differ for each of the molecules and the desired coverage is established *via* the appropriate dosing time or by thermal desorption when annealing the sample until the wanted quantity is found on the surface.

molecule	T_{doser}	T_{sample}
TBA	380 K	$T_{Au} = 250$ K $T_{Cu} \approx 100$ K
TBI	370 K	$T_{Au} < 120$ K
TBS	380 K	$T_{Au} = 260$ K
Spiropyran	380 K	$T_{Au} < 150$ K
dibromo–bianthryl	356 K	$T_{Au} < 150$ K

Table 2.3: Doser T_D and substrate T_S temperatures used for the deposition of the individual molecules and the corresponding substrate.

3 Experimental Methods

In this chapter the basic principles of the in this thesis used experimental techniques are given. It is started with a brief description of the experimental setup used for the majority of the presented results, *i.e.* molecules which are deposited on single crystals under ultra-high vacuum (UHV) conditions and analyzed with HREELS. The setup consists of a UHV chamber, separated in a preparation and spectrometer chamber. Afterwards the for our research fundamental details of the used spectroscopies are given in a nutshell since the used techniques are well established surface science methods.

3.1 Ultra High Vacuum System

Basic research on molecular switches upon their properties (adsorption geometry and switching ability) after adsorption on noble metal single crystals requires a contamination free environment and well-defined surfaces. A common approach is the conduction of experiments under ultra high vacuum conditions. In the following an introduction to the system used in this work will be given. For achieving ultra high vacuum (UHV)

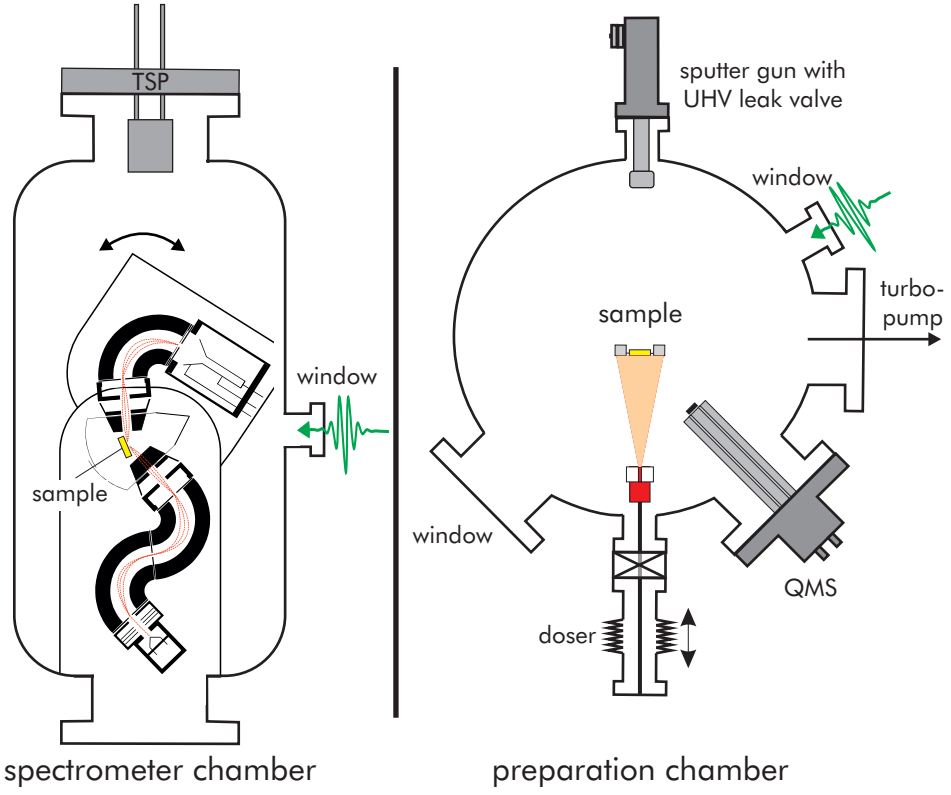

Figure 3.1: Sketch of the preparation and spectrometer level of the UHV chamber used for most of the research presented in this thesis. The upper (preparation) level is connected to a sample transfer system (not drawn) enabling an in situ exchange of the investigated substrates.

conditions a two level custom equipped stainless steel UHV chamber is pumped. A schematic depiction of the setup is given in figure 3.1. An UHV surrounding is required so that adsorption of residual gas particles onto the surface can be neglected for the duration of the experiment. The pressure achieved during the spectroscopic investigations is $\leq 1 * 10^{-10}$ mbar and the pressure in the preparation chamber is around 1 to $2 * 10^{-10}$ mbar. The chamber is separated by a gate valve: The upper half accommodates the equipment for the sample preparation and is equipped with a transfer system to exchange the used crystals without breaking the vacuum, the lower half consists of the HREELS spectrometer for the analysis. A XYZ manipulator allows the movement in all directions in space. The manipulator is equipped with a differentially pumped 360° rotational stage allowing to position the sample in the required direction. To establish vacuum a three unit pumping stage, including two turbo molecular pumps, has been used. The first one with a pumping speed of 210L/s (*Balzers* TMU 261 P), is located at the preparation chamber. It is backed up by a *Pfeiffer* TMU 071P (60 l/s) which is also used to differentially pump the rotational stage of the manipulator. Pre-vacuum conditions are generated by a *Pfeiffer* MD4 membrane pump (3.3 m^3/h). Additional pumping at the spectrometer level is established by an ion getter pump (*Varian* StarCell). To determine the pressure of the UHV, the preparation and the spectrometer chamber are equipped with *Varian* ion gauges. The composition of the residual gas can be monitored with a *Spectra* Satellite LM61 (100 amu) quadrupole mass spectrometer (QMS) which is as well used for the temperature programmed desorption (TPD) spectroscopy. Windows in both levels of the chamber allow illumination experiments in the preparation chamber and in spectrometer chamber. Illumination in the spectrometer chamber can be realized with the sample in measuring orientation.

Sample Holder

In this work a Au(111) and a Cu(111) single crystals (*MaTecK* GmbH) have been used ($\varnothing_{crystal}$ = 10 mm). Both were mounted using a pair of $\varnothing$ = 0.3 mm Ta-wires. The wires are guided through slits on the crystal edges and fixed to the legs of the exchangeable sample "boat" (see figure 3.2). The Ta-wires were also used for resistive heating of the sample. The upper Cu parts of the sample holder connect the liquid nitrogen cooled cryostat and the exchangeable lower part ("boat"). Cu is chosen because of its inertness and the high thermal and electric conductance. The boat can be used for all kinds of solid samples which can be be exchanged depending on the experimental requirements. The sample holder and "boat" are divided in a left and a right part, each contacted to an electrical feedthrough. Isolation with sufficient thermal coupling is realized by the usage of 0.5 mm thick sapphire plates. The whole setup is also isolated from the ground enabling the appliance of an additional sample potential with respect to the ground. To connect the "boat" with the sample holder the "boat" can be slipped into the sample holder as depicted in figure 3.2. The sample temperature can be measured using a type K thermocouple which is inserted into a small hole at the edge of the crystals. The thermocouple is read-out with a *Lakeshore* 340 digital PID temperature controller. Cooling is realized by a liquid nitrogen bath cryostat. It

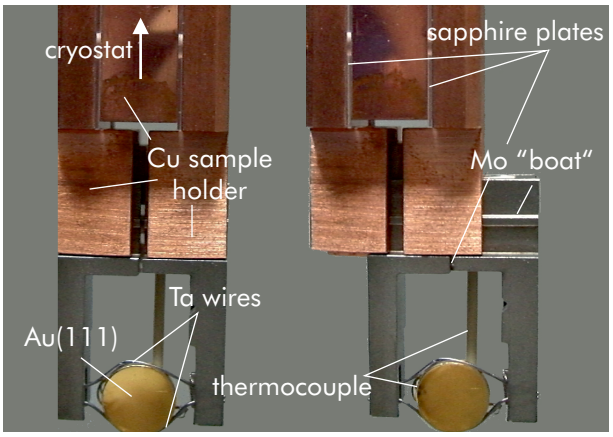

Figure 3.2: Photographs of the Cu sample holder consisting of a grounded central part connected to the liquid nitrogen cryostat and two outer parts electrically isolated by sapphire plates between the copper blocks. To demonstrate the mechanism of the exchange of the sample "boat" two photos are shown with the sample "boat" halfway and fully inserted in the Cu sample holder.

allows for minimum temperatures of $\leq$ 100 K. The crystal can be heated via resistive heating of the Ta wires holding the sample. The sample holder design is self-made and optimized for the usage with low energy electron spectroscopy methods. The front-side is flat to avoid inhomogeneous electric fields in the vicinity of the sample. To enable angle resolved measurements the rotational axis coincides with the center axis of the sample surface.

Doser

The molecules used in this thesis are kept in a separate self-made dosing unit connected to the UHV preparation chamber by a gate valve and pumped directly by an own turbo molecular pump (*Pfeiffer* TMU 071P). This enables the exchange of the molecules without breaking the preparation chamber vacuum. To adsorb the molecules onto the surface the chemical vapor deposition method is employed which requires the heating of the molecules. The doser consists of a small Ta crucible which is wrapped with a heating wire. It can be heated up to 400 K which is monitored by a type K thermocouple. Heating will increase the pressure inside the container by evaporating and accelerating the molecules. A 1 mm hole at the front side creates a conical molecular beam which can be blocked by a shutter operated by a rotational feedthrough. It blocks the direct exposition onto the sample, enhancing control over the exact dosing time and therefore the amount of the deposited material. After reaching the respective temperatures for the various investigated molecules the doser is inserted into the chamber. To control the amount of deposited molecules the deposition procedure is followed with the QMS at a representative mass of the molecule as can be seen exemplary for the dosing of TBA in figure 3.3.

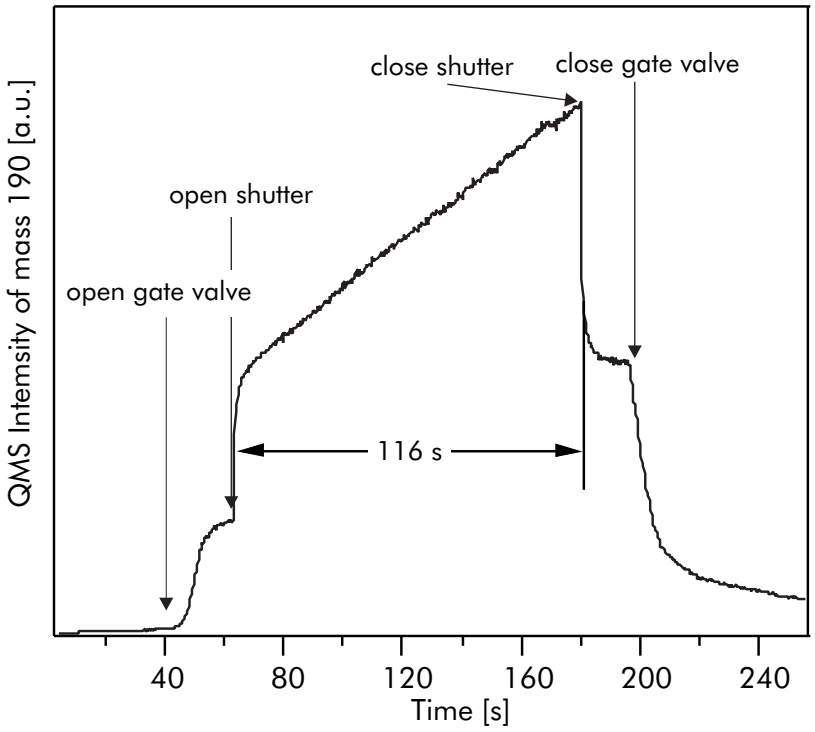

Figure 3.3: QMS signal of mass 190 detected during dosing of TBA.

Turning the shutter unblocks the path of the heated molecules onto the sample. It is closed again after the wanted dosing time has expired. Retracting the doser and shutting the gate valve allows to reach the initial base pressure within a few minutes. To reduce the sample-crucible distance (and the contamination) the dosing unit is mounted on a linear motion stage as is shown in figure 3.1.

3.2 High Resolution Electron Energy Loss Spectroscopy (HREELS)

High Resolution Electron Energy Loss Spectroscopy (HREELS) represents one of the most powerful tools to study absorption properties and geometries of adsorbates on surfaces via vibrational spectroscopy. The excitation of vibrational modes is achieved utilizing an highly monochromatic incident electron beam which is scattered at the surface and detected upon energy losses. This technique, capable of detecting adsorbate vibrations, plasmons, phonons, and electronic transitions, has been first been reported by Probst and Piper in 1967 [Pro67]. It has played (and still does) a crucial role in surface chemistry with its most important application: vibrational spectroscopy to study adsorption processes and binding properties [Iba82]. By comparison of vibrations in the gas or condensed phase with the spectra obtained from adsorbed molecules, information on the type and strength of the interactions with the surface and the effects exerted by the surface onto the molecule can be deduced. Generally vibrations can be excited by photons (infrared reflection absorption spectroscopy, IRAS), electrons (HREELS) or atoms (helium atom scattering, HAS). The advantages of using electrons for the excitation is their high sensitivity and the accessibility of the low frequency vibrations. With HREELS it is possible to detect coverages as low as 1/100 of a monolayer of CO on Pt(111) [Iba82]. Furthermore, *via* different excitation mechanisms described in the following sections, also dipole-inactive vibrations can be excited. But HREELS displays disadvantages when it comes to the resolution. HREELS typically shows resolutions above 16 cm^{-1} ($\approx$ 2 meV) for adsorbate covered surfaces whereas IRAS and atom scattering can reach resolutions below 0.8 cm^{-1} ($\approx$ 0.1 meV) [Hen94]. HREELS can be used for studies exceeding vibrational analysis. It is a versatile tool for the investigation of electronic transitions which is of use in chapter 7, where electronic HREELS enables us to measure band gaps in graphene nanoribbons on Au(111).

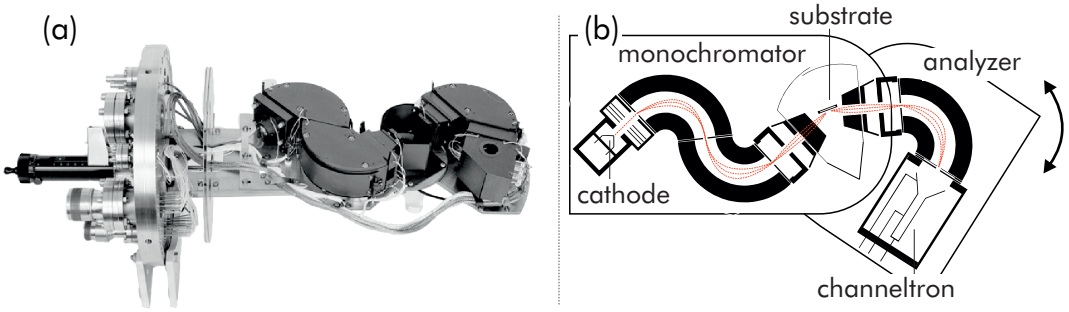

Figure 3.4: HREELS spectrometer: (a) shows the used "Delta 0.5" instrument (picture by *SPECS* GmbH) and (b) a schematic drawing of the spectrometer.

The following work has been accomplished using two different HREELS spectrometer. The work was started with an Ibach-type spectrometer using a double monochromator and a double analyzer. During the research it has been possible to purchase a more modern spectrometer (*SPECS* GmbH, "DELTA 0.5" HREELS Spectrometer)

which has been installed by the author. Figure (a) shows the used "Delta 0.5" instrument and (b) a schematic drawing of the spectrometer. The basic design of both instruments is alike, besides the exception of the usage of two 127° cylindrical sector analyzers in the Ibach-type and only one in the "DELTA 0.5" instrument. Therefore distinctions are not included in the following description. It can be divided in two sections (see figure 3.2): The first section consists of the fixed double stage monochromator, the second section of a rotatable single stage analyzer. Both sections are connected by the scattering chamber, where the sample is located during the measurements. The "DELTA 0.5" HREELS Spectrometer is able to perform measurements with high resolution ($\approx$ 2 meV/16cm^{-1}) up to loss energies of 1 eV, and in a coarse mode up to 50 eV using impact energies from 0 to 250 eV. The electron source is LaB_6 cathode from where the electrons are focussed with a lens-system into the monochromator consisting of two 127° cylindrical sector analyzers (premonochromator and monochromator). The monochromatic electron beam is then focussed by a set of electrostatic lenses on the sample within the central scattering chamber. The reflected electrons are focussed by a similar lens system on the entry slit of the analyzer, consisting as well of a 127° cylindrical sector analyzer. Finally the electrons are detected with a channeltron operated at 2.2 keV. The analyzer part is rotatable against the monochromator around the center of the scattering chamber allowing different experimental geometries (compare with chapter 3.2.1).

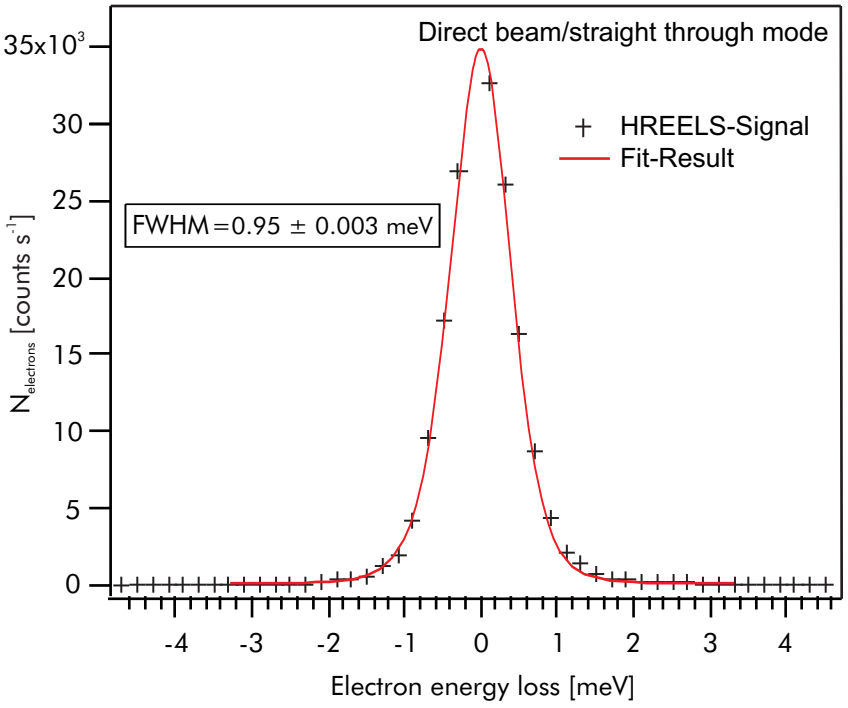

Figure 3.5: Electron energy resolution in the direct beam. The spectra is taken with a reasonable countrate, so that the corresponding spectrometer settings have been the starting point for the surface investigations.

For the investigations of adsorbate vibrations we choose primary electron energies of 3 to 4 eV and analyzing the losses in a regime up to 4000 cm^{-1}/0.5 eV. The instrument has an intrinsic resolution of about 1 meV (8 cm^{-1}) which is measured as the *full width half maximum* (FWHM) in the direct beam in the *straight through mode*. Figure 3.5 shows the corresponding spectrum. Note, that the spectrum is taken with a reasonable countrate so that the corresponding spectrometer settings have been used as a starting point for the parameters used for surface investigations.

A detailed introduction to this well established technique can be found in the review articles in references [Thi87, Roc95] and in the book by Ibach and Mils [Iba82], so that only the relevant aspects of the underlying mechanisms for this work are discussed in the following chapter.

3.2.1 Interaction Mechanisms in HREELS

For the incident, monochromatic electron beam three cases of inelastic interactions with the sample have to be considered [Iba82, Thi87]. The long range dipolar scattering concentrates the inelastic scattered electrons in a narrow lobe close to the specular reflection. HREEL spectra of adsorbates taken in the specular geometry obey IR metal surface selection rules. Short range impact scattering disperses the inelastically scattered electrons in a broad isotropic distribution. Impact scattering is not restricted to the surface selection rule. Resonance scattering (negative ion resonances) is a specific scattering mechanism dependent of the electron beam energy.

If an electron e_i^- with an initial energy of E_i interacts with an adsorbate covered surface (see figure 3.7) it can excite a vibrational quantum $\hbar\omega$ resulting in the energy of the inelastic scattered electron E_s figure

$$E_s = E_i - \hbar\omega. \tag{3.1}$$

Scanning the energy loss of the scattered electrons in the low energy direction results in HREELS spectra showing the discrete vibrational energies of the excited vibrational modes. The vibrational quantum of an single surface bound atom is given by the eigenfrequency of the harmonic oscillator $\omega = \sqrt{\frac{K}{m}}$ with K the force (spring) constant and m the oscillating mass. For vibrational modes including multiple atoms the reduced mass has to be used. Translational symmetry parallel to the surface[7] and momentum conservation lead to the following expression

$$\vec{k}_s^{\parallel} = \vec{k}_i^{\parallel} + \vec{Q} + n\vec{G}, \tag{3.2}$$

with $\vec{k}_s$ and $\vec{k}_i$ the momenta of the incoming and scattered electron, $\vec{Q}$ the momentum of the excited vibration and $\vec{G}$ a reciprocal lattice vector of the two dimensional Bravais-lattice with the integer n. In the following $n = 0$ is assumed, therefore the difference in parallel momentum of the electron before and after scattering corresponds

[7] Components of the impulse perpendicular to the surface are described as a momentum transfer to the whole crystal, so that the perpendicular component is a conserved quantity.

to the one of the excited vibrational mode.

The Dipolar Scattering Regime

Dipole scattering excites vibrational modes through the long range (≈ 100 Å) Coulomb interaction between the electron and the surface. Derived from its charge (and image charge) the incoming and scattered electron causes a time dependent long ranged electric field. This induces surface vibrations accompanied with oscillating charges thus generating an oscillating electric dipole field to be excited. For our research of organic molecules on coinage metal surfaces image charges need to be considered. For the electron in the far field vibrational modes orientated perpendicular to the surface get amplified by the image dipole, whereas parallel oscillating dipoles get extinguished. Figure 3.6 illustrates the two cases. The resulting net dipole moment is 2 μ' for perpendicular orientated dipoles μ', since the image and the real dipole are orientated alike. This leads to a surface selection rule similar to infrared spectroscopy on metals: Only vibrational modes with a component of the dipole moment orientated perpendicular to the surface can be excited. Since for metal surfaces the timescale of the motion of the valence electrons is much faster compared to the motion of the atomic nucleus this consideration is valid for static and dynamic dipole moments on metal surfaces.

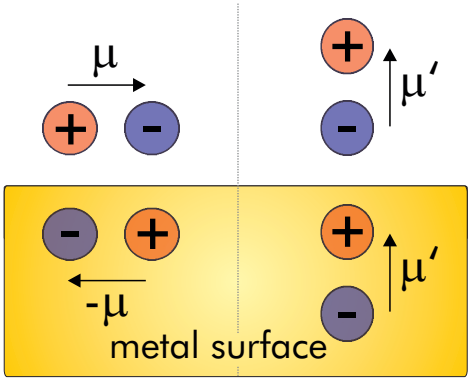

Figure 3.6: Schematic illustration of the orientation of dipoles and image dipoles on metal surfaces. On a metallic substrates perpendicular orientated dipoles get amplified to a net dipole moment of 2 μ in the far field due to the image charge in the underlying substrate. On the other hand dipole moments orientated parallel to surface get quenched for the same argumentation.

As already discussed in the general considerations in the previous chapter the perpendicular component is a conserved quantity, whereas the difference in parallel momentum of the electron before and after scattering corresponds to the one of the excited vibrational mode. The momentum loss is therefore small $\vec{k}_s^{\parallel} = \hbar\omega$. The intensity of the dipole scattered electrons exhibits a strong angular dependence. The normal measuring geometry in HREELS is the specular geometry shown in figure 3.7 with identical angles towards the surface normal of the incoming electrons and scattered electrons ($\Phi_i = \Phi_s$). In the experiment the monochromator and the analyzer are orientated $\Phi_i = \Phi_s = 60°$ towards the surface normal resulting in the highest signal intensity.

Following the quantum-mechanical theory of the inelastic scattering of slow electrons by molecules adsorbed on metal surfaces as presented in reference [Per77] we find

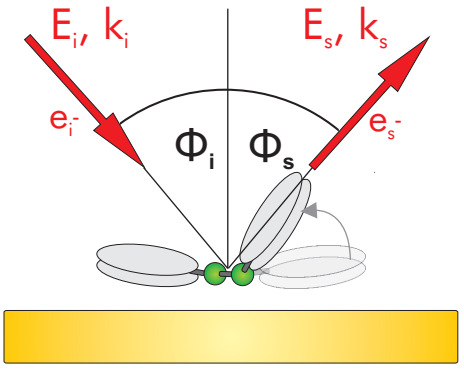

Figure 3.7: Schematic illustration of the HREELS scattering geometry for dipolar scattering. The incident electrons e_i^- possess energy E_i and impulse k_i. The angles Θ_i and Θ_s are the angles of the incident and scattered electrons with respect to the surface normal. The scattered electrons e_s^- possess energy E_s and impulse k_s. For the detection of dipolar scattered electrons the scattered electrons are detected in specular geometry: $\Phi_i = \Phi_s = 60°$.

for the cross section $\frac{d\sigma}{d\Omega}$ as a function of the scattering angle Θ_s

$$\frac{d\sigma}{d\Omega} = \left(\frac{m_e \mu e}{\pi \hbar^2}\right)^2 \frac{p_s}{p_i} \frac{1}{cos\Theta_s} \left(\frac{a_\parallel}{a^2}\right)^2, \tag{3.3}$$

with p_s and p_i the momenta of of the scattered and incident electron, $a_\parallel$ and a components of the momenta derived from transformation involving the components parallel and perpendicular of the momentum of of the scattered and incident electrons and a pre factor composed of μ, and the electron mass m_e.

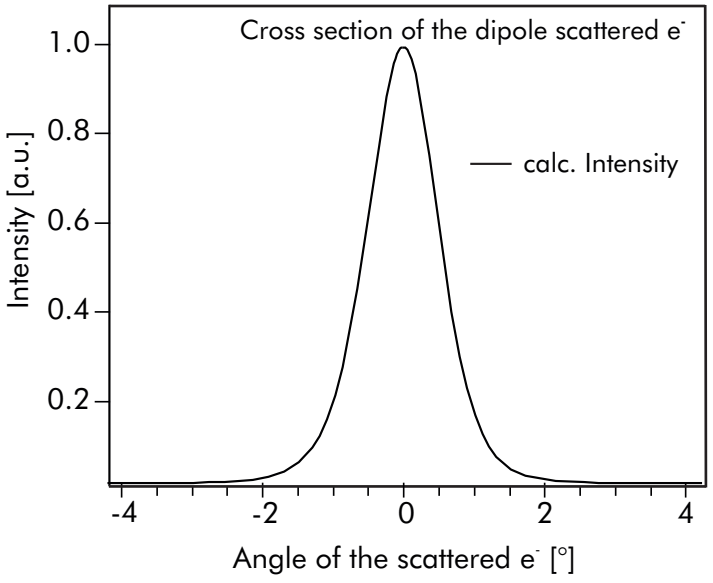

Figure 3.8: Calculated cross section of the dipole scattered electrons versus the scattering angle. The scattering angle of 0° corresponds to specular scattered electrons. In the calculation a primary electron energy of $E_0 = 3.0$ eV has been used.

Starting from *Fermis Golden Rule* the transition rate for the process in which the molecule is excited by the incoming electron from a ground state $|A>$ to the vibrational excited state $|B> \mu$ can be written as $< B|\mu_z|A >$ with μ_z the component of

the dipole moment operator of the molecule orientated perpendicular to the surface. In figure 3.8 the calculated cross section of the dipole scattered electrons is plotted versus the scattering angle. The calculation according to formula 3.3 have been carried out using an primary electron energy of $E_0 = 3.0$ eV, which is in the order of the experimentally used primary electron energies. The scattering angle is in reference to the specular angle which has been set to $\Phi_i = 60°$ in accordance to our experiments (In the figure 3.8 0° corresponds to specular geometry). In figure 3.8 the calculated cross section of the dipole scattered electrons is plotted versus the scattering angle. The calculation according to formula 3.3 have been carried out using an primary electron energy of $E_0 = 3.0$ eV, which is in the order of the experimentally used primary electron energies. The scattering angle is in reference to the specular angle (0° corresponds to specular geometry).

Our results show that for the dipolar scattered electrons the intensity is only found in a very small angular range (calculated to ± 2°) around the specular direction. This dipole lobe leads to the experimental distinguishability of the different scattering mechanisms simply by rotating the analyzer out of the specular geometry. For our experiments off-specular angles of ≥ 6° have been used.

The Impact Scattering Regime

The picture of the impact scattering mechanism is more complicated, since kinematical processes and multiple scattering events have to be included in the theoretical description [Iba82]. It requires detailed knowledge of electron/molecule scattering potential. Therefore only basic considerations are given in the following description. Opposing to the presented dipolar scattering this scattering process is short ranged (≈ 1 Å) and is considered as a direct impact of the incident electron with the atomic core potentials of the sample. Impact scattering leads to loss signals, which are detectable over a wide range out of the mirror geometry making the scattering mechanisms experimentally addressable by sufficient rotation of the analyzer out of the specular geometry (dipole lobe of dipolar scattered electrons). Opposing to dipolar scattering the detectable modes are not dependent on their orientation towards the surface, resulting in possible excitations of vibrational modes lateral and perpendicular to the surface plane. Similar to Raman spectroscopy it is possible that the interacting electron gains energy from an already excited vibration. According to reference [Thi87] the electron in this scattering mechanism is close enough to the surface that the interaction with the screening image charge can be neglected. In the off-specular geometry the count rate is usually found to be reduced by one to too orders of magnitude compared to the contribution of the dipole scattering. Therefore the influence of the impact scattered electrons on measurements in specular geometry can be neglected

Negative Ion Resonce

Negative ion resonances are not detected in the experimental part of the thesis and the brief overview is given for completeness. The negative ionresonance scattering

mechanism is well known from electron collisions between electrons and ions in the gas phase (Shape or Feshbach resonances). In this mechanism the scattered electron is transiently trapped in an unoccupied molecular orbital forming a negative ion. The lifetime of such resonant states is usually much shorter in molecules adsorbed on surfaces due to additional decay channels into the metal substrate and is therefore dependent on the coupling of the unoccupied molecular orbitals to the electronic structure of the surface. Such a state can occur, when the energy of the unoccupied state is equal to the kinetic energies of the colliding electron. The angular distribution of the scattered electrons is given by the spatial distribution of the wave function of the resonance. Therefore the cross section depends strongly from the incident angle and energy of the electron.

3.3 Vibrational Spectroscopy via Infrared-Visible SFG

A second surface sensitive vibrational technique has been used for the investigations of self assembled monolayers formed on thin gold films under wet chemical conditions. The wet chemical approach disqualifies the investigation under UHV conditions with HREELS[8]. The utilization of infrared-visible sum-frequency generation (IR-Vis SFG) has been proven to be ideal for this kind of investigations. SFG is a highly sensitive, surface specific technique with a high spectral resolution. This nonlinear optical spectroscopy is a vibrational spectroscopy method which has become an established and widely used method to explore surfaces and interfaces ranging from liquid interfaces to SAMs on metal surfaces [She84, She89, Hei91, Buc01, Bel05, Gal03, Bon00]. For our requirements utilizing light has the advantage that SFG can also be used under "real" working conditions, *i.e.* not under UHV conditions. SFG spectroscopy exploits a second order nonlinear process at interfaces with a broken inversion symmetry.

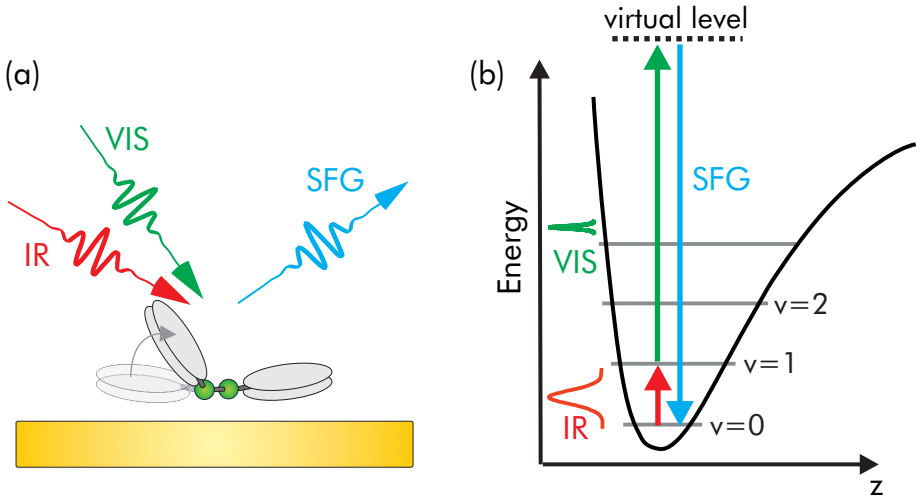

Figure 3.9: (a) Illustration of the SFG process; (b) for two beams, infrared and visible, the general scheme of an SFG process involving a resonant vibrational transition in an adsorbate layer is shown. In this three-level-system composed of a ground state $\nu = 0$, vibrational state $\nu = 1$ and an intermediate state. If the intermediate state is a virtual level, the SFG signal is dominated by the IR resonance.

For SFG two laser-pulses are overlapped on the sample, a broadband infrared ($\approx$ 150 fs, 20-30 μJ) with a bandwidth of $\approx$ 200 cm^{-1} (full width at half maximum, FWHM) laser-pulse is used together with a narrow band visible (VIS) up-conversion pulse of 7.5 μJ at ω_{Vis} = 800 nm. Both beams are p-polarized and focused onto the sample under grazing incidence of $\approx 75°$. The resulting SFG signal is spectrally dispersed and detected by an intensified CCD camera. Thus, vibrational spectra within a

[8]Measurements have been performed but with poor results.

bandwidth of ≈ 200 cm^{-1} can be obtained without scanning the IR frequency. Further experimental detail is given in reference [Fun00]. If spatial and temporal overlap is given light with the sum frequency can be observed as it is schematically shown in figure 3.9 (a). Resonant enhancement occurs for frequencies ω_{IR} within the bandwidth of the broadband IR pulse which are resonant with a vibrational transition. The general scheme of an SFG process involving a resonant vibrational transition in an adsorbate layer is shown in figure 3.9 (b).

The sum–frequency signal containing vibrational information can be observed as visible light. But its main virtue is that if the underlying medium is centrosymmetric as the in this thesis investigated gold substrates, this method is intrinsically surface sensitive.

Intense optical fields interact non-linearly with matter. Because of that, the dependence of the polarization P on the electric field E has to be expressed in higher order terms, with SFG being a second order process. In general, the resulting SFG intensity I_{SFG} is proportional to the second order polarization $P^{(2)}(\omega_{SFG} = \omega_{IR} + \omega_{Vis})$ induced by frequency mixing in the interfacial region. The of the incoming pulses induced polarization $P^{(2)}$ acts as a source for the electric fields E_{SFG} whose intensity can be expressed by:

$$I_{SFG} \propto |P^{(2)}(\omega_{SFG})|^2 \propto |\chi_S^{(2)}(\Theta)|^2 I_{IR} I_{Vis} \tag{3.4}$$

I_{IR}, I_{Vis} are the intensities of the incoming fields and $\chi_S^{(2)}(\Theta)$ the interface nonlinear susceptibility which is proportional to the density of interfacial molecules Θ. In dipole approximation $\chi_S^{(2)}(\Theta)$ vanishes in media with space-inversion symmetry. It can be separated into two parts, a resonant and a non-resonant contribution [Buc01]

$$\chi_S^{(2)}(\Theta) = \chi_{NR}^{(2)}(\Theta) + \chi_R^{(2)}(\Theta). \tag{3.5}$$

The resonant term is associated with the vibrational transition (see figure 3.9 (b)). The probed vibrations can be described by Lorentzians:

$$\chi_S^{(2)}(\Theta) = \chi_{NR}^{(2)}(\Theta) + \sum_\nu \frac{A_\nu(\theta) e^{i\phi_\nu}}{\omega_{\mathrm{IR}} - \omega_\nu + i\Gamma_\nu} \tag{3.6}$$

the resonance between the IR frequency ω_{IR} and the vibrational transition ω_ν possesses a damping constant Γ_ν. The SFG intensity can now be described as:

$$I_{SFG} \propto \left| |A_{\mathrm{NR}}(\theta)| + \sum_\nu \frac{|A_\nu(\theta) e^{i\phi_\nu}|}{\omega_{\mathrm{IR}} - \omega_\nu + i\Gamma_\nu} \right|^2 I_{\mathrm{IR}} I_{\mathrm{Vis}} \tag{3.7}$$

With the amplitudes A_{NR} and A_ν describing the strength of the non-resonant background (NRB, signal from the bare substrate) and the resonant contribution of the vibrational mode(s) ν. The respective ϕ_ν('s) take possible phase shifts between the NRB and the resonant contributions ν into account.

SFG (on metal substrates) is only sensitive to vibrational modes with a component

of the dipole moment change perpendicular to the surface. If a dipole is oscillating parallel to the metal surface, it will be screened by the image dipole created in the metal canceling the dipole moment change accompanying the molecular vibration (compare with figure 3.6). For the same reason the components of the incident IR field being parallel to the surface are screened by a metallic substrate. This leads to surface selection rules: only the component of the electric field perpendicular to the surface can couple to the vibrations and therefore only vibrations with a dipolar moment perpendicular to the surface can be excited similar to conventional IRAS-spectroscopy.

3.4 Thermal Desorption Spectroscopy

For coverage quantification and to gain insight into the adsorption behavior thermal desorption spectroscopy (TDS or TPD, temperature programmed desorption) has been employed. The QMS intensity of a mass corresponding to the investigated molecule or molecular fragment is detected as a function of the surface temperature. The usage of the *Lakeshore* temperature controller enabled us to produce highly linear heating rates typically of 1 K/s. Assuming that all adsorbed molecules exhibit equal binding sites the desorption rate R can be described using the Polanyi-Wigner-equation:

$$R = -\frac{d\Theta_{\text{ads}}}{dt} = \Theta_{\text{ads}}^{n}\nu_0 e^{\frac{-E_{des}}{k_B T}}, \tag{3.8}$$

with Θ_{ads} the number of adsorbate molecules on the surface, ν_0 the pre-exponential factor from the Arrhenius equation and n the reaction order. The desorption energy E_{des} is for non activated chemisorption processes equal to the binding energy E_B ($E_{des} = E_B$). If this expression is now connected to the desorption rate we find:

$$-\frac{d\Theta_{\text{ads}}}{dT} = \frac{dt}{dT}\Theta_{\text{ads}}^{n}\nu_0 e^{\frac{-E_{des}}{k_B T}}. \tag{3.9}$$

Using this expression we find the measured TDS spectra defined by their desorption order n resulting in typical coverage dependent shapes as can be seen in figure 3.10

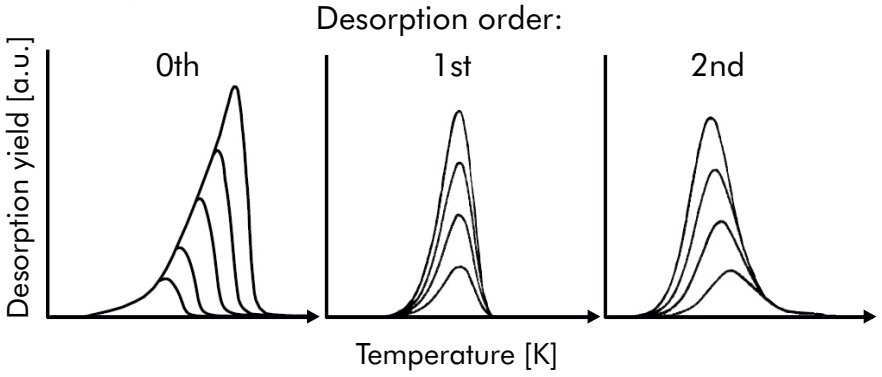

Figure 3.10: Thermal desorption spectra of 0., 1. and 2. order with a linear heating rate. Adopted from reference [Lüt95].

Since the available quadrupole mass spectrometer (QMS) is only capable to detect masses up to 200 *amu* and our investigated molecules exhibiting masses exceeding this range, we need to determine the mass of a fragment. The intensity of the signal of the fragment mass must be proportional the partial pressure of the desorbed molecule and is recorded as a function of the sample temperature. The general procedure of coverage quantification is exemplary discussed for a with tetra-*tert*-butyl-stilbene

multilayer covered Au(111) surface[9]. The mass of 190 amu corresponds to the 3,5-di-*tert*-butyl-phenyl ion and was chosen according to the already known successful TPD investigations of TBA on Ag(111) and Au(111) [Teg07, Hag07], respectively. From the coverage dependent measurements (achieved by a systematic variation of the dosing times) shown in figure 4.1 the desorption behavior of the features in the spectrum is assigned according to their desorption order.

At low coverages a broad desorption peak (α_2) is observed around 555 K, which extends to lower temperatures with increasing coverage. After saturation of this peak a second desorption feature α_1 develops at 296 K. The α_1 peak increases in height and width with increasing coverage, showing a typical zero-order desorption behavior. We therefore assign this peak to desorption from the multilayer while the α_2 peaks is associated with desorption from the first monolayer (ML).

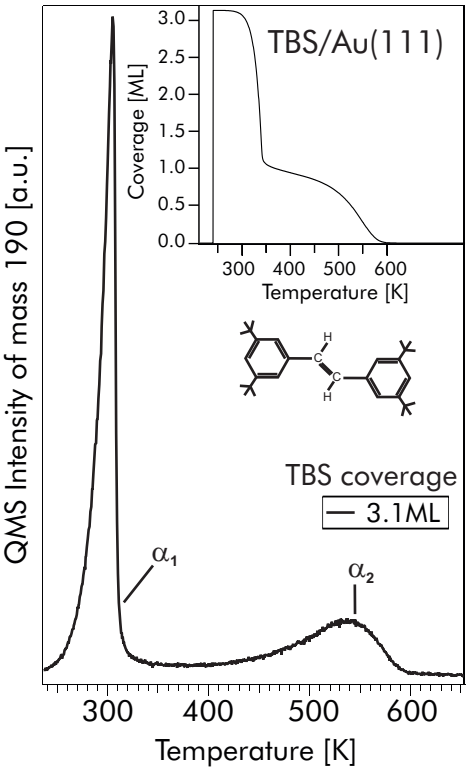

Figure 3.11: Thermal desorption spectra of 3.1 ML TBS on Au(111) recorded with a heating rate of 1 *K/s* at the fragment-mass of 190 amu. Inset: Shown is the integrated QMS signal of mass 190 for the shown TPD spectrum as a function of sample temperature used for coverage quantification. The integrated coverage from $T_S = 600 \rightarrow 370$ K is defined as one monolayer.

After the assignments of the desorption peaks with regard of their binding situation[10] we integrated the coverage in a temperature window starting from $T_S = 600$ K to $T_S = 240$ K as can be seen in the inset of figure 3.11. From the previous assignment of the α_2 peak to the monolayer we define the integrated coverage from $T_S = 600 \rightarrow 370$ K to one. From this initial calibration all investigated coverages are defined.

[9] Compare with chapter 4.1.1.

[10] The feature at higher temperatures is assigned to the surface bound monolayer and the low temperature feature is assigned to molecules bound in the second and subsequent layers explaining the identical desorption temperatures for increasing coverages.

4 *Trans / Cis*-Isomerization Reactions in Direct Contact with Noble Metal Surfaces

Various molecular switches which are able to undergo a photoinduced *trans/cis*-isomerization in solution have been studied after adsorption on noble metal surfaces by means of high resolution electron energy loss spectroscopy (HREELS). A specifically designed azobenzene derivative, *viz.* tetra-*tert*-butyl-azobenzene (TBA), is so far one of the few examples of molecular switches which have been successfully, reversible photo-isomerized after adsorption on a metal substrate, *viz.* the Au(111) surface [Ale06, Hag07, Wol09]. In TBA the phenyl rings have been equipped with bulky *tert*-butyl groups. The purpose has been to geometrically lift the functional backbone, *i.e.* the diazo-group (–N=N–), from the surface.

Note, that the photoinduced isomerization of unsubstituted azobenzene molecules bound to Au(111) is suppressed presumably because of the stronger interaction with the metal substrate and corresponding differences in the electronic and geometric structures [Com07].

However, recent experimental studies in collaboration with the group of St. Tautz (FZ Jülich) using normal incidence x-ray standing wave technique and large-scale density-functional theory calculations performed by K. Reuter *et al.* (TU München) indicate a similar distance of the photochemically active diazo bridge to the noble metal (Ag, Au) substrate for both the bare and *tert*-butyl functionalized azobenzene [McN10b, McN10a, Mer10]. Therefore the underlying mechanism governing the desired functionality may be influenced drastically by the electronic interaction with the substrate, so that purely geometrical arguments to predict the functionality of adsorbed molecules have to be taken with great caution. This demonstrates that both, the geometric and electronic structure of the complete molecule–substrate complex have to be taken into account for a successful tuning of the functionality of adsorbed molecular switches.

For the prototypical azobenzene derivative (TBA) on Au(111) it has already been shown that HREELS is an appropriate tool to investigate molecular switching at surfaces, which goes along with significant changes in the vibrational structure [Ova07].

In the following chapter the results of our HREELS investigations on the adsorption and particularly the switching properties of, structurally similar and isoelectronic to TBA, tetra-*tert*-butyl-stilbene (TBS) and tetra-*tert*-butyl-imine (TBI) on Au(111) are presented. The functional units have herein been changed from the diazo-group (–N=N–) in azobenzene (C_6H_6–N=N–C_6H_6) to the imine-group (–CH=N–) in N-benzylideneaniline (also called imine; C_6H_5–CH=N–C_6H_6) and to the vinylene-group (–HC=CH–) in stilbene (C_6H_5–CH=CH–C_6H_5). Additionally TBA has been investigated with the underlying noble metal surface varied to Cu(111) to gain insight into the influence of the electronic structure of the underlying substrate on the switching

process. It is a key goal, relevant to the development of future applications, to understand and control the structural changes of different surface-bound molecular switches. For this purpose, it is crucial to get a detailed knowledge of the adsorption geometry (molecular orientation) and the the switching properties to gain insight into the underlying elementary processes.

4.1 Photoisomerization Ability of TBS on Au(111) and TBA on Cu(111)

4.1.1 Adsorption Behavior and Photoisomerization Ability of Tetra-*tert*-butyl-stilbene on Au(111)

In order to obtain insights into the adsorption properties of TBS/Au(111) and to quantify the coverage, thermal desorption spectra were recorded as a function of TBS coverage as can be seen in figure 4.1 for different dosing times. The mass of 190 amu corresponds to the 3,5-di-*tert*-butyl-phenyl ion and was chosen according to the already known successful TPD investigations of TBA on Ag(111) and Au(111) [Teg07, Hag07], respectively.

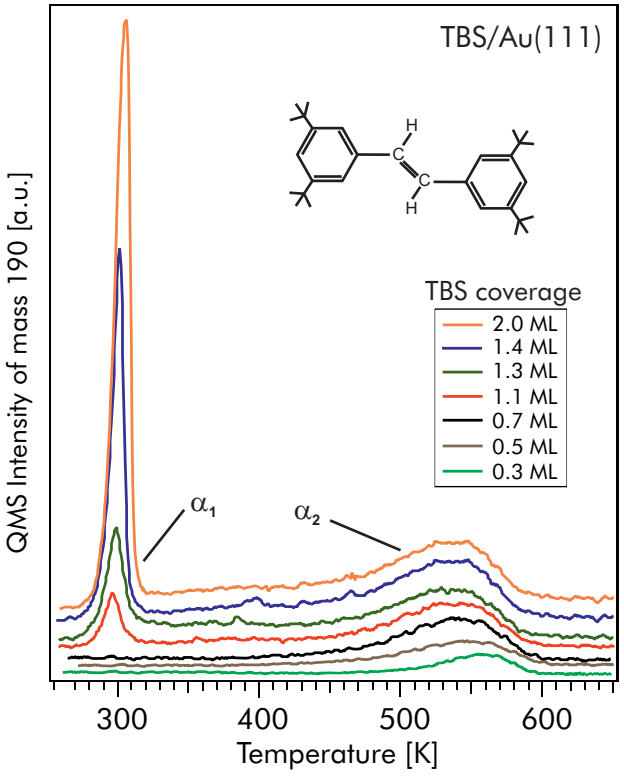

Figure 4.1: Thermal desorption spectra of TBS on Au(111) at different coverages recorded with a heating rate of 1 *K/s* at the fragment-mass of 190 amu (3,5-di-*tert*-butyl-phenyl ion) [Ley10].

At low coverages a broad desorption peak (α_2) is observed around 555 K, which extends to lower temperatures with increasing coverage. After saturation of this peak a second desorption feature α_1 develops at 296 K. The α_1 peak increases in height and width with increasing coverage, showing a typical zero-order desorption behavior. We therefore assign this peak to desorption from the multilayer while the α_2 peaks is associated with desorption from the first monolayer (ML). The thermal desorption

behavior of TBS from Au(111) is very similar to those of other aromatic compounds on noble metal surfaces, for example azobenzene derivatives [Teg07, Hag07, Óvá08], benzene [Xi94, Roc06], hexafluorobenzene [Von99], and pyridine [Zho02], respectively.

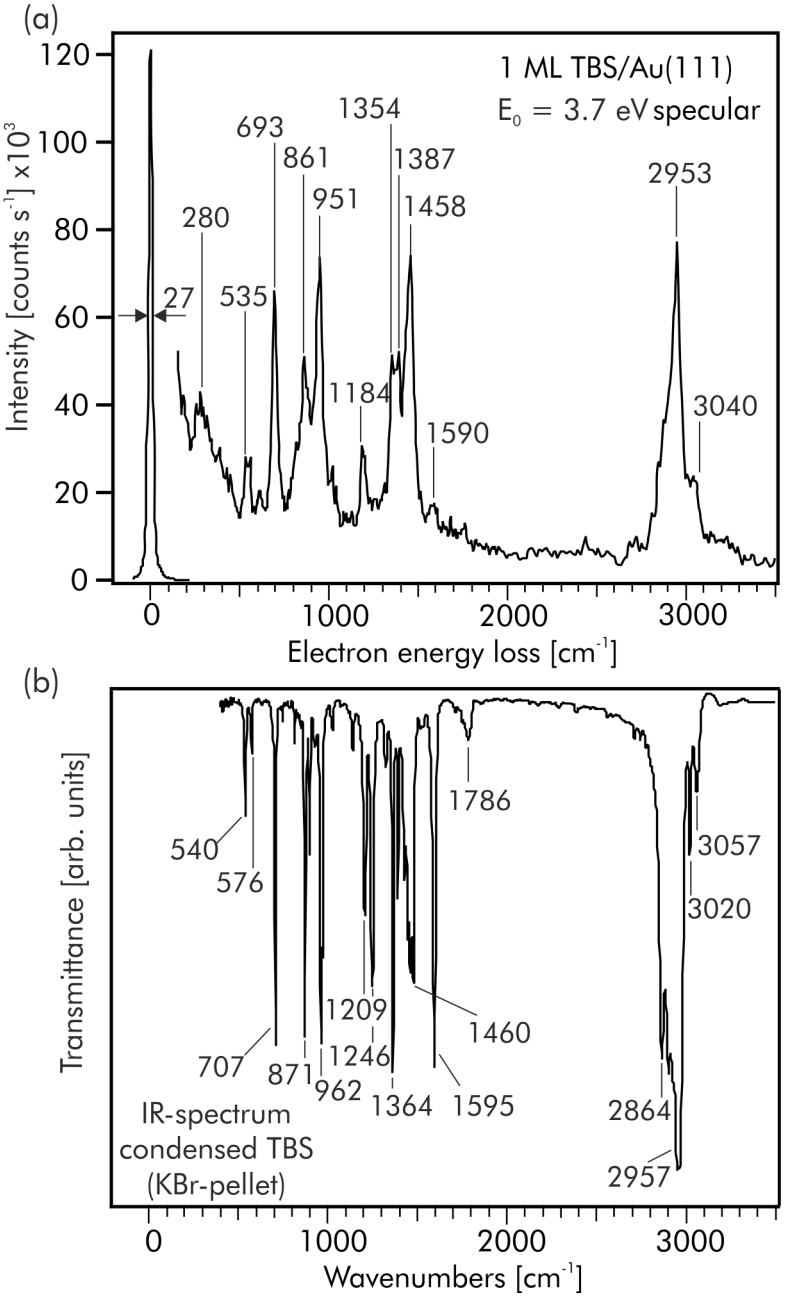

Figure 4.2: (a) HREEL spectrum of 1 ML TBS adsorbed on Au(111) recorded in specular scattering geometry with a primary electron energy of 3.7 eV. The FWHM of the elastic peak is 27 cm^{-1} (3.3 meV). (b) Fourier-transform infrared spectrum of condensed TBS (KBr-pellet) measured with a resolution of 4 cm^{-1} [Ley10].

A common observation in these systems is the substantial broadening of the desorption peak with increasing coverage in the monolayer regime. This can be attributed to repulsive interactions between the adsorbed molecules for example due to dipole-dipole interactions.

Figure 4.2 (a) shows the HREEL spectrum of 1 ML TBS adsorbed on Au(111), which was prepared by heating the multilayer-covered surface to 400 K, recorded in specular scattering geometry. For comparison, the infrared (IR) spectrum obtained for the solid state (in KBr) is displayed in figure 4.2 (b). The vibrational frequencies and their assignments for both the adsorbed and condensed TBS are listed in table 4.1 together with the literature values of vibrational modes of 0.9 ML TBA adsorbed on Au(111) [Ova07] and condensed *trans*-stilbene [Mei78, Are95, Cho97].

vibrational mode[a]	1 ML TBS [b]	cond. TBS [c]	0.9 ML TBA[d]	trans-stilbene[e]
τ(C–C)^{Ar}, δ(C–X)	424	–	–	410, 419
τ(C–C)^{Ar}	451	–	–	455
γ(C–X)	535 (da)[f]	540	–	528
δ(C–C)^{Ar}	558	576	543	541
δ(C–C)^{Ar}	609	630	–	620
τ(C–C)^{Ar}	693 (da)	707	696	692
γ(C–H)^{Ar}, ν(C–C)^{Ar}	816	813	–	847, 824
γ(C–H)^{Ar}	861 (da)	871, 889	879	848
γ(C–H)$_e$	951	962	–	966
ν(C–C)^{Ar}, δ(C–H)^{Ar}	1019	1026	1008	1028
ν(C–C)^{Ar}, δ(C–H)^{Ar}	1038	1026	–	1059
δ(C–H)^{Ar}	1184	1209	1189	1187
ν(C–C)^{Ar}	–	1246	–	1234
δ_s(CH$_3$)^t	1354	1364	1359	–
δ_s(CH$_3$)^t	1387	1390	1385	–
δ_{as}(CH$_3$)^t	1458	1460, 1477	1453	–
ν(C–C)^{Ar}	1590	1595	1584	1597
ν_s(CH$_3$)^t	2847, 2876	2864	2878	–
ν_{as}(CH$_3$)^t	2953	2957	2963	–
ν(C–H)$_e$	3011	3020	–	3029
ν(C–H)^{Ar}	3040	3057	3057	3040

Table 4.1: Vibrational frequencies (in cm^{-1}) and assignments for 1 ML TBS adsorbed on Au(111) and condensed TBS, respectively. [a] CX stands for the phenyl ring-ethylene bond; *e*, indicates the ethylene moiety; *s*, symmetric; *as*, asymmetric; ν, stretch; δ, in-plane bend; τ, torsion; γ, out-of-plane bend; *Ar*, aromatic ring; *t*, *tert*-butyl group. [b] Obtained by HREELS; present study. [c] IR spectrum recorded in KBr; present study. [d] HREELS data from tetra-*tert*-butyl-azobenzene (TBA) adsorbed on Au(111) adapted from ref. [Ova07]. [e] IR and Raman data adapted from refs. [Mei78, Are95, Cho97]. [f] The *da* indicates a strong dipole activity [Ley10].

The HREEL spectrum for the adsorbed TBS agrees well with the IR data for TBS in the solid, only small shifts towards lower energies are observed for some vibrations due to adsorption on Au(111). In both the adsorbed and condensed TBS the asymmetric CH_3 stretch mode ($\upsilon_{as} \approx 2953$ cm^{-1}) and the CH_3 deformation modes ($\delta_{as} \approx 1458$ cm^{-1}, δ_s around 1387 cm^{-1}) of the *tert*-butyl-groups as well as the out-of-plane C–H deformation of the phenyl rings and the ethylene moiety (γ(C–H) ≈ 861 cm^{-1}, γ(C–H)$_e \approx 951$ cm^{-1}) and the phenyl ring torsion mode (τ(C–C) ≈ 693 cm^{-1}) show high intensities. In contrast, the stretch modes of the aromatic rings (ν(C–C)) at 1246 and 1595 cm^{-1}, respectively, result in very high intensities in the IR spectrum of the condensed TBS, are absent or barely visible in the HREELS-spectrum.

In order to gain insights into the excitation mechanism, *i.e.*, dipole- versus impact-scattering, and to analyze the adsorption geometry of TBS on Au(111), we performed angular dependent measurements. Figure 4.3 shows a comparison of HREEL spectra recorded in specular and 9.2° off-specular geometries for 1 ML TBS/Au(111). Most

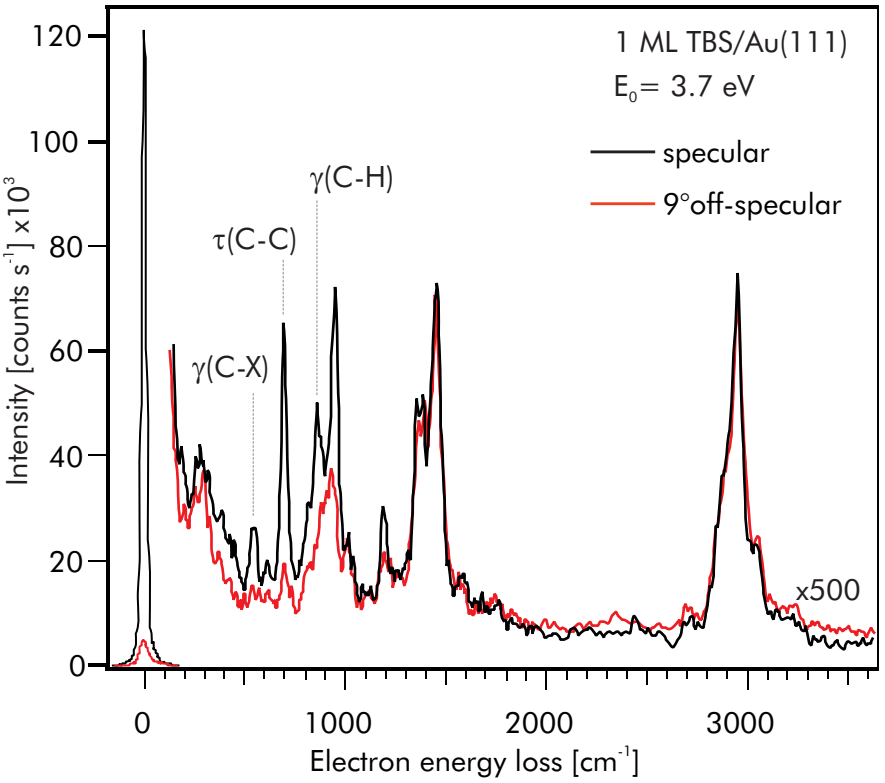

Figure 4.3: HREEL spectra of 1 ML TBS adsorbed on Au(111) recorded in specular and 9.2° off-specular scattering geometry, respectively, with a primary electron energy of 3.7 eV [Ley10]

striking is the huge intensity decrease of the out-of-plane torsion mode of the phenyl rings (τ(C–C)) at 693 cm^{-1} and the C–H bending mode (γ(C–H)) at 861 cm^{-1} in the off-specular spectrum, indicating that their intensities are originating mostly from dipole scattering in the specular spectrum (see table 4.1 for the assignment of the dipole

active modes). The strong dipole activity of the phenyl ring torsion and C–H bending modes points towards a preferential orientation of the TBS parallel to the Au(111) surface, *viz.* a planar *trans*-configuration, since in this orientation these modes have a strong dipole moment change upon vibration perpendicular to the surface. Moreover, the in-plane modes of TBS, for instance the stretch vibration of the phenyl rings at 1246 and 1595 cm^{-1} of condensed TBS observed with high intensities, are absent or barely visible in the HREELS of the adsorbed species. This corroborates the proposed planar adsorption geometry. In addition, STM measurements show that in the low-coverage regime TBS forms well-ordered islands with the molecules adsorbed in the planar configuration [Pet08] as can be seen in figure 4.4.

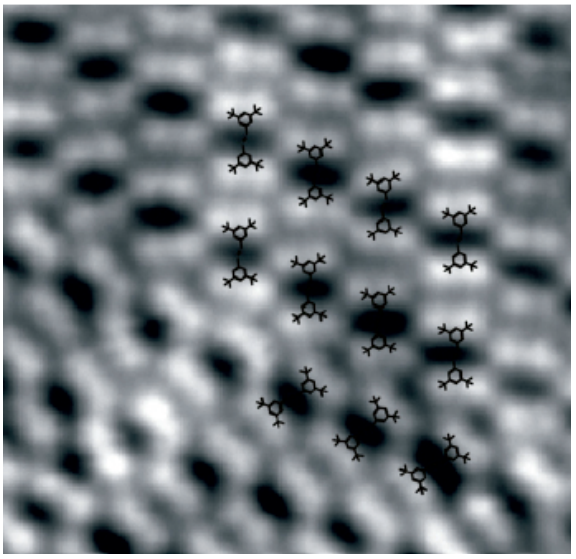

Figure 4.4: STM image of an island with close-packed tetra-*tert*-butyl-stilbene molecules on a Au(111) surface. Single molecules do appear in the STM images as four equally high lobes, which are attributed to the four tert-butyl-groups by comparison of the measured dimensions with calculated dimensions of TBS in the gas phase. The assigned molecular structure has been drawn exemplary in the STM image for some molecules. The STM picture has been adopted from the PhD thesis of M.V. Peters (HU Berlin) [Pet08].

Hence, we conclude that the adsorption behavior is similar to the one observed for TBA in direct contact with the Au(111) surface [Ale08, Mor06, Ova07]. Note that also in the liquid phase the *trans*-isomer of both azobenzene and stilbene is known to be the energetically favorable configuration [Mei92].

Photo irradiation experiments have been performed without observable changes in the vibrational structure in the HREELS spectra of TBS/Au(111). Additionally 2PPE measurements have been carried out, using femtosecond laser pulses which are generated by a 300 kHz Ti:Sapphire laser system, which pumps an optical parametric amplifier. The visible output with photon energies from 1.7 eV to 2.7 eV, respectively, can be frequency doubled in a BBO crystal to generate ultraviolet pulses (3.4–5.4 eV photon energy). No light induced changes electronic structure of surface-bound TBS are observed using different optical excitation energies ranging from 2–4.5 eV [Ley10]. Accordingly, we propose that the photoisomerization is suppressed.

Note, that the isomerization is not observed as well for STM experiments utilizing tunnel-currents and electric fields due to voltage pulses [Pet08]. In TBA/Au(111) the excitation mechanism for molecular switching has been identified to arise from a substrate-mediated charge transfer process, *viz.* the formation of a positive ion reso-

nance. Thereby excitation with photon energies above ≈ 2.1 eV leads to the generation of hot holes in the Au *d*-band, which rapidly relax to the top of the *d*-band and subsequently transfer to the HOMO level of TBA induces the isomerization [Hag08a]. In the reference [Ley10] the electronic structure of TBS adsorbed on Au(111) has been measured utilizing two-photon-photoemission spectroscopy enabling us to determine occupied and unoccupied electronic states of the molecules in direct contact with the metallic substrate. The HOMO level of TBS is located at -1.75 eV with respect to E_F, *i.e.*, at a similar energetic position as the HOMO level of TBA on Au(111), which is -1.85 eV (see chapter 2.3). Surprisingly the electronic structure is found to be almost identical, leaving the question of the quenched isomerization unanswered. One may speculate if the overlap between the Au *d*-bands and the HOMO of TBS and thus the electronic coupling is weaker compared to TBA and therefore a transfer of photoexcited Au *d*-band holes to the HOMO of TBS is unlikely. However, based on the mechanism for the photoinduced isomerization of TBA on Au(111), it is evident that a (strong) electronic coupling must be existent, *i.e.*, some degree of hybridization between the Au *d*-band and the HOMO of TBA, presumably *via* the N=N bonding or the lone pairs at the nitrogen.

Whereas the molecular switching in TBA is driven by the generation of a positive ion resonance (cation) *via* a charge transfer of holes from the Au *d*-band to the HOMO level of TBA, this mechanism is obversely not efficient in TBS/Au(111) even though the HOMO of TBS is at a similar energetic position. It is an open question if the cationic state of TBS would stimulate a conformational change. Quantum chemical calculations of the potential energy surfaces for the free TBA and TBS molecule corroborate this conclusion. They indicate that for the TBA cation larger gradients at the Franck-Condon point than for the TBS cation are exist. Furthermore in the cationic states the barrier is strongly reduced in TBA compared to TBS[11] [Ley10].

[11] Potential energy surfaces of the neutral ground state and the cationic state for the TBA and TBS, respectively, have been calculated using the B3LYP functional and a 6-31G* of Gaussian 03 program package. The calculations have been performed by P. Saalfrank *et al.*, Institut für Chemie, Universität Potsdam, SFB 658.

4.1.2 Adsorption Behavior and Photoisomerization Ability of Tetra-*tert*-butyl-azobenzene on Cu(111)

TDS has been utilized in order to obtain insights into the adsorption properties of TBA on Cu(111) and to quantify the coverage. For higher coverages a sharp desorption feature is apparent in the thermal desorption spectra around 300 K. Whereas for lower coverages almost no clear structure is resolved. The desorption behavior of the peak at ≈ 300 K resembles those of the identical molecule on other coinage metal surfaces [Teg07, Hag07, Ley07] and is similar to the previously described absorbtion behavior of TBS on Au(111) (see chapter 4.1.1.). Thus the feature at ≈ 300 K is interpreted identically, *i.e.* as the multilayer. For the other investigated TBA covered surfaces a broad desorption peak α_3 is observed with the maxima located at temperatures of $T_S^{Au(111)}$ = 525 K and $T_S^{Ag(111)}$ = 480 K [Ley07]. Surprisingly the typical monolayer behavior is not found for TBA on Cu(111). We performed HREELS measurements after annealing to temperatures of 500 K, where no further desorption is visibly in the TDS of TBA/Cu(111).

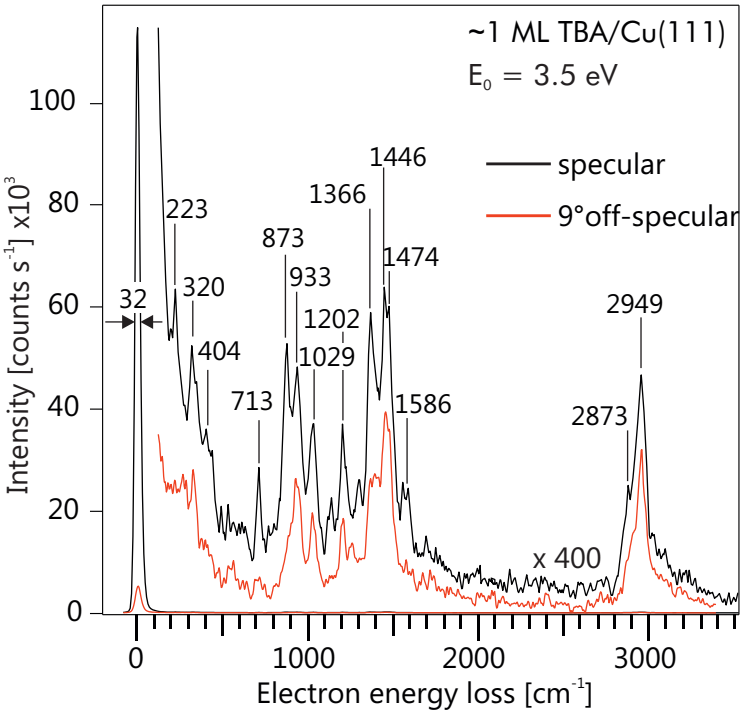

Figure 4.5: HREEL spectra of ≤ 1 ML TBA adsorbed on Cu(111) recorded in specular and 9.2° off-specular scattering geometry, respectively, with a primary electron energy of 3.5 eV, with a resolution (FWHM) of 32 cm^{-1} (4.0 meV).

The resulting spectrum shows broad vibrational features at modes around 100, 700 and 870 cm^{-1}. The observed residual vibrational features at around 700 and 870 cm^{-1} are in a frequency region where for this molecule out-of-plane modes of the aromatic

rings are found and the feature at $\approx$ 100 cm^{-1} could be the vibrational mode of a fragment bound to the Cu(111) surface. The broad vibrational features could be derived from various fragments exhibiting vibrational modes in the same energy region. Therefore a possible explanation of the "missing" monolayer in the TDS spectra could be a dissociation of the molecule during desorption[12]. The HREELS measurement have therefore been performed at an assumed monolayer coverage which has been prepared by desorbing the multilayer by heating the surface to T_S = 310 K or by deposition of the molecules on the surface kept at T_S = 310 K.

Figure 4.5 shows the HREELS spectra of around one monolayer TBA on Cu(111). We recorded HREELS spectra in specular (black line) and 9° off-specular geometry (red line) with a primary electron energy of 3.5 eV with an energy resolution of 32 cm^{-1} in the specular direction. The determined vibrational frequencies and their assignments are listed in table 4.2 together with the results from TBA on Au(111), TBA in the condensed phase [Ova07], and with literature values of the vibrational modes of (*trans*-) azobenzene [Küb60, Kel71, Bis97]. Although the azobenzene is planar (see figure 4.6

vibrational mode[a]	$\leq$ 1 ML TBA/Cu(111)[b]	0.9 ML TBA/Au(111)[c]	cond. TBA[d]	trans-azo[e]
δ(C–N)	223 (*da*)	204	–	219 (ra[f])
τ(C–C)^{Ar}	320	299	–	299[g]
τ(C–C)^{Ar}	404 (*da*)	403 (*da*)	–	403 (ra[f])
τ(C–C)^{Ar}	713 (*da*)	696 (*da*)	705	689 s
τ(C–C)^{Ar}	873 (*da*)	879 (*da*)	885	776 s
γ(C–H), δ(C–C)^{Ar}	933	921	910	927 s
ν(C–C)^{Ar},	1029	1008	1024	1020 m
ρ(CH$_3$)	1139 (*da*)	1153 (*da*)	1188	–
δ(C–N)	1202	1230	1245	1300 m
δ_s(H–C–H)(CH$_3$)	1366 (*da*)	1359 (*da*), 1385 sh	1365, 1395	–
δ_{as}(CH$_3$)	1446, 1474	1453	1463	1456 s, 1486 s
ν(C–C)^{Ar}	1586 (*da*)	1584	1602	1585 m
ν_s(C–H)(CH$_3$)	2873 sh (*da*)	2878 sh (*da*)	2865, 2900	–
ν_{as}(C–H)(CH$_3$)	2949	2951	2962	–

Table 4.2: Vibrational frequencies (in cm^{-1}) and assignments for 1 ML TBA adsorbed on Cu(111). [a] *s*, symmetric; *as*, asymmetric; ν, stretch; δ, in-plane bend; τ, torsion; γ, out-of-plane bend; *Ar*, aromatic ring; ρ, rocking.
[b] Obtained by HREELS; present study. [c] HREELS data from tetra-*tert*-butyl-azobenzene (TBA) adsorbed on Au(111) adapted from ref. [Ova07]. [d] IR spectrum recorded in KBr adapted from ref. [Ova07]. [e] IR and Raman data adapted from refs. [Küb60, Kel71]. [f] Raman spectrum recorded in CCl_4. [g] Calculated value adapted from ref. [Bis97]. Abbreviations: s, strong; m medium; sh, shoulder. The *da* indicates a strong dipole activity.

[12]Compare with the desorption behavior of nitro-spiropyran in chapter 5.1

(a)) the TBA will probably not exhibit a horizontal symmetry plane like it is idealized in figure 4.6 (b). This is supported by theoretical (Density Functional Theory) and experimental (X-ray Standing Wave) investigations together with the groups of K. Reuter and S. Tautz demonstrating that the real TBA adsorption geometry concerning the height of the diazo-bridge of the molecule above the surface is much better characterized as a 'suspended bridge' between tilted *tert*-butyl legs that is shown in figure 4.6 (c). This is derived from the almost identical adsorption heights of the diazo-group of 3.22 Å above the surface for azobenzene versus 3.28 Å for TBA/Au(111) [McN10a]. Nevertheless it is reasonable to assume that the tilting angle of the azobenzene part of the molecule remains small, so that we use an "in-plane" and "out-of-plane" in the assignments of the phenyl-ring modes.

The HREEL spectrum for the on Cu(111) adsorbed molecules agrees well with the IR data of the condensed-phase TBA with only minor energetic shifts due to the absorption on Cu(111). While in the IR spectrum of the condensed molecule the asymmetric CH_3 stretch mode (ν_{as}(C–H)(CH_3) at 2962 cm^{-1}) results in the most intense infrared absorption, this mode shows a medium intensity in the case of TBA/Cu(111). The stretch modes of the aromatic rings ν(C–C)^{Ar} at 1586 and 1029 cm^{-1} are less intense compared to the IR spectrum of the condensed phase, but show more intensity in comparison to the adsorption of TBA on Au(111). The more pronounced occurrence of these in-plane modes of the phenyl ring already hints towards a geometry on the surface with the phenyl rings slightly twisted (non-planar) as compared to the adsorption on Au(111). Accordingly the adsorption peak at 1202 cm^{-1}, assigned to the in-plane C–N deformation δ(C–N), is more pronounced compared to the adsorption on Au(111), where it was barely visible for the adsorbed species. The phenyl ring torsion modes τ(C–C)^{Ar} at 713 and 873 cm^{-1} are detected with medium intensity, whereas they show the highest intensities for TBA/Au(111).

In order to obtain insight into the excitation mechanism of the excited vibrational modes, *i.e.* dipole vs. impact scattering and to analyze the adsorption geometry further, we performed angular dependent measurements. The red curve in figure 4.5 represents the off-specular spectrum. Most striking is the intensity decrease for the out-of-plane torsion modes of the phenyl rings τ(C–C)^{Ar} at 404, 713, and 873 cm^{-1}, indicating that their intensity originates mostly from dipole-scattering in the specular spectrum. Similar to the results for TBA/Au(111) we therefore derive an orientation of the TBA in its *trans*-state which is almost planar to the surface, since in this orientation these modes would exhibit a strong dipole moment change upon vibration perpendicular to the surface. However, we conclude that the molecular orientation of TBA when adsorbed on Cu(111) is not as planar as on the Au(111) substrate, evidence is given by the smaller intensities of the out-of-plane phenyl ring torsion modes, the presence of the in-plane C–N deformation δ(C–N) of the diazo-group at 1202 cm^{-1} and the detected dipole-activity of an in-plane phenyl ring stretch mode ν(C–C)^{Ar} at 1586 cm^{-1}.

According to the photo switchable TBA, where illumination with photon energies of $h\nu \geq 2$ eV leads to a *trans*→*cis* isomerization [Hag07], we tried to induce changes in the vibrational structure by illumination with photon energies starting from $h\nu = 445$ (2.79 eV) to 248 nm (5.01 eV). Note, that with this range of photon energies

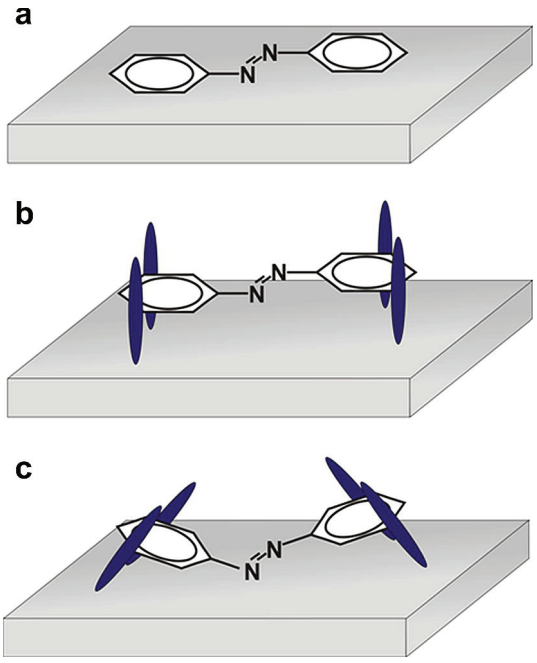

Figure 4.6: Illustration of the concept of geometric decoupling using bulky spacer groups. (a) Assumed geometry of *trans*-azobenzene on noble metal surface. (b) Ideal picture of the adsorption geometry of azobenzene equipped with four tert-butyl-groups as spacer-legs (TBA) lifting the functional backbone, *i.e.* the diazo-group, above the surface. (c) "Suspended bridge" geometry as it has been derived from X-ray standing wave measurements and DFT calculations. The figure has been adopted from the joint publication ref. [McN10a]

it should be possible to induce a direct intramolecular excitation responsible for the *trans* to *cis*-isomerization in solution (see figure 2.5). An indirectly induced isomerization likewise the TBA/Au(111)-experiment which is observed for $h\nu \geq 2$ eV [Hag08a] assuming the HOMO position of TBA being comparable upon adsorption on Au(111) and Cu(111), respectively. No changes in the HREELS spectra are observed, accordingly we propose that the photoisomerization is suppressed.

STM measurements of TBA on Cu(111) have been performed by M. Alemani *et al.* (FU Berlin) showing, consistently to the presented results, that only the *trans*-isomer is present on the surface after deposition of TBA molecules on Cu(111) as for Au(111) [Ale08]. The appearance resembles the one of TBA/Au(111) with four lobes apparent, corresponding to the *tert*-butyl-legs of the molecule. Note that the central part of the molecule and the phenyl-rings are not visible in STM spectra. But, differences in the self-assembly behavior have reported: Whereas TBA on Au(111) forms large ordered islands, disordered islands are visible on Cu(111). This fact is attributed to an enhanced molecule-substrate interaction, which could explain the "missing" monolayer in TDS measurements described at the beginning of this chapter. In accordance to our illumination experiments, no isomerization of the molecules is observed on Cu(111) but on Au(111) when utilizing voltage pulses from the STM tip [Ale08].

The similarities in the adsorption geometries of azobenzene and TBA at Cu(111) and Au(111) derived from the HREELS measurement strongly hint that the purely geometrical arguments that have been underlying the bulky spacer group concept have to be reassessed. Instead, the present analysis supports the suggestion of P. Tegeder and co-workers that for understanding the mechanism of the photo-induced switching functionality the detailed electronic structure of the metal substrate in combination

with the influenced electronic structure of the molecular switch in direct contact with the substrate is much more important than previously thought.

In the model presented in reference [Hag08a] we explain the switching (non-switching) of TBA on Au(111) (and Ag(111), respectively,) by assuming that the incident photon creates a hole in the metal, which exhibits an ultra fast decay to the d-band upper edge located ≈ 2.1 eV below the Fermi-energy E_F (see figure 2.2 (a)). In the case of Au(111), this hole can then transfer to the highest occupied molecular orbital (HOMO) of TBA. In contrast to Ag(111) where the d-band is ≈ 2 eV lower lying and thus preventing the overlap with the HOMO hindering the isomerization. In the present case for TBA on Cu(111) the position of the d-band is close to the d-band position of Au(111) (-2.1 eV in reference to E_F; see figure 2.2 (b)), which does not explain *a priori* the quenched isomerization of TBA on Cu(111). A possible explanation for the quenched isomerization behavior of TBA/Cu(111) is given in ref. [Ale08]. A stronger molecule-substrate interaction caused by the Cu(111) substrate is utilized as an explanation. They conclude that a strong interaction could potentially hinder the isomerization process by introducing both a larger barrier for lifting up parts of the molecule and an increased steric hindrance to the necessary molecular motion imposed by the neighboring molecules.

Alternatively, changes in the electronic interaction between molecules and substrate could affect the isomerization mechanism by modifying the electronic states of the *trans-* (and *cis-*) isomers as well as the connecting transition structure and therefore (strongly) influence the resulting potential energy surface[13]. Moreover, the surface corrugation might play an important role, since the three-dimensional *cis*-isomer could selectively be destabilized and therefore become non-addressable. The important influence of the molecule-surface interaction on the isomerization process becomes apparent when comparing the above discussed results with the behavior of TBA on Au(111).

[13]Compare with the "inverted" thermal isomerization behavior of TBI on Au(111) in chapter 4.2 or the modified equilibrium structure of spiropyran on Au(111) in chapter 5.

4.2 Coverage and Temperature Dependent Isomerization of an Imine Derivative

In this chapter HREELS has been employed to analyze thermally activated changes in the geometrical structure of the photochromic molecular switch 3,3',5,5'-tetra-tert-butyl-imine (TBI) adsorbed on Au(111). In contrast to azobenzene and its derivatives, imine-based switches have only been scarcely investigated on metal surfaces.

The author is only aware of two publications. Both studies have been performed in the group of P. Tegeder at the FU Berlin. The same molecules (TBI) as in the recent study have been investigated adsorbed on Au(111) with 2PPE spectroscopy, but the focus of this investigation has been set to the electronic structure of the molecule-metal interface [Hag10].

It was found for another imine derivative, namely carboxy-benzylideneaniline (CBA), adsorbed on Au(111) that the molecule adopts a planar *trans*-configuration in the first monolayer. This is despite the strong non-planar geometry of the molecule in solution (Compare with chapter 2.2.2.). In this HREELS study we found that illumination with UV-light at 355 nm of CBA in direct contact with Au(111) ($\leq$ 1 ML) causes no changes in the vibrational structure, whereas for higher coverages ($>$ 1 ML) we observed pronounced modifications which we assigned to a *trans* $\rightarrow$ *cis* isomerization. The backreaction has been achieved by thermal activation, when heating the surface to 273 K. We proposed a direct intramolecular electronic excitation analogue to the molecule in solution since the second and subsequent layers are decoupled from the surface [Óvá10].

The study on 3,3',5,5'-tetra-tert-butyl-imine (TBI) is motivated by our previous work on 3,3',5,5'-tetra-tert-butyl-azobenzene (TBA), since imine is structurally similar and isoelectronic to azobenzene, which is the most thoroughly investigated molecular switch in solution and in case of physisorbed molecules on metal surfaces, a photoinduced isomerization has so far been demonstrated only for the specifically designed TBA adsorbed on Au(111). Our intention is to analyze the adsorption and particularly the switching properties of the adsorbed molecule when changing the central functional unit from the diazo-group (–N=N–) in azobenzene to the imine-group (–C=N–) in N-benzylideneaniline (also called imine; C_6H_5–CH=N–C_6H_6).

4.2.1 Coverage Quantification

For coverage quantification and to gain insight into the adsorption behavior of TBI on Au(111) thermal desorption spectroscopy has been employed. Figure 4.7 shows the TPD spectra at mass 57 amu taken after dosing TBI with varying dosing times. The Au(111) surface has been cooled to $T_S \approx 200$ K during deposition, while the doser has been heated to $T_D \approx 358$ K. The broad high temperature TPD feature between 440 and 590 K is assigned to the monolayer. Therefore its area, when the peak is saturated, is taken as a reference for the coverage estimation. With increasing coverage this peak starts to emerge at 525 K, for 0.3 ML the peak maximum is located at 511 K, whereas for the saturated monolayer the peak maximum is located at 480 K. This is typical for 2nd order desorption (see chapter 3.4). For low coverages in the sub-monolayer regime the adsorbed TBA binds more strongly to the substrate, increasing coverage leads to a denser packing and increasing adsorbate-adsorbate repulsion, e.g. originating from dipole-dipole-interaction, and therefore to the observed shift of the peak maximum to lower temperatures.

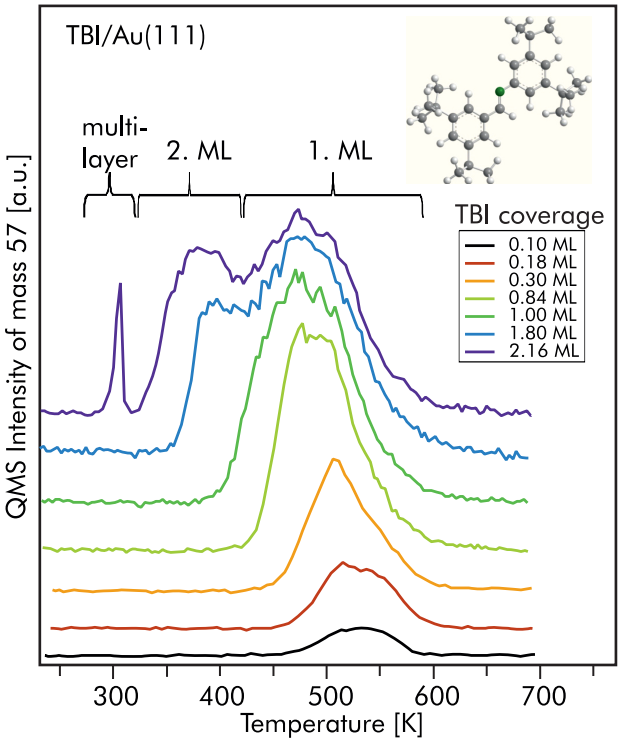

Figure 4.7: Coverage quantification by means of thermal desorption spectroscopy of TBI adsorbed on Au(111). Shown is the measured signal for mass 57 amu ($C_4H_9^+$) for different dosing times.

After saturation of the first monolayer we observe the appearance of a second peak located between 320 and 440 K with 2nd order desorption behavior, which we assign to

the second monolayer, since its area is equivalent to approximately the area of the first monolayer. At lower temperatures we find the multilayer with 0th order desorption kinetics (spectra for higher coverages not shown in figure 4.7). Complete desorption for coverages exceeding one ML is given after annealing to $T_S = 317$ K.

In the following all molecular layers have been prepared dosing the wanted amount of molecules on the Au(111) surface held at $T_S \approx 200$ K ($T_D \approx 358$ K) by choosing the appropriate dosing time. All HREELS investigations have been followed by recording a complete TPD to assure the amount of molecules on the substrate.

4.2.2 Analysis of the Adsorption Geometry

To analyze the adsorption geometry of TBI adsorbed on Au(111), we deposited one monolayer on the substrate held at a temperature of $T_S = 200$ K. Afterwards angular-dependent HREELS measurements in specular and 9° off-specular geometries (see figure 4.8) at a sample temperature of ≈ 100 K have been carried out. The energy of the primary electrons was set to 3.5 eV with a resolution of 17.5 cm^{-1} (≈ 2.2 meV), measured as the full width at half maximum (FWHM) of the elastic peak.

The complete assignment of all measured vibrational frequencies is listed in table 4.3 together with the experimental values of vibrational modes of N-benzylideneaniline (imine) in the condensed and liquid phase (references [Ost67, Z.89]), theoretical values obtained by normal coordinate analysis and DFT studies (references [Koz93, Gae07]). The results obtained for a previous HREELS study of TBA on Au(111) (reference [Ova07]) has been taken into account as well, since the investigated azobenzene derivative is equipped as well with four *tert*-butyl groups and is therefore isoelectronic and structurally close to TBI.

It is apparent that several vibrational modes detected in the IR spectra of the condensed molecules (or in solution) are absent or barely visible in the HREELS spectra of the on gold adsorbed species. Therefore the modes, which are absent in the measurements of the surface bound species are quenched upon adsorption on the metal substrate. Noteworthy is that no vibrational modes in the region above 1500 and below 2800 cm^{-1} are observed. In the specular spectrum several vibrational features are detected. First, we discuss only the absence of the vibrational modes which are assigned to in-plane modes ν(CC) of the benzylidene and aniline ring of the molecule located at 1568 (1570) ([Gae07]), and 1584 cm^{-1} ([Z.89]), respectively. Furthermore the stretch mode of the imine group ν(C=N) reported at 1638 cm^{-1} in reference [Gae07] is absent[14]. The missing vibrational modes are located either in the planes of the phenyl rings or in the plane of the imine group. Therefore we conclude that for the absorbed molecule the latter modes are missing most likely because of a parallel orientation of the molecule to the metal surface. The absence of the in-plane stretch modes ν(CC) and ν(C=N) leads us to the classification of the in the vibrational HREELS detected mode at 1183 cm^{-1} to the ρ(CH3) rocking mode of the *tert*-butyl legs. In the literature this region exhibits as well the ν(C-*ph*) and ν(N-*ph*) stretch vibrations, which are not likely to be detected for the preliminary assumed adsorption geometry with the imine group

[14]For comparison the IR spectrum of condensed TBI is shown in the lower part of figure 4.8

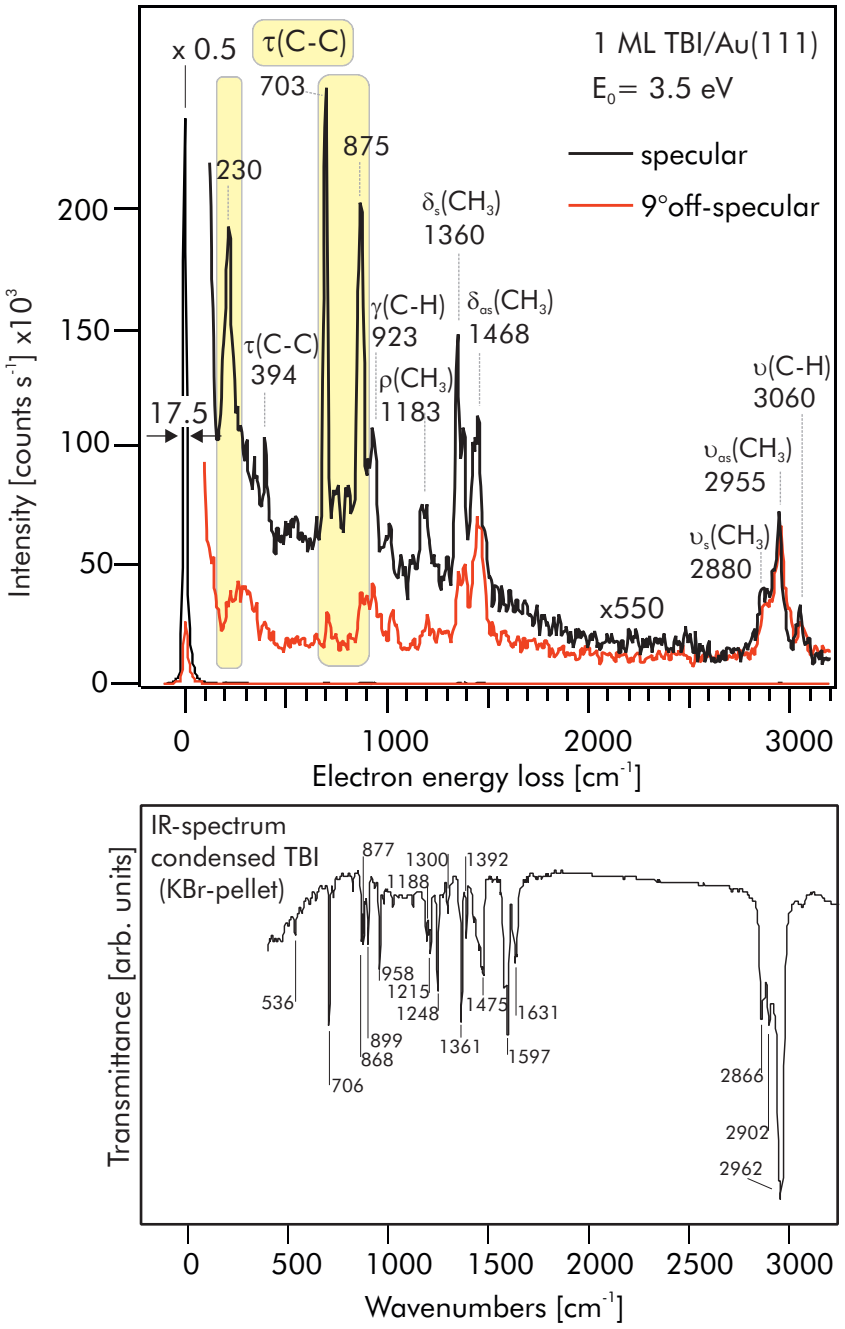

Figure 4.8: HREEL spectra of 1ML TBI adsorbed on Au(111) recorded in specular and 9° off-specular scattering geometry. The primary electron energy was set to 3.5 eV. The resolution is 17.5 cm^{-1} ($\approx$ 2.2 meV) [Mie11]. For comparison the IR-spectrum of the condensed TBI (KBr-pellet) is shown. The IR-spectrum has been taken in the group of R. Haag, Chemistry Department, FU Berlin.

and the phenyl rings lying parallel to the surface. The observed vibrational modes between 2800 and 3100 cm^{-1} arise from symmetric and asymmetric C–H stretch modes which are attributed to the CH_3 parts of the *tert*-butyl legs. These modes are therefore not valuable for the geometrical analysis since their orientation is expected to be such, that a component of the dipole moment change perpendicular to the surface is present for all kinds of possible adsorption geometries.

In order to gain further information on the adsorption geometry of TBI in the monolayer regime, we carried out angular-dependent HREELS measurements in specular (solid black line) and off-specular geometry (solid red line) (see figure 4.8).
We discuss here the relevant angular dependent vibrational modes for the determination of the adsorption geometry.

Most striking are the pronounced intensity drops of the out-of-plane torsion modes of the phenyl rings ((C-C)), at 230, 703, and 875 cm^{-1} [Z.89, Ova07] in the off-specular spectrum, indicating that their intensities in the specular spectrum mainly originate from dipole scattering. The strong dipole activity of the phenyl ring torsion modes arises from an orientation, where these modes have a strong dipole moment change upon vibration perpendicular to the surface.

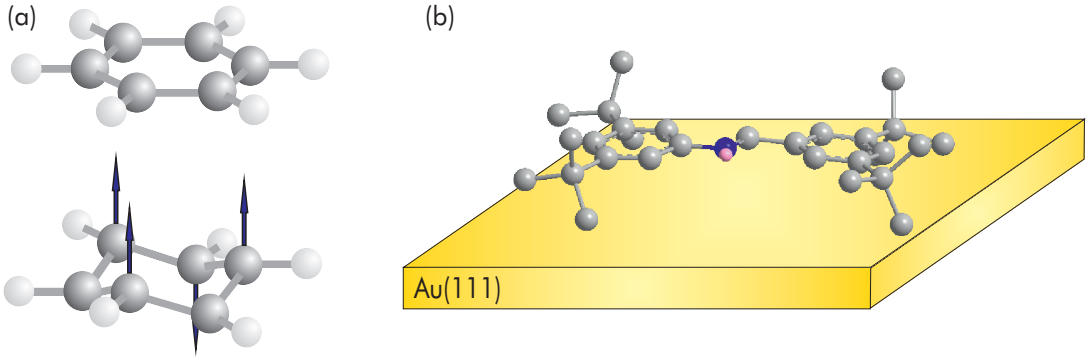

Figure 4.9: (a) Sketch of a phenyl ring and the corresponding out-of-plane phenyl ring torsion mode $\tau(C{-}C)$ to the vibrational feature at 703 cm^{-1} (see figure 4.8). Arrows indicate movement of the carbon atoms out of their former position in the plane of the phenyl ring. (b) Assumed planar adsorption geometry of TBI (shown without hydrogen atoms) on Au(111) due to the strong dipole activity of the out-of-plane phenyl ring torsion modes at 217, 703, and, 875 cm^{-1} (see Fig. 4.8).

Figure 4.9 (a) shows one of the dominant phenyl ring torsion modes of the HREELS spectra of one ML TBI adsorbed on Au(111) (see figure 4.8), *i.e.*, the out-of-plane torsion mode at 703 cm^{-1} [Gün96]. Due to the strong dipole activity of these modes, we conclude that the preferred orientation of the planar phenyl rings must be parallel or almost parallel towards the surface. Note that a similar adsorption behavior has been observed for TBA and the stilbene analogue on Au(111) [Ova07, Ley10]. Accordingly, the HREEL data indicates a planar geometry of the molecules when adsorbed on Au(111) as can be seen in figure 4.2.3 (b).

Our experimental findings are in contrast to the known geometry of the free molecules. According to experimental [EB71, Bür70] and theoretical [Pat85, Gae07] studies, the trans-isomer exhibits a highly non-planar configuration, which is caused by the conjugation between the aniline ring and the nitrogen lone pair resulting in torsion angles of the two rings about the imine group of $\approx 55^\circ$ and 10°, respectively[15].

vibrational mode	TBI/Au(111)[a]	experimental[b]	theoretical[c]
τ(CC), *ph*	230 (*da*)	275	–
τ(CC), *ph*; δ(CN)	294	299	–
τ(CC), *ph*	394 (*da*)	403	–
τ(CC), *ph*	703 (*da*)	692, 696	–
ring-vibration^{op}	–	750	–
δ^{op}(*ph*)	–	–	765
δ(C-*ph*)	–	–	766
τ(CC), *ph*	875 (*da*)	879	–
δ(N-*ph*)	875 (*da*)	–	879
γ(CH), *ph*; δ(CC),Ph	923	921	–
ν(CC), *ph*	1023	1008	–
ρ(CH3)	1183 (*da*)	1153	–
ν(C-*ph*); ν(N-*ph*)	–	1189	1170; 1199
δ_s(HCH)(CH3)	1360 (*da*)	1359	–
δ(CH), imine	1360 (*da*)	1370	1366
δ_{as}(HCH),CH3; ν(CC), *ph*	1468	1453	–
ν(CC), benzylidene ring	–	–	1568
ν(CC), aniline ring	–	–	1570, 1584
ν(C=N), imine group	–	1613	1638
ν_s(CH), CH_3	2880	2879	–
ν(CH)	2895	–	2906
ν_{as}(CH), CH_3	2955	2951	–
ν(CH), *ph*	3060	3000-3085	–

Table 4.3: Vibrational frequencies (in cm^{-1}) and assignments for a monolayer TBI adsorbed on Au(111).
s, indicates symmetric; *as*, asymmetric; ν, stretch; δ, in-plane bending; γ, out-of-plane bending; τ, torsion, ρ rocking, *ph* = phenylring.
[a] Values obtained from present HREELS study of 1 ML TBI adsorbed on Au(111) at sample temperatures of $T_S = 200$ K.
[b] Experimental assignments taken from references [Ost67, Z.89, Ova07] (solid state and solution IR and Raman spectra of N-benzylideneaniline, TBA/Au(111) HREELS measurement).
[c] theoretical assignments taken from references [Koz93, Gae07] (values obtained by normal coordinate analysis and DFT studies for N-benzylideneaniline).

[15] For details see chapter 2.2.2.

Despite the known geometry of the *trans*-isomer in the condensed or liquid phase, we support the observed planar adsorption geometry with results from a density functional theory study by D. Jacquemin *et al.*, where a calculated forced-planar geometry for unsubstituted N-benzylideneaniline is reported. The ground-state of this geometry is found to be 0.09 eV (71 cm^{-1}) [Jac09] higher in energy compared to the twisted ground-state geometry. This small energetic shift can probably be easily compensated by the interaction via van der Waals interaction between the flat lying phenyl rings and the gold substrate for planar TBI molecules.

Further proof of the proposed adsorption geometry illustrated in figure 4.9 (b) is given in the joint publication together with the group of L. Grill, FHI Berlin (see reference [Mie11]). Here, STM images of TBI on Au(111) after annealing the surface to approximately the same surface temperature as in the present HREELS study (T_S^{STM} = 230 K) show that the TBI molecules adsorbes in two different types of ordered islands. Either in a zigzag pattern or in ordered rows[16], similar to the behavior of TBA molecules on Au(111) which adsorb in their planar *trans*-geometry [Ale06]. Single molecules do appear in the STM images as four equally high lobes, which are attributed to the four *tert*-butyl-groups by comparison of the measured dimensions with calculated dimensions of TBI in the gas phase. Hence, there is no indication for a rotation of the phenyl rings out of the plane. Therefore and due to the resemblance of the STM images to the known images of TBA/Au(111) in its *trans*-state, the adsorption geometry is assigned to a planar *trans*-state of TBI on Au(111).

[16]The edge of an island of ordered rows can be seen in figure 4.12 (a). The assigned molecular structure has been drawn exemplary in the STM image for some molecules.

4.2.3 Thermally Induced Isomerization of 1ML TBI/Au(111)

We studied the effect of illumination on the vibrational structure of the TBI/Au(111) system. Light exposure with varying photon doses at 355 and 445 nm (3.5 and 2.8 eV), respectively, of 1 ML TBI adsorbed on Au(111) provoked no changes in the vibrational structure, *viz.*, no modification of the adsorption geometry is observed. We propose that the photoisomerization is suppressed for coverages $\leq$ 1 ML. Presumably, this arises from the electronic interaction between the molecules and the metallic substrate leading to ultrashort lifetimes of molecular excited states believed to be responsible for the isomerization.

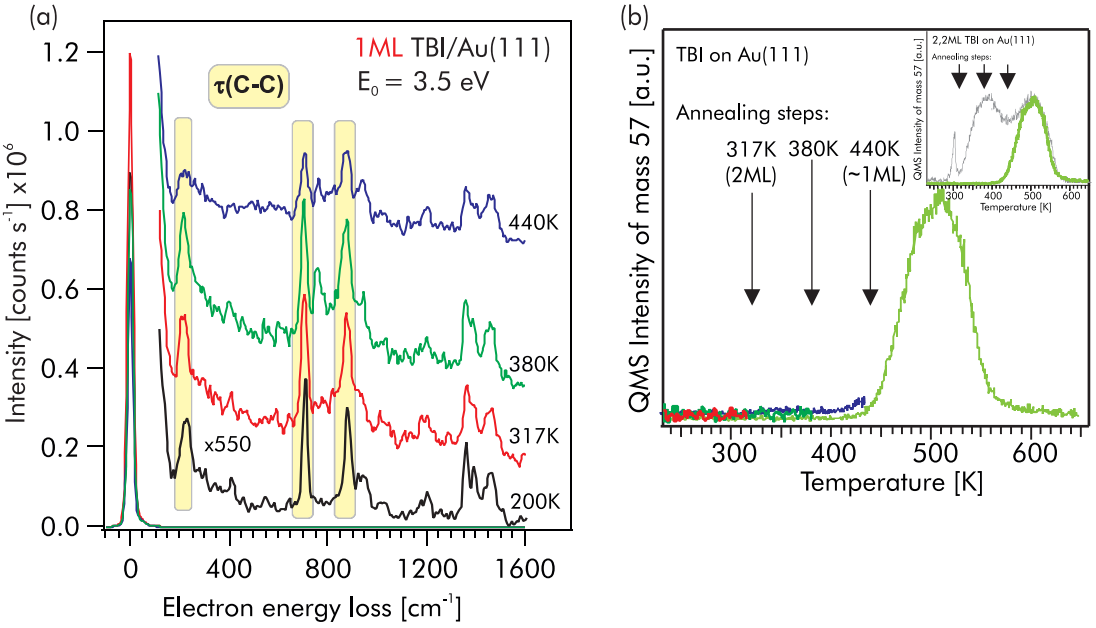

Figure 4.10: (a) HREELS spectra of 1 ML TBI on Au(111) deposited at a sample temperature of 200 K and after annealing to different temperatures, recorded in specular geometry with a primary electron energy of 3.5 eV. The resolution has been $\leq$ 20 cm^{-}1 (2.5 meV) for all measurements. The sample was heated for 2 min at the given temperatures, using a heating rate of 1 K/s, and subsequently cooled down to T_S = 100 K. (b) TPD spectra taken for the annealing steps. Shown is the signal for mass 57 amu ($C_4H_9^+$) as a function of temperature for the single annealing steps. Inset: For comparison the annealing steps and the subsequent full TPD to T_S = 650 K are plotted together with the TPD of 2.2 ML.

We performed HREELS measurements to gain insight into the molecular geometry following thermal activation. Figure 4.10 (a) shows HREELS spectra taken after deposition of 1 ML of the TBI molecules at T_S = 200 K and subsequent annealing steps to 317, 380 and 440 K. The resolution has been $\leq$ 20 cm^{-1} (2.5 meV) for all measurements. The single annealing steps have been performed in front of the QMS to assure that we started with the wanted quantity of molecules on the substrate,

i.e. one monolayer. Figure 4.10 (b) shows the QMS signal of mass 57 for the single heating steps. After the final HREELS measurement a full TPD to T_S = 650 K has been recorded. The HREELS spectra of the *trans*-TBI are dominated by the intense phenyl ring torsion modes which are highlighted in figure 4.10 (a)[17] located at 230, 703, and 880 cm^{-1} up to heating temperatures of 380 K, due to the planar (*trans*-) adsorption geometry (see figure (b)). After heating the sample to 440 K a very strong intensity decrease of theses vibrational modes is observed, which we assign to a conformational change to *cis*-isomers with one phenyl ring pointing upwards, in analogy to the HREELS measurements of the *trans* to *cis*-isomerization of TBA on Au(111) [Ova07] and in comparison to the taken STM-images (figure 4.12 (a)). Note that the spectral changes are not caused by a reduced TBI coverage, since thermal desorption spectroscopy shows basically no desorption at these conditions (see blue line in figure 4.10 (b)). Therefore we assign the observed changes to a *trans* to *cis* isomerization of TBI on Au(111) which is illustrated in figure 4.11.

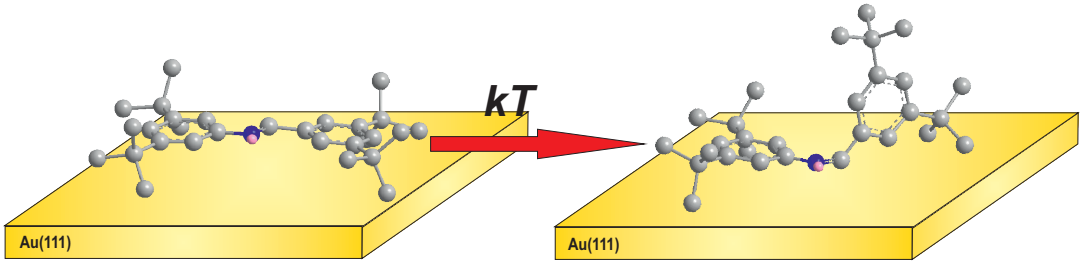

Figure 4.11: Schematic illustration of the measured adsorption geometries of *trans*-TBI/Au(111) and for *cis*-TBI/Au(111), found at 210 K and after annealing to T_S > 380 K, respectively.

Since it is known that isomerization of this class of molecules can also be achieved by STM manipulation [Ale06, Cho06, Hen06, Dri08, Ale08], attempts have been made by L. Grill *et al.* to achieve a switching of the TBI molecules on Au(111) by applying voltage pulses to a single molecule. For two different manipulation strategies ((i) to increase the voltage up to ± 2.5 V and (ii) using small voltages and high currents up to 100 nA) no isomerization could be induced [Mie11].

However, directly after adsorption, some of the molecules appear as bright spots in the STM image (see figure 4.12 (a)) with an apparent height of 3.9 ± 0.3 Å above the surface, while for the protrusions of the *trans*-isomers appear at 2.4 ± 0.2 Å. A characteristic height profile across such a feature is presented in figure 4.12 (b). These bright spots are typically found either in small, disordered islands or at the border of large islands. Only in few cases they are located inside ordered islands. It is very important that these spots have a similar appearance compared to TBA molecules in their *cis*-form [Dri08], which exhibit an apparent height of 4.1 ± 0.3 Å. Moreover, three small protrusions are visible close to the bright lobe (inset in figure 4.12 (a)), in similarity

[17] Compare with chapter 4.2.2.

to TBA molecules, where these weaker protrusions could be assigned to the *tert*-butyl legs of the molecule by comparison with calculations [Dri08].

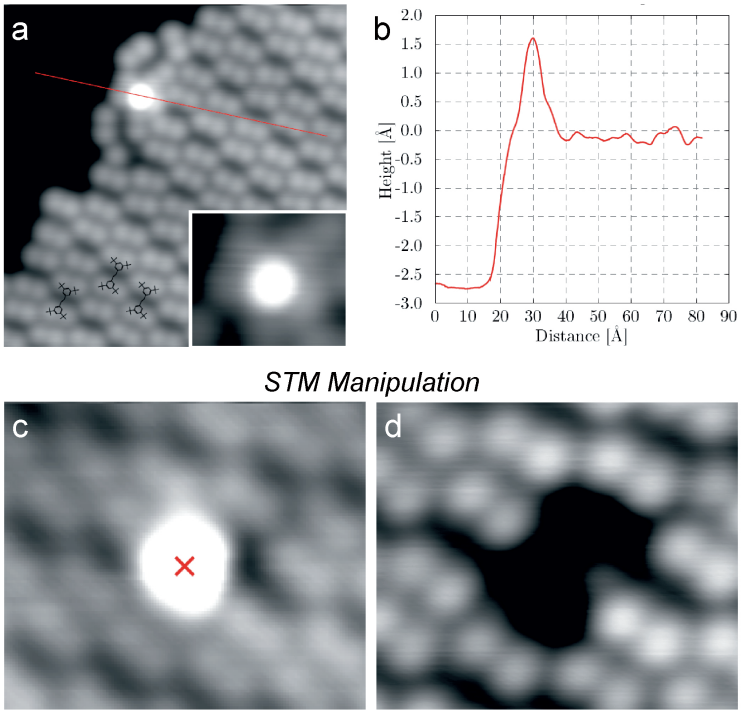

Figure 4.12: (a) STM image (9.4 × 9.4 nm^2) of an island with close-packed TBI molecules, one of them appearing as a bright protrusion. The inset (1.9 × 1.7 nm^2) shows the area of the bright protrusion, revealing the typical appearence with two weaker protrusions at the left side and one at the right side of the bright spot. (b) Height profile along the line in (a): the average spot height above the gold surface is 3.9 ± 0.3 . (c,d) STM images (both 4.7 × 4.0 nm^2) of the same surface area before (c) and after (d) a voltage pulse is applied with the STM tip above the bright protrusion (marked as a cross in (c)). During the pulse, the voltage is increased linearly during 1 min from 1 to 2.5 V (with a tunneling current up to 7 nA). The STM pictures have been taken in cooperation with the group of L. Grill, FHI Berlin [Mie11].

The observation of molecule removal during STM manipulation is shown in figure 4.12 (c-d). When applying a voltage pulse above an individual molecule (at the marked cross in figure 4.12 (c)), it is sometimes observed that the entire protrusion vanishes from its former area (see subsequent STM image in figure 4.12 (d)). In its place, a hole is found in the molecular island instead, which exhibits a contour that precisely resembles the rectangular shape of a single *trans*-isomer. Together with their typical appearance, we therefore assign these bright lobes to individual *cis*-isomers of the TBI molecules.

It is known that for this kind of molecules switching can be achieved when sufficient thermal energy is supplied to overcome the activation barrier. In the STM measure-

ments annealing experiments have been performed. Remarkably, the number of bright spots, which are assigned to the *cis*-species, rises strongly, when heating up the surface to temperatures up to T_S = 468 K. Note, that for this temperatures desorption starts, therefore the appearance of more spots is not likely to be related to contamination. The experimental findings of this STM study support the assignment of the thermally induced changes in the HREELS spectra to a thermally activated *trans*→*cis*-isomerization

If the assignment of both investigations (HREELS and STM) is correct, than this behavior is highly surprising regarding the known thermally activated *cis* to *trans* relaxation for *cis*-TBA on Au(111) [Hag07].

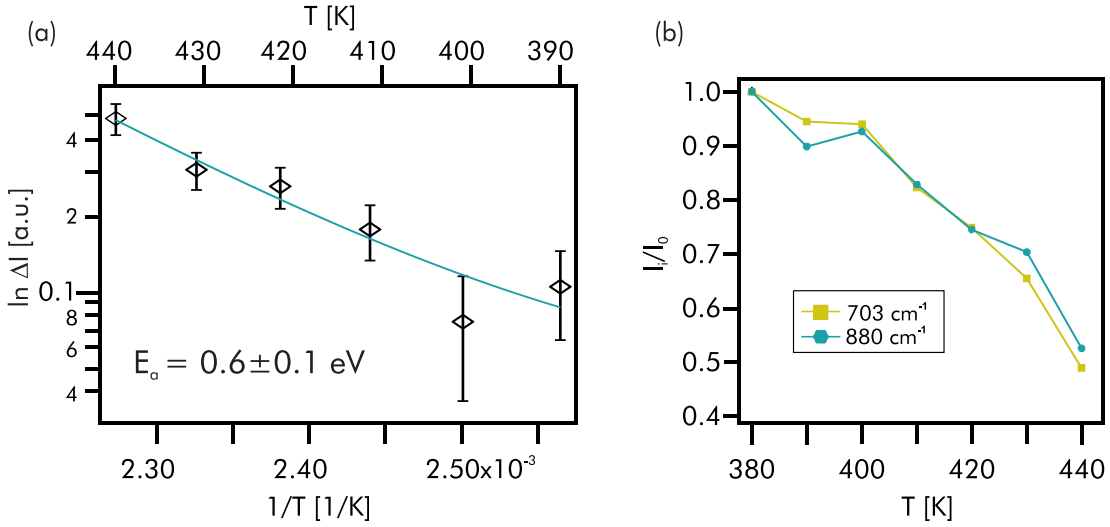

Figure 4.13: (a) Logarithmic intensity change ln $\Delta I = ln((I_0 - I_i)/I_0)$ of the phenyl ring torsion mode at 880 cm^{-1} as a function of the substrate temperature. The fit (solid line) and the activation energy (E_A) for the thermally induced *trans* to *cis* isomerization of TBI on Au(111) were obtained by using the Arrhenius expression given in equation 4.11. (b) Relative intensity change I_i/I_0 of two phenyl ring torsion modes at 703 and 880 cm^{-1} as a function of the substrate temperature.

Considering the reverted equilibrium between the two isomers when adsorbed on Au(111), it is desirable to gain insight into the origin of the larger stability of the *cis*-isomer on the gold substrate. Therefore we studied the changes of the vibrational loss intensities during the thermally induced *trans* to *cis* isomerization, providing a quantitative insight into the activation barrier. Specifically, the temperature induced intensity changes of the phenyl ring torsion modes at 703 and 880 cm^{-1} (see 4.13 (b)), respectively, were used as a quantitative measure for the reaction. The activation energy (E_A) is determined from the relative change in peak intensity

$$\triangle I_i = \frac{I_{317K} - I_{iK}}{I_{317K}} \tag{4.10}$$

between the *trans*-TBI covered surface at 317 K and the same surface annealed to a particular temperature, using the Arrhenius-like expression

$$\Delta I = I_p \exp\left(-E_A/k_B T\right) \tag{4.11}$$

(with I_p an intensity pre-exponential factor and k_B the Boltzmann constant [Ova07]).

Note that the temperature series was done on a freshly prepared film for each temperature step. At each particular temperature the same annealing times (2 min) have been used. As can be seen in 4.13 (b) the intensity of both modes shows the same temperature dependent behavior. From these measurements we derived a value of 0.6 ± 0.1 eV for the activation energy (see figure 4.13 (a)). In comparison, for free imine derivatives in solution the barrier between the stable *trans*- and the metastable *cis*-form is around 1 eV [Gae07]. Thus, we found a barrier reduction of 0.4 eV for the surface bound TBI, indicating that the potential energy landscape is significant different from that in the free molecule. Moreover, at the surface, the *cis*-isomer turned out to be the energetically more stable species, reversing the situation known for the TBI in the liquid phase.

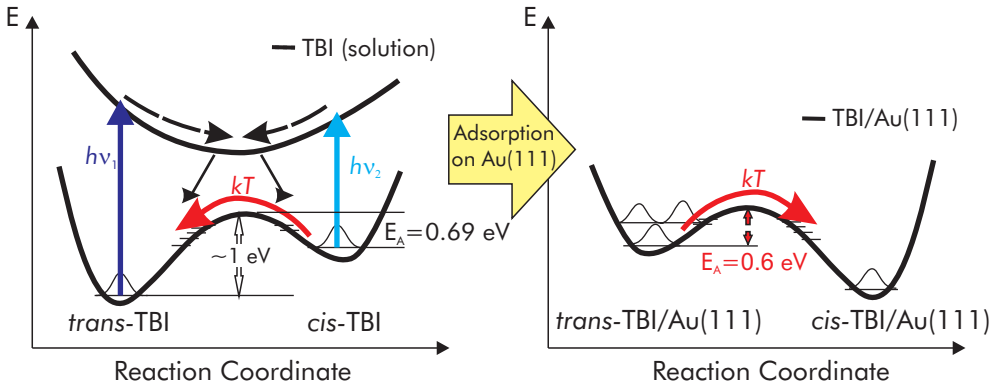

Figure 4.14: Scheme of the potential energy landscape of the TBI molecule in solution and after adsorption on Au(111). Also shown are the known excitation mechanisms and the activations barriers for the thermal relaxation of the molecule from its meta-stable to its stable ground state, *i.e.* *cis*→*trans* for TBI in solution, and *trans*→*cis* for TBI/Au(111), respectively.

Figure 4.14 schematically shows the potential energy landscape for TBI in solution and after adsorption on Au(111) regarding the "inverted" isomerization behavior and the determined barrier for the thermal *trans*→*cis* isomerization of TBI/Au(111) according to our experimental results. Shown are as well the known excitation mechanisms, *i.e.* photoexcitation to the excited state and thermally activated relaxation from the meta-stable *cis*- to the stable *trans*-isomer, for TBI in solution.

While the *trans*- TBI molecules interact rather weakly with the Au(111) surface, due to the tert-butyl legs and in similarity with the TBA molecules [Hag07], this might be different when they are in the *cis*-state, because the lone pair electrons of the N atom can eventually reach the metal surface. A possible enhanced molecula/substrate interaction could be given by the lone pair electrons with the metal substrate. Such an interaction would be sterical more likely with the molecule in the *cis* state.

4.2.4 Thermally and Coverage Induced Isomerization: 2ML TBI/Au(111)

We investigated the adsorption and thermal isomerization behavior of the bilayer regime of TBI on Au(111). Figure 4.15 (a) shows HREELS spectra taken after deposition of 2 ML of the TBI molecules at T_S = 210 K and subsequent annealing steps to 317, 380 and 440 K. Identical to our investigation of 1 ML TBI/Au(111). The resolution has been $\leq$ 20 cm^{-1} (2.5 meV) for all measurements. The single annealing steps have been performed in front of the QMS to assure that we started with the wanted quantity of molecules on the substrate, *i.e.* the bilayer. Figure 4.10 (b) shows the QMS signal of mass 57 for the single heating steps. After the final HREELS measurement a full TPD to T_S = 650 K has been recorded.

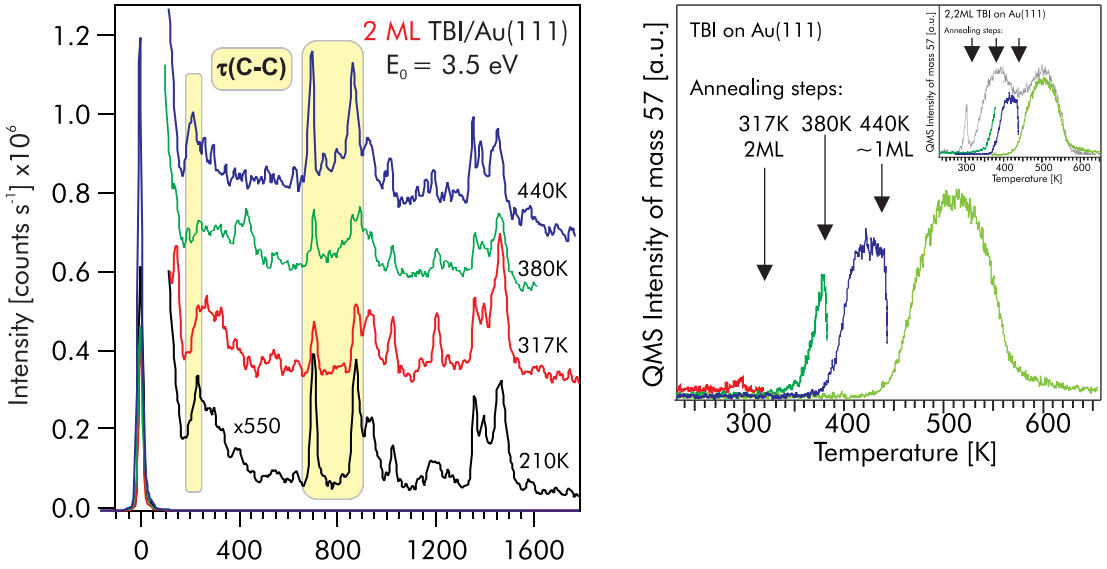

Figure 4.15: (a) HREELS spectra of 2 ML TBI on Au(111) deposited at a sample temperature of 210 K and after annealing to different temperatures, recorded in specular geometry with a primary electron energy of 3.5 eV. The resolution has been $\leq$ 20 cm^{-1} (2.5 meV) for all measurements. The sample was heated for 2 min at the given temperatures, using a heating rate of 1 K/s, and subsequently cooled down to T_S = 100 K. Highlighted are the phenyl ring torsion modes τ(CC), since they are used as a measure for the isomerization state. (b) TPD spectra taken for the different annealing steps. Shown is the measured signal of mass 57 amu as a function of temperature for the single annealing steps. Inset: For comparison the annealing steps and the subsequent full TPD to T_S = 650 K are plotted together with the TPD of 2.2 ML.

When adsorbing a bilayer on Au(111) at sample temperatures of T_S = 210 K (black line in figure 4.15) we find the vibrational structure of the two monolayers covered surface to be identical with the one found for a single monolayer on Au(111) dosed at T_S = 200 K (black line in figure 4.10). Especially the high intensities of the dipole active phenyl ring torsion modes in the spectra taken at $T_S \approx$ 210 K (highlighted in figure 4.15), which has been used to characterize the isomerization behavior, closely

resembles the one found for 1 ML TBI/Au(111). Therefore the adsorption geometry of the bilayer is assigned to a planar (*trans*-) geometry, consistent with the discussion of the adsorption geometry for the first layer[18].

The HREELS spectra of the *trans*-TBI in the second layer are dominated by the intense phenyl ring torsion modes τ(CC) which are highlighted in figure 4.15 (a) located at 230, 700, and 880 cm^{-1}. But already the first annealing step to 317 K leads to a very strong intensity decrease of these vibrational modes, which we assign to a conformational change to *cis*-isomers with one or both of the phenyl rings pointing upwards, in analogy to the HREELS measurements of the *trans* to *cis* isomerization of 1 ML TBI on Au(111) in chapter 4.2.3. Note, that at this annealing temperature[19] almost no desorption is visible as can be seen in figure 4.15 (b). Therefore we assign the observed changes to a *trans* to *cis* isomerization of 2 ML TBI on Au(111). When annealing to sample temperatures of 380 K, the intensity of the τ(CC) marker modes stays unchanged within the precision of the measurement. As it is expected for the bilayer, this annealing temperature leads to desorption of TBI molecules as can be seen in figure 4.15 (b).

To summarize the experimental findings for the bilayer so far, the *trans*→*cis* isomerization is already observed at lower temperatures (317 K for 2 ML compared to 440 K for 1 ML TBI/Au(111)) when the surface coverage is unchanged and the vibrational fingerprint stays unchanged when heating to 380 K desorbing ≈ 50 % of the second layer. But when the surface is heated to 440 K, which is exactly equivalent to the complete desorption of the bilayer, the intensity of the marker modes fully recovers (blue line in figure 4.15 (a)). Following our previous interpretation of the adsorption geometry, we conclude that the entire removal of the second (*cis*-) layer leads to a full monolayer of *trans*-isomers on the surface. The fact that different molecular configurations are found for equal coverages annealed at the same temperature is highly surprising and shows that a delicate balance of the influences of substrate/adsorbate- versus adsorbate/adsorbate interaction may govern the switching properties of molecular switches on surfaces. Starting with different coverages and heating up the surface to T_S = 440 K, equivalent to the removal of the second layer for 2ML/TBI and no desorption for 1ML/TBI, leads to a different isomerization state of 1 ML TBI on Au(111).

After we performed the final heating step to 440 K, which led to the emergence of the *trans*-monolayer TBI on gold, we repeated the annealing step at T_S = 440 K this time for 5 minutes, consecutively cooled the sample to 100 K and took another HREEL spectrum. The result clearly shows the strong decrease of the τ(CC) marker modes prototypical for the *cis*-isomer of TBI. This resembles the known isomerization behavior for 1 ML TBI/Au(111) as it has been discussed in chapter 4.2.3.

The observed isomerization states of TBI/Au(111) when starting with a two monolayers coverage on the Au(111) surface after performing the above described heating steps are summed up in figure 4.16. Hence the adsorption geometry for both coverage regimes after adsorbing at T_S ≈ 200 K is the *trans*-state, we believe that TBI adsorbs

[18] Compare with chapter 4.2.2.

[19] Corresponding to the multilayer desorption temperature

Coverage:	2 ML	2 ML	1.5 ML	1 ML	1 ML
Switching State:	*trans*	→ *cis* →		*trans*	*cis*
Temperature T_S:	210K, 2 min	317K, 2 min	380K, 2 min	440K, 2 min	440K, 5 min

Figure 4.16: The determined switching states of TBI/Au(111) starting from two monolayers coverage adsorbed on the Au(111) surface at T_S = 210 K and after heating the sample to T_S = 317, 380, and 440 K, respectively.

from the stable *trans*-state in the gas-phase. Whereas the molecules for coverages exceeding one monolayer switch to the *cis*-state by sample heating, we find the molecules in their initial *trans* adsorption geometry after removal of the second layer. The fact that the *trans*→*cis* isomerization for the second layer takes place already at lower temperatures could be understandable when considering the weaker bond strength of the second layer[20]. The finding of a *trans*-layer after removal of the second layer is surprising. A possible explanation could be given by the assumption that if parts of the multilayer desorb the monolayer density would be increased when the molecules switch to the *cis*-state (and further incorporation of molecules from the second layer). This gain in adsorption energy could overcompensate the energy cost for isomerization. Further annealing leads to the desorption of molecules (now in their *cis*-state) and leaves open space for the isomerization back to the planar *trans*-isomer. When heating the *trans*-layer for longer times at 440 K we find a *trans*→*cis* isomerization, similar to the one observed for the results starting with one monolayer coverage (see chapter 4.2.3). We believe that the two observed *cis*-species are not identical, arising from their binding situation, *i.e.* directly bond to the gold substrate for coverages $\leq$ 1 ML or their binding situation being influenced by the surrounding molecules. One reason for the different *cis*-states depending on the environment is already discussed in the end of the last chapter and could be due to a possible chemical interaction of the nitrogen lone pair with the metal surface resulting in an increased coupling to the substrate for coverages $\leq$ 1 ML. Hints for the presence of two different *cis*-species are found in the HREELS-spectra in figures 4.10 and 4.15. For the *cis*-species in figure 4.10 starting with a coverage of $\approx$ 1 ML an additional vibrational mode is detected at $\approx$ 760 cm^{-1} which is not detected for the *cis*-species observed at 2 ML starting coverage (see figure 4.15). Assignment of this mode has not been made since in this energetic range a variety of possible vibrational modes is found. It possesses an energy to high to result from a gold-molecule vibrational mode but additional vibrational modes could occur if the geometry of this stabilized *cis*-species (or the force constant of vibrational modes) is altered due to the additional coupling to the substrate.

[20]Compare with the lower desorption temperatures of the second layer in figure 4.7.

4.2.5 Summary

In this contribution high resolution electron energy loss spectroscopy (HREELS) has been employed to analyze thermally activated changes in the geometrical structure of the photochromic molecular switch 3,3',5,5'-tetra-tert-butyl-imine (TBI) adsorbed on Au(111). TBI in solution undergoes an optically induced isomerization between a stable *trans*- and a metastable *cis*-isomer. Measurements have been performed for two coverage regimes: The monolayer and the bilayer regime. For both coverages all molecules are found in the *trans*-state after deposition at sample temperatures of $T_S = 210$ K, but conformational changes upon heating are observed, which are assigned to a switching process, *e.g.* isomerization to the *cis*-state. When heating the sample to $T_S = 440$ K two different scenarios are observed depending on the starting coverage.

Annealing of a monolayer leads to an increasing number of *cis*-isomers, pointing towards an "inverted" thermal isomerization behavior, since it is known for the molecules in solution that the *trans*-isomer is the more stable compound which results in a thermal *cis* to *trans* relaxation upon sufficient heating [Mie11].

We investigated the changes in the vibrational loss intensities during the trans to cis transition to gain a quantitative insight into the activation barrier governing the thermally induced *trans* to *cis* isomerization. The activation energy E_A is determined using an Arrhenius-like expression. From these measurements we derived a value of 0.6 ± 0.1 eV for the activation energy (see figure 4.13 (a)). Thus, we found a barrier reduction of 0.4 eV for the surface bound TBI, indicating that the potential energy landscape is significant different from that in the free molecule. Moreover, at the surface, the *cis*-isomer turned out to be the energetically more stable species, reversing the situation known for the TBI in the liquid phase. The reason for this surface-mediated effect could be a stronger coupling of the central imine part of the molecule in its *cis*-configuration to the Au(111) surface, as compared to the *trans*-state. This would be sterical only possible for the *cis*-isomer.

Whereas for a bilayer the temperature induced *trans*→*cis* isomerization of the TBI can be monitored as well, but complete desorption of the second layer at $T_S = 440$ K leads to the formation of a *trans*-monolayer. The fact that different molecular configurations are found for equal coverages annealed at the same temperature is highly surprising and shows that adsorbate/substrate-interactions and coverage dependent effects may govern the switching properties of molecular switches on surfaces. When annealing this *trans*-monolayer further we observe a *trans*→*cis* isomerization similar to the one observed with 1 ML TBI/Au(111) as the starting condition.

We believe that the two observed *cis*-species are not identical, arising from their binding situation, *i.e.* directly bond to the gold substrate for coverages ≤ 1 ML or their binding situation being influenced by the surrounding molecules. One reason for the different *cis*-states depending on the environment is discussed in chapter 4.2.3 and could be due to a possible chemical interaction of the nitrogen lone pair with the metal surface resulting in an increased coupling to the substrate for coverages ≤ 1 ML.

5 Nitro-spiropyran on Au(111)

In this chapter the results of our studies for a second class, besides the already reviewed molecules which undergo a *trans/cis*-isomerization, of prototypical molecular switches are given. Molecules that undergo a reversible, optically and thermally induced ring openining/closing-reactions, *e.g.* spiropyran-, spirooxazin-, and benzopyranderivatives, have attracted great attention because of the drastic change of the molecular properties through the formation and breaking, respectively, of an intramolecular bond.

We investigated the chemical transformation between spiropyran (SP) and merocyanine (MC) on a Au(111) surface. In figure 5.1 the in this chapter measured 1,3,3-trimethylindolino-6-nitrobenzopyrylospiran is displayed as an ball-and-stick model.

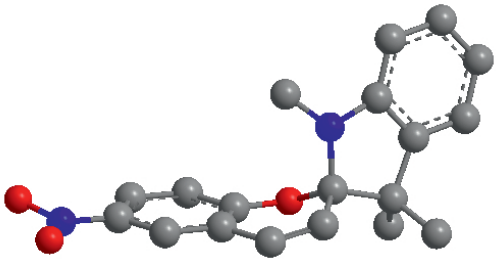

Figure 5.1: Ball-and-stick model of 1,3,3-trimethylindolino-6-nitrobenzopyrylospiran (spiropyran, SP). The geometry of the closed spiropyran is determined by the sp^3 hybridized carbon atom resulting in an twisted orientation with a perpendicular alignment between the indoline and the benzopyran group.

The SP-to-MC transformation follows a multistep pathway where the C–O bond breaking in the spiropyran is the rate determining step [Cot04]. The fission of the bond triggers a complete change of fundamental molecular properties including the molecular structure and the charge distribution. Starting from the colorless, three-dimensional SP form the molecules transform to the closed MC form exhibiting a planar, conjugated conformation which is highly chemical active and can be found in a zwitterionic state possessing a large dipole moment.

Up till now most experiments concerning the ring-opening/closing reaction have been performed in solution. Here the ring-opening process can be triggered by illumination with UV light. Irradiation with visible green light on the other hand is responsible for the ring-closing reaction. Furthermore the molecule can be transformed from its open photocolored MC form to its thermodynamically stable parent compound SP *via* a thermally induced back-reaction[21]. The huge change in the molecular properties has led to a wide prediction of possible applications, including storage devices [Par89, Ber00, Ray02], molecular sensors and detectors [Byr06] and to induce reversible chemical and/or optical properties of organic-inorganic interfaces as a novel concept in chemical sensing [Rad07].

A key point of this work is to achieve reversible changes in the molecular conformation for adsorbed molecules. This is of fundamental importance for the incorporation of the molecular functionality into functional devices. It is well known that the potential energy surfaces are affected when the molecules are condensed on the surface [Hag08a, Wol09]. The changes in the ground state potential energy surface is capable

[21] For details see chapter 2.2.5.

of modifying the equilibrium structure [Hen08, Hen07b, Pia08]. Even the chemically inert gold surface can exhibit a non-covalent interaction with the adsorbates which is strong enough to influence the molecular conformation [Hen07a] and can even cause consequent shifts of the thermodynamic equilibrium[22]. From STM measurements it is reported that spiropyran molecules form ordered structures when adsorbed on Au(111) [Hua07], but reports of stable phases of the open merocyanine isomer remain absent.

Based on our results we emphasize, that the usage of metal surfaces and clusters is well suited to mediate the reaction and to stabilize former metastable states of molecular switches.

[22]Compare as well with chapter 4.2.

5.1 Coverage Quantification of Nitro-spiropyran on Au(111)

To gain control over the exact coverage of the trimethyl-6-nitro-spiropyran adsorbed on Au(111), we performed TPD measurements for different dosing times. The spiropyran exhibits a molecular mass of 322 amu which exceeds the upper instrumental limit which is at 100 amu for the used mass spectrometer. Therefore we had to choose a fragment which is correlated with the desorption rate of the spiropyran (see chapter 3.4). Figure 5.2 shows a detail of a residual gas analysis (RGA) performed before and after evaporating spiropyran in the UHV-preparation chamber.

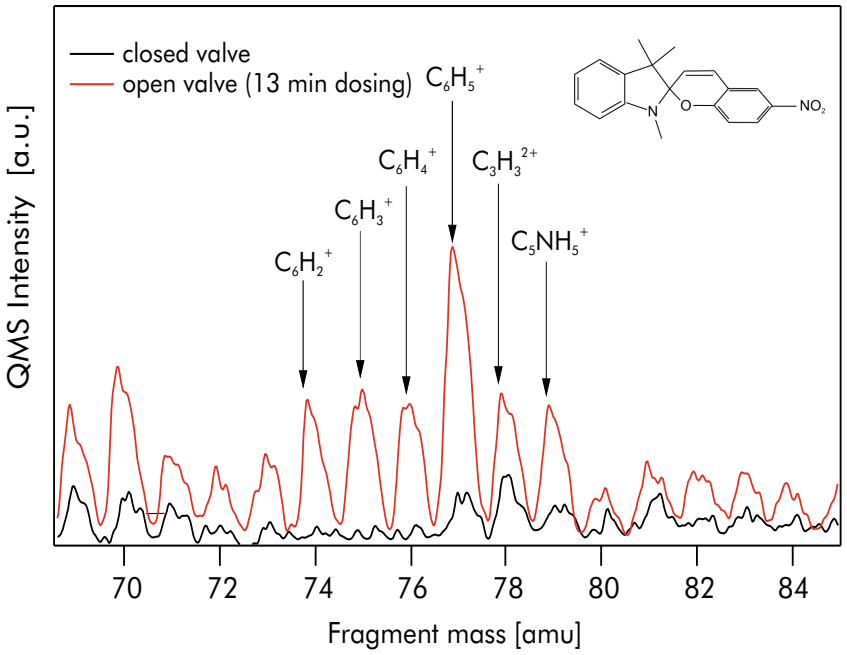

Figure 5.2: RGA spectra before (solid black line) and after evaporation of spiropyran (solid red line) shown in a regime between mass 69 and 85 amu. The spectra have been taken before (with the valve closed between the UHV-preparation chamber and the evaporator) and after dosing the spiropyran for 13 min.

The first spectra (solid black line) has been taken with the gate valve between the preparation chamber and the evaporator being closed and the second spectra (solid red line) shows the results with an open valve after 13 minutes of dosing with a doser temperature of $T_D = 358$ K. The highest intensity is found for the fragment of an ionized phenylring ($C_6H_5^+$) at 77 amu.

Neighboring peaks have been assigned to further C_6H_X-ions, double ionized fragments ($C_3H_3^{2+}$) and a fragment which can be deduced from an ionized phenylring carrying an additional nitrogen atom.

Figure 5.3 shows TPD spectra at mass 77 amu taken after dosing spiropyran with increasing dosing times from 1 to 16 min. We did not define the coverage for one mono-

layer as it is possible that the molecules dissociate during desorption as can be seen in figure 5.4 and is discussed later on. After adsorbing > 1 ML, the multilayer peak starts to develop at $T_S \approx 365$ K , gaining in height and width.

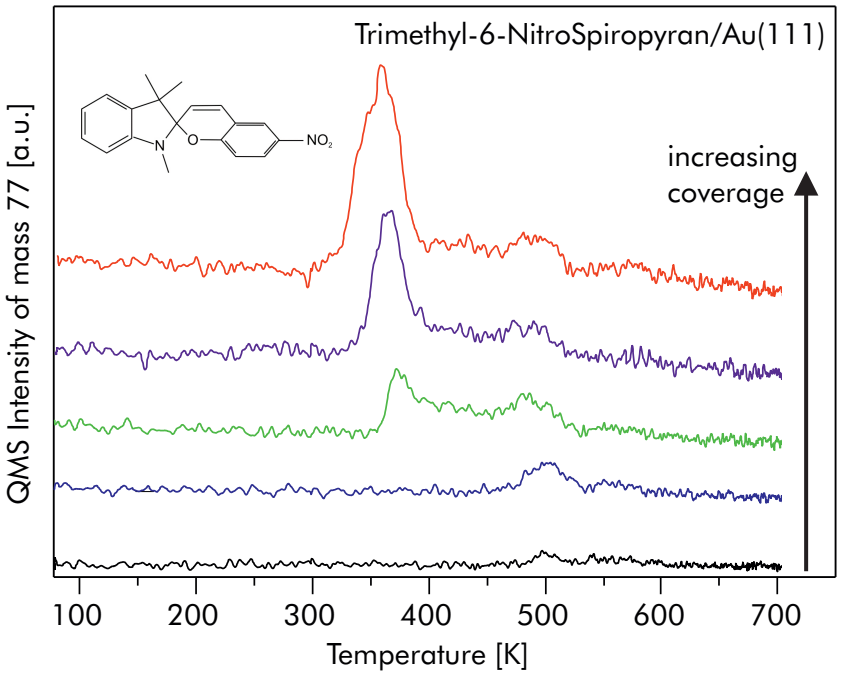

Figure 5.3: TPD spectra of spiropyran on Au(111) taken at mass 77 amu for different dosing times.

HREELS measurements have been performed after the execution of a full TPD spectrum, where the adsorbate covered (≈ 0.5 ML Spiropyran on Au(111)) surface has been heated up to $T_S = 700$ K.

The resulting HREELS spectrum is shown in figure 5.4 as a solid black line. It clearly shows that even after exceeding the desorption temperature about ≈ 200 K fragments of the molecule remain adsorbed on the gold surface.

Two major, rather broad contributions are observed, the maxima located at ≈ 420 and ≈ 770 cm^{-1}, respectively. The former region is characteristic of C–C torsion modes τ(C–C), whereas the latter typically corresponds to C–H bending modes γ(C–H). The excited vibrational features exhibit a broad energetic distribution, which is most likely caused by vibrations of various fragments in an energy regime close to the original vibrational mode.

Performing a full sample preparation cycle of Argon sputtering at p=$2*10^{-6}$ mbar followed by an annealing step of the sample at $T_S = 800$ K leads to a complete removal of the described features (see solid red line in figure 5.4). We conclude that the trimethyl-6-nitro-spiropyran dissociates at least partially during the thermal desorption. A possible reason for the strong interaction with gold substrate is discussed in the results section in chapter 5.3.

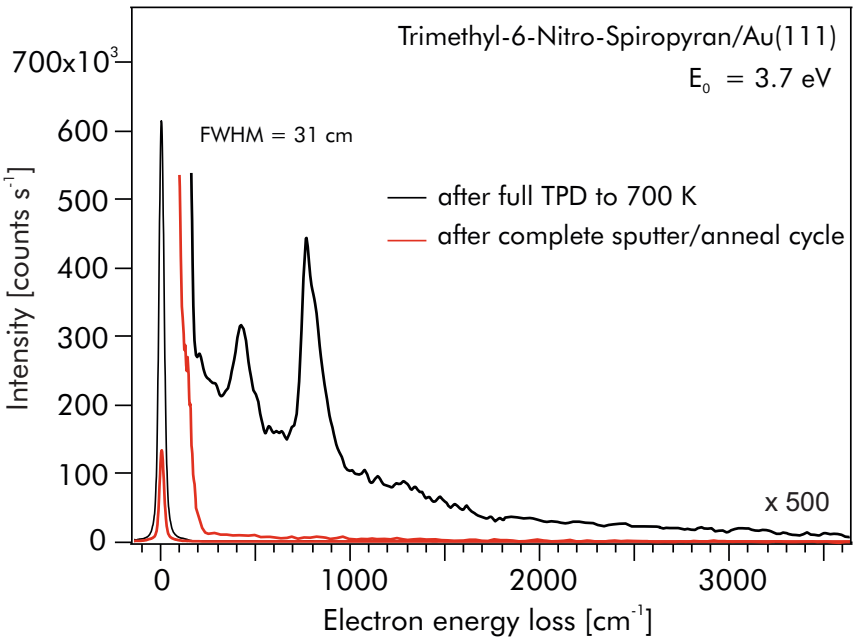

Figure 5.4: HREEL spectra of spiropyran on Au(111) taken with primary electron energies of $E_0 = 3.7$ eV after annealing at 700 K (solid black line) and after a full sputter/anneal cycle (solid red line), respectively.

For further experiments the preparation of adsorbate covered surfaces has only been performed for freshly prepared Au(111) surfaces.

5.2 Thermally Activated Ring-Opening Reaction

The adsorption behaviour of a sub-monolayer spiropyran on Au(111) as a function of substrate temperature has been studied by means of STM in the group of J. I. Pascual in the physics department of the FU Berlin[23]. The molecular layer has been deposited on a cold Au(111) surface and the STM experiments have been performed at a temperature of 5 K using a custom-made low-temperature STM. When annealing the surface at temperatures T_S ≥220 K, the molecular layer undergoes an ordering transition[24]. The resulting STM image is shown in figure 5.5 (a) revealing the formation of extended self-assembled domains.

Within these extended molecule covered areas a structure is noticeable, revealing that the islands are composed of molecular rows along which the molecular orientation alternates (see inset of figure 5.5 (a)). Despite the observed anisotropic structure, the domains show an overall rounded shape. This indicates that the intermolecular interaction is of comparable strength both in the direction and across the direction of the rows. The herringbone reconstruction of the Au(111) surface can be recognized unperturbed underneath the adsorbed molecular layer indicating that the molecules populate weakly bond adsorption states. This result is known for several low-temperature phases of organic molecules adsorbed on Au(111) [FT06].

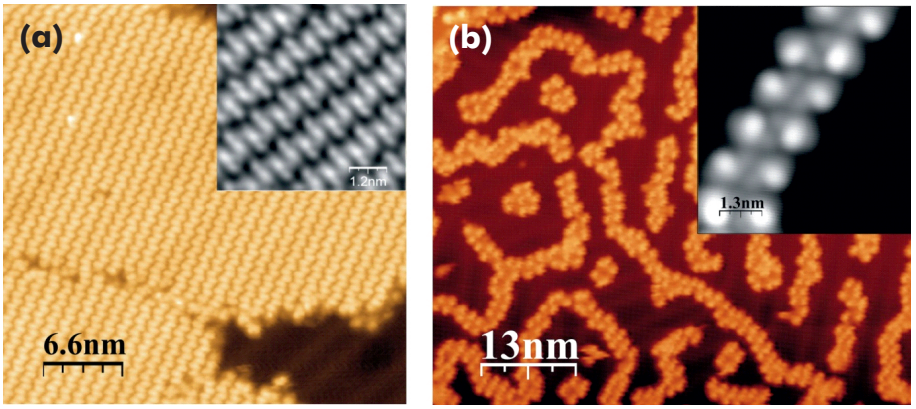

Figure 5.5: (a) STM image of adsorbate-covered Au(111) surface annealed at $T_S \approx 240$ K. The height of the molecular islands oscillates around 0.3 ± 0.1 nm depending on the applied sample bias. Inset: High-resolution STM image showing an alternating alignment of molecules along rows. (b) STM image of adsorbate-covered Au(111) surface annealed at $T_S \approx 300$ K. Inset: High-resolution STM image showing that the molecular chains exhibit an intramolecular pattern composed of a 0.1 nm high planar oval structure with a 0.25 nm high internal lobe. Figures adopted from joint publication [Pia09].

From the STM images it is not *a priori* possible to distinguish between the open or closed form, but the high-resolution STM image (inset of figure 5.5 (a)) exhibits that

[23] Subproject A1 of the SFB 658.

[24] STM and HREELS measurements have also been performed directly after the adsorption at 170 K resulting in a disordered phase of the adsorbate.

all molecules feature the same shape and orientation on the surface. This demonstrates that only one molecular species is present in the observed domains. The intramolecular chirality could equally be explained by the presence of the chiral SP or prochiral MC isomers. The structure and the dimensions of the unit cell (1.2 nm $*$ 1.1 nm) agree with the previous observation reported in reference [Hua07], which where attributed to the SP isomer.

When the surface is heated to temperatures of $T_S \approx 300$ K, the appearence of the adsorbate layer change drastically. The former resolved two-dimensional molecular islands disappear, and a new phase composed of molecular chains is observed (figure 5.5 (b)). Here the chains do show a preference to follow the underlying herringbone structure of the Au(111) surface, which expresses an enhanced interaction with the metal surface. Furthermore, as a characteristic of long-range repulsive interaction among chains, lateral packing is not observed. The described repulsive behavior has been observed for ensembles of of organic molecules with large dipole moments or charge transfer on metal surfaces [Bab07, Yok07, FT06]. Summarizing, this expresses a stronger interaction of the high-temperature phase with the metal substrate. The described transformation is not reversible, confirming that the chain-structure is the thermodynamically stable configuration on Au(111)[25]. The inset of figure 5.5 (b) shows a close up view of a molecular chain. The chain structure is explained by the packing of molecular dimers (for details see reference [Pia09]). Each molecule appears as an asymmetric oval feature with one higher lobe (0.25 nm high) on one side.

Summarizing the results obtained by the STM measurements, the two observed phases are associated with a structure entirely formed by one of the two different isomers of the parent spiropyran compound. Driven by thermal activation and the presence of the metal substrate the conversion from on to the other compound is found to be complete. However, the STM images do not provide a definitive assignment of the molecular isomers or orientations that appear in each phase.

In order to verify the proposed adsorption geometry of the spiropyran on Au(111) as a function of substrate temperature, *viz.* the observed phase transition, we performed angular-dependent HREELS measurements. The HREEL spectra were recorded in both specular ($\theta_i = \theta_r = 60°$) and off-specular ($\theta_i = 50.8°$, corresponding to 9.2° off-specular; $\theta_r = 60°$) scattering geometry at a sample temperature of ≈ 100 K. The energy of the primary electrons was set to 3.7 eV with an overall resolution of ≤ 4 meV, measured as the full width at half maximum (FWHM) of the elastic peak.

Figure 5.6 (a) shows the HREEL spectra of a submonolayer spiropyran/Au(111) after deposition of the molecules on a a cold Au(111) surface annealed to a substrate temperature of 240 K and recorded in specular and 9.2° off-specular scattering geometries. In figure 5.6 (b) the adsorbate covered surface, again dosed on a cold substrate, has been annealed to $T_S \approx 323$ K.

[25] All STM measurements have been performed after subsequent cooling to $T_S \approx 5$ K following the performed annealing steps.

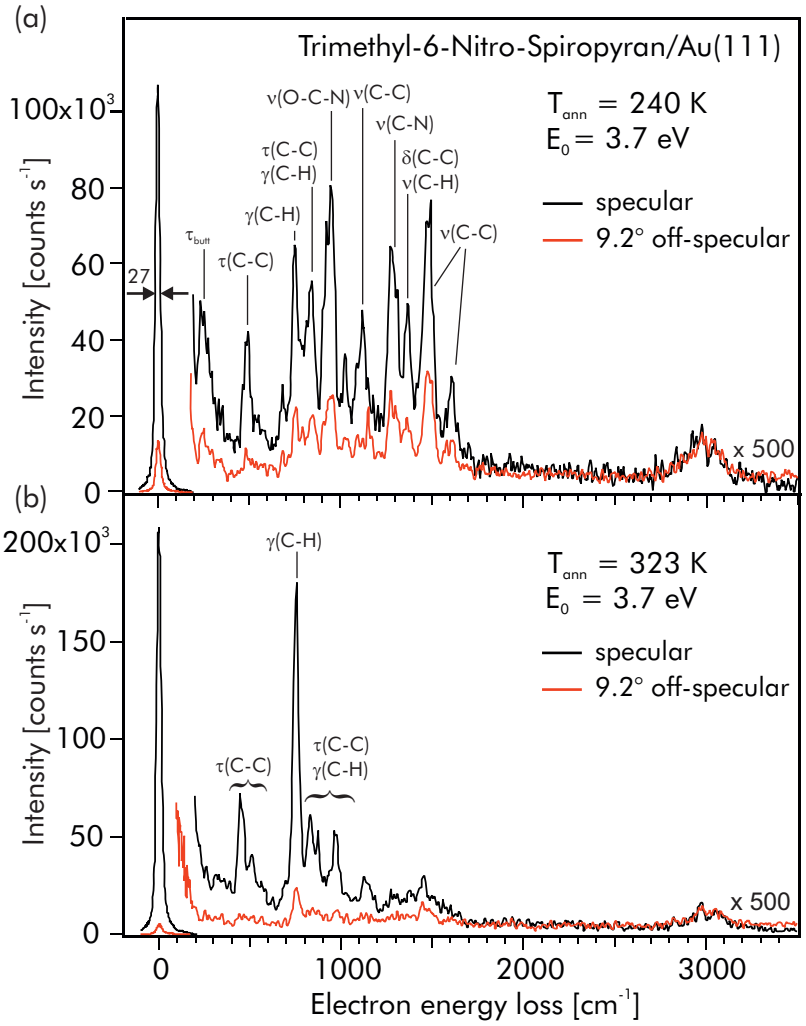

Figure 5.6: (a) HREELS spectra of a sub-monolayer SP on Au(111) annealed to a substrate temperature of 240 K (Phase A) recorded in specular and 9.2° off-specular scattering geometry, respectively, with a primary electron energy of 3.7 eV. (b) HREELS spectra of a sub-monolayer SP/Au(111) annealed to a substrate temperature of 323 K (Phase B) [Pia09].

The vibrational frequencies and their assignments are listed in table 5.1 together with the literature values of vibrational modes of spiropyran in the condensed and liquid phase [DM07, Cot00, Sch67], benzopyran [Nav05], and nitrobenzene [Lap79, Cla03].

The vibrational fingerprints of the molecular layer after annealing at the two temperatures are very different and are interpreted as a SP→MC ring-opening reaction upon annealing. In the specular spectrum several vibrational features are detected, here we discuss only the angular dependency of the vibrational modes which are relevant for the determination of the adsorption geometry [26].

[26]For the detailed assignment of all vibrational modes see table 5.1.

In figure 5.6 (a) ($T_S \approx 240$ K) strong intensities of the vibrations of the phenyl ring torsion (out-of-plane, τ(C–C) at 492 and 844 cm^{-1}), C–H deformation (out-of-plane, γ(C–H) at 753, 844 and 927 cm^{-1}), as well as C–C stretch (ν(C–C) at 1473, and 1492 cm^{-1}) and C–C deformation (in-plane, δ(C–C) 947 and 1369 cm^{-1}) modes are observed. None of these modes shows a particular strong dipole activity, indicating that the closed-form (spiropyran) is existent, with only one of the phenyl rings orientated parallel to the surface and the other one perpendicular, respectively.

The observation of the O–C–N stretch vibration (ν_s(O–C–N) at 947 cm^{-1}) and of the butterfly torsion modes involving the pyran and phenyl rings (τ_{butt} at 256 and 279 cm^{-1}) are a strong indication for the presence of the spiropyran isomer with the benzopyran unit of the molecule lying parallel to the surface. Additionally, the strong intensity of the C–N (1273 cm^{-1}) and N-CH_3 (1311 cm^{-1}) stretch vibrations are indicating that the indoline moiety of the molecule is standing upright on the surface (as schematically shown in the left side of figure 5.7).

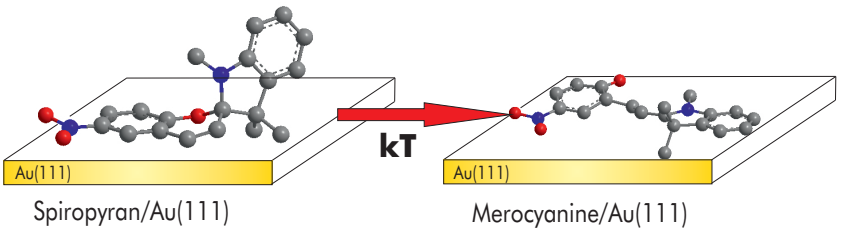

Figure 5.7: Schematic illustration of the measured adsorption geometries for the spiropyran and for the thermally activated merocyanine on Au(111), found after annealing the surface to $T_S \approx 240$ and 323 K, respectively.

Further evidence for the proposed absorption geometry is given by the absence of the symmetric and asymmetric stretch modes of the NO_2 group, which are normally located at 1348 and 1523 cm^{-1}, respectively. Note that in the case of a perpendicular orientation of the benzopyran unit one would expect intense NO_2 stretch vibrations due to a high dipole activity.

After annealing the surface at $T_S = 323$ K (see figure 5.6 (b)) the picture is completely changed. Most striking is the absence of the butterfly torsion modes τ_{butt}, the O–C–N stretch vibration ν_s(O–C–N) and the in-plane modes located above ≈ 1200 cm^{-1}, which mostly correspond to C–C stretch modes. The disappearance of the τ_{butt} and the ν_s(O–C–N) mode is explained by the occurrence of the ring-opening reaction. The almost complete absence of the in-plane modes above ≈ 1200 cm^{-1} and the strong dipole activity of the C–H deformation and phenyl ring torsion modes (out-of-plane γ(C–H) at 754, 844 and 927 cm^{-1}; τ(C–C) at 492 and 844 cm^{-1}) clearly indicates a parallel orientation (flat lying) of the merocyanine isomer with respect to the surface.

Furthermore, the flat lying adsorption geometry of the merocyanine obviously leads to a more homogeneous film, resulting in a smaller scattered elastic electron beam (reduced diffuse scattering), which causes an increase in the elastic beam intensity by

vibrational mode[a]	Phase A[b]	Phase B[b]	Spiropyran[c]	Benzopyran[d]	Nitrobenzene[e]
δ(C–H)	247 m[f]	–	–	–	254
τ_{butt}[g], δ(C–H), τ(C–C)	256 m	261 w		269	–
τ_{butt}, δ(C–H), τ(C–C)	279 m	–	–	269	–
τ(C–C)	298 m	301 w	–	–	304
τ(C–C)	337 w	332 w	–	335	–
δ(C–C)	353 w	355 w	–	343	–
δ(C–C)	385 vw	387 w	–	–	392
τ(C–C)	450 w	445 vs (da)[h]	–	442	–
τ(C–C), δ(C–H)	492 s	508 s (da)	–	506	–
$\tau(NO_2)$	534 w	534 w	–	–	532
δ(C–C)	685 m	687 w	–	–	681
γ(C–H)	753 s	754 vs (da)	748	740	–
ν(C–C), τ(C–C), γ(C–H)	844 s	838 s (da)	–	859	852
γ(C–H), τ(C–C)	872 w	874 s (da)	–	875	–
γ(C–H), δ(C–C), δ(C–H)	927 vs	927 vw	–	938	935
ν_s(O–C–N)	947 vs	–	954	–	–
γ(C–H)	–	964 s (da)	–	–	975
γ(C–H), δ(CCN)	1024 m	1026 w	1026	–	1021
ν_{as}(C–H,CH_3)	1092 m	1090 w	1090	–	–
γ(C–H), ν_{as}(C–C)	1118 s	1120 m	1123	1118	–
δ(C–H), ν(C–C)	1150 m	1150 vw	–	1158	1162
ν(C–N)	1273 s	1274 w	1278	–	–
ν(N–CH_3)	1311 s	1309 w	1314	–	–
δ(C–C), ν(C–H)	1369 s	1369 w	–	1385	–
ν(C–C), δ_{as}(CH_3)	1473 vs	1451 m	1466	1464	1479
ν(C–C)	1492 vs	–	–	1498	–
ν(C–C)	1576 w	–	1570	1586	1586
ν(C–C)	1608 m	–	–	1606	1590
ν(C=C)	1644 w	–	1642	–	–
ν_{as}(CH_3)	2973 w	2973 w	2969	–	–
ν(C–H)	3074 w	3074 w	–	3064	3082

Table 5.1: Vibrational frequencies (in cm^{-1}) and assignments for a sub-monolayer trimethyl-6-nitro-spiropyran adsorbed on Au(111). Phase A is prepared by annealing the sample to 240 K and phase B to 323 K. [a] *s*, indicates symmetric; *as*, asymmetric; υ, stretch; δ, in-plane bending; γ, out-of-plane bending; τ, torsion. [b] Obtained by HREELS; present study. [c] IR data of spiropyran adapted from Refs. [DM07, Cot00, Sch67]. [d] IR and Raman data of benzopyran adapted from Ref. [Nav05]. [e] IR and Raman data of nitrobenzene adapted from Refs. [Lap79, Cla03]. [f] m, indicates medium; w, weak; s, strong, vs, very strong; vw, very weak. [g] $\tau_{butt.}$ is the butterfly torsion between the pyran and phenyl ring. [h] The *da* indicates a strong dipole activity.

a factor of two compared to the intensity from the spiropyran-covered surface. The right side of figure 5.7 illustrates the assumed orientation of the merocyanine isomer on Au(111).

On the basis of our HREELS results, we conclude that a thermally induced ring-opening reaction of spiropyran takes places at Au(111) surface near room temperature,

with the merocyanine isomer being the thermodynamically more stable species. The observed effect is thus opposite to the known behavior of the molecule in solution, where merocyanine compounds are unstable and undergo a thermally induced ring-closing reaction. After photocoloration of the parent spiropyran compound, the open isomers undergo the thermal back reaction, returning to the thermodynamically more stable closed form in the time scale of seconds or minutes at room temperature. It is thus significative that on a relatively inert metal surface like Au(111) the reaction is completely reverted, turning the open merocyanine into the most stable form. This result introduces the conceptually attractive possibility of using inorganic substrates to balance the equilibrium between open and closed isomers simply by tuning the strength of the interaction with the metal substrate [Pia09].

5.3 Activation Barrier of the Ring-Opening Reaction

Considering the reverted stability between the two isomers when adsorbed on Au(111), it is desirable to gain insight into the origin of the larger stability of merocyanine on the gold substrate. A probable effect is that the activation energy for dissociating the C–O bond is lowered significantly by the presence of the metal surface. To determine the activation barrier between both isomers in the thermally induced SP→MC conversion, we annealed in steps of $\leq$ 10 K between 230 and 323 K for equal annealing times. As can be seen in figure 5.8, the chosen temperatures correspond to phases where the ring-opening reaction has not been activated or fully achieved, respectively.

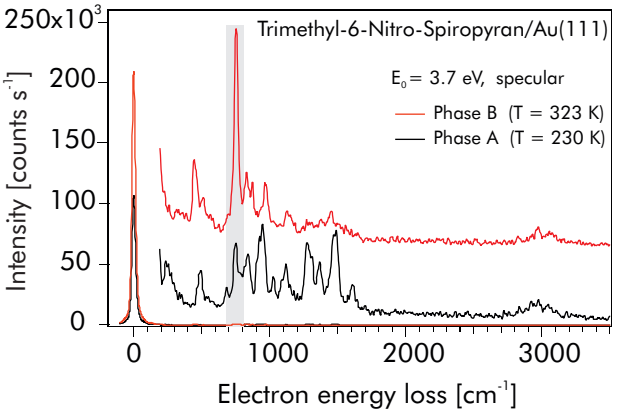

Figure 5.8: Comparison of the vibrational structures of the phase A and phase B. During the SP→MC transition the largest change in the intensity of the vibrational modes is measured for the γ(C–H) deformation mode at 754cm^{-1} (shadowed).

In order to obtain a quantitative insight into the activation barrier governing the ring-opening reaction we have performed an analysis of the reaction kinetics using the changes in the vibrational spectra of the molecular layer during the SP→MC transition [Pia09].

The kinetic analysis, i.e., the determination of the activation energy (E_A) was carried out as follows: the adsorbate-covered surface was annealed to 230 K to generate an ordered film. Afterwards an HREEL spectrum was taken, than the sample was heated up to a specific temperature and subsequently cooled down to 100 K followed by a HREELS measurement. This procedure was done for equal annealing times (10 minutes) at the particular temperature in each case on a freshly prepared film[27].

In particular, the change in the intensity of the γ(C–H) deformation mode at 754 cm^{-1} (see figure 5.8) is used as a quantitative measure for the reaction, *viz.* we correlated the intensity change $\triangle\, I_i^{754\ cm^{-1}}$ as a function of substrate temperature with the amount of molecules which performed the ring opening. The relative intensity is hereby defined as the intensity between the peak maximum and the averaged noise level in the region between 1800 and 2800 cm^{-1}, where no vibrational features are observed. The error bar is determined by the averaged noise level.

[27]For every temperature step the surface has been sputtered and annealed to guarantee a similar initial situation for the experiment.

The activation energy E_a is determined by determining the relative change in the intensity $\triangle$I of the vibrational mode at 754 cm^{-1} between the SP-covered surface (at 230 K) and the substrate annealed to a particular temperature

$$\triangle\, I_i = \frac{I_{iK} - I_{230K}}{I_{230K}} \tag{5.12}$$

and relating it to the Arrhenius-like expression

$$\triangle\, I = I_0 exp\left(-\frac{E_A}{k_B T_{ann}}\right), \tag{5.13}$$

where I_0 is an intensity pre-exponential factor and k_B is the Boltzmann constant.

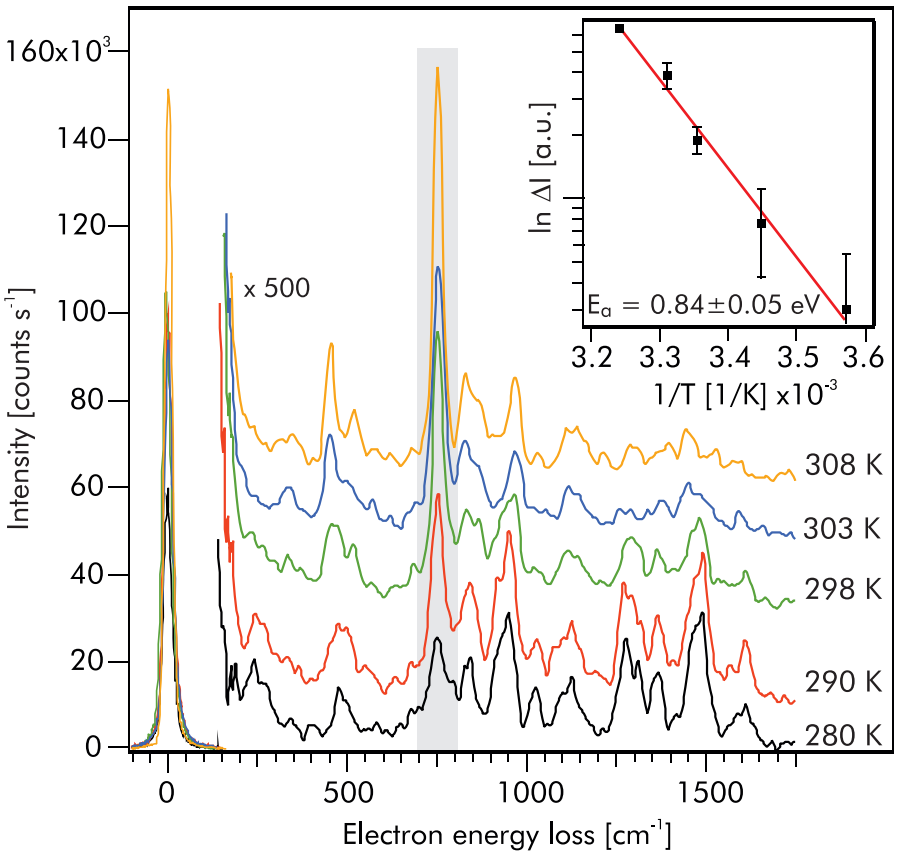

Figure 5.9: HREEL spectra of ≈ 0.7 ML spiropyran on Au(111) as a function of substrate temperature recorded in specular scattering geometry with a primary electron energy of 3.7 eV. For clarity only spectra taken at 280 to 308 K are shown in a frequency regime up to 2000 cm^{-1}. The modes at ≈ 3000 cm^{-1} do not show major changes in the performed measurements. Inset: The intensity change of the out-of-plane C–H bending mode at 754 cm^{-1} as a function of the substrate temperature is used to elucidate the activation energy (E_a) for the ring opening reaction of spiropyran on Au(111) *via* an Arrhenius plot [Pia09].

Figure 5.9 shows spectra taken at temperatures around the transition point from

SP→MC which happens in a temperature window between 280 and 310 K. In the inset the intensity change $\triangle\ I_i^{754\ cm^{-1}}$ is plotted as a function of the inverse temperature and fitted using equation 5.13. The activation energy is derived to $E_A = 0.84 \pm 0.05$ eV, which is surprisingly close to the reported values of spiropyran in solution[28] [Gor01], which can be attributed to the weakly adsorbed state of spiropyran on Au(111).

Even if the the presence of the metal surface does not seem to significantly lower the barrier for the the C–O bond cleavage in the ring-opening reaction, it may still balance the equilibrium energetics towards the merocyanine isomer if an additional mechanism is responsible for the stabilization of the MC molecules on the surface. From the estimated structures we conclude that the planar conjugated form of the MC form is expected to interact with the electronic states of the gold substrate, thus hindering the back-reaction. It is known for the MC isomer to exist in a zwitterionic state, where the large dipole moment of the molecule is expected to interact strongly with the metal surface through the creation of image charges increasing the molecule-metal bond. The results from the HREELS measurements of the at 700 K annealed molecule/Au(111) surface (see figure 5.4), which show remaining C–C torsion modes τ(C–C)and C–H bending modes γ(C–H), led to the conclusion that the trimethyl-6-nitro-spiropyran dissociates at least partially during the thermal desorption. This observation do support the discussed strong interaction of the MC isomer with the substrate.

Also from the basis of the geometry of the molecules on the substrate it is possible to argue for the larger stability of the MC isomer on the surface. The SP→MC reaction requires simply the cleavage of a C–O bond, which is well possible for molecules embedded in ordered domains. In contrast, the back-reaction MC→SP would require the previous removal of the indoline from the surface. The addition of these forces to the C–O bond formation would lead to a significant increase in the activation barrier for the closing of the adsorbed MC isomer.

For the free spiropyran molecule, photoadsorption of UV light with wavelength of 245 nm and 345 nm induces the ring-opening process, whereas the closing reaction is achieved under illumination with green light at $h\nu = 550$ nm. The presence of the surface can open up new possible indirect excitation channels and alter the position of the molecular electronic states underlying the reaction. An Nd:YAG-laser has been chosen as a light source with its fundamental wavelength either doubled to $h\nu = 532$ nm, 2.33 eV or tripled to 355 nm, 3.49 eV and experiments have been carried out with the collaborating group of J. Pascual *et al.*. As a result we have to conclude that photo excitation of the ring-opening/closing reaction is hindered due to adsorption on Au(111). Most likely the lifetime of the electronically excited molecular orbitals is drastically reduced in presence of the substrate due to additional relaxation channels into the substrate. This could lead to the observed quenching of the photoisomerization. The already discussed inverted stabilization of the merocyanine due to a strong binding could hinder the folding processes in the ring-closing reaction.

[28] $E_a = 0.77$ - 0.98 eV, depending on the solvent.

5.4 Summary

Concluding, we have shown that spiropyran undergoes a thermally induced ring-opening reaction due to adsorption on Au(111) contrary to the known behavior in solution. We have shown that it is possible to detect and analyze the adsorption geometry of both phases, *i.e.* the spiropyran isomer and the merocynine isomer, of the parent spiropyran molecule adsorbed on Au(111) employing HREEL spectroscopy. For the spiropyran we determined an adsorption geometry where the benzopyran moiety of the closed form is lying flat on the surface and the indoline unit is orientated perpendicular to the surface. For the open merocyanine isomer we found evidence, clearly indicating a parallel orientation (flat lying) with respect to the surface. Molecular switches on metallic substrates exhibit different properties than in solution, essentially as a result of their condensation into ordered molecular phases and their interaction with the (metal) substrate. Here we have shown that the thermal stability of a prototypical molecular switch is strongly modified due to adsorption on Au(111). In contrast to the behavior known for the molecule in solution we found the open MC isomer to be more stable when adsorbed on Au(111).

Furthermore, it was possible to gain insight into the energetics of the thermally induced ring-opening reaction. The molecules undergo a complete ring-opening reaction near room temperature resulting in phases of merocyanine/Au(111). We determined the activation energy to $E_a = 0.84 \pm 0.05$ eV which is surprisingly close to the known values of nitr-spiropyran in solution. Therefore the origin of the larger stability of the open form is associated with a larger interaction with the surface which could be enhanced by the zwitterionic character of merocyanine.

On the basis of our results, we foresee a strategy for tuning the stability and the photoswitchable properties of metal-supported spiropyran-based thin films by choosing an optimum combination of organic functionalization and inorganic substrate. The selection of substrate materials with a different electronic structure and bonding strength could facilitate a tuning of the potential energy landscape. This could not only open up possibilities of guiding the ring-opening/closing reaction to the favored isomer but also exploiting the additional possible activation and decay pathways mediated by the substrate could lead to a new functionality [Pia09].

6 SFG Analysis of Molecular Switches Incorporated in SAMs

Up to this chapter we discussed results obtained for physisorbed or weakly chemisorbed molecular switches on metal surfaces, which were prepared via evaporation under UHV conditions. A second approach has been to anchor the photoswitchable molecules via an anchoring group (head group) covalently to the substrate. The terminal functional group is separated from the head group by a spacer unit (linker) and thereby determines the chemical or functional properties of the surface [Ulm96, Sch04, Sch00, Lov05]. The sample preparation has been realized *ex-situ* under wet chemical conditions which allow to systematically anchor complex molecular units with a preferred orientation to the surface. The wet chemical conditions make it possible to obtain monolayers of well-ordered molecular ensembles through self-assembly, *i.e.* self-assembled monolayers (SAMs). Via modification of the anchor group (and the linker) the strength of the electronic coupling can be modified in a well-directed manner and accordingly the adsorbate/substrate interaction, *e.g.* charge transfer, can be investigated. By using appropriate substituents linked to the functional unit and/or anchor groups with different footprints it is possible to vary the lateral (adsorbate/adsorbate) interaction in order to study cooperative effects within the molecular layer.

The investigation and characterization of chromophore containing self-assembled monolayers, which are formed by covalent binding of sulfides or disulfides to a solid surface, *e.g.* gold or silver, is seen as a very promising approach towards the development of materials with novel optical and electronic properties [Kri05]. Most common is the usage of one-dimensional linkers like alkanethiols for the preparation of SAMs on gold [Wöl09, vdM10]. Molecular switching which involves geometrical changes, *e.g.* the *trans/cis* isomerization of azobenzene, is efficient in solution, but it is obvious that the transition from the *trans*- to the *cis*-isomer requires a certain amount of free volume. This restriction is already obvious when one compares the switching properties of the azobenzene compound in solution with the properties of azobenzene in its crystalline form. Whereas the process of the isomerization is on a rather short timescale in solution, in the condensed form isomerization is hardly achieved even after vast illumination times. In a densely packed and highly ordered film, for instance in azobenzene-substituted alkanethiols on gold, the free volume needed for the isomerization is limited and therefore the photoinduced switching is restricted due to steric hindrance [Jun08]. Moreover π-aggregation of the attached chromophores is a known problem that changes or is even able to suppress the switching ability [Kri05, Thy07]. For instance electronic intermolecular coupling can result in an ulrafast delocalization of the excited exciton on the femtosecond timescale within the layer [Gah10]. Here the excitation energy is delocalized faster than it can be transferred to the nuclear coordinate which is a strong constraint to photoswitching of well-ordered SAMs with a tight packing density.

However it has been shown for highly ordered films of aromatic azobenzene biphenyls adsorbed on Au (and Pt) that cooperative light-induced transformation is observed for

whole domains and is highly effective [Pac07, Fer08, Cri11].

In this work we studied (i) the photoisomerisation of an azobenzene-functionalized SAM on a gold surface in which the azobenzene unit is connected to a tripodal linker system (see chapter 6.1) and (ii) investigated SAMs containing azobenzene biphenyls, where we performed dilution experiments by introducing lateral spacer molecules to the SAM (see chapter 6.2).

Sum-frequency generation (SFG) vibrational spectroscopy (see chapter 3.3) has been employed to investigate the orientation of the functional molecules towards the surface and therefore to analyze the switching state of the system. In both molecular systems ((i) and (ii)) the azobenzene carries an additional cyano (-C≡N) group in the *para* position of the outer phenyl ring which acts as a marker group for the SFG and therefore permits a direct measure of the switching state. SFG is a well-known nonlinear technique for studying interfaces. These studies include liquid interfaces, SAMs on metal surfaces, electrochemical and catalytic reactions to dynamics and kinetics at interfaces due to the temporal resolution of the SFG [She89, She84, Hei91, Buc01, Bel05, Wan05, Bon00, Gal03, GD08]. We demonstrate that SFG is a highly suitable technique to determine the reversible photoinduced *trans/cis* isomerization of an azobenzene-functionalized SAM and therefore is a sensitive tool to analyze the molecular structure of functional surfaces [Wag09].

6.1 Azobenzene-Functionalized Tripodal SAM

The first azobenzene functionalized SAM we studied by means of SFG spectroscopy has been designed following the recently developed concept of using three-dimensional linkers with a tetrahedral core unit [Jia03, Shi06, Gal02]. It is known for these type of molecules functionalized with an azobenzene moiety that the photoisomerisation ability is preserved on a single molecular level when the isolated system is bound to a Au(111) surface or to the apex of an Au-coated cantilever tip of an atomic force microscope [Tak06b, Tak06a, Tak10]. If the functionality of these molecules when incorporated in a self assembled monolayer is preserved has not been proven so far. We investigated an azobenzene-linker-conjugate with tetrahedrical shape which has been synthesized by K. Rück-Braun *et al.*[29] in the chemistry department of the TU Berlin [Zar08].

The tripodal linkersystem with an adamantane core and an azobenzene headgroup has been introduced to gain sufficient control of the orientation of the headgroup with regard to the surface and to control the headgroup to surface distance. For immobilization on metal surfaces the system provides three thioester groups (see fig. 6.3 (b)). However, it should be pointed out that in previous studies it has been shown that the anchoring of all three thiols in systems with tetrahedral shape is elusive [Shi06] and that a XPS study revealed that the average number of bond thiols ranges from 1.5 to 2 for various tripodal systems [Wei05]. Therefore to make a higher flexibility accomplishable a methylene unit has been introduced between the anchoring moiety and the phenyl ring on top of the adamantane core.

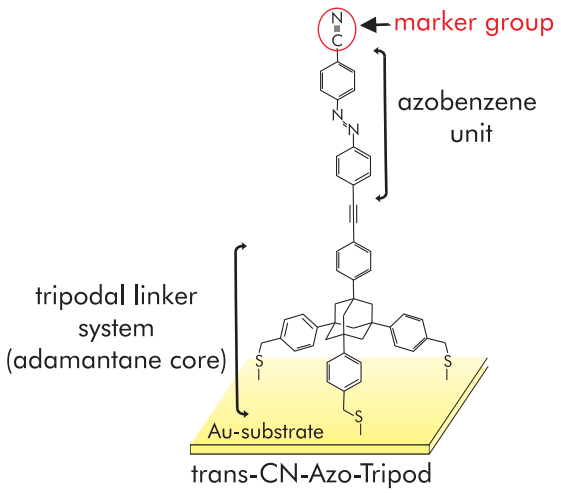

Figure 6.1: Drawing of the investigated azobenzene functionalized tripodal molecule bound to a gold surface assuming that all three thiol groups anchor to the substrate. The three anchoring groups of the linker system generate a footprint with a sidelength of 12-15 Å minimizing obstructive ascendancies for the isomerization due to possible sterical hindrance. The azobenzene carries an additional cyano group as a marker group for SFG vibrational spectroscopy.

The azobenzene headgroup contains an additional nitrile (-CN) functionality in *para*-position of the outer phenyl ring which acts as a marker for the vibrational spectroscopy (see fig. 6.1). The control of the orientation of the photochromic moity and it's marker is crucial for the experiment due to the vanishing electric field components

[29] Subproject B6 of the SFB 658 "Elementary Processes in Molecular Switches at Surfaces"

of the incident IR light parallel to the metal surface. Since in dipole approximation at metal surfaces *surface selection rules* do apply, only vibrations with a component of the dipole moment change normal to the surface are observable. Therefore the orientation of the marker group parallel to the surface normal is decisive and permits a direct measure of the switching state.

The intention of this measurement is to analyze the photoisomerization behavior of the described molecules organized in a SAM bound to the metal substrate. This brings up the necessity to gain knowledge of the photochromic behavior of the compound in solution so that the data of the surface sensitive measurement can be set in reference.

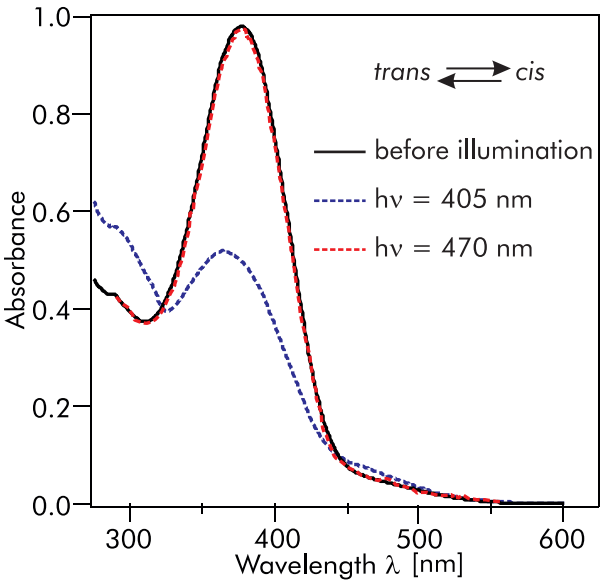

Figure 6.2: UV/Vis absorption spectrum of the tripodal azobenzene-linker-conjugate (see fig. 6.3 (b)) in solution (CH_2Cl_2) before and after illumination with light at 405 nm and 470 nm. Exposure at 405 nm leads to a decrease of the absorbance at the $\pi - \pi^*$ absorption band at around 380 nm and to an increase of the $n - \pi^*$ absorption band around 470 nm due to a *trans* $\rightarrow$ *cis* isomerization. Illumination with light of 470 nm wavelength induces the back reaction to the initial state (*cis* $\rightarrow$ *trans*).

In the liquid phase, direct electronic excitation induces the isomerization of azobenzene and its derivatives *via* a $n - \pi^*$ (S_1) and $\pi - \pi^*$ (S_2) electronic excitation, respectively. In figure 6.2 the UV/Vis absorption spectra of the azobenzene-linker-conjugate highly diluted in dichloromethane (CH_2Cl_2) before and after illumination with light at 405 nm and 470 nm is shown. The intense absorption band at $\approx$ 380 nm belongs to the S_2 transition which can be assigned to the symmetry-allowed $\pi - \pi^*$ electronic excitation of *trans*-azobenzene (see chapter 2.2.1). Comparison with the corresponding maximum of the UV/Vis absorption spectrum of pure azobenzene in figure 2.5 shows a red shift of this band of $\approx$ 30 nm, which can be explained with the expanded π-system of the azobenzene-linker-conjugate in comparison to with unsubstituted azobenzene. The energy of the $\pi - \pi^*$ transition decreases in consequence of the conjugation. Due to this red shift the S_2 transition starts to overlap with the energetically lower lying $n - \pi^*$ transition. The corresponding absorption band around 470 nm belongs to the symmetry-forbidden S_1 transition.

Illumination at 405 nm leads to a drastic drop in intensity of the $\pi - \pi^*$ absorption

band at 380 nm and to a hypsochromic shift of the associated maximum of ≈ 10 nm. In addition an increase in the absorbance of the $n - \pi^*$ transition can be observed. The described effects due to illumination at 405 nm can be assigned to the *trans* → *cis* isomerization. On the other hand, light exposure at 470 nm drives the *cis* → *trans* isomerization leading to recovery of the absorbance at 470 nm.

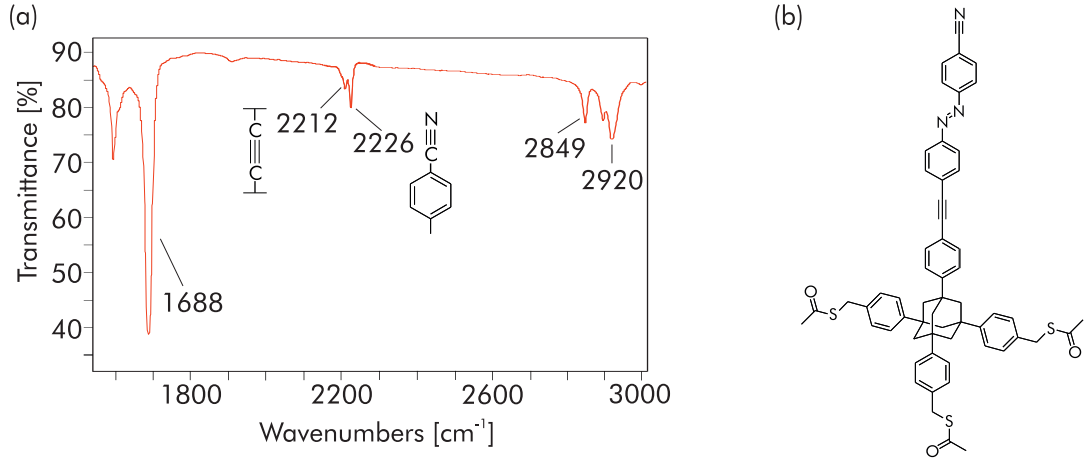

Figure 6.3: (a) Part of the attenuated total reflectance FT-IR spectrum of the tripodal azobenzene-linker-conjugate shown in (b). At 2212 cm^{-1} and 2226 cm^{-1} we find the stretch vibrations of the -C≡C- and -C≡N triple bond, respectively. (b) Structure of the *trans* isomer of the investigated azobenzene derivative with thioester protection groups.

Figure 6.3 (a) shows a part of a FT-IR spectrum using attenuated total reflectance (ATR) taken with a *Nicolet Avatar 360* routine use mid-IR (∼400-4000 wavenumbers) spectrometer with a resolution of ≈ 0.5 wavenumbers[30]. It is known that for most cases the -C≡N triple bond stretch vibration results in a strong signal and is in the range of 2260 to 2200 cm^{-1}, whereas the -C≡C- triple bond stretch vibration is a little lower in energy (2260-2150 cm^{-1}) [Hes91]. Therefore the vibrational mode at 2226 cm^{-1} is assigned to the -C≡N marker group and the vibrational feature at 2212 cm^{-1} to the -C≡C- stretch mode. The other vibrational modes shown in figure 6.3 (a) can be assigned to the C=O-stretch vibration at 1688 cm^{-1} and the aliphatic C-H stretching vibrations between 2800 cm^{-1} and 3000 cm^{-1} [Hes91, Ban99, Bru07].

[30]data courtesy of K. Rück-Braun *et al.*

6.1.1 Sample Preparation

To investigate the photochemical behavior, the molecules have been applied to a gold substrate (200nm gold film evaporated on a quartz plate). The gold substrate was flame annealed and then immersed in a solution of 1 mg of the azobenzene tripod conjugate dissolved in 2.2 ml of 2:1 ethanol-THF solution. For the *in situ* deprotection of the thioacetate 15 μl of a 28 % aqueous solution of NH_3 was added and the reaction mixture was degassed for 20 min under a stream of argon. To achieve the self assembly of the film the gold substrates have been immersed for 24 hours in the dark and under Ar atmosphere. After immersion the samples were carefully rinsed with copious amounts of THF then dried in an argon stream. Afterwards the samples were kept in dark in Ar filled containers until the SFG measurements, to avoid oxidation of the sulfur. For the SFG experiments the adsorbate covered surfaces were mounted in a small chamber under argon atmosphere.

6.1.2 Analysis of the Ground State Geometry

In figure 6.4 (a) a broadband IR-VIS-SFG spectrum of the azobenzene-functionalized SAM is shown in the frequency regime between $\approx$ 2080 and 2350 cm^{-1}.

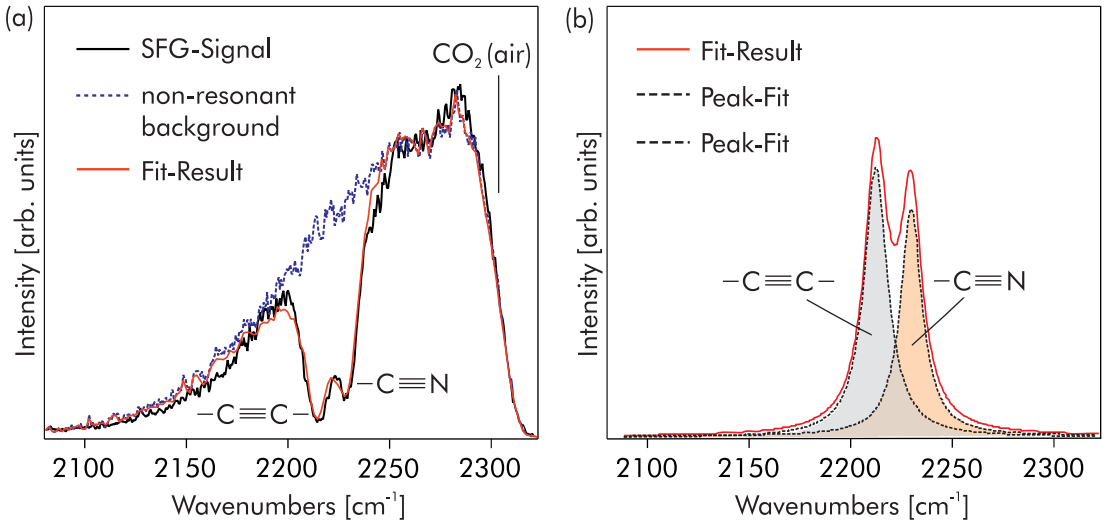

Figure 6.4: (a) Broadband IR-VIS-SFG spectrum in the frequency window of the -C≡N and -C≡C- stretch vibration of the azobenzene-functionalized SAM. Also shown are the non-resonant background measured from the bare gold substrate (dotted blue line) and a fit using two Lorentzian resonances (solid red line), which models the experimental data nicely. Starting around 2349 cm^{-1} all infrared intensity is absorbed by the asymmetric CO_2 stretch vibration of air. The relative phase of the vibrational modes with respect to the non-resonant contribution governs the lineshape of the measured spectrum in the region of the resonances. (b) Two Lorentzian fits for the vibrational resonances result in ratio of the amplitudes between the -C≡C- and -C≡N modes of 1 : 0.87 [Wag09].

Note that the measurements were performed under ambient conditions and that the -C≡N stretch vibration is expected between 2200 and 2260 cm^{-1}, thus in a frequency region where C-H modes and vibrations of air constituents like H_2O or CO_2 do not interfere. Two distinct vibrational modes are visible at 2215 and 2228 cm^{-1}, which are assigned after comparison with the ATR FT-IR (see fig. 6.3 (b)) to the modes of the -C≡C- and -C≡N stretch vibrations, respectively. Since the experiments werer performed under ambient conditions the ambient conditions of the measurements all infrared intensity is absorbed above 2349 cm^{-1} by the asymmetric CO_2 stretch vibration of air. Additionally a fit using two Lorentzian resonances (see equation 3.7) and the non-resonant background taken from a pure gold substrate is shown. The IR intensity is proportional to this non-resonant contribution. The fit describes the measured spectrum conclusively. The lineshape of the SFG signal depends strongly on the relative phase ϕ_q of the vibrational modes with respect to the non-resonant background. In our case the phases of the -C≡C- and -C≡N stretch vibrations can be determined to $\phi_q = 3/4\pi$ and $\phi_q = 1/4\pi$, respectively, leading to the observed shape of the SFG spectrum which resembles an IR absorption spectrum. The two Lorentzian resonances obtained from the fit are shown in figure 6.4 (b). Comparison of the amplitudes of the -C≡C- and -C≡N modes show a ratio of $1 : 0.87$.

As previously stated, IR-active groups can only contribute to a SFG-Signal if the dipole moment change of the vibration exhibits a component parallel to the surface normal. Therefore, the appearance of the strong -C≡C- and -C≡N vibrational signals points towards a preferential orientation in which the azobenzene linker conjugate adopts a perpendicular or nearly perpendicular orientation towards the surface. The almost identical ratio between the two observed vibrational modes implies that the molecule is most likely in *trans* configuration, which is in analogy with the investigations of the molecule in solution, where the *trans* isomer is the energetically more stable one.

6.1.3 Photoinduced Conformational Changes

In the following we investigate the effect of illumination on the vibrational structure of the functionalized surface. After illumination of the sample with a laser diode at a wavelength of 405 nm and a photon dose (number of photons, n_p) of $n_p \approx 10^{18}$ cm^{-2} the SFG spectrum shown in figure 6.5 was taken. Light exposure at this wavelength leads to a significant decrease in the amplitude of the -C≡N vibrational mode, whereas the -C≡C- stretch vibration stays constant (see figure 6.5(b)). This indicates that no radiation induced damage occurs and that the orientation of the linker system towards the surface stays unchanged. The ratio of the amplitudes between both modes after illumination is determined to $1 : 0.46$, which corresponds to a decrement in the amplitude of the -C≡N mode of ≈ 50 % compared to the non-illuminated film.

We assign the change in the vibrational structure to a photoinduced *trans* → *cis* isomerization of the azobenzene unit. The former perpendicular (or nearly perpendicular) orientation (see Fig. 6.1) of the CN-group towards the surface is not given anymore for the *cis* isomer, grounding the drop in amplitude of the corresponding vibrational

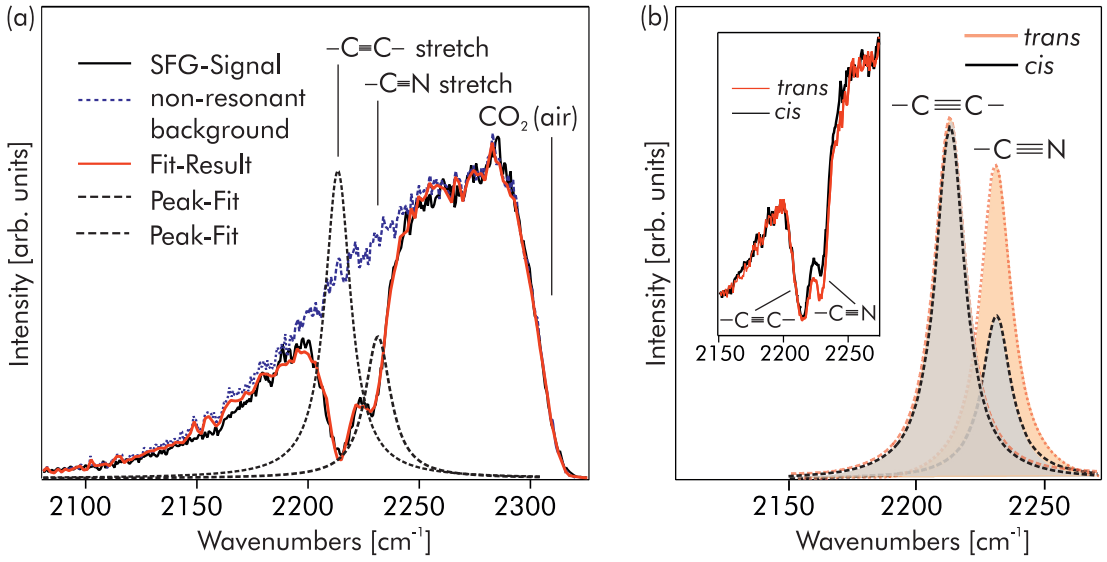

Figure 6.5: (a) Broadband IR-VIS-SFG spectrum of the azobenzene functionalized SAM after illumination with a laser diode at $h\nu = 405$ nm ($n_p \approx 10^{18}$ cm^{-2}). The ratio of the amplitudes between the -C≡C- and -C≡N modes is 1 : 0.49, *i.e.*, the amplitude of the -C≡C- vibrational mode drops ≈ 50 % due to the *trans* → *cis* isomerization, whereas the amplitude of the -C≡N mode and therefore the orientation of the linker system stays constant. (b) Comparison between the fits using Lorentzian resonances before (*trans* configuration) and after illumination (*cis* configuration). Inset shows the raw SFG data before and after illumination with $h\nu = 405$ nm [Wag09].

mode. Please note that, in principle, polarization-dependent experiments would allow the estimation of the orientation of the *p*-cyanophenyl moiety. This evaluation of the experimental data would require profound knowledge of the optical properties of the interface, especially information about the hyperpolarizability tensor is indispensable [Buc01, Wan05, Gal03]. Since these essential values are not identified for the investigated system, we refrained from a polarization-dependent analysis.

In order to estimate the relative amount of switched molecules in the SAM and to compare this value with the one for the free molecules in solution, a discussion about to what extent the vibrational mode of the cyano marker group of the *cis* isomer contributes to the measured -C≡N amplitude in the SFG-signal is needed. One can think of two possible scenarios:

(i) when the molecule is in its *cis* configuration the -C≡N mode does not contribute to the signal, i.e. there is no component of the vibrational dipole moment change perpendicular to the surface or (ii) the -C≡N vibrational mode of the *cis* isomer still contributes to the signal.

For the first case, (i), the -C≡N mode must be parallel to the surface to lead along to a vanishing dipole moment change perpendicular to the surface. Assuming that the tilting angle of ≈ 120° along this axis between the *trans*- and the *cis*-isomer is the

same as for the free molecule, this configuration would be possible if the molecules are tilted ≈ 30° to the surface. The observed decrease of ≈ 50 % in the amplitude of the -C≡N signal after illumination indicates that half of the molecules which originally contributed to the signal in the *trans* configuration no longer make a contribution. For case (ii), the *cis* isomers contribute to the measured -C≡N signal, the amount of switched molecules must be even larger to provoke a reduction of 50 %. Therefore the lower limit for the amount of molecules undergoing the *trans* → *cis* isomerization is ≈ 50 %. For comparison, the amount of switched molecules in the liquid phase is ≈ 55 % in the photostationary state, calculated from the intensities of the absorption bands associated with the $\pi - \pi^*$ transition (see Chapter 6.1) in the UV/Vis absorption spectrum before (*trans*-isomer) and after illumination with $h\nu = 405$ nm (see Fig. 6.2).

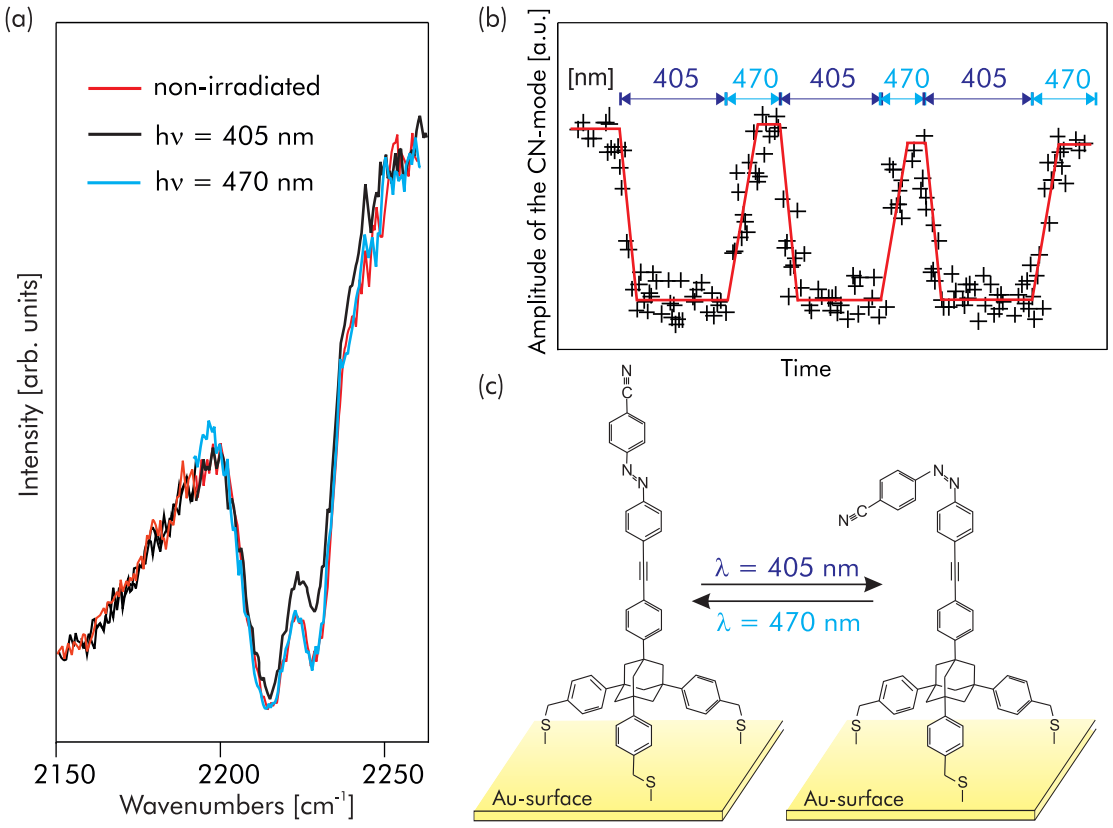

Figure 6.6: (a) SFG spectra of the azobenzene-functionalized SAM before and after light exposure with $h\nu = 405$ and 470 nm. (b) Change in the amplitude of the -C≡N mode in the SFG signal as function of the illumination time with the two different wavelength ($h\nu = 405$ and 470 nm), demonstrating the light-induced reversible changes in the vibrational structure due to the *trans/cis* isomerization. (c) Scheme of the reversible *trans/cis* isomerization process of the immobilized azobenzene linker conjugate [Wag09].

To drive the reverse process, i.e., the *cis* → *trans* isomerization, we performed illumination experiments with $h\nu = 470$ nm. From illumination experiments of the molecule in solution it is known that illumination in the visible (blue) range (see Fig. 6.2) stimulates the back reaction. The results show that for the self-assembled monolayer of the molecules on a gold substrate in its *cis* state (≈ 50 % *cis* isomers) a photon dose of $n_P \approx 6 \times 10^{19}$ cm^{-2} at a wavelength of 470 nm restores the amplitude of the -C≡N mode. The same SFG amplitude can be retrieved as from the SAM with the incorporated azobenzene linker conjugate in its *trans* configuration (see Fig. 6.6 (a)).

The results of alternating light exposure with the two different wavelength of 405 nm and 470 nm clearly demonstrates that the changes in the -C≡N mode are reversible as shown in Fig 6.6 (b). We propose that the observed reversible changes in the vibrational structure can be associated with a structural change of the SAM, which we assign to a reversible isomerization process as depicted in Fig. 6.6 (c). The 405 nm light drives the *trans* → *cis* whereas the reverse process (*cis* → *trans*) can be stimulated by 470 nm light. With using the tripodal linker system with the adamantane core, which generates a triangular footprint with a sidelength of ≈ 15 Å [Zar08], allows the reversible isomerization which is associated with a significant structural change due to a sufficient free volume to prevent steric hindrance. As already addressed in Chapter 6.1 the sketch in Fig. 6.6 (c) might not represent the true situation concerning the anchoring of all three thiol groups to the gold substrate [Shi06, Wei05, Wei06].

If we want to gain insight into the photoinduced isomerization of the azobenzene-functionalized SAM we have to consider two scenarios: (i) the photons induce a direct (intramolecular) electronic excitation within the adsorbate[31] and (ii) the incident photons indirectly drive the process, so that the underlying metal substrate acts as the chromophore, where hot electrons (or holes) are generated and then attached to the adsorbate, creating a negative (or positive) ion resonance. It is known for the liquid phase that a direct electronic excitation drives the isomerization of azobenzene and we propose that a direct optical excitation drives as well the isomerization of the immobilized azobenzene linker conjugate. Since the tripodal linker system results in a weak interaction between the metal substrate and the functional azobenzene unit, *viz.* the azobenzene is electronically decoupled. Therefore it is likely that the electronic structure of the adsorbed molecule will be very similar to the molecule in the liquid phase, *i.e.*, the absorption bands should be barely modified. Therefore, photoexcitaion at $h\nu = 405$ nm leads to *trans* → *cis* isomerization, whereas excitation at $h\nu = 470$ nm drives the back reaction (*cis* → *trans*), analogous to the liquid phase. In contrast, a photoinduced substrate mediated charge transfer process has been proposed for the photoisomerization of a physisorbed azobenzene derivative adsorbed on the Au(111) surface [Hag08a]. In this case photoexcitation with energies above 2.2 eV leads to a hole formation in the d-bands of the Au(111) which is followed by a hole transfer to the highest occupied molecular orbital, inducing the isomerization.

[31] For case (i) details are given in chapter 6.1.

6.1.4 Quantification of the Isomerization Process

In order to quantify the light-induced reversible isomerization of the azobenzene functionalized SAM on the gold surface, we evaluated the effective cross sections for both, the *trans* → *cis* ($\sigma_{eff}(cis)$) and the *cis* → *trans* ($\sigma_{eff}(trans)$) reaction. Since the total amount of *cis* isomers as a function of photon dose is unknown, we used the change in the amplitude of the -C≡N stretch mode as a measure for the switching process, *i.e.*, we correlated the observed changes as a function of photon dose with the number of switched molecules (see Fig. 6.7). By using an exponential saturation function we can

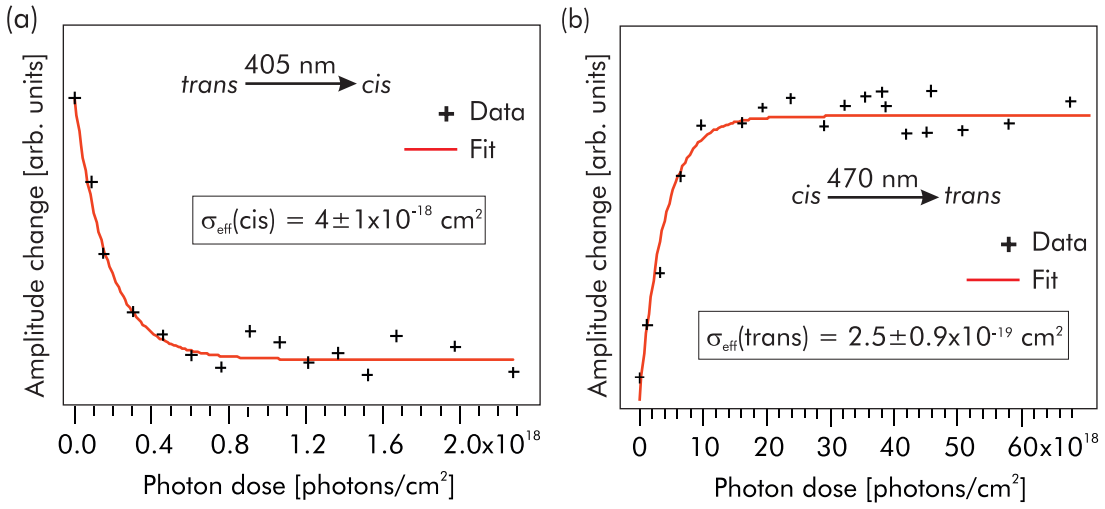

Figure 6.7: Change of the amplitude of the -C≡N mode as a function of photon dose. (a) Decrease of the amplitude of the -C≡N mode as a function of photon dose at $h\nu$=405 nm due to the *trans* → *cis* isomerization. (b) Increase of the amplitude of the -C≡N mode as a function of photon dose at $h\nu$=470 nm due to the *cis* → *trans* isomerization. The solid lines in (a) and (b) represent fits using the exponential saturation function 6.14 [Wag09].

estimate an effective cross section

$$\triangle A = \triangle A_{\infty}(1 - \exp -(\sigma_{eff} \cdot n_p)) \tag{6.14}$$

where △ A is the change in the amplitude of the -C≡N mode, $\triangle A_{\infty}$ corresponds to the asymptotic change in the -C≡N amplitude and n_p is the number of photons (photon dose). In figure 6.7 the fits according to equation 6.14 are represented by solid lines. From these fits we can derive an effective cross section of $\sigma_{eff}(cis) = 4 \pm 1 \times 10^{-18}$ cm^{-2} at 405 nm for the *trans* → *cis* isomerization, and $\sigma_{eff}(trans) = 2.5 \pm 0.9 \times 10^{-19}$ cm^{-2} for the back reaction(*cis* → *trans*).

The difference of approximately one order of magnitude between the cross sections is most likely related to the different absorption cross sections in the UV/Vis absorption spectra (see Fig. 6.2). While the excitation at 405 nm leads to strong absorption band due to the $\pi \rightarrow \pi^{\star}$ transition, excitation at 470 nm induces a symmetry forbidden

$n \rightarrow \pi^\star$ transition. Therefore the observed absorption band is much less pronounced. Assuming that the quantities of the switched molecules in solution and in the SAM are similar, *i.e.*, *ca.* 50 % (see chapter 6.1.3), then the photoisomerization cross sections for the azobenzene-functionalized SAM closely resemble the ones known for azobenzene and its derivatives in the liquid phase. This demonstrates the strong decoupling of the functional azobenzene unit from the metallic substrate due to the tripodal linker system.

6.2 Azobenzene Biphenyl SAMs

Further approaches have been attempted to overcome the problem of steric hindrance in tightly packed photochromic SAMs. For instance studies on conformationally flexible alkylthiols featuring azobenzene headgroups which form single component SAMs, have been reported to exhibit only a weak or vanishing photo-response. To overcome this cutback mixed SAMs where azobenzene-containing molecules are incorporated in a matrix of shorter alkanethiol SAMs have been suggested. Indeed, photoisomerization has been achieved when diluting the function [Yas03, Kum08].

However, it has been observed that the π-stacking of the aromatic units of the azobenzene-containing molecules leads to phase separation of the two components. Furthermore it can not be excluded that the seen effects of the isomerization are restricted to either single or few molecules adsorbed at domain boundaries or defect sites. In such locations the anchoring of the molecules is weaker and the packing density is lower which leads to a energetically less stable situation allowing the photoisomerization. Another route is to introduce lateral spacers, *e.g.* sterically bulky ethyl groups at the *ortho*-position with respect to the diazo group [Han10] or *para*- carborane in the alkyl chain [Ito05], yielding in a high photoisomerization capacity.

Nevertheless it has been shown recently for highly ordered and tightly packed single component azobenzene-containing SAMs on Au(111), formed by chemisorption of molecules exhibiting a rather high conformational rigidity compared to conformationally flexible thiolated azobenzenes sustaining aliphatic units, that collective switching of entire molecular 2D crystalline domains can be achieved [Pac07]. In this approach towards an controlled photochromic switchable surface the usage of a thiolated azobiphenyl molecule leads to a reported isomerization yield of $\approx$ 96 % [Elb08, Fer08]. In this chapter we present SFG vibrational spectroscopy results obtained for a single-

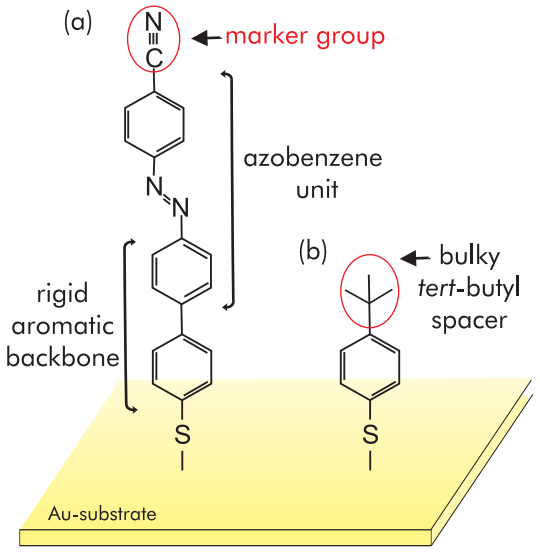

Figure 6.8: (a) Sketch of a single immobilized azobiphenyl molecule on gold. The rigid character of the aromatic backbone is supposed to result in a geometry of the 2D packing being governed by π-stacking. The molecules are expected to exhibit a tight packing at the supramolecular level originated by this π-π interchain interaction. The outer phenyl ring of the azobenzene carries an additional cyano group in *para* position which acts as a marker group for SFG spectroscopy. (b) (4-*tert*-butylphemyl)methanethiol is used as a lateral spacer for the dillution experiments. The rather bulky *tert*-butyl headgroup is supposed to introduce sufficient free volume for the isomerization in between the functional molecules.

component and a two-component self-assembled monolayer on gold. The design of the molecules follows the approach of a rather rigid aromatic backbone through the usage of an azobenzene biphenyl (see Figure 6.8 (a))[32]. Again the azobenzene headgroup is equipped with an additional nitrile functionality in the *para*-position of the phenyl ring which acts as a marker for the SFG spectroscopy. It is expected that the π-conjugated backbone will lead to a tight packing since the π-π intermolecular interactions are mostly responsible for the geometry of the 2D packing, whereas for alkanethiol SAMs the geometry is mainly governed by the head group/substrate interaction. Furthermore, because of its similar structure to arenethiols, a mainly planar conformation can be expected [Yan00] leading to long range order with π-π interchain interaction which could promote the induced isomerization of a few molecules over many adjacent molecules.

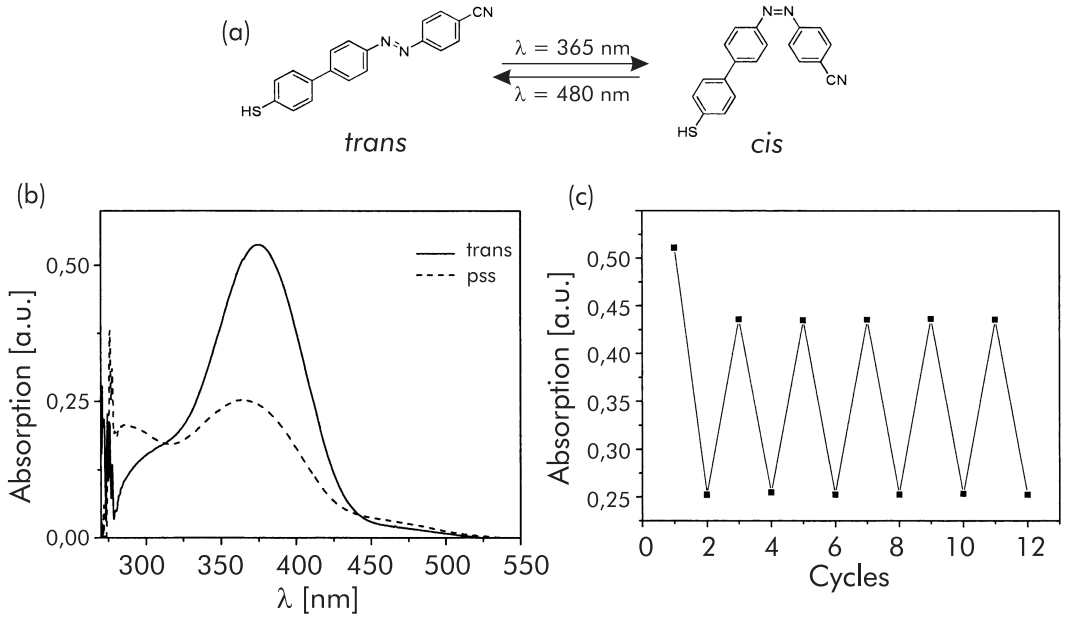

Figure 6.9: (a) Structure of the investigated azobenzene derivative in its *trans* and *cis* geometry, as well as the corresponding wavelengths to induce the isomerization in either direction (*trans* $\rightarrow$ *cis* and *cis* $\rightarrow$ *trans*, respectively). (b) UV/Vis absorption spectrum of the azobenzene biphenyl compound solved in benzene ($c = 1.02 * 10^{-5}$ mol/l). Solid line represents the spectrum of the molecules in their groundstate (*trans*), dotted line shows the spectrum of the photostationary state (pss) when illuminating with light at $\lambda = 365$ nm. (c) Change in absorption measured at $\lambda = 365$ nm before and after illumination with $\lambda = 365$ nm and $\lambda = 480$ nm, respectively. Reproduced from Ref. [Zar11].

In Figure 6.9 (b) the UV/Vis-adsorption spectra of the azobenzene compound (see Figure 6.9 (a)) solved in benzene ($c = 1.02 * 10^{-5}$ mol/l) are shown before and after

[32]Synthesis by the group of K. Rück-Braun, Subproject B6 of the SFB 658.

illumination with light at $h\nu = 365$ nm and $h\nu = 480$ nm, respectively. At $\lambda = 375$ nm we find the maximum of the symmetry-allowed $\pi - \pi^*$ electronic excitation of the *trans* species. This redshift of ≈ 35 nm, compared to pure azobenzene in solution, is expected for a conjugated system (compare with Chapter 6.1). After illumination with UV light at $h\nu = 365$ nm a decrease of the absorbance of the $\pi - \pi^*$ absorption band of ≈ 50 % can be observed accompanied by a shift of the corresponding maximum of 8 nm to higher energies. In the photostationary state which is enriched with the *cis*-isomer we find the typical increasing absorption band of the $n - \pi^*$ electronic excitation around 480 nm. This feature is less pronounced due to the fact that the accordant electronic excitation is symmetry forbidden and through the overlap with the dominant $\pi - \pi^*$ absorption band.

The back reaction (*cis* $\rightarrow$ *trans*) can be induced when exciting the $n - \pi^*$ transition with photons at $h\nu = 480$ nm. In Figure 6.9 (c) the change in the amplitude of the absorption band at $\lambda = 365$ nm in the UV/vis spectrum is displayed after alternating illumination with the two different wavelengths $h\nu = 365$ and 480 nm. Even after extended repetition (12 cycles of illumination either with $h\nu = 365$ or 480 nm) no decrease in the absorption is detected in the photostationary state. However, one has to note that the former ground state intensity of the absorption band at 365 nm (corresponding to the absorption of cycle 1 in Figure 6.9 (c)) can not be reached by means of inducing the *cis* $\rightarrow$ *trans*-isomerization with light but rather an *trans*-isomer enriched photostationary state (pss) is established with the relative amount of *trans*-isomers being stable after repeated light driven *cis/trans*-isomerization cycles.

6.2.1 Sample Preparation of the Azobenzene Biphenyl SAMs

Again the molecules have been applied to a gold substrate (200nm gold film evaporated on a quartz plate). The gold substrate was flame annealed and then immersed at room temperature in a solution of 1 mg of the azobenzene biphenyl conjugate dissolved in 2.0 ml of 2:1 ethanol-THF solution. To achieve the self assembly of the molecules the gold substrates have been immersed for 24 hours in the dark and under Ar atmosphere. After immersion the samples were carefully rinsed with copious amounts of THF then dried in an argon stream. Afterwards the samples were kept in dark in Ar filled containers until the SFG measurements, to avoid oxidation of the sulfur. For the SFG experiments the adsorbate covered surfaces were mounted in a small chamber under argon atmosphere.

6.2.2 Analysis of the Ground State Geometry

In figure 6.10 the broadband IR-VIS-SFG spectrum of the azobenzene biphenyl functionalized SAM is shown in the frequency window of the -C≡N vibrational mode, which is expected between 2200 and 2260 cm^{-1} [Hes91]. Since the measurements were performed under ambient conditions the central wavelength of the femtosecond-IR pulse is selected such that the resulting SFG spectrum is in a range where it does not interfere with the asymmetric CO_2 stretch vibration of air ($\nu_{as}(CO_2) \approx 2350\ cm^{-1}$).

The intensity of the signal is proportional to the non-resonant contribution, which

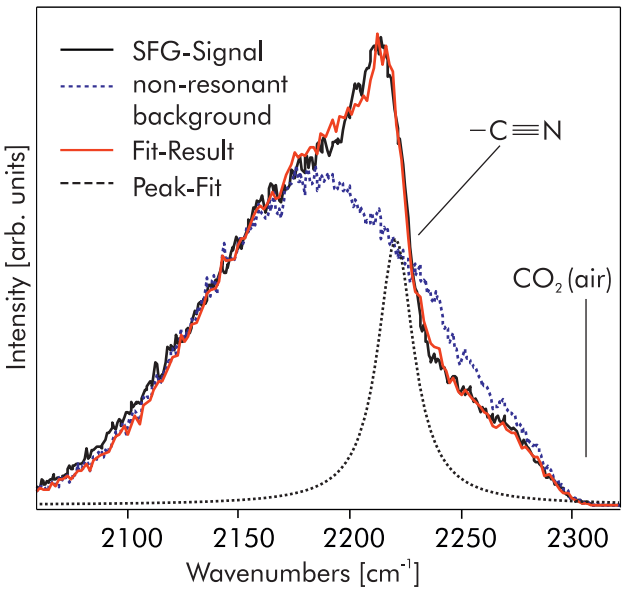

Figure 6.10: Broadband IR-VIS-SFG spectrum of the azobenzene biphenyl SAM on gold in the frequency regime between ≈ 2080 and 2350 $cm^{-}1$ (black solid line). The blue dotted line represents the non-resonant background measured from the bare gold substrate and the red solid line represents a fit using one Lorentzian resonance (black dotted line) and the non-resonant background, which is in good agreement with the experimental data.

is as well depicted in the spectrum. Additionally a fit using one Lorentzian resonance and the non-resonant background, taken from the bare gold substrate, is shown. At 2220 cm^{-1} a strong vibrational feature is observed, which is assigned to the -C≡N triplebond stretch vibration (compare with chapter 6.1.2). Since the relative phase ϕ_q of vibrational modes can lead to completely different lineshapes in the SFG signal, exact statements are often only possible after a detailed analysis using equation 3.7. With a relative phase of $\phi_q = 0.81\pi$ of the Lorentzian resonance the lineshape of the SFG signal is convincingly described.

In addition *surface selection rules* for metals are governing the observable vibrations (see chapter 3.3). For this reason and for the fact that the amplitude of the vibrational mode is strong and in the same regime as observed for the azobenzene-functionalized tripodal SAM (see Chapter 6.1) we propose that the molecules adopt a preferred orientation where the alignment of the molecules leads to a perpendicular or almost perpendicular geometry towards the surface and that the azobenzene is most likely in its *trans* configuration, which is as well the energetically favorable configuration in solution. This assumption seems to be legitimate not only when comparing with our previous study on the functionalized SAMs with the tripodal linker system, but when comparing with STM-results obtained by Giuseppina Pace *et al.* from chemically comparable molecules on gold films which show a tight packing behavior of the *trans*-species in large domains at the surface [Pac07].

The energetic position of the -C≡N stretch vibration is $\approx$ 8 cm^{-1} shifted to lower energies in comparison to the azobenzene-functionalized tripodal SAM. Generally the -C≡N stretch vibration shifts to lower energies when conjugated [Hes91]. The observed red shift is surprising since comparison of the molecular structure of the two different investigated functionalized SAMs shows that for the tripodal molecules the conjugation of the system is expected to be more pronounced due to the triple bond between the azobenzene and the linker system (see Figure 6.1). This fact is expressed when comparing the UV/Vis-absorption spectra of the two dissimilar species. We find for both functionalized conjugates in solution that the maximum of the S_2 electronic excitation in the UV/Vis spectra, which leads to the *trans* $\rightarrow$ *cis* isomerization, exhibits an offset towards lower energies compared to unsubstituted azobenzene. The larger redshift of the maximum of the adsorption band of the $\pi - \pi^*$ electronic excitation for the tripodal azobenzene-linker-conjugate can be easily explained by the stronger conjugation of this system.

Therefore this behavior is attributed to the expected higher packing density of the azobenzene biphenyl SAMs due to an enhanced molecule/molecule interaction compared to the tripodal SAMs. These packing density dependent lateral interactions within the adsorbed layer (*e.g.* dipole-dipole coupling and through-metal interaction *versus* static or chemical effects like intermolecular repulsion or reduced back-donation) can not be distinguished in the present experiment [Hol92, Hof83]. Most likely enhanced dipole-dipole interaction, where the oscillating molecules interact via their through-space dipolar field, does not lead to the observed shift since increasing coverage (packing density) results in a shift to higher frequencies when expressing the potential energy as a sum of simple pairwise dipole-dipole interactions [Ham65].

6.2.3 Illumination Experiments on Azobenzene Biphenyl SAMs

In this chapter we discuss the SFG results obtained from illumination experiments on the vibrational and therefore geometrical structure of the azobenzene-functionalized SAM. Corroborated by the UV-visible spectroscopy results, which revealed that the molecule itself represents an optically addressable molecular switch, we performed irradiation experiments with a solid state laser diode at $h\nu$ = 405 nm and a diode array at $h\nu$ = 470 nm in order to trigger the direct (intramolecular) excitation. Furthermore, we tried to induce the photoisomerization *via* possible indirect excitation mechanisms. Utilizing photons with higher energies the substrate could act as an electron donor and the isomerization could be achieved by attachment of hot electrons to an unoccupied molecular orbital (negative ion resonance). On account of this we illuminated the SAM with UV light from a KrF-Excimer laser ($h\nu$ = 248 nm, 5.0 eV). Figure 6.11 shows the results of the illumination experiments with $h\nu$ = 405 nm and $h\nu$ = 470 nm, respectively.

Starting from the presumed scenario of a preferred orientation of the molecules perpendicular or nearly perpendicular to the surface in which the azobenzene adopts its *trans* geometry, we tried to induce the *trans* $\rightarrow$ *cis* isomerization with blue light at $h\nu$ = 405 nm likewise the observed isomerization of the solved molecules. 30 min

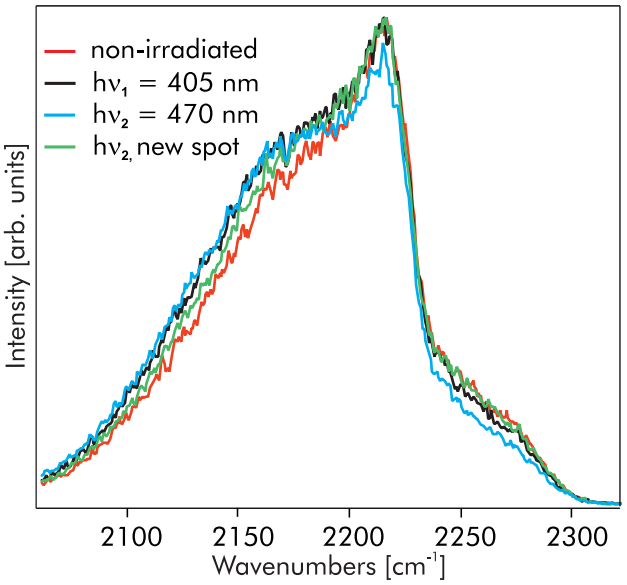

Figure 6.11: (a) SFG spectra of the azobenzene-functionalized SAM before and after light exposure with $h\nu = 405$ and 470 nm and on a fresh spot after illumination with $h\nu = 470$ nm. Neither illumination with $h\nu = 405$ nor 470 nm did lead to any reproducible changes in the vibrational structure of the azobenzene-functionalized SAM. Apparent small changes after illumination with $h\nu = 470$ nm has been disproved after changing to fresh spots within the illuminated area (exemplary spectra shown).

of illumination with a photon dose of $n_p \approx 5 * 10^{18}$ cm^{-2} does not lead to significant changes in the SFG spectrum. Subsequently we illuminated the sample with photon energies of $h\nu = 470$ nm ($n_p \approx 10^{18}$ cm^{-2}). Small changes in the spectrum seemed to be observable, but when we scanned over the sample within the illuminated area it became blatant that the vibrational structure and therefore the configuration of the molecules incorporated in the SAM does not change (exemplary spectra shown in figure 6.11). Variation of the exposure times up to $n_p \approx 10^{19}$ cm^{-2} as well as the usage of the KrF-Excimer laser did not lead to detectable changes within the spectra.

6.2.4 Two-Component Azobenzene-Functionalized SAMs

Considering the results from the azobenzene biphenyl SAMs which did not show any changes in the vibrational structure for different kinds of excitations, we followed a different approach. We derived that the molecules are well ordered and feature a preferred upright orientation towards the surface with an assumed high packing density. The reason for the quenched isomerization of the single-component azobiphenyl SAM could be related to sterical hindrance, due to neighboring molecules, which block the required space for geometrical changes. A related problem could be associated with the π-stacking of the molecules. On one hand it is known that the π-stacking governs the packing density towards closest-packing [Yan00], which is assumed to cause the formation of systems where the photoisomerization of whole domains is feasible [Pac07, Fer08, Cri11]. On the other hand the π-stacking, which is the interaction between the aromatic systems in adjacent molecules, could be responsible for the quenching of the excited state responsible for the isomerisation (*i.e.*, the π^*-orbital) due to a fast decay of the photoexcited electron. The importance of intralayer electronic coupling has recently been shown by Cornelius Gahl *et al.*. They investigated an azobenzene-functionalized alkanethiol *via* X-ray and UV/vis spectroscopy [Gah10]. They found the structural arrangement of the molecules following the self-assembly principles of aliphatic-aromatic SAMs and to be very comparable to the investigated closed-packed biphenyls of references [Pac07, Fer08]. Whereas the decoupling from the surface through the alkanethiol linker is effective, they found a broadening and a blue-shift of ≈ 0.6 eV for the π-π^* transition in the UV/Vis-spectra of the SAM relative to the corresponding absorption maximum of the molecules in solution. This energy shift of the excitation corresponds to a delocalization time on the order of 1 fs. It is plausible that this fast excitonic delocalization within the layer quenches the isomerization reaction which takes ≈ 1 ps [Näg97, Fuj01].

Both possible constraints may be overpowered when introducing spacer molecules in between the functional molecules. Photoinduced conformational changes have been observed for photochromic systems (*i.e.*, azobenzenes [Yas03] and diarylethenes [Kat06]) when chemisorbed in a hosting alkanethiol monolayer. But isomerization has only been observable for molecules at domain boundaries. At these distinct adsorption sites it is known that the packing density and the potential energy landscape are strongly influenced. For functional molecules incorporated in rigid matrixes of shorter tether molecules, which allow the azobenzene moiety to protrude from the matrix, the azobenzene-functionalized molecules are found to be photoactive [Kum08].

In this work (4-*tert*-butylphemyl)methanethiol (see figure 6.8 (b)) is employed to act as a lateral spacer and is introduced to the SAM formation process in solution with a factor of 10(spacer-molecules):1(azobenzene biphenyls)[33]. In figure 6.12 the broadband IR-VIS-SFG spectrum of the two component SAM is shown. The SFG-signal is fitted using the non-resonant background and one Lorentzian resonance. The fit-result is not fully conclusive and shows a deviation especially in the regime between 2250 cm^{-1} and 2300 cm^{-1}. Nevertheless, the fit has been restricted to only one Lorentzian resonance

[33] see chapter 6.2.1 for details of the preparation procedure

since originated from the two components in the SAM this follows the only possible vibration in the chosen frequency window.

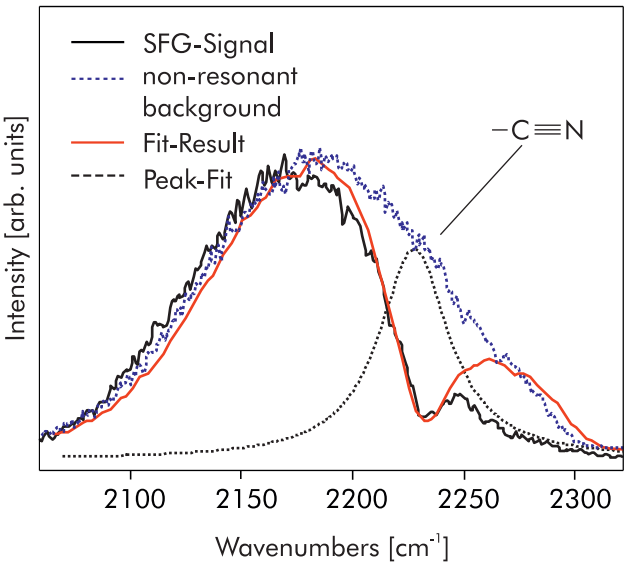

Figure 6.12: SFG signal (black solid line) of the mixed SAM containing (4-*tert*-butylphemyl)methanethiol as a lateral spacer and azobenzene biphenyl. The SFG-signal is fitted using the non-resonant background (blue dotted line) and one Lorentzian resonance (black dotted line). The fit has been restricted to only one Lorentzian resonance. At 2223 cm^{-1} we find the -C≡N triplebond vibrational feature. Derived from the fit we find a relative phase of ϕ_q = -1/2π of the resonance with respect to the background.

At 2223 cm^{-1} we find the vibrational feature, which is assigned to the -C≡N stretch vibration. Derived from the fit we find a relative phase of ϕ_q = -1/2π of the Lorentzian resonance with respect to the non-resonant background. When we compare the results from the fit with the ones that we obtained for the single component SAM (see chapter 6.2.2) a change in the phase is expected (compare with chapter 6.1.2) since it expresses the interference of the SFG-signal with the non-resonant signal, which obviously changed due to the modified molecular layer. When we compare the amplitudes A_q and the full width half maximum Γ_q of the two cases, we find that the ratio of the amplitudes for the mixed SAM and the single-component SAM is 0.77 : 1 and the full width half maximum Γ_q more than doubled. The fact that we observe a broadening of the vibrational mode for the two component SAM usually expresses a situation, where the ordering of the molecular ensemble is disturbed which causes changes in the potential energy landscape of the -C≡N mode due to the chemically different surroundings. Since the ratio A_q is proportional to the number of oscillators the decrease in amplitude is expected. One has to consider as well that the *surface selection rules* fore metal-substrates would lead as well to a lowering of the amplitude, when a disordering of the layer and therefore more random orientations of the oscillators towards the surface are expected. Anyhow the fact that amplitude only drops ≈ 13% is surprising regarding the high dilution of the functional molecules in the formation process. It seems most likely that the admixture of the spacer molecules in the process of the SAM formation hinders the formation of well orientated domains and that the spacers themselves could be displaced to large amounts during the 24 hours self assembly process where the system finds its energetically most stable configuration.

Irradiation of the sample with wavelength of 405, 470, and 248 nm were performed. The illumination experiments with varying photondoses did not lead to observable changes in the SFG spectra.

6.3 Summary

In summary, we have studied the reversible, photoinduced *trans/cis* isomerization of an azobenzene-functionalized SAM on a gold surface using a tripodal linker system and investigated SAMs on gold containing azobenzene biphenyls. In both approaches a cyano marker group is employed to directly investigate the switching state of the azobenzene.

The results demonstrate that the tripodal linker system results in an electronically decoupling of the optically active molecular orbitals of the azobenzene from the electronic structure of the underlying gold substrate. Furthermore the usage of a rather bulky linker system guarantees a sufficient lateral spacing which enables the photoisomerization. To our point of view this seems to be crucial if we compare the obtained results for the tripodal linker to the results of the thiolate azobiphenyl rigid rod molecule, where no photoinduced conformational changes could be observed both for the single-component SAM as well for the diluted SAM with introduced spacer molecules. In consequence of the weak adsorbate-adsorbate and adsorbate-substrate interaction of the tripodal azobenzene derivative, the switching behavior of the azobenzene incorporated into the SAM closely is analogous to the free molecule in solution. We propose a direct (intramolecular) electronic excitation mechanism responsible for the observed *trans* $\rightarrow$ *cis* isomerization at illumination with $h\nu = 405$ nm and the back reaction *cis* $\rightarrow$ *trans* at $h\nu = 470$ nm. A goal for the future would be to incorporate substituents, which exhibit an integrated functionality themselves, which could be activated by the photoinduced conformational change of the functional unit. For instance hydrophillic, polar groups as substituents could change essential characteristics of the surface as chemical reactivity, wetting properties, and the non-linear optical properties when the geometry of the substituents towards the surface is transformed exploiting the steric changes induced by the molecular switching.

7 Bottom Up Fabrication of Graphene Nanoribbons

Graphene, a flat two dimensional monolayer of sp^2-bonded carbon atoms, densely packed in a honeycomb lattice, has despite of its short history attracted tremendous attention. Its strict two-dimensionality combined with the extremely high crystal quality makes it a fascinating model system with outstanding electronic and transport properties. In terms of fundamental physics concerning the peculiar electronic properties graphene no longer needs any further proof of importance [Gei07]. This is highlighted by the award of the Nobel-Prize to A. Geim and K. Novoselov from the *University of Manchester* for their years of work on graphene including the fabrication technique, the *Scotch tape technique*, which led to the first observation of the anomalous quantum Hall effect [Gei10].

However, graphene is a zero-gap semiconductor which makes it unsuitable for the use in nano electronics, where carrier type and transport need to be controlled precisely. Therefore new classes of carbon nanostructures such as one dimensional carbon nanotubes or narrow stripes of graphene, *i.e.* graphene nanoribbons (GNR), hold great promise for new generations of nanodevices. Although the parent material graphene exhibits semi-metallic behavior quantum confinement and edge effects are predicted to determine the electronic nature of all graphene nanoribbons with width $\leq$ 10 nm to be semi-conducting [Eza06, Son06a, Tao11]. GNRs are basically based on single layers of graphene that exhibit different chirality depending on the angle at which it is cut. Depending on how the uncombined edges are configured, *e.g.* either in an armchair or a zigzag configuration (as can be seen in figure 2.15), GNRs have been predicted divergent electronic and magnetic properties. The variable electronic properties, which include metalic/semimetallic behavior, tunable size of the band gap and the presence of one-dimensional edge states with unusual magnetic structure [Fel11] are strongly dependent on the ribbon width and the edge structure [Fuj96, Wak01, Bar06, Son06b].

Although to date there are a number of fabrication methods known from literature, *e.g.* the unzipping of carbon nanotubes [Kos09, Eli10, Tao11] as well as lithographic [Han07], and chemical methods [Yan08, Dat08], the reliable production of atomically precise GNRs with width smaller than 10 nm remains a challenge. L. Grill (FHI Berlin) and St. Hecht (HU Berlin) introduced the concept of the on-surface synthesis[34]. In our investigations we follow the bottom-up approach which has been proposed and successfully operated by Cai *et al.* [Cai10]. They reported a surface-supported GNR synthesis using the precursor monomer 10,10'-dibromo-9,9'-bianthryl. In the bottom-up approach the chirality and width of the ribbon are now defined by the choice of the precursor molecule, which may open up a wide variety of possible GNRs steered by the right chemical design of the precursor. Another big advantage is as well that the fabrication takes place *in sito*, therefore it is possible to measure the specific properties of the GNRs on a clean surface under UHV conditions.

[34] Compare with chapter 2.4

In this study, employing electronic HREELS, we report the first measurement of the band gap of a sub-nanometer wide atomically precise GNR which is an important property of the GNR and is therefore well suited as a benchmark for theoretical calculations.

7.1 Sample Preparation

The Au(111) crystal was mounted on a liquid-nitrogen-cooled cryostat, which is capable of establishing a temperature regime between 90 to 800 K *via* resistive heating. Samples of graphene nanoribbons were prepared *in-situ* by evaporating the precursor molecule 10,10'-dibromo-9,9'-bianthryl by means of a home-built effusion cell held at 450 K at a crystal temperature of $\approx$ 100 K. The crystal was cleaned prior to deposition using a standard procedure of sputtering (Ar+) and subsequent annealing at 800 K. In order to characterize the adsorbate layer thickness, temperature programmed desorption (TPD) was employed monitoring a characteristic fragment (anthracene) of the precursor molecule with a mass of 176 amu while heating the substrate resistively with a heating rate of 1 K/s. Although the sub-monolayer coverage can not be determined in this manner due to the formation of nanoribbons [35], one can distinguish the monolayer from subsequent layers and remove the multilayer(s) by heating. In our fabrication steps of the surface supported GNRs we followed the basic steps described in reference [Cai10] (see figure 7.3): In a first step we annealed the surface at T_S = 470 K which leads to the dehalogenation of the precursor monomers, where the dehalogenated intermediates form linear polymers due to single covalent C-C bonds. After a second annealing step at T_S = 670 K intramolecular cyclodehydrogenation of the polymeric chain is achieved. This leads to a fully aromatic system and therefore to the formation of the N = 7 armchair GNR. Each step has been followed with vibrational HREELS to determine the respective configuration (see chapter 7.2).

[35] Although the nanoribbons are expected to be physisorbed at a low binding energy, the large contact area to the substrate results in an inability to desorb thermally at temperatures up to 800 K.

7.2 Characterization of the On-Surface Synthesized GNRs

As described in chapter 7.1 we followed each step of the fabrication process of the GNR by means of vibrational HREELS. Figure 7.1 shows the HREELS spectrum of $\leq$ 1 ML 10,10'-dibromo-9,9'-bianthryl on Au(111) annealed at T_S = 470 K. At this temperature it is reported for the precursor monomer to dehalogenate and to form covalent C-C bonds between the now dehalogenated intermediates resulting in polymer chains. We annealed for 10 min to provide sufficient thermal energy for the the C–Br dissociation and to enhance surface mobility of the species to establish a sufficient polymer chain formation.

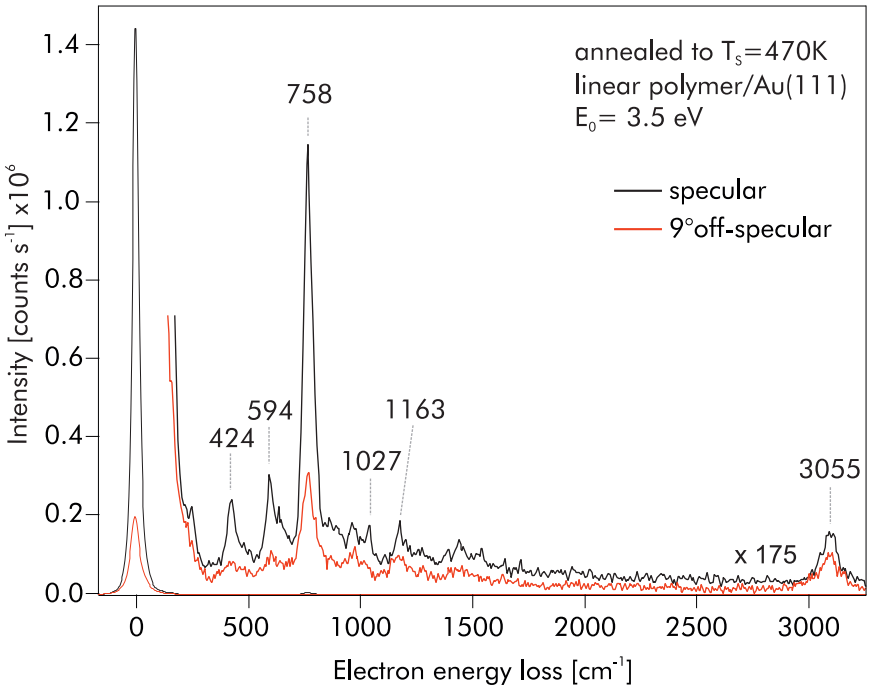

Figure 7.1: HREEL spectrum of $\leq$ 1 ML 10,10'-dibromo-9,9'-bianthryl on Au(111) annealed at T_S = 470 K taken in specular (solid black line) and in 9° off-specular (solid red line) geometry recorded with a primary electron energy of E_0 = 3.5 eV. The FWHM of the elastic peak is 32 cm^{-1} (4.0 meV) in the specular and 46 cm^{-1} (5.8 meV) for the off-specular recorded spectrum, respectively. Please note that the resolution is negatively influenced by the high count rate. The choice favoring the higher count rate instead of better resolution was made because of the rather simple structure of the vibrational loss spectrum.

We recorded the HREEL spectrum in specular (solid black line) and in 9° off-specular (solid red line) geometry with primary electron energies of E_0 = 3.5 eV. The FWHM of the elastic peak is 32 cm^{-1} (4.0 meV) in the specular and 46 cm^{-1} (5.8 meV) for the off-specular recorded spectrum, respectively. The vibrational frequencies and their assignments are listed in table 7.1 together with the results obtained for the GNR

covered gold surface (see figure 7.2). In the specular spectra of HREELS, the signals contains both dipole- and impact scattered components [Iba82]. The C–H stretch mode (ν(C–H) $\approx$ 3055 cm^{-1}) and the out-of-plane C–H wagging mode (γ(C–H) $\approx$ 758 cm^{-1}) as well as out-of-plane edge modes at $\approx$ 594 cm^{-1} and out-of-plane modes of the carbon atoms of the aromatic rings (τ(C–C) $\approx$ 424 cm^{-1}) show high intensities. Vibrational structure is detected with low intensities in the region from $\approx$ 800 to 1500 cm^{-1}.

vibrational mode	linear polymer*	GNR*	assignment
τ(C–C)	424 (*sda*)	404 (*sda*)	410[a]
oop edge modes	594 (*sda*)	609 (*sda*)	630[b], 500-650[c]
γ(C–H)	758 (*da*)	793 (*sda*)	790[d]
in plane modes	1027	–	–
(scissoring) δ(C–H)	1163	–	1150[d]
ν(C–H)	3055	–	3000-3100[e]

Table 7.1: Vibrational frequencies (in cm^{-1}) and assignments for the linear-polymer phase and the GNR phase on Au(111), respectively.
oop, out-of-plane; ν, stretch; δ, in-plane bend; τ, torsion; γ, out-of-plane bend.
* Obtained by HREELS; present study.
Theoretical and/or experimental vibrational data adapted from: [a] [She88], [b] [Maz11], [c] [Mal09], [d] [Luo10], [e] [Gün96] for assignment of the vibrational modes. The *da* indicates a mainly dipole active mode, *sda* indicates a strong dipole activity.

In order to gain insights in the excitation mechanism and to be able to analyze the adsorption geometry of the linear polymers on the surface (see figure 7.3), we performed angular dependent measurements. The out-of-plane edge modes at $\approx$ 594 cm^{-1} and the out-of-plane modes of the carbon atoms of the aromatic rings at $\approx$ 424 cm^{-1} exhibit a huge intensity decrease, the out-of-plane C–H wagging mode (γ(C–H) $\approx$ 758 cm^{-1}) a pronounced intensity decrease in the off-specular spectrum, indicating that their intensities are originating mostly from dipole scattering in the specular spectrum (see table 7.1 for the assignment of the dipole active modes). The strong dipole activity of the C–H wagging and out-of-plane modes at $\approx$ 424 and $\approx$ 594 cm^{-1} point towards a preferential orientation of the linear polymers lying mostly flat on the Au(111) surface. Since in this configuration these modes possess a strong dipole moment change upon vibration perpendicular to the surface.

Because of the single C–C bond in the linear polymer phase the aromatic rings exhibit an tilt angle towards the surface which has been confirmed by STM in reference [Cai10]. Indeed our measurements support the reported molecular arrangement. We observe the C–H stretch mode ν(C–H) at $\approx$ 3055 cm^{-1} with a weak dipole activity indicating that dipole moment change of this vibrational mode exhibits a component parallel to the surface normal. Therefore we confirm the geometry shown in figure 7.3 (i).

Figure 7.2 shows the HREELS spectrum after annealing the linear polymer covered

Au(111)-surface at T_S = 670 K for 10 minutes. This further annealing at 670 K is the final step in the surface assisted synthesis of the GNR on gold. Here we induce an intramolecular cyclodehydrogenation of the polymer chain resulting in the N=7 armchair ribbon which is shown in figure 7.3 (ii). We recorded the HREEL spectrum again in specular (solid black line) and in 9° off-specular (solid red line) geometry with a primary electron energy of E_0 = 3.5 eV. The FWHM of the elastic peak is 31 cm^{-1} (3.9 meV) in the specular and 46 cm^{-1} (5.7 meV) for the off-specular recorded spectrum, respectively. In comparison to the specular spectrum of the linear polymer phase the count rate in the elastic peak gains one order of magnitude to 14 $*10^6$ counts per second. Only three vibrational excitations are observable after the cyclodehydrogenation step, the out-of-plane edge modes at ≈ 609 cm^{-1}, and the out-of-plane modes of the carbon atoms of the aromatic rings at ≈ 404 cm^{-1}, and the out-of-plane bend mode C–H (γ(C–H) ≈ 793 cm^{-1}). The extremely high count rate and the very pronounced out-of-plane (few) detected vibrational modes express an extreme electronic smoothness of the molecule covered surface.

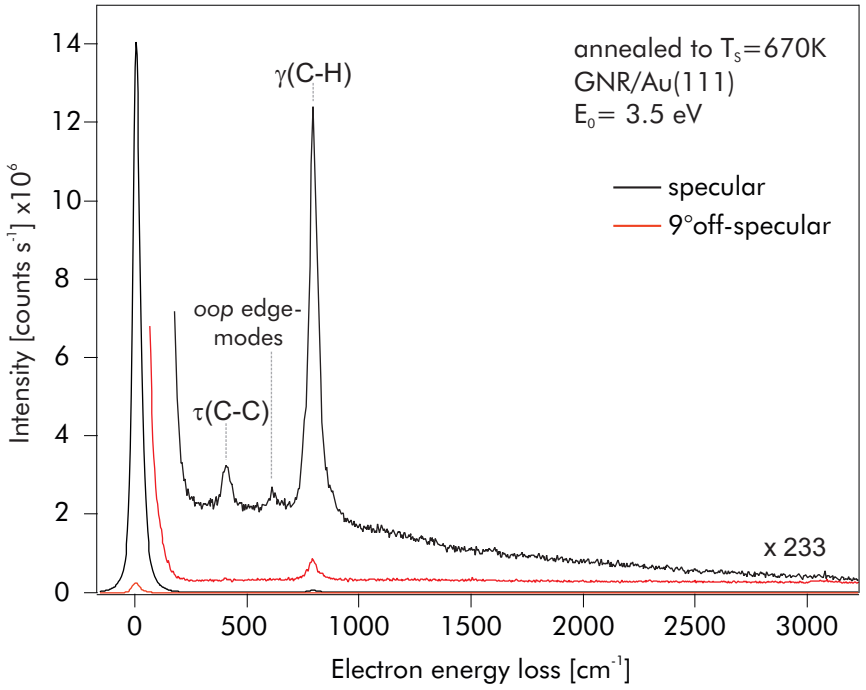

Figure 7.2: HREEL spectrum of ≤ 1 ML 10,10'-dibromo-9,9'-bianthryl on Au(111) annealed at T_S = 670 K recorded in specular (solid black line) and in 9° off-specular (solid red line) geometry recorded with primary electron energies of E_0 = 3.5 eV. The FWHM of the elastic peak is 31 cm^{-1} (3.9 meV) in the specular and 46 cm^{-1} (5.7 meV) for the off-specular recorded spectrum, respectively.

It has been reported in the supplementary information of reference [Cai10] and in a theoretical DFT study using the local-density approximation [Gil10] that the mode

we observe at 404 cm^{-1} in our study[36] is caused by the transverse-acoustic fundamental mode (1-TA). In this mode all atoms of one half of the nanoribbon move in-phase and in opposite direction than the atoms of the other half, resulting in a strong width dependent mode. We conclude differently, as it is obvious from the spectra obtained from the GNR phase (see Figure 7.2). The mode at 404 cm^{-1} exhibits a very strong dipole activity equivalent to a pronounced orientation of the dipole moment change perpendicular to the surface. We conclude that its origin lies in an out-of-plane torsion mode of the phenyl rings. This conclusion is backed up by a theoretical study where only one mode is found for armchair nanoribbons in the vicinity of 400 cm^{-1} which shows no width dependent and corresponds mainly to out-of-plane modes [Maz11].

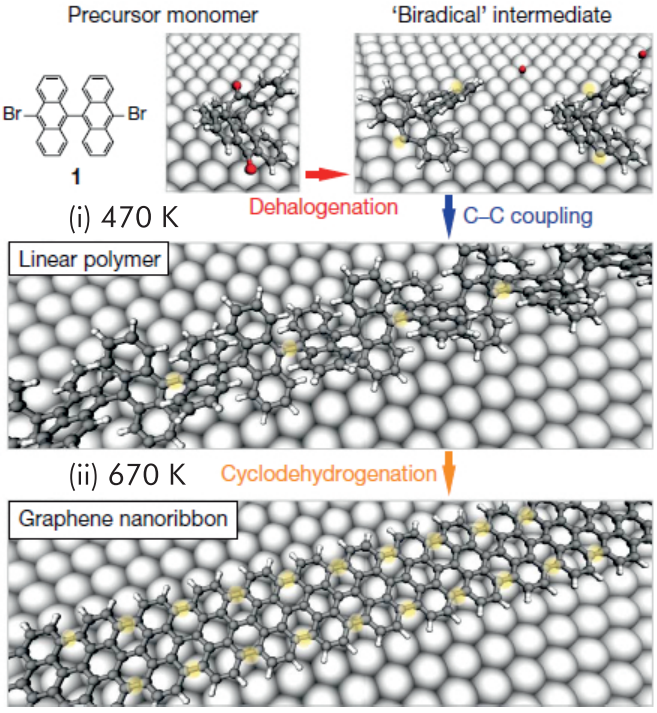

Figure 7.3: Bottom up fabrication of atomically precise GNRs. (1) shows the precurser monomer 10,10'-dibromo-9,9'-bianthryl. Basic steps for the bottom-up fabrication of the nanoribbons from bianthryl (1) monomers to straight N = 7 GNRs:
(i) In a first step heating the surface to 470 K leads to a surface-assisted dehalogenation of the monomer followed by a C-C coupling resulting in the linear polymer phase (polyanthrylene)
(ii) Further annealing at 670 K induced intramolecular cyclodehydrogenation of the polymer chain resulting in the N=7 armchair ribbon.
Picture is adopted from reference [Cai10].

All three observed modes exhibit a strong dipole activity derived from the comparison with the HREELS spectrum taken at 9° off-specular geometry (red solid line). The strong dipole activity of the out-of-plane modes and the complete absence of vibrational excitations in the regime $\geq$ 800 cm^{-1}, which is governed by in-plane vibrational edge modes (C–H) leads us to the conclusion that the GNR phase is established with an tremendously high efficiency. Especially the complete absence of the former relative intense C–H stretch vibration is a clear proof for the planar adsorption geometry of the GNRs on the Au(111)-surface.

Hence this corroborates the proposed planar adsorption geometry and the successful bottom-up fabrication of the GNR schematically shown in figure 7.3.

[36] found at 396 cm^{-1} in [Cai10] derived from Raman spectroscopy, and at $\approx$ 410 cm^{-1} in [Gil10] derived from DFT calculations for a nanoribbon width = 7.5 Å.

7.3 Investigation of the Electronic Structure of the GNR

We investigated the electronic structure of the GNR with employing the HREELS spectrometer by means of measuring electronic transitions occurring in the adsorbate covered surface at a primary electron energy of 15 eV. Electronic EELS with energies of ≈ 10 eV was first used to study surface electronic excitations on semiconductor and insulator surfaces to determine the energy gap between valence and conduction band [Roc95] which makes it an appropriate tool for our aim of investigating the band-gap/electronic structure of the GNR. To gain confidence in this technique we started with measurements of thick multilayers of 10,10'-dibromo-9,9'-bianthryl (≥15 ML) adsorbed on Au(111). In figure 7.4 an exemplary spectrum of ≈ 15 ML on Au(111) dosed at a sample temperature of $T_S \approx 100$ K is shown.

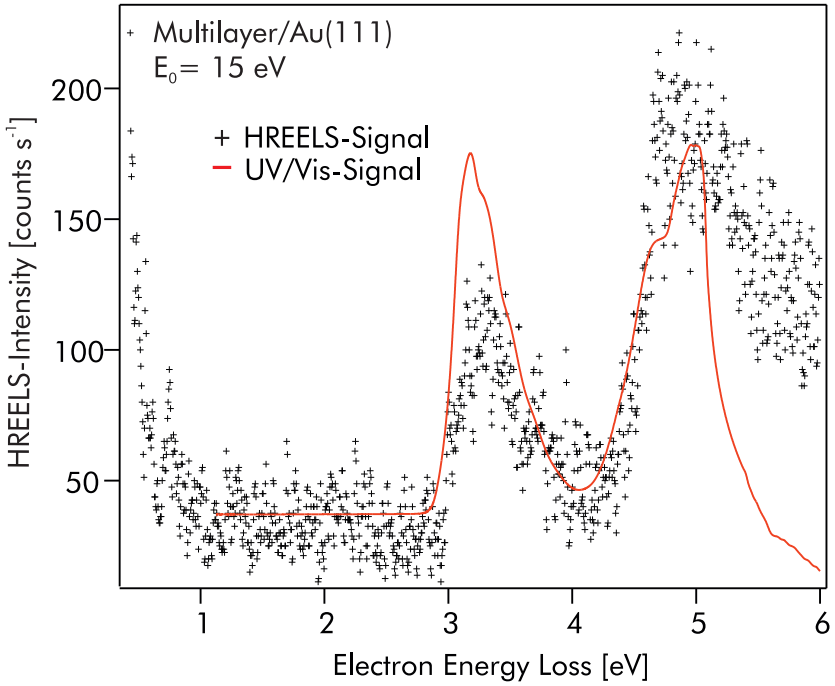

Figure 7.4: HREEL spectrum of a thick multilayer (≥15 ML) of 10,10'-dibromo-9,9'-bianthryl adsorbed on Au(111). In the HREELS experiment the primary electron energy has been set to $E_0 = 15$ eV and the electron energy loss has been analyzed in an energy regime up to 6 eV (≈ 48390 cm^{-1}) to investigate electronic excitations. The fwhm is 19 meV (153 cm^{-1}). For comparison the UV/Vis absorption spectrum of the same molecule in solution is plotted against the same energy axes in arbitrary units (solid red line). The comparison exhibits a qualitatively good agreement in the energetic positions of the observed electronic excitations.

The spectrum is shown in an electron energy loss regime between 0.7 and 6 eV, where typically the first electronic transitions between the occupied and unoccupied molecular orbitals are expected. The fwhm of the elastic peak is 19 meV. On the

low energy side of the spectrum the shoulder of the elastic peak is visible. Between 1 and 3 eV the spectrum exhibits no measured excitations followed by two distinct features which we assign to electronic excitations located[37] at 3.3 and 4.9 eV, respectively, supported by the UV/Vis absorption spectrum. To gain further knowledge about the electronic structure of the molecule we performed UV/Vis absorption measurements of the molecule solved in chloroform. The result is also shown in figure 7.4. The comparison exhibits a very good congruence depending the energetic positions of the observed electronic excitations showing that the method is suited to determine the electronic structure (electronic transitions).

The UV/Vis absorption spectrum exhibits a more detailed view of the fine structure of the observed electronic transition. In figure 7.5 we fitted the UV/Vis data using five Gaussians. The fit describes the measured data conclusively. From this we derive five electronic excitations, were the energetically lowest lying is assigned to the HOMO to LUMO transition at 3.12 eV. Further peak positions are at 3.30, 3.62, 4.78, and 5.00 eV [38].

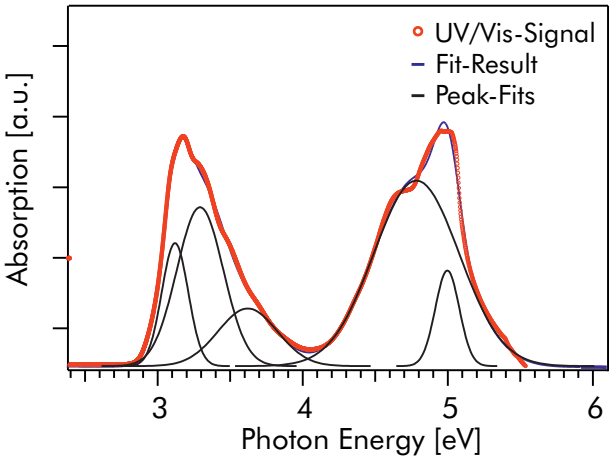

Figure 7.5: UV/Vis absorption spectrum of 10,10'-dibromo-9,9'-bianthryl in solution (red dots) and a fit (solid blue line) using 5 Gaussians. The fit describes the measured absorbance conclusively. The energetically lowest lying feature is assigned to the HOMO to LUMO transition at 3.12 eV. Further peak positions are at 3.30, 3.62, 4.78, and 5.00 eV.

Figure 7.6 shows a series of spectra starting with the spectrum from the clean gold substrate (black markers) followed by the multilayer spectrum (red markers) and the spectra of the linear polymer phase (annealed at 470 K; blue markers) and the GNR phase (annealed at 670 K; green markers), respectively. All spectra have been taken in specular geometry at sample temperatures of $T_S \approx 100$ K. To exclude that for the chosen primary electron energy of $E_0 = 15$ eV no underlying structure of electronic excitations of the bare gold substrate interferes with the later performed measurements

[37] The energetic position is determined by the position of the maximum intensity of the corresponding peak.

[38] Structure optimizations have been performed with Gaussian09 using the B3LYP hybrid functional by L. Bogner, FU Berlin. The electronic transitions determined from the yielded molecular orbital gaps show two basically two electronic transitions at around 3.4 (HOMO→LUMO) and 4.7 eV (HOMO-2→LUMO and HOMO→LUMO+2) with a substructure revealing three transition for the gap around 3.4 eV and two transitions for the gap around 4.7 eV. The energetic differences (in the order of 1/100 eV) found in the substructures are "physically unlikely". The overall trend is comparable. The results are given Appendix A.

of the adsorbate covered surface we took a spectrum of the freshly prepared Au(111) surface. For the clean Au(111) surface no distinct features are observed. Thereafter we deposited a thick multilayer (≈ 15 ML) on the cold gold substrate ($T_S \approx 100$ K). The results are already discussed above (see Fig. 7.4).

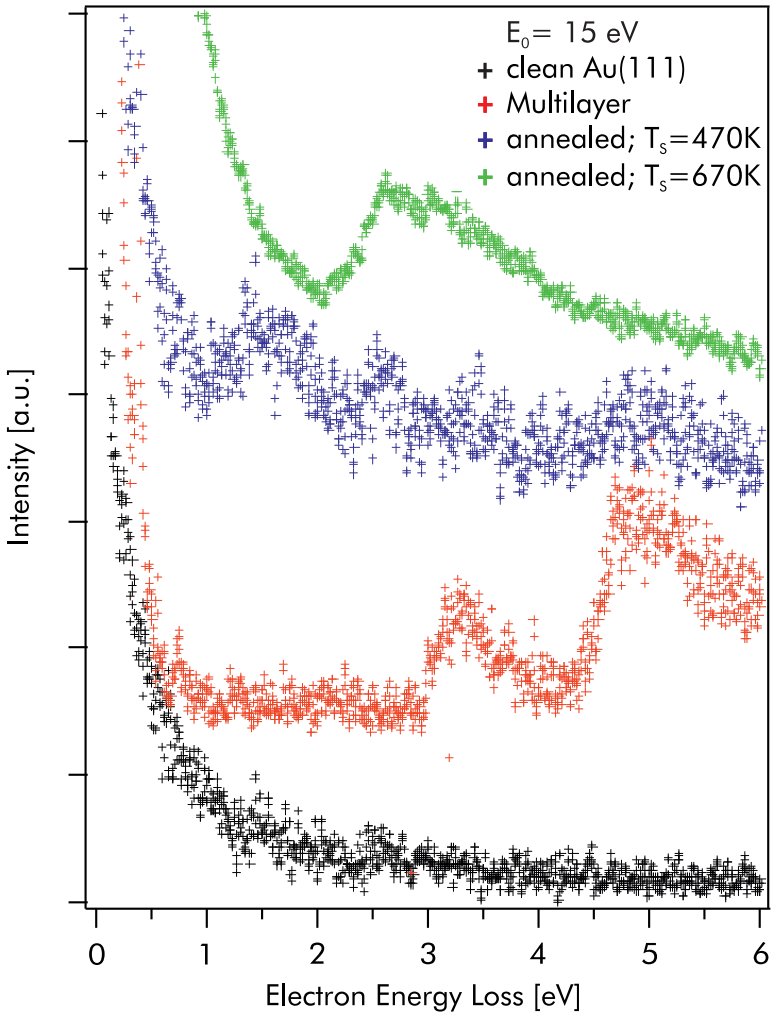

Figure 7.6: HREELS spectra taken with a primary electron energy of $E_0 = 15$ eV. Shown is a series of data as a function of annealing temperature, *viz.* the different steps in the formation process of the GNRs starting with the spectrum from the clean gold substrate. All spectra have been taken in specular geometry, the fwhm for all spectra is ≈ 20 meV. For clarity the spectra are vertically shifted with respect to their baseline.

When we heat the surface for 10 min to $T_S = 470$ K the precursor molecules dehaligonate and form covalent C-C bonds between the now dehalogenated intermediates resulting in polymer chains. The result supports the observed on-surface synthesis detected with vibrational HREELS. The electronic structure is obviously changed for the single phases formed during the annealing steps. For the now linear polymer covered

surface we found a more diverse electronic structure. Starting at lower energies we find features in the spectrum at ≈ 1.6 and ≈ 2.6 eV followed from two electronic excitations, *i.e.* ≈ 3.4 and ≈ 5.0 eV, found in the regime of the observed electronic excitations of the multilayer covered substrate. When heating the surface further to $T_S = 670$ K to achieve the the formation of fully aromatic GNRs by cyclodehydrogenation we observe in the region between 2 to 4.2 eV loss energy a broad feature. The feature exhibits a clear double peak structure. The description of the electronic structure is given in more detail later in the text. The energetic transitions are summarized in table 7.2.

system	electronic transition [eV]
multilayer/Au(111)[a]	≈ 3.3 and ≈ 4.9
lin. polymers/Au(111)[b]	1.6, 2.6, 3.4, and 5.0
GNR/Au(111)[c]	2.60, and 3.07

Table 7.2: Electronic transitions all phases investigated on Au(111).
[a] The electronic transitions for the multilayer phase are determined by the position of the maximum intensity of the corresponding peak.
[b] The electronic transitions for the linear polymer phase are determined by the position of the maximum intensity of the corresponding peak.
[c] The electronic transitions for the GNR phase are derived from the fit shown in figure 7.7

Our aim of the investigation of the GNRs on Au(111) was to gain insight into the electronic structure of the sample. Especially the width dependent band gap is of high interest for possible future applications of nanoribbons. Although graphene nanoribbons have been extensively studied in literature [Nak96, Bar06, Eza06, Son06b, Son06a, Cha11] the band gap of nanoribbons is to date only measured for lithographically patterned GNRs with a width ≥ 15 nm [Han07]. For nanoribbons with a width ≤ 10 nm the author is only aware of a study for chemically derived nanoribbons [Li08]. Here the fabrication is achieved by centrifugation of exfoliated commercial expandable graphite, with an edge structure of unknown precision.

It is well known that particularly the structure of the edge and the electronic edge states determine the electronic properties of the nanoribbons. Similar to carbon nanotubes (CNTs) the energy gap depends on the width and on the crystallographic orientation of the GNR [Nak96]. Therefore differences in the results for the fundamentally different approaches of fabrication, *i.e.* top-down *versus* bottom-up approaches, are understandable due to the expected different structural and chemical precision of the resulting GNRs. Due to the bottom up approach[39] resulting in atomically precisely fabricated nanoribbons investigated in this study we expect our measurements to give benchmarking results for the band gap. To our knowledge this is the first time that the electronic structure of an atomically precise graphene nanoribbon with a width of ≤ 1 nm is measured[40].

[39] following reference [Cai10]
[40] Scanning tunneling microscopy (STM) investigations by Cai *et al.* of the system yield a ribbon width of 7.5 Å.

Figure 7.7 shows a close view on the electronic HREELS spectrum of the GNR covered gold. The broad feature at 2 to 4.2 eV due to the electronic excitation exhibits a clear double peak structure. Therefore we fitted the spectrum in this region using two Gaussians. The fit is displayed as a solid red line in the measured spectrum. The energetic positions of the two electronic transitions are determined to 2.6 and 3.1 eV, respectively.

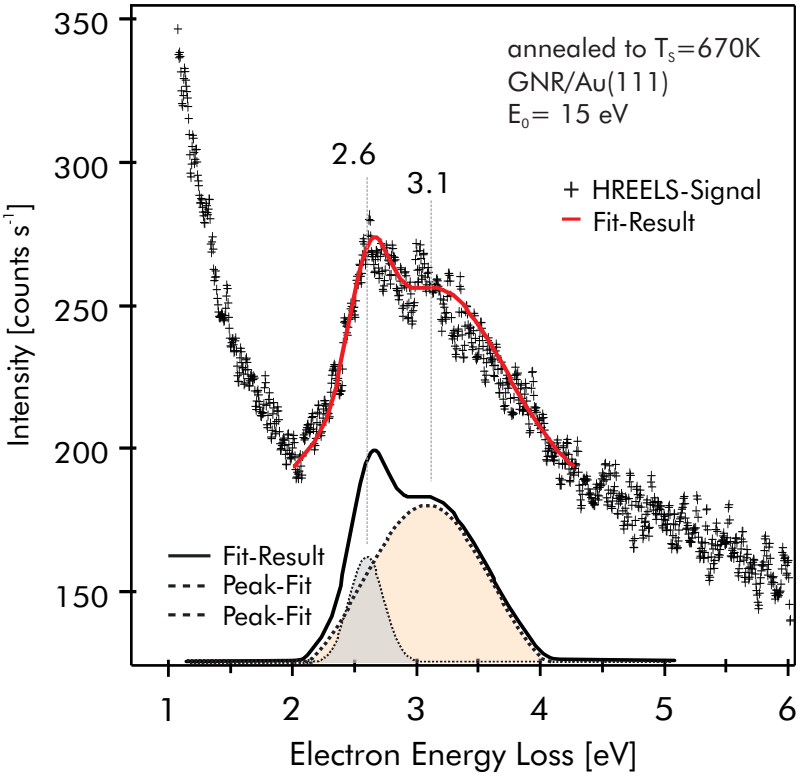

Figure 7.7: HREELS spectrum of the GNR-covered gold surface recorded at a primary electron energy of $E_0 = 15$ eV shown in an electron energy loss regime from 0.7 to 6 eV. The spectrum is fitted (solid red line) using two Gaussian peaks located at 2.6 and 3.1 eV, respectively. Two electronic transitions are observed located at 2.6 and 3.1 eV. The energetically lowest lying transition can be assigned to the band gap of the system.

The energetically lowest lying transition can be assigned to the transition from the highest occupied band, *i.e.* the valence band, of to the lowest unoccupied band, *i.e.* the conduction band. Whereas the higher lying transition located at 3.1 eV could either be caused by the transition from the highest occupied band -1 to the lowest unoccupied band or by the transition from the highest occupied band to the lowest unoccupied band +1. The two possible electronic transitions underlying the peak at 3.1 eV electron energy loss are indistinguishable with the use technique.

The lowest transition energy corresponds to the band gap of the system which thus is directly measured in the presented electronic HREELS experiment. When we compare the determined value for the investigated N = 7 GNR with a width of 7.5 Å with

the width-dependent band gap calculations by Son *et al.* in the local density approximation we find a rather large offset of around 1 eV as can be seen in figure 7.8 [Son06b].

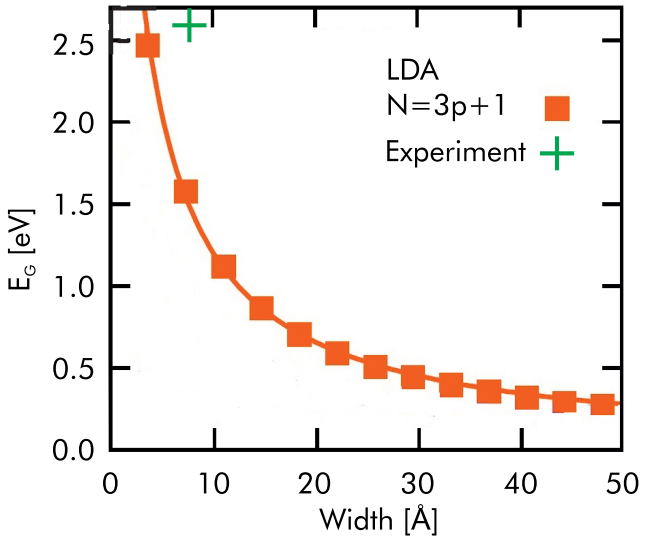

Figure 7.8: Comparison of the in the present work measured band-gap for the GNR (width = 7.5 Å, N = 7, p = 2) adsorbed on Au(111) (green cross) to the width-dependent local-density approximation (LDA) calculations from Son *et al.* for Na=3p+1 wide nanoribbons (red curve taken from [Son06b]).

In a another theoretical study by Barone *et al.* employing different functionals[41] the band gap is determined to 1.5 eV for PBE and 2.1 eV for the HSE calculations [Bar06]. Using the HSE functional, they predict a doublet structure in a calculated optical spectrum of a N = 7 armchair nanoribbon resembling the observed structure of the measured electronic transitions.

[41] (i) One is the PBE realization of the generalized gradient approximation CGA and (ii) HSE, the screened exchange hybrid density functional.

7.4 Summary

In summary, we have demonstrated that the bottom-up approach presented in reference [Cai10] is feasible and that HREELS is an excellent technique to follow the respective steps of the *in situ* GNR fabrication for the prototypical armchair ribbon of width N=7. We were able to confirm the radical addition reaction to form linear polymers during a first thermal activation at T_S = 470 K and the surface-assisted cyclodehydrogenation at a second annealing step at T_S = 670 K which is the final step in the formation of the GNRs. Only vibrational modes of the wanted chemical end-product are observable in the vibrational HREELS spectrum after the last fabrication step. We have to conclude that the by Cai *et al.* presented bottom-up approach results in chemically pure GNRs. Within the accuracy of the method in use there is no experimental proof of unwanted side-products.

Furthermore employing primary electron energies of E_0 = 15 eV, HREELS has been proven to be a powerful tool which enables us to directly measure the band gap of the GNRs on Au(111). Despite the intriguing width- and shape-dependent electronic properties of GNRs, especially the possible engineering of the band gap, predicted by calculations and their great future regarding possible applications this is the first measurement of the band-gap of a chemically pure sub nanometer GNR.

As a key feature we were able to determine the band gap and a second electronic transition at 2.60 and 3.07 eV, respectively. GNRs incorporated into transistors have already shown excellent electronic properties with on/off ratios of more than 100.000 : 1 [Bul08]. The in this study presented result for the size of the band gap fits in the overall trend of an opening gap with decreasing GNR width presented in theoretical work by Son *et al.* and Barone *et al.*. Values for the band gap of the N = 7 GNR are reported to: 1.6 eV [Son06b], 1.5 and 2.1 eV [Bar06], depending on the used functionals. Therefore the presented results could be of interest as a benchmark for further theoretical calculations. For nanoribbons with a width $\leq$ 10 nm the author is only aware of a study for chemically derived nanoribbons [Li08]. Here, following the trend for the measured nanoribbons, the band gap of a sub-nanometer wide ribbon would be an order of magnitude lower. Once again we would like to point out that the reliable production of atomically precise nanoribbons remains a big challenge for top-down approaches.

Our results, combined with the known band gaps for GNRs of width $\geq$ 10 nm [Han07, Li08], clearly show that the usage of a rational design of GNR width (and shape) opens up the possibility to precisely tailor the band gap to achieve the wanted electrical properties for the use in technical applications. The bottom up fabrication method seems to be ideal to produce atomically precise nanoribbons but is limited in means of the availability of precursor molecules resulting in a successful on-surface synthesis. To our knowledge only the in the present study investigated precursor molecule and a precursor which forms chevron-type nanoribbons are known to date [Cai10]. Nevertheless this methods holds great promise, with the development of a wider range of (chemically pure or doped) precursor molecules, for a wide range of nanostructures with desired physical properties.

8 Summary

The present work focuses on the investigation of molecular switches on coinage metal substrates by vibrational spectroscopies utilizing electrons or photons. In this thesis four different kinds of adsorbate/substrate systems have been presented. The main goal was to achieve comprehensive understanding of the various factors determining the switching ability given by the interaction of the adsorbed molecules with the metal substrate. For this purpose molecules capable of undergoing photoinduced *trans/cis*-isomerizations and ring-opening/closing reactions in solution have been investigated mainly on Au(111) by means of high resolution electron energy loss spectroscopy (HREELS). In a second experimental approach we investigated azobenzene functionalized self assembled monolayers (SAMs) which are formed *ex-situ* under wet chemical conditions on gold. Sum-frequency generation (SFG) vibrational spectroscopy is used to determine changes in the geometry of the molecules accompanying the *trans/cis*-isomerization. In the last part of the thesis we have been exploring the potential of a bottom-up fabrication of graphene nanoribbons (GNRs) on Au(111) studied by vibrational and electronic HREELS.

In the study of the first kind of adsorbate/substrate systems various molecular switches which are able to undergo a photoinduced *trans/cis*-isomerization in solution we investigated their adsorption geometry and isomerization behavior on metal substrates. We systematically changed the photochemically active group and studied its dependence on the switching ability. Furthermore we varied the substrate from Au(111) to Cu(111) for the azobenzene derivative tetra-*tert*-butyl-azobenzene (TBA). TBA/Au(111) is so far one of the few systems where a photoinduced *trans/cis*-isomerization of the adsorbed species is feasible. We investigated three isoelectronic molecules which are the respective derivatives of azobenzene (TBA), imine (TBI) and stilbene (TBS) equipped with four *tert*-butyl groups at the phenyl-rings supposed to decrease the coupling strength between adsorbate and surface. Depending on the photochemically active group changing from the diazo-group (–N=N–) in TBA to the imine-group (–HC=N–) in TBI and to the vinylene-group (–HC=CH–) in TBS we observed considerable differences in their isomerization behavior. We find for all three molecules a planar adsorption geometry of the respective *trans*-isomer after deposition on the metal surface. This is despite the known twisted *trans*-geometry for free imine molecules and already shows the influence of the substrate. Whereas photoinduced switching for TBA on Au(111) is feasible it is quenched for TBS and TBI on Au(111) as well as for TBA on Cu(111). The molecular switching in TBA/Au(111) is driven by the generation of a positive ion resonance (cation) *via* a charge transfer of holes from the Au *d*-band to the HOMO level of TBA. This mechanism is obversely not efficient in TBS and TBI on Au(111) and TBA on Cu(111), even though the HOMO level of TBS as well as the *d*-band of Cu are at similar energetic positions compared to TBA/Au(111).

For TBI on Au(111) we found an thermally activated *trans*→*cis*-isomerization. When sufficiently heated all molecules are found in their *cis*-state. This is in disagreement for the molecules in solution where the *trans*-isomer represents the energetically

more stable compound. We were able to gain a quantitative insight into the reaction deriving the activation energy to $E_A = 0.6 \pm 0.1$ eV. Compared to the free molecules we find the barrier reduced about 0.4 eV showing the strong influence of the substrate on the potential energy landscape resulting in an "inverted" thermal isomerization behavior. At a bilayer of TBI on Au(111) we observe the thermal *trans*→*cis*-isomerization already at lower temperatures. After complete desorption of the second layer we find the molecules in the *trans*-conformation again. This is opposing to the experiments of a starting coverage of one monolayer where only *cis*-isomers are present after thermal activation expressing that the isomerization behavior is coverage dependent. A second annealing step leads to a further *trans*→*cis*-isomerization similar to the findings for one monolayer starting coverage. We deduce this behavior to non-identical *cis*-species depending on their binding situation to the surrounding. A possible reason could be given by the presence of a stronger interaction of the lone pair of the nitrogen in the *cis*-conformation with the surface for coverages ≤ 1 ML leading to an increased coupling and quenching of the back reaction.

As the second adsorbate/substrate system we studied 1,3,3-trimethylindolino-6-nitrobenzopyrylospiran (spiropyran, SP) on Au(111). Spiropyran undergoes a photo and thermally induced bidirectional ring-opening/closing reaction between the stable spiropyran and the meta-stable, isomeric merocyanine (MC). From angular dependent HREELS measurements we could analyze the adsorption geometry. On Au(111) the molecules are present in their three dimensional, closed SP form. The benzopyran moiety of the closed form is lying flat on the surface and the indoline unit is orientated perpendicular to it. Annealing of the molecular layer induces tremendous changes in the vibrational fingerprint. We found evidence for the appearance of the open MC isomer orientated parallel on the Au(111) surface (flat lying). It is significative that on a relatively inert metal surface like Au(111) the thermal stability is reverted, turning the open merocyanine into the most stable form. This result introduces the conceptually attractive possibility of using inorganic substrates to balance the equilibrium between open and closed isomers simply by tuning the strength of the interaction with the metal substrate. The back reaction could not be induced neither by temperature nor by photons. We were able to derive the activation energy for the thermally induced ring-opening reaction to $E_A = 0.84 \pm 0.05$ eV being surprisingly close to the reported values of spiropyran in solution. This excludes the possibility that the activation energy for the dissociation of the C–O bond in the ring opening is lowered by the presence of the metal. The reason for the stability inversion could be given by a zwitterionic state of MC stabilizing the open isomer on the metal substrate. Note, that photoswitching could not be observed in either direction, possibly due to a reduction of the life-time of the photoexcited state through additional decay channels to the metal.

SFG vibrational spectroscopy is employed to investigate the reversible, photoinduced *trans/cis*-isomerization of an azobenzene-functionalized self-assembled monolayer (SAM) on gold using a tripodal linker system. In addition we studied azobenzene biphenyl SAMs on gold. In both molecules a cyano-group at the outer phenyl-ring is used as a direct measure of the switching state. We found effective cross sections for the reactions

of σ_{eff} (*cis*) = 4 ± 1 × 10^{-18} cm^2 at 405 nm (*trans*→*cis*) and σ_{eff} (*trans*) = 2.5 ± 1 × 10^{-19} cm^2 at 470 nm (*cis*→*trans*), both are similar to the cross sections found for the free molecule in solution. The results demonstrate that the tripodal linker system results in an electronically decoupling of the optically active molecular orbitals of the azobenzene from the electronic structure of the underlying gold substrate. Furthermore the bulky linker system guarantees a sufficient lateral spacing which enables the reversible photoisomerization. To our point of view this seems to be crucial if we compare the obtained results for the tripodal linker to the results of the thiolate azobiphenyl molecule, where no photoinduced conformational changes could be observed both for the single-component SAM as well for a diluted SAM with introduced spacer molecules. In consequence of the weak molecule/molecule and molecule/metal interaction of the tripodal azobenzene derivative, the switching behavior of the azobenzene incorporated into the SAM is analogous to the free molecule in solution. Therefore we propose a direct (intramolecular) electronic excitation mechanism.

We have shown that the bottom-up fabrication of GNRs on the Au(111) surface starting with 10,10'-dibromo-9,9'-bianthryl as the precursor molecule is feasible and that vibrational HREELS is an excellent technique to follow the preparation steps of the *in-situ* GNR fabrication for the prototypical N=7 armchair ribbon of width ≈ 7.5 Å. After the final fabrication step only vibrational modes of the wanted chemical end-product are observable in the spectrum. Employing primary electron energies of E_0 = 15 eV electronic HREELS has been proven to be a powerful tool which enables us to directly measure the band gap of the GNRs on Au(111). As a key feature we were able to determine the band gap and a second electronic transition at 2.6 and 3.1 eV, respectively. We report the first measurement of the band gap of a sub-nanometer wide atomically precise GNR on Au(111), which is an important property of the GNR and is therefore well suited as a benchmark for theoretical calculations. The bottom up fabrication method seems to be ideal to produce atomically precise nanoribbons. Our results clearly show that the usage of a rational design of GNR width (and shape) by the choice of the right precursor molecule opens up the possibility to precisely tailor the band gap to achieve the wanted electrical properties for the use in technical applications.

Summarizing we could gain insight into the dependence of the switching process regarding molecule/substrate-interactions and molecule/molecule-interactions. These interactions govern the adsorption geometry and electronic structure of the surface bound species as well as they are responsible for steric hindrance and intra-layer electronic coupling strength. From our results we conclude that the physical mechanism governing the desired functionality may be influenced drastically by the electronic interaction with the substrate, so that purely structural arguments to predict the functionality of adsorbed molecules have to be taken with great caution. This demonstrates that both, the geometric and electronic structure of the complete molecule–substrate complex have to be taken into account for a successful reversible photoisomerization of surface bound molecular switches. A route for future investigations could be in the choice of semi-metals and semi-conductors as the underlying substrates, since additional decay

channels of the excited states provided by the coupling to the metallic substrate are believed to be a major factor responsible for the prevalent quenching of photoinduced molecular switching on surfaces.

A Structure optimization of 10,10'-Dibromo-9,9'-bianthryl

Structure optimizations of 10,10'-Dibromo-9,9'-bianthryl have been performed with Gaussian09 using the hybrid functional B3LYP with the Pople basis set (6-31G(d)).

MO gaps	6-31G(d)
LUMO+2 - LUMO+1	1.27 eV
LUMO+1 -LUMO	0.003 eV
LUMO - HOMO	3.422 eV
HOMO - HOMO-1	0.006 eV
HOMO-1 - HOMO-2	1.271 eV

Table A.1: Orbital gaps yielded with B3LYP/6-31G(d).

Resulting electronic transitions:

electronic transition	6-31G(d)
HOMO→LUMO	3.422 eV
HOMO-1→LUMO	3.428 eV
HOMO→LUMO+1	3.425 eV
HOMO-2→LUMO	4.693 eV
HOMO→LUMO+2	4.692 eV

Table A.2: Resulting electronic transitions from the calculated orbital gaps. The energetic differences found in the substructures are "physically unlikely".

References

[Ale06] M. Alemani, M.V. Peters, S. Hecht, K.-H. Rieder, F. Moresco, & L. Grill. *Electric Field-Induced Isomerization of Azobenzene by STM.* J. Am. Chem. Soc. **128**, (2006) 14446.

[Ale08] Micol Alemani, Sofia Selvanathan, Francisco Ample, Maike V. Peters, Karl-Heinz Rieder, Francesca Moresco, Christian Joachim, Stefan Hecht, & Leonhard Grill. *Adsorption and Switching Properties of Azobenzene Derivatives on Different Noble Metal Surfaces: Au(111), Cu(111), and Au(100).* The Journal of Physical Chemistry C **112**, 28, (2008) 10509. URL `http://pubs.acs.org/doi/abs/10.1021/jp711134p`.

[Are95] Juan Francisco Arenas, Isabel Lopez Tocon, Juan Carlos Otero, & Juan Ignacio Marcos. *A Priori Scaled Quantum Mechanical Vibrational Spectra of trans- and cis-Stilbene.* The Journal of Physical Chemistry **99**, 29, (1995) 11392. URL `http://pubs.acs.org/doi/abs/10.1021/j100029a015`.

[Asa93] Tsutomu Asano, Hiroyuki Furuta, Hans Joerg Hofmann, Renzo Cimiraglia, Yuho Tsuno, & Mizue Fujio. *Mechanism of thermal Z/E isomerization of substituted N-benzylideneanilines. Nature of the activated complex with an sp-hybridized nitrogen atom.* The Journal of Organic Chemistry **58**, 16, (1993) 4418. URL `http://pubs.acs.org/doi/abs/10.1021/jo00068a042`.

[Bab07] Ashleigh E. Baber, Stephen C. Jensen, & E. Charles H. Sykes. *Dipole-Driven Ferroelectric Assembly of Styrene on Au111.* Journal of the American Chemical Society **129**, 20, (2007) 6368. URL `http://pubs.acs.org/doi/abs/10.1021/ja0709526`. PMID: 17472383.

[Bal03] V. Balzani, A. Credi, & M. Venturi. *Molecular Devices and Machines - A Journey into the Nano World.* Wiley-VCH: Weinheim, 2003.

[Bal08] Vincenzo Balzani, Alberto Credi, & Margherita Venturi. *Molecular Machines Working on Surfaces and at Interfaces.* ChemPhysChem **9**, 2, (2008) 202. URL `http://dx.doi.org/10.1002/cphc.200700528`.

[Ban99] C. N. Banwell & E. M. McCash. *Molekülspektroskopie.* R. Oldenbourg Verlag, 1999.

[Bar90] J. V. Barth, H. Brune, G. Ertl, & R. J. Behm. *Scanning tunneling microscopy observations on the reconstructed Au(111) surface: Atomic structure, long-range superstructure, rotational domains, and surface defects.* Phys. Rev. B **42**, 15, (1990) 9307. URL `http://link.aps.org/doi/10.1103/PhysRevB.42.9307`.

[Bar06] V. Barone, O. Hod, & G. E. Scuseria. *Electronic Structure and Stability of Semiconducting Graphene Nanoribbons.* Nano Letters **6**, 12, (2006)

2748. URL http://pubs.acs.org/doi/abs/10.1021/nl0617033. PMID: 17163699.

[Baz11] Maciej Bazarnik, Jorg Henzl, Ryszard Czajka, & Karina Morgenstern. *Light driven reactions of single physisorbed azobenzenes.* Chem. Commun. **47**, 27, (2011) 7764. URL http://dx.doi.org/10.1039/C1CC11578B.

[Bel05] M. A. Belkin & Y. R. Shen. *Non-linear optical spectroscopy as a novel probe for molecular chirality.* International Reviews in Physical Chemistry **24**, 2, (2005) 257 . URL http://search.ebscohost.com/login.aspx?direct=true&db=aph&AN=18979686&site=ehost-live.

[Ber36] E. Bergmann & A. Weizmann. *Dipole Moment and moleculare structure. XVII. The dipole moment of azo dyes and some similiar substances.* Trans. Faraday Soc. **32**, (1936) 1318.

[Ber71] R. C. Berthelson. *Techniques of Chemistry: Photochromism, Vol 3.* Wiley-Interscience, New York, 1971.

[Ber76] U. Berns, G. Heinrich, & H. Guesten. *Solvent dependency of the thermal cis trans isomerization of donor/acceptor-substituted N-benzylideneaniline.* Zeitschrift fuer Naturforschung **31B(7)**, (1976) 953.

[Ber00] Garry Berkovic, Valeri Krongauz, & Victor Weiss. *Spiropyrans and Spirooxazines for Memories and Switches.* Chemical Reviews **100**, 5, (2000) 1741. URL http://pubs.acs.org/doi/abs/10.1021/cr9800715.

[Bis97] Nandita Biswas & Siva Umapathy. *Density Functional Calculations of Structures, Vibrational Frequencies, and Normal Modes of trans- and cis-Azobenzene.* The Journal of Physical Chemistry A **101**, 30, (1997) 5555. URL http://pubs.acs.org/doi/abs/10.1021/jp970312x.

[Bon00] Mischa Bonn, Christian Hess, Stephan Funk, James H. Miners, Bo N. J. Persson, Martin Wolf, & Gerhard Ertl. *Femtosecond Surface Vibrational Spectroscopy of CO Adsorbed on Ru(001) during Desorption.* Phys. Rev. Lett. **84**, 20, (2000) 4653.

[Bro06] Wesley R. Browne & Ben L. Feringa. *Making molecular machines work.* Nat Nano **1**, 1, (2006) 25. URL http://dx.doi.org/10.1038/nnano.2006.45.

[Bru07] Paula Yurkanis Bruice. *Organische Chemie.* Pearson Education Deutschland, 2007.

[Buc01] M. Buck & M. Himmelhaus. *Vibrational spectroscopy of interfaces by infrared–visible sum frequency generation.* Journal of Vacuum Science & Technology A: Vacuum, Surfaces, and Films **19**, 6, (2001) 2717. URL http://link.aip.org/link/?JVA/19/2717/1.

[Bul08] Kevin Bullis. *Graphene Transistors*. Technology Review (Cambridge: MIT Technology Review, Inc). URL http://www.technologyreview.com/Nanotech/20119/.

[Bür70] H. B. Bürgi & J. D. Dunitz. *Crystal and Molecular Structures of Benzylideneaniline, Benzylideneaniline-p-carboxylic acid and p-methylbenzylidene-p-nitroaniline*. HCA **53**, 7, (1970) 1747. URL http://dx.doi.org/10.1002/hlca.19700530724.

[Byr06] Robert Byrne & Dermot Diamond. *Chemo/bio-sensor networks*. Nat Mater **5**, 6, (2006) 421. URL http://dx.doi.org/10.1038/nmat1661.

[Cai10] Jinming Cai, Pascal Ruffieux, Rached Jaafar, Marco Bieri, Thomas Braun, Stephan Blankenburg, Matthias Muoth, Ari P. Seitsonen, Moussa Saleh, Xinliang Feng, Klaus Mullen, & Roman Fasel. *Atomically precise bottom-up fabrication of graphene nanoribbons*. Nature **466**, 7305, (2010) 470. URL http://dx.doi.org/10.1038/nature09211.

[Cha11] A. J. Chaves, G. D. Lima, W. de Paula, C. E. Cordeiro, A. Delfino, T. Frederico, & O. Oliveira. *Dynamical gap generation in graphene nanoribbons: An effective relativistic field theoretical model*. Phys. Rev. B **83**, (2011) 153405.

[Chi97] Alexander K. Chibisov & Helmut Görner. *Photoprocesses in Spiropyran-Derived Merocyanines*. The Journal of Physical Chemistry A **101**, 24, (1997) 4305. URL http://pubs.acs.org/doi/abs/10.1021/jp9625691.

[Cho97] Cheol Ho Choi & Miklos Kertesz. *Conformational Information from Vibrational Spectra of Styrene, trans-Stilbene, and cis-Stilbene*. The Journal of Physical Chemistry A **101**, 20, (1997) 3823. URL http://pubs.acs.org/doi/abs/10.1021/jp970620v.

[Cho06] B.-Y. Choi, S.-J. Khang, S. Kim, H. Kim, H.W. Kim, Y.J. Song, J. Ihm, & Y. Kuk. *Conformational Molecular Switch of the Azobenzene Molecule: A Scanning Tunneling Microscopy Study*. Phys. Rev. Lett. **96**, (2006) 156106.

[Cla03] John Clarkson & W. Ewen Smith. *A DFT analysis of the vibrational spectra of nitrobenzene*. Journal of Molecular Structure **655**, 3, (2003) 413 . URL http://www.sciencedirect.com/science/article/pii/S0022286003003168.

[Com07] Matthew J. Comstock, Niv Levy, Armen Kirakosian, Jongweon Cho, Frank Lauterwasser, Jessica H. Harvey, David A. Strubbe, Jean M. J. Freacutechet, Dirk Trauner, Steven G. Louie, & Michael F. Crommie. *Reversible Photomechanical Switching of Individual Engineered Molecules at a Metallic Surface*. Phys. Rev. Lett. **99**, 3, (2007) 038301. URL http://link.aps.org/doi/10.1103/PhysRevLett.99.038301.

[Cot00] Grazia Cottone, Rosina Noto, Gianfranco La Manna, & Sandro L. Fornili. *Ab initio study on the photoisomers of a nitro-substituted spiropyran.* Chemical Physics Letters **319**, 1-2, (2000) 51 . URL http://www.sciencedirect.com/science/article/pii/S0009261400000956.

[Cot04] Grazia Cottone, Rosina Noto, & Gianfranco La Manna. *Theoretical study of spiropyran-merocyanine thermal isomerization.* Chemical Physics Letters **388**, 1-3, (2004) 218 . URL http://www.sciencedirect.com/science/article/pii/S0009261404003343.

[Cri11] Nuria Crivillers, Emanuele Orgiu, Federica Reinders, Marcel Mayor, & Paolo Samori. *Optical Modulation of the Charge Injection in an Organic Field-Effect Transistor Based on Photochromic Self-Assembled-Monolayer-Functionalized Electrodes.* Advanced Materials **23**, 12, (2011) 1447. URL http://dx.doi.org/10.1002/adma.201003736.

[Dat08] Sujit S. Datta, Douglas R. Strachan, Samuel M. Khamis, & A. T. Charlie Johnson. *Crystallographic Etching of Few-Layer Graphene.* Nano Letters **8**, 7, (2008) 1912. URL http://pubs.acs.org/doi/abs/10.1021/nl080583r. PMID: 18570483.

[DM07] R. Delgado-Macuil, M. Rojas-López, V.L. Gayou, A. Ordua-Diaz, & J. Diaz-Reyes. *ATR spectroscopy applied to photochromic polymer analysis.* Materials Characterization **58**, 8-9, (2007) 771 . URL http://www.sciencedirect.com/science/article/pii/S1044580306003561. XIV International Materials Research Congress: Symposium 7, XIV International Materials Research Congress.

[Dri08] Carlo Dri, Maike V. Peters, Jutta Schwarz, Stefan Hecht, & Leonhard Grill. *Spatial periodicity in molecular switching.* Nat Nano **3**, 11, (2008) 649. URL http://dx.doi.org/10.1038/nnano.2008.269.

[Dür03] H. ans Bouas-Laurent H. Dürr (Hg.). *Photochroism - Molecules and Systems.* Elsevier Science, Amsterdam, 2003.

[EB71] M. Ashraf El-Bayoumi, M. El-Aasser, & F. Abdel-Halim. *Electronic spectra and structures of Schiff's bases. I. Benzanils.* Journal of the American Chemical Society **93**, 3, (1971) 586. URL http://pubs.acs.org/doi/abs/10.1021/ja00732a004.

[Eck84] H. Eckhardt, L. Fritsche, & J. Noffke. *Self-consistent relativistic bandstructure of noble metals.* Journal of Physics F .

[Elb08] Mark Elbing, Alfred Blaszczyk, Carsten von Hänisch, Marcel Mayor, Violetta Ferri, Christian Grave, Maria Anita Rampi, Giuseppina Pace, Paolo Samori, Andrei Shaporenko, & Michael Zharnikov. *Single Component Self-Assembled Monolayers of Aromatic Azo-Biphenyl: Influence of the Packing*

Tightness on the SAM Structure and Light-Induced Molecular Movements. Adv. Funct. Mater. **18**, 19, (2008) 2972. URL http://dx.doi.org/10.1002/adfm.200800652.

[Eli10] Ana Laura Elias, A. R. Botello-Mendez, D. Meneses-Rodriguez, Viviana Jehova Gonzalez, Daniel Ramirez-Gonzalez, Lijie Ci, Emilio Munoz-Sandoval, Pulickel M. Ajayan, Humberto Terrones, & Mauricio Terrones. *Longitudinal Cutting of Pure and Doped Carbon Nanotubes to Form Graphitic Nanoribbons Using Metal Clusters as Nanoscalpels*. Nano Letters **10**, 2, (2010) 366. URL http://pubs.acs.org/doi/abs/10.1021/nl901631z. PMID: 19691280.

[Eza06] Motohiko Ezawa. *Peculiar width dependence of the electronic properties of carbon nanoribbons*. Phys. Rev. B **73**, 4, (2006) 045432.

[Fan90] D. Fanghänel, G. Timpe, & V. Orthman. In A. V. El'tsov (Hg.), *Organic Photochromes*. Consultants Bureau, New York, 1990 105.

[Fel11] H. Feldner, Z. Y. Meng, T. C. Lang, F. F. Assaad, S. Wessel, & A. Honecker. *Dynamical Signatures of Edge-State Magnetism on Graphene Nanoribbons*. arxiv .

[Fer01] B. L. Feringa. *Molecular Switches*. Wiley-VCH, Weinheim, 2001.

[Fer08] V. Ferri, M. Elbing, G. Pace, M. Dickey, M. Zharnikov, P. Samori, M. Mayor, & M. A. Rampi. *Light-Powered Electrical Switch Based on Cargo-Lifting Azobenzene Monolayers*. Angewandte Chemie International Edition **47**, 18, (2008) 3407. URL http://dx.doi.org/10.1002/anie.200705339.

[Fey60] R. P. Feynman. *There's plenty of room at the bottom*. Engineering and Science **23**, (1960) 22.

[Fis52] E. Fischer & Y. Hirshberg. J. Chem. Soc. 4522.

[Fis57] Ernst Fischer & Yael Frei. *Photoisomerization Equilibria Involving the CN Double Bond* (1957). URL http://dx.doi.org/doi/10.1063/1.1743834. Journal article.

[Fla68] John B. Flannery. *Photo- and thermochromic transients from substituted 1',3',3'-trimethylindolinobenzospiropyrans*. Journal of the American Chemical Society **90**, 21, (1968) 5660. URL http://pubs.acs.org/doi/abs/10.1021/ja01023a003.

[FT06] I. Fernandez-Torrente, K. J. Franke, N. Henningsen, G. Schulze, M. Alemani, Ch. Roth, R. Rurali, N. Lorente, & J. I. Pascual. *Spontaneous Formation of Triptycene Supramolecules on Surfaces*. The Journal of Physical Chemistry B **110**, 41, (2006) 20089. URL http://pubs.acs.org/doi/abs/10.1021/jp065149x.

[Füc06] G. Füchsel, T. Klamroth, J. Dokic, & P. Saalfrank. *On the Electronic Structure of Neutral and Ionic Azobenzenes and Their Possible Role as Surface Mounted Molecular Switches.* J. Phys. Chem. B **110**, (2006) 16337.

[Fuj96] Mitsutaka Fujita, Katsunori Wakabayashi, Kyoko Nakada, & Koichi Kusakabe. *Peculiar Localized State at Zigzag Graphite Edge.* Journal of the Physical Society of Japan **65**, 7, (1996) 1920. URL `http://jpsj.ipap.jp/link?JPSJ/65/1920/`.

[Fuj01] T. Fujino, S. Y. Arzhantsev, & T. J. Tahara. The Journal of Physical Chemistry A **105**, (2001) 8123.

[Fun00] S. Funk, M. Bonn, D. N. Denzler, Ch. Hess, M. Wolf, & G. Ertl. *Desorption of CO from Ru(001) induced by near-infrared femtosecond laser pulses* **112**, 22, (2000) 9888. URL `http://dx.doi.org/doi/10.1063/1.481626`.

[Gae07] Alexander Gaenko, Ajitha Devarajan, Laura Gagliardi, Roland Lindh, & Giorgio Orlandi. *Ab initio DFT study of Z-E isomerization pathways of N-benzylideneaniline.* Theoretical Chemistry Accounts: Theory, Computation, and Modeling (Theoretica Chimica Acta) **118**, (2007) 271. URL `http://dx.doi.org/10.1007/s00214-007-0319-1`. 10.1007/s00214-007-0319-1.

[Gah10] Cornelius Gahl, Roland Schmidt, Daniel Brete, Erik R. McNellis, Wolfgang Freyer, Robert Carley, Karsten Reuter, & Martin Weinelt. *Structure and Excitonic Coupling in Self-Assembled Monolayers of Azobenzene-Functionalized Alkanethiols.* Journal of the American Chemical Society **132**, 6, (2010) 1831. URL `http://pubs.acs.org/doi/abs/10.1021/ja903636q`. PMID: 20099853.

[Gal02] Elena Galoppini, Wenzhuo Guo, Wei Zhang, Paul G. Hoertz, Ping Qu, & Gerald J. Meyer. *Long-Range Electron Transfer across Molecule: Nanocrystalline Semiconductor Interfaces Using Tripodal Sensitizers.* Journal of the American Chemical Society **124**, 26, (2002) 7801. URL `http://pubs.acs.org/doi/abs/10.1021/ja025840n`. PMID: 12083934.

[Gal03] P. Galetto, H. Unterhalt, & G. Rupprechter. *The molecular orientation of CO on Pd(1 1 1) A polarization-dependent SFG study.* Chem. Phys. Lett. **367**, (2003) 785.

[Gar00] Antonio A. Garcia, Suman Cherian, Jin Park, Devens Gust, Frank Jahnke, & Rohit Rosario. *Photon-Controlled Phase Partitioning of Spiropyrans.* The Journal of Physical Chemistry A **104**, 26, (2000) 6103. URL `http://pubs.acs.org/doi/abs/10.1021/jp0003757`.

[GD08] Julianne M. Gibbs-Davis, Jennifer J. Kruk, Christopher T. Konek, Karl A. Scheidt, & Franz M. Geiger. *Jammed Acid-Base Reactions at Interfaces.* Journal of the American Chemical Society **130**, 46, (2008) 15444. URL `http://pubs.acs.org/doi/abs/10.1021/ja804302s`. PMID: 19006409.

[Gei07] A. K. Geim & K. S. Novoselov. *The rise of graphene*. Nat Mater **6**, 3, (2007) 183. URL http://dx.doi.org/10.1038/nmat1849.

[Gei10] A. Geim & K. Novoselov (2010). URL http://nobelprize.org/nobel_prizes/physics/laureates/2010/press.html.

[Gil10] Roland Gillen, Marcel Mohr, & Janina Maultzsch. *Symmetry properties of vibrational modes in graphene nanoribbons*. Phys. Rev. B **81**, 20, (2010) 205426. URL http://link.aps.org/doi/10.1103/PhysRevB.81.205426.

[Gor01] Helmut Gorner. *Photochromism of nitrospiropyrans: effects of structure, solvent and temperature*. Phys. Chem. Chem. Phys. **3**, 3, (2001) 416. URL http://dx.doi.org/10.1039/B007708I.

[Gri07] L. Grill, M. Dyer, L. Lafferentz, M. Persson, M. V. Peters, & S. Hecht. *Nano-architectures by covalent assembly of molecular building blocks*. Nat Nanotechnol. **2 (11)**, (2007) 687.

[Gri08] Leonhard Grill. *Functionalized molecules studied by STM: motion, switching and reactivity*. Journal of Physics: Condensed Matter **20**, 5, (2008) 053001. URL http://stacks.iop.org/0953-8984/20/i=5/a=053001.

[Gün96] H. Günzler & H. M. Heise. *IR-Spektroskopie*. VCH, Weinheim, 1996.

[Hag07] Sebastian Hagen, Felix Leyssner, Dhananjay Nandi, Martin Wolf, & Petra Tegeder. *Reversible switching of tetra-tert-butyl-azobenzene on a Au(1 1 1) surface induced by light and thermal activation*. Chemical Physics Letters **444**, 1-3, (2007) 85 . URL http://www.sciencedirect.com/science/article/B6TFN-4P4NPKH-6/2/028e837ff46253f99ee31a314d1fbd5e.

[Hag08a] Sebastian Hagen, Peter Kate, Felix Leyssner, Dhananjay Nandi, Martin Wolf, & Petra Tegeder. *Excitation mechanism in the photoisomerization of a surface-bound azobenzene derivative: Role of the metallic substrate.* Journal of Chemical Physics **129**, 16, (2008) 164102. URL http://search.ebscohost.com/login.aspx?direct=true&db=aph&AN=35102431&site=ehost-live.

[Hag08b] Sebastian Hagen, Peter Kate, Maike Peters, Stefan Hecht, Martin Wolf, & Petra Tegeder. *Kinetic analysis of the photochemically and thermally induced isomerization of an azobenzene derivative on Au(111) probed byÂ two-photon photoemission*. Applied Physics A: Materials Science & Processing **93**, (2008) 253. URL http://dx.doi.org/10.1007/s00339-008-4831-5. 10.1007/s00339-008-4831-5.

[Hag10] Sebastian Hagen, Ying Luo, Rainer Haag, Martin Wolf, & Petra Tegeder. *Electronic structure and electron dynamics at an organic molecule/metal interface: interface states of tetra- tert -butyl-imine/Au(111)*. New Journal of

Physics **12**, 12, (2010) 125022. URL http://stacks.iop.org/1367-2630/12/i=12/a=125022.

[Ham65] R.M. Hammaker, S.A. Francis, & R.P. Eischens. *Infrared study of intermolecular interactions for carbon monoxide chemisorbed on platinum.* Spectrochimica Acta **21**, 7, (1965) 1295 . URL http://www.sciencedirect.com/science/article/B6W98-44W571K-4C/2/3c1714a8ae7acc96ce8588b89974e58c.

[Ham95] B. Hammer & J. K. Norskov. *Why gold is the noblest of all the metals.* Nature **376**, 6537, (1995) 238. URL http://dx.doi.org/10.1038/376238a0.

[Han02] Wen-Ge Han, Timothy Lovell, Tiqing Liu, & Louis Noodleman. *Density Functional Studies of the Ground- and Excited-State Potential-Energy Curves of Stilbene cis/rans Isomerization.* ChemPhysChem **3**, 2, (2002) 167. URL http://dx.doi.org/10.1002/1439-7641(20020215)3:2<167::AID-CPHC167>3.0.CO;2-G.

[Han07] Melinda Y. Han, Barbaros Ozyilmaz, Yuanbo Zhang, & Philip Kim. *Energy Band-Gap Engineering of Graphene Nanoribbons.* Phys. Rev. Lett. **98**, 20, (2007) 206805.

[Han10] Mina Han, Daisuke Ishikawa, Takumu Honda, Eisuke Ito, & Masahiko Hara. *Light-driven molecular switches in azobenzene self-assembled monolayers: effect of molecular structure on reversible photoisomerization and stable cis state.* Chem. Commun. **46**, 20, (2010) 3598. URL http://dx.doi.org/10.1039/B921801G.

[Hec06] S. Hecht & M. Peters. *Synthese des Moleküls/Experiment unveröffentlich* .

[Hei91] T. F. Heinz. *Second-Order Nonlinear Optical Effects at Surfaces and Interfaces.* Elsevier, Amsterdam, 1991.

[Hen94] M. Henzler & W. Göpel. *Oberflächenphysik des Festkörpers.* Oberflächenphysik des Festkörpers, 1994.

[Hen06] J. Henzl, M. Mehlhorn, H. Gawronski, K.-H. Rieder, & K. Morgenstern. *Reversible cis-trans Isomerization of a Single Azobenzene Molecule.* Angew. Chem. Int. Ed. **45**, (2006) 603.

[Hen07a] N. Henningsen, K. J. Franke, I. F. Torrente, G. Schulze, B. Priewisch, K. Rück-Braun, J. Doic, T. Klamroth, P. Saalfrank, & J. I. Pascual. *Inducing the Rotation of a Single Phenyl Ring with Tunneling Electrons.* The Journal of Physical Chemistry C **111**, 40, (2007) 14843. URL http://pubs.acs.org/doi/abs/10.1021/jp0741861.

[Hen07b] Jörg Henzl, Thomas Bredow, & Karina Morgenstern. *Irreversible isomerization of the azobenzene derivate Methyl Orange on Au(1 1 1).* Chemical

Physics Letters **435**, 4-6, (2007) 278 . URL http://www.sciencedirect.com/science/article/pii/S0009261407000103.

[Hen08] N. Henningsen, R. Rurali, K. Franke, I. Fernandez-Torrente, & J. Pascual. *Trans to cis isomerization of an azobenzene derivative on a Cu(100) surface.* Applied Physics A: Materials Science & Processing **93**, (2008) 241. URL http://dx.doi.org/10.1007/s00339-008-4840-4. 10.1007/s00339-008-4840-4.

[Hes91] Manfred Hesse, Herbert Meier, & Bernd Zeeh. *Spektroskopische Methoden in der organischen Chemie.* Georg Thieme Verlag Stuttgart . New York, 1991.

[Hof83] Friedrich M. Hoffmann. *Infrared reflection-absorption spectroscopy of adsorbed molecules.* Surface Science Reports **3**, 2-3, (1983) 107 . URL http://www.sciencedirect.com/science/article/B6TVY-46D7040-D/2/67e0d56d4531cae156a6b2faa5d5da5e.

[Hol92] Peter Hollins. *The influence of surface defects on the infrared spectra of adsorbed species.* Surface Science Reports **16**, 2, (1992) 51 . URL http://www.sciencedirect.com/science/article/B6TVY-46G39DJ-F/2/d9fd7802434682987862ef69737e33bb.

[Hua07] Tian Huang, Zhenpeng Hu, Bing Wang, Lan Chen, Aidi Zhao, Haiqian Wang, & J. G. Hou. *Observation of Hierarchical Chiral Structures in 8-Nitrospiropyran Monolayers.* The Journal of Physical Chemistry B **111**, 25, (2007) 6973. URL http://pubs.acs.org/doi/abs/10.1021/jp071193g.

[Iba82] H. Ibach & D. Mills. *Electron Energy Loss Spectroscopy and Surface Vibrations.* Academic Press New York, N. Y., 1982.

[Iba90] H. Ibach & H. Lüth. *Festkorperphysik: Einführung in die Grundlagen.* Springer Verlag Berlin, Heidelberg, 1990, 3. Aufl.

[Iri00] M. Irie. *Photochromism: Memories and Switches - Introduction.* Chemical Reviews **100**, 5, (2000) 1683. URL http://pubs.acs.org/doi/abs/10.1021/cr9800681. PMID: 11777415.

[Ito05] Masayuki Ito, Takashi Tsukatani, & Hisashi Fujihara. *Preparation and characterization of gold nanoparticles with a ruthenium-terpyridyl complex, and electropolymerization of their pyrrole-modified metal nanocomposites.* J. Mater. Chem. **15**, 9, (2005) 960. URL http://dx.doi.org/10.1039/B412406E.

[Jac09] Denis Jacquemin, Adele D. Laurent, Eric A. Perpete, & Jean-Marie Andre. *An ab initio simulation of the UV/visible spectra of N-benzylideneaniline dyes.* Int. J. Quantum Chem. **109**, 15, (2009) 3506. URL http://dx.doi.org/10.1002/qua.22303.

[Jia03] Huahua Jian & James M. Tour. *En Route to Surface-Bound Electric Field-Driven Molecular Motors*. The Journal of Organic Chemistry **68**, 13, (2003) 5091. URL http://pubs.acs.org/doi/abs/10.1021/jo034169h.

[Jun97] T.A. Jung, R.R. Schlittler, & J.K. Gimzewski. *Conformational identification of individual adsorbed molecules with the STM*. Nature **386**, (1997) 696.

[Jun08] Ulrich Jung, Belinda Baisch, Daniel Kaminski, Klaus Krug, Annika Elsen, Tobias Weineisen, Diego Raffa, Jochim Stettner, Claudia Bornholdt, Rainer Herges, & Olaf. Magnussen. *Structure and redox behavior of azobenzene-containing monolayers on Au(111): A combined STM, X-ray reflectivity, and voltammetry study.* J. Electroanal. Chem. **619-620**, (2008) 152.

[Kat06] N. Katsonis, T. Kudernac, M. Walko, S. J. van der Molen, B. J. van Wees, & B. L. Feringa. *Reversible Conductance Switching of Single Diarylethenes on a Gold Surface*. Adv. Mater. **18**, 11, (2006) 1397. URL http://dx.doi.org/10.1002/adma.200600210.

[Kel71] B. Kellerer, H.H. Hacker, & J. Brandmüller. *Structure of azobenzene and tolane in solution Raman spectra of azobenzene, azobenzene-d10, p,p'-azobenzene-d2, azobenzene-15N2, and tolane*. Indian. J. Pure Appl. Phys. **9**, (1971) 903.

[Kin97] N. R. King, E. A. Whale, A. Davis, F.and Gilbert, & G. Mitchell. *Effect of media polarity on the photoisomerisation of substituted stilbene, azobenzene and imine chromophores*. J. Mater. Chem. **7**, 4, (1997) 625. URL http://dx.doi.org/10.1039/A607980F.

[Kok06] Anton Kokalj. http://www.xcrysden.org/ (2006).

[Kos09] Dmitry V. Kosynkin, Amanda L. Higginbotham, Alexander Sinitskii, Jay R. Lomeda, Ayrat Dimiev, B. Katherine Price, & James M. Tour. *Longitudinal unzipping of carbon nanotubes to form graphene nanoribbons*. Nature **458**, (2009) 872.

[Koz93] L. I. Kozhevina, E. B. Prokopenko, V. I. Rybachenko, & E. V. Titov. *The vibrational spectra and force constants of benzylideneaniline and its fluoroderivatives*. Journal of Molecular Structure **295**, (1993) 53 . URL http://www.sciencedirect.com/science/article/pii/002228609385007H.

[Kri05] Volker Kriegisch & Christoph Lambert. *Self-Assembled Monolayers of Chromophores on Gold Surfaces*. In Frank Würthner (Hg.), *Supermolecular Dye Chemistry*, Bd. 258 von *Topics in Current Chemistry*. Springer Berlin / Heidelberg, 2005 585–585. URL http://dx.doi.org/10.1007/b135682. 10.1007/b135682.

[Küb60] R. Kübler, W. Lüttke, & S. Weckherlin. Z. Elektrochem. **64**, (1960) 650.

[Kum08] Ajeet S. Kumar, Tao Ye, Tomohide Takami, Byung-Chan Yu, Austen K. Flatt, James M. Tour, & Paul S. Weiss. *Reversible Photo-Switching of Single Azobenzene Molecules in Controlled Nanoscale Environments.* Nano Letters **8**, 6, (2008) 1644. URL `http://pubs.acs.org/doi/abs/10.1021/nl080323%2B`. PMID: 18444688.

[Lap79] J. D. Laposa. *Vibrational spectra of nitrobenzene-d5.* Spectrochimica Acta Part A: Molecular Spectroscopy **35**, 1, (1979) 65 . URL `http://www.sciencedirect.com/science/article/pii/0584853979800677`.

[Lew82] J. W. Lewis & C. Sandorfy. *An infrared study of the photoisomerization of N-benzylideneaniline.* Canadian Journal of Chemistry **60**, 13, (1982) 1720. URL `http://www.nrcresearchpress.com/doi/abs/10.1139/v82-235`.

[Ley07] Felix Leyssner. *Diplomarbeit: Adsorption und elektronische Struktur des molekularen Schalters tetra-tert-butyl-Azobenzol auf Ag(111) und Au(111).* Dissertation, AG Wolf, FB Physik, FU Berlin (2007).

[Ley10] Felix Leyssner, Sebastian Hagen, Laszlo Ovari, Jadranka Dokic, Peter Saalfrank, Maike V. Peters, Stefan Hecht, Tillmann Klamroth, & Petra Tegeder. *Photoisomerization Ability of Molecular Switches Adsorbed on Au(111): Comparison between Azobenzene and Stilbene Derivatives.* The Journal of Physical Chemistry C **114**, 2, (2010) 1231. URL `http://dx.doi.org/10.1021/jp909684x`.

[Li08] Xiaolin Li, Xinran Wang, Li Zhang, Sangwon Lee, & Hongjie Dai. *Chemically Derived Ultrasmooth Graphene Nanoribbon Semiconductors.* Science **319**, (2008) 1229.

[Lov05] J. Christopher Love, Lara A. Estroff, Jennah K. Kriebel, Ralph G. Nuzzo, & George M. Whitesides. *Self-Assembled Monolayers of Thiolates on Metals as a Form of Nanotechnology.* Chemical Reviews **105**, 4, (2005) 1103. URL `http://pubs.acs.org/doi/abs/10.1021/cr0300789`.

[Luo10] Guangfu Luo, Hong Li, Lu Wang, Lin Lai, Jing Zhou, Rui Qin, Jing Lu, Wai-Ning Mei, & Zhengxiang Gao. *Polarized Vibrational Infrared Absorption of Graphene Nanoribbons.* The Journal of Physical Chemistry C **114**, 15, (2010) 6959. URL `http://pubs.acs.org/doi/abs/10.1021/jp912000x`.

[Lüt95] H. Lüth (Hg.). *Surfaces and Interfaces of Solid Materials.* 3. ed. Berlin etc.: Springer-Verlag, 1995.

[Mal09] S. Malola, H. Hakkinen, & P. Koskinen. *Comparison of Raman spectra and vibrational density of states between graphene nanoribbons with different edges* (2009). URL `http://dx.doi.org/10.1140/epjd/e2008-00256-2`.

[Maz11] F. Mazzamuto, J. Saint-Martin, A. Valentin, C. Chassat, & P. Dollfus. *Edge shape effect on vibrational modes in graphene nanoribbons: A numerical*

study. Journal of Applied Physics **109**, 6, (2011) 064516. URL http://link.aip.org/link/?JAP/109/064516/1.

[McN10a] Erik R. McNellis, Christopher Bronner, Jorg Meyer, Martin Weinelt, Petra Tegeder, & Karsten Reuter. *Azobenzene versus 3,3',5,5'-tetra-tert-butylazobenzene (TBA) at Au(111): characterizing the role of spacer groups*. Phys. Chem. Chem. Phys. **12**, 24, (2010) 6404. URL http://dx.doi.org/10.1039/C001978J.

[McN10b] Erik R. McNellis, Giuseppe Mercurio, Sebastian Hagen, Felix Leyssner, Jörg Meyer, Serguei Soubatch, Martin Wolf, Karsten Reuter, Petra Tegeder, & Stefan Tautz. *Bulky spacer groups - A valid strategy to control the coupling of functional molecules to surfaces?* Chemical Physics Letters **499**, 4-6, (2010) 247 . URL http://www.sciencedirect.com/science/article/pii/S0009261410012960.

[Mei78] Z. Meic & H. Güsten. *Vibrational studies of trans-stilbenes–I. Infrared and Raman spectra of trans-stilbene and deuterated trans-stilbenes*. Spectrochimica Acta Part A: Molecular Spectroscopy **34**, 1, (1978) 101 . URL http://www.sciencedirect.com/science/article/pii/0584853978801937.

[Mei92] Herbert Meier. *The Photochemistry of Stilbenoid Compounds and Their Role in Materials Technology*. Angewandte Chemie International Edition in English **31**, 11, (1992) 1399. URL http://dx.doi.org/10.1002/anie.199213993.

[Mei93] Z. Meic, G. Baranovic, & Suste T. J.Mol. Struct. **196**, (1993) 163.

[Mer10] G. Mercurio, E. R. McNellis, I. Martin, S. Hagen, F. Leyssner, S. Soubatch, J. Meyer, M. Wolf, P. Tegeder, F. S. Tautz, & K. Reuter. *Structure and Energetics of Azobenzene on Ag(111): Benchmarking Semiempirical Dispersion Correction Approaches*. Phys. Rev. Lett. **104**, 3, (2010) 036102. URL http://link.aps.org/doi/10.1103/PhysRevLett.104.036102.

[Mie11] Johannes Mielke, Felix Leyssner, Matthias Koch, Stephan Meyer, Ying Luo, Sofia Selvanathan, Rainer Haag, Petra Tegeder, & Leonhard Grill. *Imine Derivatives on Au(111): Evidence for "Inverted" Thermal Isomerization*. ACS Nano **0**, 0. URL http://pubs.acs.org/doi/abs/10.1021/nn103297e.

[Mor04] F. Moresco. *Manipulation of large molecules by low temperature STM: model systems for molecular electronics*. Phys. Rep. **399**, (2004) 175.

[Mor06] F. Moresco. *Daten vor der Veröffentlichung/ private communication* .

[Mor11] Karina Morgenstern. *Switching individual molecules by light and electrons: From isomerisation to chirality flip*. Progress in Surface Science **86**, 5-

8, (2011) 115 . URL http://www.sciencedirect.com/science/article/pii/S0079681611000207.

[Mus82] R.G Musket, W. McLean, C.A. Colmenares, D.M. Makowiecki, & W.J. Siekhaus. *Preparation of atomically clean surfaces of selested elements: a review.* Appl. of Surf. Science **10**, (1982) 143.

[Näg97] T. Nägele, R. Hoche, W. Zinth, & J. Wachtveitl. *Femtosecond photoisomerization of cis-azobenzene.* Chem. Phys. Letters **272**, (1997) 489.

[Nak96] Kyoko Nakada, Mitsutaka Fujita, Gene Dresselhaus, & Mildred S. Dresselhaus. *Edge state in graphene ribbons: Nanometer size effect and edge shape dependence.* Phys. Rev. B **54**, 24, (1996) 17954.

[Nav05] Amparo Navarro, Juan Jesus López Gonzalez, A. Garcia Fernandez, Istvan Laczik, & Gabor Pongor. *Structural and vibrational study of isochroman.* Chemical Physics **313**, 1-3, (2005) 279 . URL http://www.sciencedirect.com/science/article/pii/S0301010405000285.

[Ost67] B. Ostrowska & T. Trainer. Acta. Phys. Polon. **33**, (1967) 111.

[Ova07] Laszlo Ovari, Martin Wolf, & Petra Tegeder. *Reversible Changes in the Vibrational Structure of Tetra-tert-butylazobenzene on a Au(111) Surface Induced by Light and Thermal Activation.* The Journal of Physical Chemistry C **111**, 42, (2007) 15370. URL http://pubs.acs.org/doi/abs/10.1021/jp075274o.

[Óvá08] László Óvári, Jutta Schwarz, Maike V. Peters, Stefan Hecht, Martin Wolf, & Petra Tegeder. *Reversible isomerization of an azobenzene derivative adsorbed on Au(1 1 1): Analysis using vibrational spectroscopy.* International Journal of Mass Spectrometry **277**, 1-3, (2008) 223 . URL http://www.sciencedirect.com/science/article/pii/S1387380608001620. Electron-induced atomic and molecular processes: A special issue honoring Eugen Illenberger on his 65th birthday.

[Óvá10] László Óvári, Ying Luo, Felix Leyssner, Rainer Haag, Martin Wolf, & Petra Tegeder. *Adsorption and switching properties of a N-benzylideneaniline based molecular switch on a Au(111) surface* (2010). URL http://dx.doi.org/doi/10.1063/1.3460647. Journal article.

[Pac07] Giuseppina Pace, Violetta Ferri, Christian Grave, Mark Elbing, Carsten von Hänisch, Michael Zharnikov, Marcel Mayor, Maria Anita Rampi, & Paolo Samori. *Cooperative light-induced molecular movements of highly ordered azobenzene self-assembled monolayers.* Proceedings of the National Academy of Sciences **104**, 24, (2007) 9937. URL http://www.pnas.org/content/104/24/9937.abstract.

[Pal00] Krzysztof Palczewski, Takashi Kumasaka, Tetsuya Hori, Craig A. Behnke, Hiroyuki Motoshima, Brian A. Fox, Isolde Le Trong, David C. Teller, Tetsuji Okada, Ronald E. Stenkamp, Masaki Yamamoto, & Masashi Miyano. *Crystal Structure of Rhodopsin: A G Protein-Coupled Receptor*. Science **289**, 5480, (2000) 739. URL http://www.sciencemag.org/content/289/5480/739.abstract.

[Par89] D. A. Parthenopoulos & P. M. Rentzepis. *Three-Dimensional Optical Storage Memory*. Science **245**, 4920, (1989) 843. URL http://www.sciencemag.org/content/245/4920/843.abstract.

[Pat85] Lalit N. Patnaik & Sarojini Das. *Conformation of p-dimethylaminobenzylidene-p-nitroaniline, p-nitrobenzylidene-p-dimethylaminoaniline, their stilbene and azobenzene derivatives*. Int. J. Quantum Chem. **27**, 2, (1985) 135. URL http://dx.doi.org/10.1002/qua.560270204.

[Per77] B. N. J. Persson. *Theory of inelastic scattering of slow electrons by molecules absorbed on metal surfaces*. Solid State Communications **24**, 8, (1977) 573 . URL http://www.sciencedirect.com/science/article/pii/0038109877901661.

[Pet08] Maike V. Peters. *Photoschaltbare Katalysatoren, Dissertation*. Dissertation, Humboldt-Universität zu Berlin (2008).

[Pia08] M. Piantek, J. Miguel, M. Bernien, C. Navio, A. Krüger, B. Priewisch, K. Rück-Braun, & W. Kuch. *Adsorption of carboxymethylester-azobenzene on copper and gold single crystal surfaces*. Applied Physics A: Materials Science & Processing **93**, (2008) 261. URL http://dx.doi.org/10.1007/s00339-008-4825-3. 10.1007/s00339-008-4825-3.

[Pia09] Marten Piantek, Gunnar Schulze, Matthias Koch, Katharina J. Franke, Felix Leyssner, Alex Krüger, Cristina Navio, Jorge Miguel, Matthias Bernien, Martin Wolf, Wolfgang Kuch, Petra Tegeder, & Jose Ignacio Pascual. *Reversing the Thermal Stability of a Molecular Switch on a Gold Surface: Ring-Opening Reaction of Nitrospiropyran*. Journal of the American Chemical Society **131**, 35, (2009) 12729. URL http://pubs.acs.org/doi/abs/10.1021/ja901238p. PMID: 19722719.

[Pro67] F. M. Probst & T. C. Piper. J. Vac. Sci. Technol. **4**, (1967) 53.

[Rad07] Aleksandar Radu, Silvia Scarmagnani, Robert Byrne, Conor Slater, King Tong Lau, & Dermot Diamond. *Photonic modulation of surface properties: a novel concept in chemical sensing*. Journal of Physics D: Applied Physics **40**, 23, (2007) 7238. URL http://stacks.iop.org/0022-3727/40/i=23/a=S06.

[Rau03a] H. Rau. *Azo compounds*. In H. D"urr & H. Bouas-Laurent (Hg.), *Studies in Organic Chemistry, Photochroism-Molecules and Systems*, Bd. 40. Amsterdam, 2003 165–192.

[Rau03b] H. Rau. *Photochromism-Molecules and Systems*. Elsevier, Amsterdamm, 2003.

[Ray02] Francisco M. Raymo & Silvia Giordani. *All-optical processing with molecular switches*. Proceedings of the National Academy of Sciences **99**, 8, (2002) 4941. URL `http://www.pnas.org/content/99/8/4941.abstract`.

[Ren10] Wencai Ren, Riichiro Saito, Libo Gao, Fawei Zheng, Zhongshuai Wu, Bilu Liu, Masaru Furukawa, Jinping Zhao, Zongping Chen, & Hui-Ming Cheng. *Edge phonon state of mono- and few-layer graphene nanoribbons observed by surface and interference co-enhanced Raman spectroscopy*. Phys. Rev. B **81**, 3, (2010) 035412. URL `http://link.aps.org/doi/10.1103/PhysRevB.81.035412`.

[Roc95] M. Rocca. *Low-energy EELS investigation of surface electronic excitations on metals*. Surface Science Reports **22**, 1-2, (1995) 1 . URL `http://www.sciencedirect.com/science/article/pii/0167572995000046`.

[Roc06] T. J. Rockey, M. Yang, & H.-L. Dai. *Adsorption Energies, Inter-adsorbate Interactions, and the Two Binding Sites within Monolayer Benzene on Ag(111)*. J. Phys. Chem. B **110**, (2006) 19973.

[Sch67] Cajetan Schiele & Günther Arnold. *Zur struktur der photochromen form des spiro-6-nitro-[2H-1-benzopyran-2,2'-1',3',3'-trimethylindolins]*. Tetrahedron Letters **8**, 13, (1967) 1191 . URL `http://www.sciencedirect.com/science/article/pii/S0040403900906658`.

[Sch00] Frank Schreiber. *Structure and growth of self-assembling monolayers*. Progress in Surface Science **65**, 5-8, (2000) 151 . URL `http://www.sciencedirect.com/science/article/B6TJF-428DK9M-1/2/ad6737541afffca8cd2d8cce759e5d51`.

[Sch04] Frank Schreiber. *Self-assembled monolayers: from 'simple' model systems to biofunctionalized interfaces*. Journal of Physics: Condensed Matter **16**, 28, (2004) R881. URL `http://stacks.iop.org/0953-8984/16/i=28/a=R01`.

[Sch08] Roland Schmidt, Erik McNellis, Wolfgang Freyer, Daniel Brete, Tanja Giessel, Cornelius Gahl, Karsten Reuter, & Martin Weinelt. *Azobenzene-functionalized alkanethiols in self-assembled monolayers on gold*. Applied Physics A: Materials Science & Processing **93**, (2008) 267. URL `http://dx.doi.org/10.1007/s00339-008-4829-z`. 10.1007/s00339-008-4829-z.

[Sch11] Michael Schulze. *Diplomarbeit: Electronic and adsorption properties of azobenzenes adsorbed on noble metal surfaces.* Dissertation, AG Tegeder, FB Physik, FU Berlin (2011).

[She84] Y. R. Shen. *The principles of nonlinear optics.* New York, Wiley-Interscience, 1984.

[She88] N. Sheppard. *Vibrational spectroscopic studies of the structure of species derived from the chemisorption of hydrocarbons on metal single-crystal surfaces.* Annu Rev Phys Chem. **39**, (1988) 589.

[She89] Y. R. Shen. *Surface properties probed by second-harmonic and sum-frequency generation.* Nature **337**, 6207, (1989) 519. URL `http://dx.doi.org/10.1038/337519a0`.

[Shi06] Yasuhiro Shirai, Long Cheng, Bo Chen, & James M. Tour. *Characterization of Self-Assembled Monolayers of Fullerene Derivatives on Gold Surfaces: Implications for Device Evaluations.* Journal of the American Chemical Society **128**, 41, (2006) 13479. URL `http://pubs.acs.org/doi/abs/10.1021/ja063451d`. PMID: 17031961.

[Son06a] Young-Woo Son, Marvin L. Cohen, & Steven G. Louie. *Energy Gaps in Graphene Nanoribbons.* Phys. Rev. Lett. **97**, 21, (2006) 216803.

[Son06b] Young-Woo Son, Marvin L. Cohen, & Steven G. Louie. *Half-metallic graphene nanoribbons.* Nature **444**, (2006) 347.

[Tak06a] Daiko Takamatsu, Yoko Yamakoshi, & Kenichi Fukui. *Control of probe function in noncontact atomic force microscopy using photo-responsive molecular tip.* e-Journal of Surface Science and Nanotechnology **4**, (2006) 249.

[Tak06b] Daiko Takamatsu, Yoko Yamakoshi, & Kenichi Fukui. *Photoswitching Behavior of a Novel Single Molecular Tip for Noncontact Atomic Force Microscopy Designed for Chemical Identification.* The Journal of Physical Chemistry B **110**, 5, (2006) 1968. URL `http://pubs.acs.org/doi/abs/10.1021/jp056986m`.

[Tak10] Daiko Takamatsu, Kenichi Fukui, Safwan Aroua, & Yoko Yamakoshi. *Photoswitching tripodal single molecular tip for noncontact AFM measurements: synthesis, immobilization, and reversible configurational change on gold surface.* Org. Biomol. Chem. **8**, 16, (2010) 3655. URL `http://dx.doi.org/10.1039/C002657C`.

[Tam00] Naoto Tamai & Hiroshi Miyasaka. *Ultrafast Dynamics of Photochromic Systems.* Chemical Reviews **100**, 5, (2000) 1875. URL `http://pubs.acs.org/doi/abs/10.1021/cr9800816`. PMID: 11777424.

[Tao11] Chenggang Tao, Liying Jiao, Oleg V. Yazyev, Yen-Chia Chen, Juanjuan Feng, Xiaowei, Zhang, Rodrigo B. Capaz, James M. Tour, Alex Zettl, Steven G. Louie, Hongjie Dai, & Michael F. Crommie. *Spatially resolving edge states of chiral graphene nanoribbons.* Nature Physics .

[Teg07] P. Tegeder, S. Hagen, F. Leyssner, M.V. Peters, S. Hecht, T. Klamroth, P. Saalfrank, & M. Wolf. *Electronic structure of the molecular switch tetra-*tert*-butyl-azobenzene adsorbed on Ag(111)* (2007). URL `http://dx.doi.org/10.1007/s00339-007-4047-0`.

[Thi87] P A Thiry, M Liehr, J J Pireaux, & R Caudano. *Electron Interaction Mechanisms in High Resolution Electron Energy Loss Spectroscopy.* Physica Scripta **35**, 3, (1987) 368. URL `http://stacks.iop.org/1402-4896/35/i=3/a=024`.

[Thy07] Sujatha Thyagarajan, Aiping Liu, Olumide A. Famoyin, Massimiliano Lamberto, & Elena Galoppini. *Tripodal pyrene chromophores for semiconductor sensitization: new footprint design.* Tetrahedron **63**, 32, (2007) 7550 . URL `http://www.sciencedirect.com/science/article/B6THR-4NS2GBS-3/2/1915bc5b0ea67c4545f2b5b30abd41b0`.

[Ulm96] Abraham Ulman. *Formation and Structure of Self-Assembled Monolayers.* Chemical Reviews **96**, 4, (1996) 1533. URL `http://pubs.acs.org/doi/abs/10.1021/cr9502357`. PMID: 11848802.

[vdM10] Sense Jan van der Molen & Peter Liljeroth. *Charge transport through molecular switches.* Journal of Physics: Condensed Matter **22**, 13, (2010) 133001. URL `http://stacks.iop.org/0953-8984/22/i=13/a=133001`.

[Von99] T. Vondrak & X.-Y. Zhu. *Two-Photon Photoemission Study of Heterogeneous Electron Transfer: C6F6 on Cu(111).* The Journal of Physical Chemistry B **103**, 17, (1999) 3449. URL `http://pubs.acs.org/doi/abs/10.1021/jp9846983`.

[Wag09] Steffen Wagner, Felix Leyssner, Christian Kordel, Sebastian Zarwell, Roland Schmidt, Martin Weinelt, Karola Ruck-Braun, Martin Wolf, & Petra Tegeder. *Reversible photoisomerization of an azobenzene-functionalized self-assembled monolayer probed by sum-frequency generation vibrational spectroscopy.* Phys. Chem. Chem. Phys. **11**, 29, (2009) 6242. URL `http://dx.doi.org/10.1039/B823330F`.

[Wak01] Katsunori Wakabayashi. *Electronic transport properties of nanographite ribbon junctions.* Phys. Rev. B **64**, 12, (2001) 125428. URL `http://link.aps.org/doi/10.1103/PhysRevB.64.125428`.

[Wal91] David H. Waldeck. *Photoisomerization dynamics of stilbenes.* Chemical Reviews **91**, 3, (1991) 415. URL `http://pubs.acs.org/doi/abs/10.1021/cr00003a007`.

[Wan05] Hong-Fei Wang, Wei Gan, Rong Lu, Yi Rao, & Bao-Hua Wu. *Quantitative spectral and orientational analysis in surface sum frequency generation vibrational spectroscopy (SFG-VS).* International Reviews in Physical Chemistry **24**, 2, (2005) 191. URL http://www.informaworld.com/10.1080/01442350500225894.

[Wei71] Karl Weiss, Charles H. Warren, & Gunnar Wettermark. *cis-trans isomerization about the carbon-nitrogen double bond. Structures of the isomers of N-benzylideneaniline.* Journal of the American Chemical Society **93**, 19, (1971) 4658. URL http://pubs.acs.org/doi/abs/10.1021/ja00748a003.

[Wei05] Lingyun Wei, Hugo Tiznado, Guangming Liu, Kisari Padmaja, Jonathan S. Lindsey, Francisco Zaera, & David F. Bocian. *Adsorption Characteristics of Tripodal Thiol-Functionalized Porphyrins on Gold.* The Journal of Physical Chemistry B **109**, 50, (2005) 23963. URL http://pubs.acs.org/doi/abs/10.1021/jp0537005.

[Wei06] Tobias Weidner, Andreas Kramer, Clemens Bruhn, Michael Zharnikov, Andrey Shaporenko, Ulrich Siemeling, & Frank Trager. *Novel tripod ligands for prickly self-assembled monolayers.* Dalton Trans. , 23, (2006) 2767. URL http://dx.doi.org/10.1039/B515727G.

[Wet65] J.; Sousa J.; Dogliotti L. Kinetics Wettermark, G.; Weinstein. *Kinetics of Cis-Trans Isomerization of para-Substituted N-Benzylideneanilines.* J. Phys. Chem. **69**, (1965) 1584.

[Wil93] I. Willner & B. Willner. *Chemistry of Photobiological Switches in: Biological Applications of Photochemical Switches.* Wiley&Sons, New York, 1993.

[Wol09] Martin Wolf & Petra Tegeder. *Reversible molecular switching at a metal surface: A case study of tetra-tert-butyl-azobenzene on Au(1 1 1).* Surface Science **603**, 10-12, (2009) 1506 . URL http://www.sciencedirect.com/science/article/pii/S0039602809000326. Special Issue of Surface Science dedicated to Prof. Dr. Dr. h.c. mult. Gerhard Ertl, Nobel-Laureate in Chemistry 2007.

[Wöl09] Christof Wöll. *Interfacial Systems Chemistry: Towards the Remote Control of Surface Properties.* Angewandte Chemie International Edition **48**, 45, (2009) 8406. URL http://dx.doi.org/10.1002/anie.200902974.

[Xi94] Ming Xi, Michael X. Yang, Sam K. Jo, Brian E. Bent, & Paul Stevens. *Benzene adsorption on Cu(111): Formation of a stable bilayer* (1994). URL http://dx.doi.org/doi/10.1063/1.468041. Journal article.

[Yan00] Guohua Yang, Yile Qian, Chaiwat Engtrakul, Lawrence R. Sita, & Gang-yu Liu. *Arenethiols Form Ordered and Incommensurate Self-Assembled Monolayers on Au(111) Surfaces.* The Journal of Physical Chemistry B **104**, 39, (2000) 9059. URL http://pubs.acs.org/doi/abs/10.1021/jp001611g.

[Yan08] Xiaoyin Yang, Xi Dou, Ali Rouhanipour, Linjie Zhi, Hans Joachim Räder, & Klaus Müllen. *Two-Dimensional Graphene Nanoribbons*. Journal of the American Chemical Society **130**, (2008) 4216.

[Yas03] Satoshi Yasuda, Tohru Nakamura, Mutsuyoshi Matsumoto, & Hidemi Shigekawa. *Phase Switching of a Single Isomeric Molecule and Associated Characteristic Rectification*. Journal of the American Chemical Society **125**, 52, (2003) 16430. URL `http://pubs.acs.org/doi/abs/10.1021/ja038233o`.

[Yok07] Takashi Yokoyama, Tomonori Takahashi, Kazuteru Shinozaki, & Masakuni Okamoto. *Quantitative Analysis of Long-Range Interactions between Adsorbed Dipolar Molecules on Cu(111)*. Phys. Rev. Lett. **98**, 20, (2007) 206102. URL `http://link.aps.org/doi/10.1103/PhysRevLett.98.206102`.

[Z.89] Meic Z. & Baranovic G. *Vibrational spectra of trans-N-benzylideneaniline and its isotopomers*. Pure Appl. Chem. **61**, 12, (1989) 2129.

[Zar08] Sebastian Zarwell & Karola Rück-Braun. *Synthesis of an azobenzene-linker-conjugate with tetrahedrical shape*. Tetrahedron Letters **49**, 25, (2008) 4020 . URL `http://www.sciencedirect.com/science/article/B6THS-4S9P5KY-3/2/14beeb332ca5c365c792a9a8405fd516`.

[Zar11] S. Zarwell. *Doktorarbeit: Photoschalter-Linker-Konjugate: Design, Synthesen und Charakterisierungen*. Dissertation, Fakultät II - Mathematik und Naturwissenschaften der Technischen Universität Berlin (2011).

[Zhi03] V.V. Zhirnov, III Cavin, R.K., J.A. Hutchby, & G.I. Bourianoff. *Limits to binary logic switch scaling - a gedanken model*. Proceedings of the IEEE **91**, 11, (2003) 1934 .

[Zho02] Q. Zhong, C. Gahl, & M. Wolf. *Two-photon photoemission spectroscopy of pyridine adsorbed on Cu(1 1 1)*. Surface Science **496**, 1-2, (2002) 21 . URL `http://www.sciencedirect.com/science/article/pii/S0039602801015023`.

List of Publications

Publications within this thesis

F. Leyssner, C. Bronner, St. Meyer, and P. Tegeder *Measurement of the electronic structure of a sub-nanometer wide bottom-up fabricated graphene nanoribbon* to be published (2011)

G. Mercurio, E. McNellis, I. Martin, S. Hagen, F. Leyssner, S. Soubatch, J. Meyer, M. Wolf, P. Tegeder, F.S. Tautz, and K. Reuter. *Structure and energetics of azobenzene at Ag(111): Benchmarking semi-empirical dispersion correction approaches.* ESRF Highlights 2010

J. Mielke, F. Leyssner, M. Koch, St. Meyer, Y. Luo, S. Selvanathan, R. Haag, P. Tegeder and L. Grill. *Imine derivatives on Au(111): Evidence for "inverted" thermal isomerization.* ACS Nano 5 (2011) 2090-2097.

E.R. McNellis, G. Mercurio, S. Hagen, F. Leyssner, J. Meyer, S. Soubatch, M. Wolf, K. Reuter, P. Tegeder, and F.S. Tautz. *Bulky Spacer Groups – A Valid Strategy to Control the Coupling of Functional Molecules to Surfaces?* Chem. Phys. Lett., 499 (2010) 247-249.

L. Óvári, Y. Luo, F. Leyssner, R. Haag, M. Wolf, and P. Tegeder. *Adsorption and switching properties of a N-benzylideneaniline based molecular switch on a Au(111) surface.* J. Chem. Phys., 133 (2010) 044707-1/-8.

G. Mercurio, E. McNellis, I. Martin, S. Hagen, F. Leyssner, S. Soubatch, J. Meyer, M. Wolf, P. Tegeder, F.S. Tautz, and K. Reuter. *Structure and energetics of azobenzene at Ag(111): Benchmarking semi-empirical dispersion correction approaches.* Phys. Rev. Lett., 104 (2010) 036102-1/-4

F. Leyssner, S. Hagen, L. Óvári, J. Dokic, P. Saalfrank, M. V. Peters, S. Hecht, T. Klamroth, and P. Tegeder. *Photoisomerization ability of molecular switches adsorbed on Au(111): Comparison between azobenzene and stilbene derivatives.* J. Phys. Chem. C, 114 (2010) 1231-1239.

M. Piantek, G. Schulze, M. Koch, K.J. Franke, F. Leyssner, A. Krüger, C. Navío, J.Miguel, M. Bernien, M. Wolf, W. Kuch, P. Tegeder, and J.I. Pascual. *Reversing the thermal stability of a molecular switch on a gold surface: ring-opening reaction of nitro-spiropyran.* J. Am. Chem. Soc., 131 (2009) 12729-12735

S. Wagner, F. Leyssner, C. Kördel, S. Zarwell, R. Schmidt, M. Weinelt, K. Rück-Braun, M. Wolf, and P. Tegeder. *Reversible photoisomerization of an azobenzene-functionalized self-assembled monolayer probed by sum-frequency generation vibrational spectroscopy.* Phys. Chem. Chem. Phys., 11 (2009) 6242-6248

Publications concerning other topics

F. Leyssner, M. Koch, St. Meyer, Y. Luo, R. Haag, and P. Tegeder. *Invited presentation of research: Coverage and temperature dependent isomerization of tetra-tert-butyl-imine on Au(111).* Bunsen-Magazin, 13. Jahrgang, 5 (2011) 148.

S. Hagen, P. Kate, F. Leyssner, D. Nandi, M. Wolf, and P. Tegeder. *Excitation Mechanism in the Photoisomerization of a Surface-bound Azobenzene Derivative: Role of the Metallic Substrate.* J. Chem. Phys., 129 (2008) 164102/1-164102/8.

S. Hagen, F. Leyssner, D. Nandi, M. Wolf, and P. Tegeder. *Reversible Switching of tetra-tert-butyl-Azobenzene on a Au(111) Surface Induced by Light and Thermal Activation.* Chem. Phys. Lett., 444 (2007) 85-90.

P. Tegeder, S. Hagen, F. Leyßner, M.V. Peters, S. Hecht, T. Klamroth, P. Saalfrank, and M. Wolf. *Electronic structure of the molecular switch tetra-tert-butyl-azobenzene adsorbed on Ag(111).* Appl. Phys. A, 88 (2007) 465-472.

Academic curriculum vitae

For reasons of data protection,
the curriculum vitae is not included in the online version.

Acknowledgments

I would like to thank all the people who have supported my work but it would be impossible to name all of them. I am very grateful for the help I received during this work.

First and most important I want to express my gratitude to Prof. Petra Tegeder, who has been already my supervisor during my Diploma thesis and is to a large amount responsible for the successful continuance of my scientific work. It has been a pleasure to join her young work group. The support has been ideal over the shared years at the FU and the time spend together at or off work will be missed. Thank you!

I also want to thank Prof. Nacho Pascual for becoming second referee of this thesis and for his interest in my work. The exchange of ideas (and equipment) has always been fruitful and every meeting with him has been a pleasure.

I would like to thank Prof. Martin Wolf and the members of his former workgroup at the FU Berlin. Here I began my work on molecular switches during my Diploma and started the work underlying the present thesis. The conditions and support have always been and still are exceptional.

Dr. Sebastian Hagen, you showed me everything in the lab. I always appreciated your enthusiastic work style: less talking more action! I am happy that we are still in contact and continue our mutual after work sports activities.

Matthias Koch has been an amazing diploma student, thanks for everything.

Michael Meyer, I have been your best man at your wedding otherwise I would believe that we are married. We spent the last 25 years, with small discontinuities, "learning" together starting from primary school. Surprisingly, it is still great to have you around, thanks!

I would also like to say thank you to the new team (which I already worked with for three years now): Christopher Bronner, Erwan Varene, Michael Schulze and the "young-guns" Stephan Meyer and Lea Bogner and the rest of the people who I had the chance to work with. It has been a pleasure working with you and the positive atmosphere in the group made even the longest discussions, Lab catastrophes and conferences spend together livable.

Dietgard Mallwitz and Peter West have to be named for their great support at diverse problems related to administration and the *Feuerzangenbowle* at the Christmas parties.

All the members of the groups who we collaborated with during this work have always been supportive. Prof. Katharina Franke, PD Dr. Leonhard Grill, Prof. Rainer Haag, Prof. Stefan Hecht, Prof. Wolfgang Kuch, Prof. Karsten Reuter, Prof. Karola

Rück-Braun, Prof. Saalfrank and Prof. Martin Weinelt and the members of their work groups have been of help during this work. The number of work groups mentioned shows how efficient the collaborations in the SFB 658 *Molecular Switches on Surfaces* have been and how much fun it was working in an environment like this.

I have to mention the collaborations with the group of Stefan Tautz, which enabled two beamtimes at the European Synchrotron Radiation Facility in Grenoble. To Dr. Sergey Soubatch and Giuseppe Mercurio who endured long hours with me during the measurements: it has been great to get to know you guys!

Acknowledgements have to be given to people outside the scientific community as well: First of all I thank Vanessa who always encouraged me and has been a great support over the past years. I am looking forward to what life brings next. I am grateful to have a family like mine, you made everything look easier. All of my friends, you have been my backing and I am still amazed how you kept interest in my work and helped me to gain distance from it.